

Department of Neuroanatomy,  
Theoretical Medicine and Biosciences,  
Faculty of Medicine  
Saarland University, Homburg/Saar

# **A LOCAL, PERI-ACTIVE ZONE ENDOCYTIC MACHINERY AT PHOTORECEPTOR SYNAPSES IN CLOSE VICINITY TO SYNAPTIC RIBBONS**

A thesis submitted to the Faculty of Medicine in fulfilment of the  
requirements for the degree of

**Doctor of Philosophy (Ph.D.)**

At the Saarland University

2014

Submitted by

Silke Wahl

Date of birth: 27.09.1982

Place of birth: Neunkirchen, Saar

Supervisor:

Co-supervisor:

*Dedicated to my parents, family & friends*

# Contents

<b>Summary</b>	<b>7</b>
<b>Zusammenfassung</b>	<b>9</b>
<b>1 Introduction</b>	<b>11</b>
1.1. The mammalian eye	11
1.2. Ribbon synapse of retina	14
1.3. RIBEYE is the major component of synaptic ribbon	16
1.4. The functional role of RIBEYE in ribbon synapses	18
1.5. Synaptic vesicle cycle at ribbon synapses	19
1.5.1. Exocytosis	19
1.5.2. Endocytosis	20
1.5.2.1. Clathrin-mediated endocytosis	20
1.5.2.2. Clathrin-independent endocytosis	36
1.6. working hypothesis	36
<b>2 Material and Methods</b>	<b>38</b>
2.1. Materials	38
2.1.1. Antibodies	38
2.1.2. Secondary antibodies	41
2.1.3. Animal tissue	41
2.1.4. Buffers and Media	42
2.2. Methods	43
2.2.1. Immunofluorescence microscopy	43
2.2.1.1. Immunolabeling of cryo-sections	43
2.2.1.2. Immunolabelling of 0.5 $\mu$ m-thin resin sections: Embedding procedure	43
2.2.1.3. Immunolabelling procedure for use with 0.5 $\mu$ m-thin	44

resin sections	
2.2.1.4. Control incubations	44
2.2.1.5. Direct-Labeling of primary antibodies (mouse anti-CtBP2) with fluorophores (DyLight 488/DyLight650)	44
2.2.1.6. Triple immunolabelling for super-resolution structured illumination microscopy (SR-SIM)	45
2.2.1.7. Blocking of antibodies: Preabsorption experiments	45
2.2.1.8. Super-resolution structured illumination microscopy (SR-SIM)	46
2.2.2. Postembedding immunogold electron microscopy: Tissue embedding and immunogold labelling procedure	46
2.2.3. SDS-Page	47
2.2.4. Western blots	47
2.2.5. Isolation of photoreceptors from the mature mouse retina	48
2.2.6. Analysis of synaptic ribbon-associated endocytic activity in synaptic terminals of isolated mouse photoreceptors	49
<b>3 Results</b>	<b>50</b>
3.1. Testing of antibodies	50
3.2. Localisation of dynamin	50
3.3. Localization of Dynamin interacting-proteins	60
3.4. Proof of specificity	64
3.5. Hight resolution analysis	66
3.6. Localisation of other endocytic proteins	69
<b>4 Discussion</b>	<b>82</b>
<b>5 Further projects</b>	<b>88</b>

<b>6 References</b>	<b>89</b>
<b>7 Abbreviations</b>	<b>107</b>
<b>8 List of figures</b>	<b>110</b>
<b>9 Acknowledgement</b>	<b>112</b>
<b>10 Curriculum Vitae</b>	<b>113</b>
<b>11 Publications</b>	<b>114</b>

## **Summary**

Photoreceptor ribbon synapses are continuously active synapses with large active zones that contain synaptic ribbons. Synaptic ribbons are anchored to the active zones and are associated with large numbers of synaptic vesicles. The base of the ribbon that is located close to L-type voltage-gated  $\text{Ca}^{2+}$ -channels is a hotspot of exocytosis. The continuous exocytosis at the ribbon synapse needs to be balanced by compensatory endocytosis. Recent analyses indicated that vesicle recycling at the synaptic ribbon is an important determinant of synaptic signaling at the photoreceptor synapse. To get insights into mechanisms of vesicle recycling at the photoreceptor ribbon synapse, I localized major endocytic proteins in photoreceptor synapses of the mouse retina.

Endocytosis requires the coordinated assembly of a large number of proteins at the plasma membrane. Dynamin is a mechanoenzyme important for most forms of endocytosis. Clathrin is an important coat protein, needed for many but not all forms of endocytosis. Other dynamin/clathrin-associated proteins mediate different functions in the endocytic cycle.

Therefore, in the present study, I analyzed the localization of dynamin, amphiphysin, endophilin, synaptojanin, syndapin, clathrin and calcineurin in the mouse retina. For this purpose, I used conventional epifluorescence microscopy, super-resolution structured illumination microscopy (SR-SIM) and immunogold electron microscopy.

I found that major endocytic proteins (i.e. dynamin, syndapin, amphiphysin, and calcineurin) are indeed highly enriched around the active zone and the synaptic ribbon, in a peri-active zone localization. Other endocytic proteins, i.e. endophilin and synaptojanin, are diffusely distributed throughout the entire presynaptic terminal. The specificity of the presented immunolabellings were carefully controlled by various control experiments. Furthermore, I presented evidence for two clathrin heavy chain variants being present in photoreceptor terminals. One variant is enriched around the synaptic ribbon in a peri-active zone localization, whereas the other is localized in the entry region of the terminal probably at an endosomal compartment.

In agreement with the focal enrichment of major endocytic proteins at the synaptic ribbon, I observed a preferential uptake of sulforhodamine (SR101), a fluid phase

-Summary-

endocytosis marker, and FM1-43 dye in close vicinity to the synaptic ribbon in mouse photoreceptor terminals. This endocytic activity depends on dynamin, because SR101 uptake was completely blocked by dynasore, a specific inhibitor of dynamin activity.

These data proposes that the presynaptic peri-active zone surrounding the synaptic ribbon complex is not only a hotspot of exocytosis, it is also a hot spot of endocytosis in photoreceptor ribbon synapses. This endocytotic activity depends on dynamin.

## **Zusammenfassung**

Photorezeptor Ribbonsynapsen sind kontinuierlich aktive Synapsen mit großen aktiven Zonen, die synaptische Ribbons enthalten. Synaptische Ribbons sind in der aktiven Zone verankert und mit einer großen Anzahl synaptischer Vesikel assoziiert. Die Basis des Ribbons ist in der aktiven Zone unmittelbar neben den spannungsgesteuerten  $Ca^{2+}$  - Kanälen vom L-Typ immobilisiert. Dort findet die Exozytose synaptischer Vesikel besonders intensiv statt. Die kontinuierliche Exozytose an den Ribbonsynapsen muss durch Endozytose kompensiert werden. Jüngste Untersuchungen haben gezeigt, dass das Zur-Verfügung-Stellen von synaptischen Vesikeln am synaptischen Ribbon ebenfalls eine wichtige Determinante für die synaptische Signalübertragung in den Photorezeptorsynapsen ist. Um einen Einblick in den endozytotischen Membranverkehr in den Photorezeptor-Ribbonsynapsen zu erhalten, habe ich wichtige, an der Endozytose beteiligte, Proteine in Photorezeptorsynapsen in der Retina von Mäusen lokalisiert.

Endozytose benötigt die koordinierte Aktivität einer großen Anzahl von Proteinen. Dynamin ist ein Mechano-Enzym, das für die meisten Formen der Endozytose wichtig ist. Clathrin ist ein wichtiges Mantel-Protein, das für viele, aber nicht für alle Formen der Endozytose benötigt wird. Andere Dynamin- bzw. Clathrin- assoziierte Proteine vermitteln verschiedene Schritte im endozytotischen Weg.

Daher habe ich in der vorliegenden Studie die Lokalisation von Dynamin, Amphiphysin, Endophilin, Synaptojanin, Syndapin, Clathrin und Calcineurin in der Retina von Mäusen untersucht. Zu diesem Zweck habe ich konventionelle Epifluoreszenzmikroskopie, Höchstauflösende Mikroskopie mit strukturierter Belichtung (SR-SIM) und Immunogold-Elektronenmikroskopie angewendet.

Dabei fand ich heraus, dass wesentliche endozytotische Proteine (d.h. Dynamin, Synadapin, Amphiphysin und Calcineurin) in der Tat stark um die aktive Zone und den synaptischen Ribbon angereichert sind. Andere endozytotische Proteine, d.h. Endophilin und Synaptojanin, sind dagegen diffus in der präsynaptischen Terminale verteilt. Die Spezifität der gezeigten Immunfärbungen wurde sorgfältig durch verschiedene Kontrollexperimente überprüft. Desweiteren habe ich Beweise für die Existenz zweier Varianten der schweren Clathrin-Ketten in den Photorezeptorterminalen aufgezeigt.

## -Zusammenfassung-

Eine Clathrin-Variante ist um den synaptischen Ribbon konzentriert und in der peri-aktiven Zone lokalisiert, während die andere in der Eingangsregion der synaptischen Terminale, wahrscheinlich in einem endosomalen Kompartiment, gelegen ist. In Übereinstimmung mit der fokalen Anreicherung von wichtigen endozytotischen Proteinen um den synaptischen Ribbon herum, habe ich eine präferentielle Aufnahme von Sulforhodamin (SR101), einem Marker für Flüssigphase-Endocytose, und FM1-43 Farbstoff in unmittelbarer Nähe zum synaptischen Ribbon in Photorezeptor-Terminalen von Mäusen beobachten können. Diese endozytotische Aktivität ist funktionell abhängig von Dynamin, da die Aufnahme von SR101 durch die Anwesenheit von Dynasore, einem spezifischen Inhibitor der Dynamin-Aktivität, komplett blockiert werden konnte.

Diese Ergebnisse lassen darauf schließen, dass die präsynaptische peri-aktive Zone, welche den synaptischen Ribbonkomplex umgibt, nicht nur ein Schwerpunkt exozytotischer Aktivität, sondern auch ein Schwerpunkt endozytotischer Aktivität in Photorezeptor-Ribbonsynapsen ist. Diese endozytotische Aktivität ist abhängig von Dynamin.

## **1. Introduction**

The visual system is extraordinary in the quantity and quality of information it supplies about the world. It is a complex systems that involves several stages and several steps of parallel information processing in various areas of the central nervous system (tom Dieck and Brandstätter, 2006). In general it consists of the eye, the optical nerve, the tractus opticus, the corpus geniculatum laterale and different brain areas. The initial stage of this system is the eye, a sophisticated sensory organ. It can even detect a single photon and transmits the signal to the higher brain center. To be able to perform these demanding tasks sensory neurons in the eye contain specialized synapses called ribbon synapses (Schmitz, 2009).

### **1.1. The mammalian eye**

The eye is a fluid-filled sphere enclosed by three layers of tissue (Figure 1). The outer layer is composed of the sclera and the transparent light-permeant cornea. The middle tissue layer contains the iris, the ciliary body and the choroid. The innermost layer of the eye, the retina, contains neurons that are sensitive to light and capable of transmitting visual signals to higher brain center via the optic nerve (for review, see Purves et al., 2001).

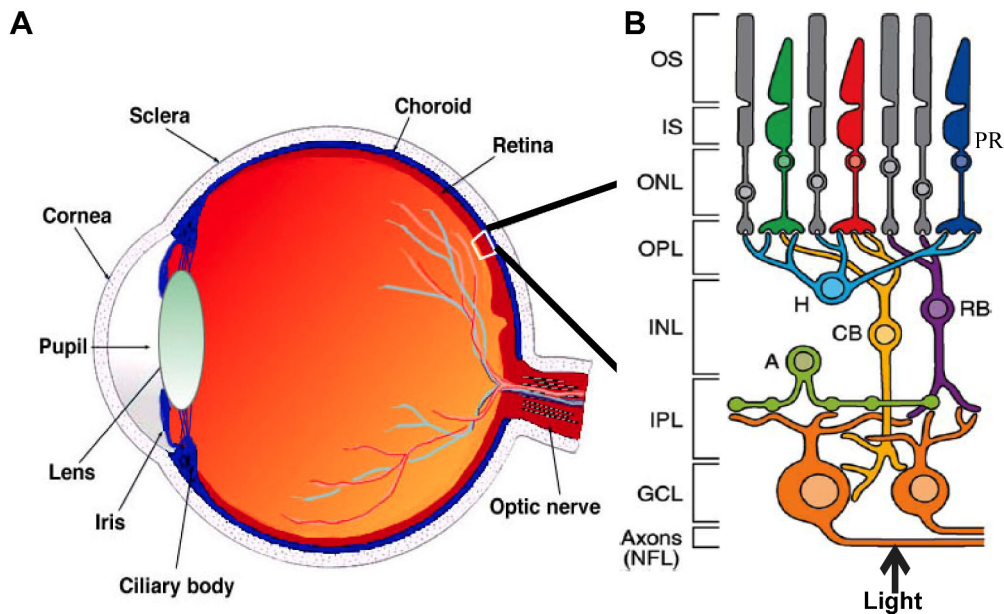


**Figure 1 (A) Section through the adult human eye** (<http://webvision.med.utah.edu>). **(B) Schematic representation of main retinal neurons.** Abbreviations: OS, outer segment; IS, inner segments; ONL, outer nuclear layer; OPL, outer plexiform layer; INL, inner nuclear layer; IPL, inner plexiform layer; GCL, ganglion cell layer; PR, photoreceptor; A, amacrine cells; H, horizontal cells; RB, rod bipolar cells; CB, cone bipolar cells; The arrow indicates light pathway in the retina.

During the embryonic development, the retina is formed as part of the neuroectoderm, a specialised part of the ectoderm, which also develops into the central nervous system (CNS). The retina, unlike the central nervous system, comprises only of few classes of neurons. It is a highly organised structure and easily accessible and it serves as a model system to study CNS functions. The mature mammalian retina consists of two distinct parts, i.e. neural retina and the single layered retinal pigment epithelium.

The neural retina is an intricate network of sensory and higher order neurons that processes in parallel many different aspects of visual signals, e.g. brightness, darkness, contrast, colour and motion (Wässle, 2004). There are five main types of neurons in the retina: photoreceptors, bipolar cells, ganglion cells, horizontal cells, and amacrine cells.

Their somata are located in the three nuclear layers of the retina, which are separated by the two synaptic layers (Figure 2).

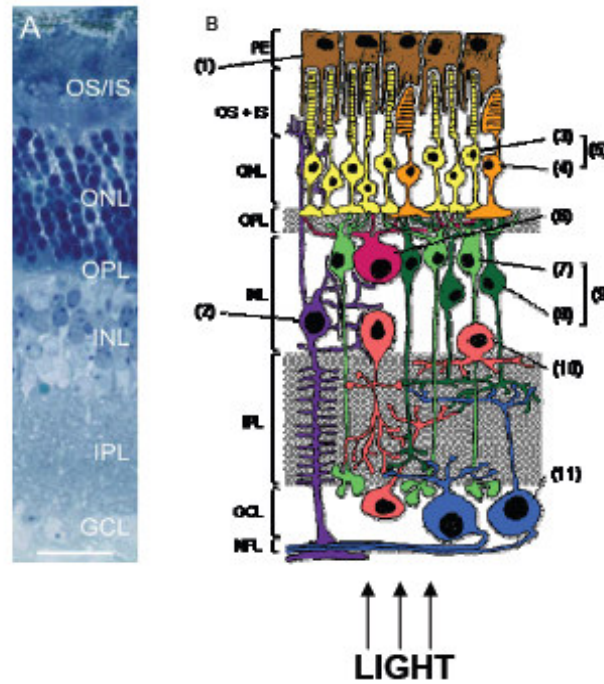


**Figure 2 Schematic overview of the mammalian retina.**

**A)** Toluidine blue-stained vertical cryostat section of retina showing the various retinal layers (OS/IS contains the outer and inner segments of the rod and cone photoreceptors; outer nuclear layer (ONL) containing the somata of the photoreceptors, outer plexiform layer (OPL) or first synaptic region, inner nuclear layer (INL) containing the somata of the second order neurons, i.e. horizontal, bipolar and amacrine cells, inner plexiform layer (IPL) or second synaptic region, ganglion cell layer (GCL) containing the somata of the ganglion cells and of displaced amacrine cells) (Tom Dieck *et al.*, 2006).

**B)** Vertical section through a mammalian retina. (Obtained from MPI for Brain research, Frankfurt) The following cell types are shown: retinal pigment epithelium (PE, 1), Müller cells (2), photoreceptors (5), rods (3), and cones (4), horizontal cells (6), bipolar cells (9): rod - (7) and cone bipolar cells (8), amacrine cells (10), ganglion cells (11). The arrows show the direction of the light falling into the eye (and through the layer of the retina). Abbreviations. OS, outer segment; IS, inner segment. Scale: 20µm.

The photoreceptor layer contains the outer segments (OS) and inner segments (IS) of rod and cone photoreceptors. The axons of these photoreceptors as well as the dendrites of horizontal and bipolar cells are located in the outer nuclear layer (ONL) and the outer plexiform layer (OPL). In the inner nuclear layer (INL), the cell bodies of horizontal, bipolar, amacrine, Müller glia and interplexiform cells are found. The inner plexiform layer (IPL) contains the axons of bipolar cells, amacrine cells as well as the dendrites of ganglion cells. The ganglion cell layer (GCL) consists of the cell bodies of ganglion cells and displaced amacrine cells and astrocytes in the area around the optical nerve. The axons of the ganglion cells form the nerve fiber layer. They traverse the retina, collect in a bundle at the optic disc, and leave the eye to form the optic nerve.

The major route of information flow through the retina is processed through a three-neuron chain. Light is detected by the photoreceptors (1st neuron) and transformed into a neuronal signal that is transmitted to the bipolar cells (2nd neuron). They are carrying the signal from the OPL to the IPL, where the signal is passed to the dendrites of the ganglion cells (3rd neuron). Their axons run in the fiber layer of the retina and collect at the optic disk to form the optic nerve, which carries all visual information from the eye to the higher visual brain areas.

This chain requires a number of synapses with different properties in signal transmission. Indeed, various types of structurally and functionally distinct synapses are present in the retina: the faster electrical synapses, the physically transmitting conventional chemical synapses and the ribbon synapses that transmit their signals tonically and in a graded fashion (Heidelberger et al., 2005).

## **1.2. Ribbon synapse of retina**

Graded synaptic output requires the release of several hundreds to several thousands of synaptic vesicles per second (Parson and Sterling, 2003; Sterling and Matthews, 2005; Heidelberger et al., 2005). To accomplish this level of performance, the sensory neurons of the eye and the cochlea maintain large pool of fast releasable vesicles and are equipped with a special type of chemical synapses, the ribbon synapses (Dowling et al., 1987; Fuchs et al., 2003). These are unique chemical synapses characterized by presynaptic specialisation, the synaptic ribbon.

The synaptic ribbon is a large presynaptic sheet-like structure with a lamellar organization and associated with the active zone (Sterling et al., 1998; Schmitz, 2009). Synaptic ribbons are surrounded and physically in touch with a large amount of synaptic vesicles which are positioned by the ribbon in close proximity to the active zone. In electron micrographs the ribbons appear mostly bar shaped (Sjöstrand et al., 1953) (Figure 3). This appearance was also revealed by three-dimensional reconstructions, which provides the synaptic ribbon with a huge surface area. This surface area is around  $0.77\mu\text{m}^2$  big in mammalian rods (Sterling and Matthews, 2005) (Figure 3). The rod mammalian photoreceptor ribbon is approximately 35nm thick and juts up to  $1\mu\text{m}$  in deep into the presynaptic cytoplasm.

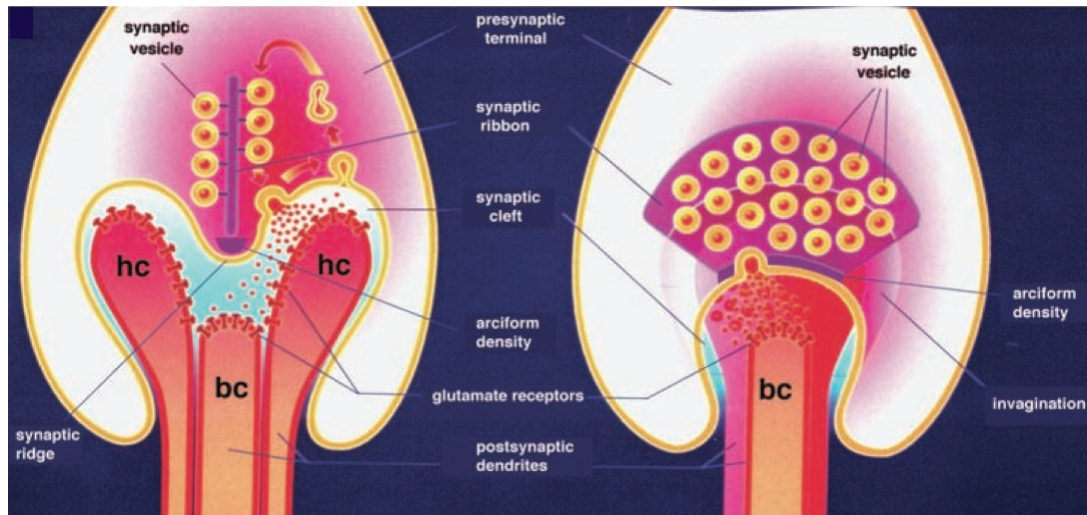


**Figure 3 Schematic diagramme of photoreceptor ribbon synapses.** The bar-shaped ribbon (left panel) is actually a cross-section of a plate-like structure that is bended along the invaginated photoreceptor presynaptic plasma membrane in a crescent, -shaped manner (right panel). The postsynaptic dendritic profiles of horizontal and bipolar cells are depicted in a simplified manner (Schmitz, 2009).

The photoreceptor ribbon is not directly connected with the active zone. It is anchored via the arciform density, which is located within a small evagination of the presynaptic plasma membran, the synaptic ridge. The ridge contains clusters of presynaptic L-type voltage-gated calcium-channels. Due to an overall invagination of the presynaptic plasma membrane, the arciform density has a curved shape. The synaptic ribbon adopts this shape and becomes a horseshoe shaped appearance (Figure 4).

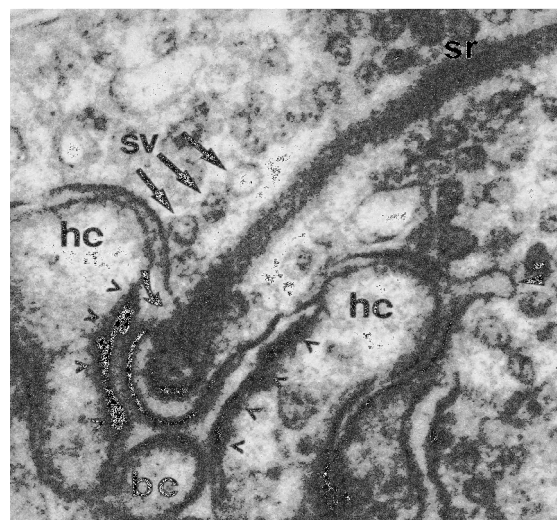


**Figure 4 Ultrastructure model for assembly of synaptic ribbon.** EM picture of a photoreceptor ribbon synapse, Abbreviation: sr-synaptic ribbon, sv-synaptic vesicle, hc-horizontal cell, bc-bipolar cell (Schmitz, 2009).

The shape of the ribbon and the number of tethered vesicles varies between the different types of photoreceptors and bipolar cells in the retina.

The small terminals of the rod photoreceptors usually contain a single large synaptic ribbon, which is several 100nm in height, 1µm in depth and shows horseshoe shaped structure, which is clearly visible at the light microscopical level. Around 770 synaptic vesicles usually bind to a rod synaptic ribbon (Sterling and Matthews, 2005).

130 of the 770 total vesicles are found in a basal row at the membran-anchored end of the synaptic ribbon and are considered as "docked " vesicles for immediated release. The other remaining synaptic vesicles, the "tethered " vesicles, are associated to the ribbon in a more distal row.

The terminals of the cone photoreceptors are larger than the rod terminals and contain several ribbons (10-12 ribbons per terminal) with shorter active zones contacted by invaginating postsynaptic elements. By light microscopy, the ribbons in a cone terminal appear like a chain of dots. The individual ribbons are slightly shorter (~ 1µm long; 0.2µm high) if you compare them with the one of the rods (~2µm long; 0.4µm high.) The total ribbon surface and the number of ribbon-tethered vesicles is much larger in the cones than in the rods (Sterling and Matthews, 2005; Jackman et al., 2009; Heidelberger et al., 2005).

The terminals of the rod and cone bipolar cells in the IPL contain several small ribbons that are opposed by two non-invaginating postsynaptic processes of amacrine and ganglion cells. Bipolar cell ribbons, like cone photoreceptor ribbons, have a dot-like appearance by light microscopy due to their relative small size (tom Dieck *et al.*, 2006). Ribbon synapses of goldfish bipolar cells for expamle contain 45 to 65 small ribbons. Each of them binds around 110 vesicles from which 22 are docked. In total, they bind approximately 1200 docked vesicles (von Gersdorff, 2001).

### **1.3. RIBEYE is the major component of synaptic ribbon**

RIBEYE is the only known protein component specific for synaptic ribbons. Its identification shed breakthrough information on the molecular structure of synaptic ribbons (Schmitz *et al.*, 2000).

RIBEYE consists of a unique aminoterminal, proline rich A-domain (563aa) to which, as published until now, no homologous proteins exists, while the caboxyterminal B-

domain (425aa) is largely identical to the nuclear co-repressor protein CtBP2 (Schmitz et al., 2000) (Figure 5). CtBP2 and RIBEYE are splice variants of the CtBP2 gene (Schmitz *et al.*, 2000; Corda *et al.*, 2006).

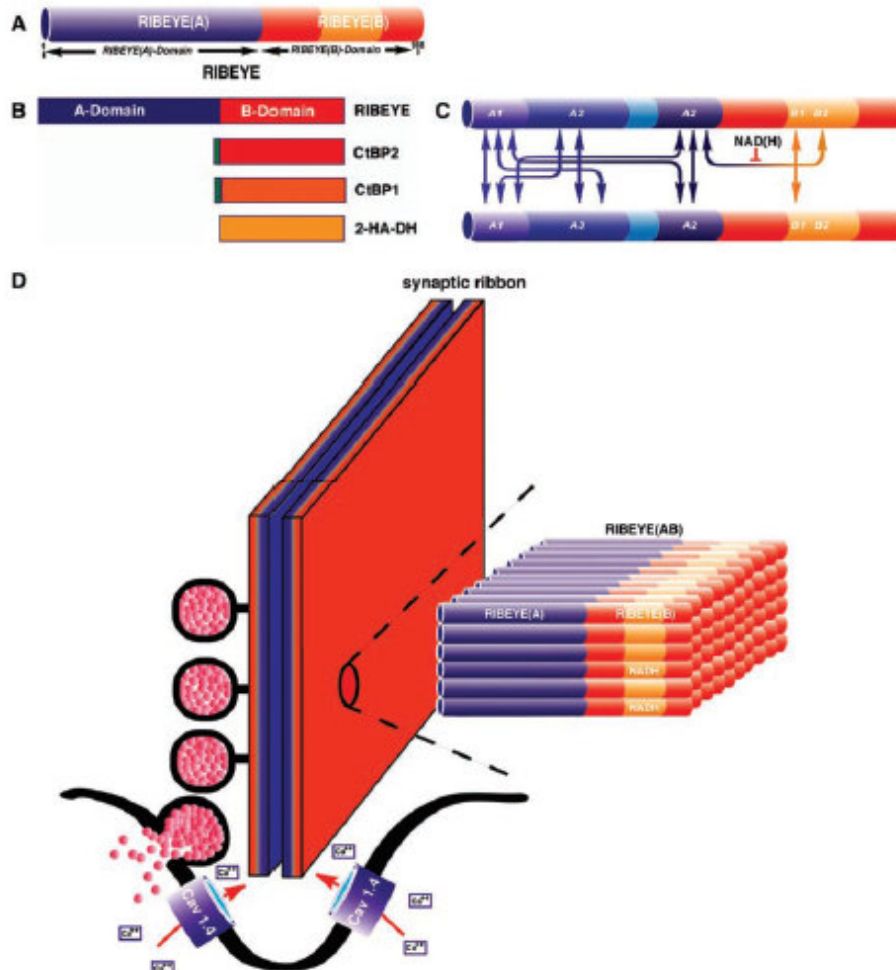


**Figure 5 RIBEYE is the main structural element of synaptic ribbons.** Schematic depiction of the domain structure of RIBEYE, (A, B) RIBEYE consists of a unique aminoterminal A-domain and a carboxyterminal B-domain which is identical to CtBP2 except for the first 20 N-terminal amino acids. RIBEYE (B)-domain/CtBP2 is related to CtBP1 and binds NAD(H). RIBEYE (B)/CtBP2 and CtBP1 evolutionarily developed from a family of D-isomer-specific 2-hydroxy acid dehydrogenases (2-HA-DH). (C) Multiple RIBEYE-RIBEYE interaction sites are present in the A- and B-domains of RIBEYE. In the A-domain, 3 RIBEYE docking sites are present, denoted as “A1,” “A2,” and “A3.” The B-domain contains 2 RIBEYE interaction sites, “B1” and “B2.” These interaction sites allow multiple RIBEYE-RIBEYE interactions as indicated by the arrows. Heterotypic RIBEYE(A)-RIBEYE(B) interactions are inhibited by NAD(H). (D) Highly simplified schematic working hypothesis on how the synaptic ribbon could be built from RIBEYE subunits. A RIBEYE-containing scaffold is suggested to be glued together via RIBEYE-RIBEYE interactions. At the base of the synaptic ribbon, L-type voltage-gated Ca<sup>2+</sup> channels are clustered. The poreforming unit of these channels in rod synapses (Cav1.4) is schematically depicted. The arciform density is not shown. (A-D).

CtBP2 and CtBP1 constitute together a family of transcriptional co-repressors. CtBP1 was found to be a C-terminal binding protein for the adenovirus E1A-protein (Schaeper et al., 1995) and CtBP2 was subsequently observed as a close structural and functional homolog of CtBP1 (Katsanis et al., 1998). The structure of RIBEYE and its gene lead to the suggestion that RIBEYE is a fusion protein of a preexisting protein (CtBP2) and a novel N-terminal domain (Schmitz et al., 2000). Several studies indicated that RIBEYE is the major component of synaptic ribbons (Schmitz et al., 2000; Zensek et al., 2002; Wan et al. 2005; Magupalli et al., 2008). This suggests that it has also a major influence on the function of synaptic ribbons.

#### **1.4. The functional role of RIBEYE in ribbon synapses**

Knockdown experiments in zebrafish using morpholino-based silencing techniques show that the knockdown of RIBEYE leads to disappearance of synaptic ribbons except for a small stump (Wan et al., 2005).

The RIBEYE (A)-domain appears to have a predominantly structural role, whereas the B-domain probably points to the cytoplasmic face of the synaptic ribbon where it binds NADH (Magupalli *et al.*, 2008; Alpadi *et al.*, 2008). RIBEYE can polymerize via interactions between its A- and B- domains to form vesicle-associated structures, similar to spherical synaptic ribbons. NADH may promote the assembly of synaptic ribbons by favoring homotypic and inhibiting heterotypic interaction between the RIBEYE(A)- and RIBEYE(B)-domains (Magupalli *et al.*, 2008). Heterologous expression of full-length RIBEYE generated electron-dense spherical structures that resembled spherical synaptic ribbons of inner hair synaptic ribbons (Magupalli *et al.*, 2008). The modular assembly hypothesis of synaptic ribbons from individual RIBEYE subunits provides also an explanation for the assembly of synaptic ribbons from smaller RIBEYE subunits. The assembly of synaptic ribbons from RIBEYE subunits likely is a multistep process, which also includes the synaptic spheres, spherical synaptic ribbon-like structures (Schmitz, 2009).

## 1.5. Synaptic vesicle cycle at ribbon synapses

### 1.5.1. Exocytosis

Ribbon synapses transmit graded changes of membrane potential into modulations of continuous, tonic exocytosis of synaptic vesicles (Jackman et al., 2009; for review, see Heidelberger et al., 2005; Schmitz, 2009; Mercer and Thoreson, 2011).

TIRF analyses have shown that the basal end of the synaptic ribbon is a hotspot of exocytosis (Zenisek et al., 2000). The presynaptic release sites are localized within an invagination of the presynaptic plasma membrane where they contact the dendritic tips of secondary neurons (for review see Schmitz, 2009). Most amazingly, ribbon synapses are equipped with a roughly similar set of synaptic proteins as conventional synapses, although the physiological properties of ribbon synapses are quite distinct (Heidelberger et al., 2005; Thoreson 2007; Zanazzi and Matthews 2009).

The membran fusion in ribbon synapses is also driven by the formation of trans-SNARE complexes consisting of v- and t-SNAREs (Südhof and Rothman, 2009). The specific composition of SNARE complexes differs to some extent between different types of ribbon synapses and in comparison to conventional synapses (Heidelberger et al., 2005; Thoreson 2007; Zanazzi and Matthews 2009). For example, syntaxin 3b replaces syntaxin 1 as Q-SNARE in retinal ribbon synapses while in hair cells and pinealocytes syntaxin 1 appears to be present (Zanazzi and Matthews, 2009).

In ribbon synapses, the  $\text{Ca}^{2+}$  sensitivity of exocytosis appears to be unusually high. Tonic release is induced by intracellular  $\text{Ca}^{2+}$  at around  $1\mu\text{M}$  in photoreceptor synapses. In ribbon synapses release can already be elicited at submicromolar intracellular  $\text{Ca}^{2+}$  concentrations. Furthermore there is a linear relationship between exocytosis and intracellular  $\text{Ca}^{2+}$  concentrations (Thoreson et al., 2004; Heidelberger et al. 2005; Thoreson 2007). The  $\text{Ca}^{2+}$  dependence and kinetics of exocytosis vary considerably between different types of ribbon synapses and also within one type of ribbon synapses (Johnson et al., 2008).

Also, if you compare rod and cone terminals with each other, the intraterminal  $\text{Ca}^{2+}$  concentration is different and their release kinetics too. Cones show faster release kinetics than rods. This correlates with a higher  $\text{Ca}^{2+}$  concentration in cones in comparison to rods (Rabl et al. 2005; Sheng et al., 2007; Thoreson et al., 2007).

The entry of  $\text{Ca}^{2+}$  through voltage-gated  $\text{Ca}^{2+}$  channels drives the fusion of synaptic vesicles at the presynaptic plasma membrane of ribbon synapses. These are predominantly L-type  $\text{Ca}^{2+}$  channels that do not (or very slowly) inactivate and stay open even during prolonged depolarization. This property is important to maintain continuous neurotransmitter release. The  $\text{Ca}^{2+}$  channels are located close to the plasma membrane-anchored end of the synaptic ribbon (Zanazzi and Matthews, 2009).

The continuous exocytosis at the ribbon synapse needs to be balanced by compensatory endocytosis to avoid synaptic depression and replenish vesicle pools (Schweizer and Ryan, 2006; Wu et al., 2007; Smith et al. 2008).

### **1.5.2. Endocytosis**

In general, different modes of endocytosis exist. In retinal bipolar cells at least two are known from electrophysiological analyses, a fast retrieval mechanism and a slow one (Smith et al. 2008). The fast one ( $\tau \sim 1-2$  seconds) is clathrin independent, regulated by presynaptic  $\text{Ca}^{2+}$  and is selectively inhibited by high intracellular chloride. A link between exocytosis and fast endocytic membrane retrieval could be the influx of presynaptic  $\text{Ca}^{2+}$  (Wu et al., 2007). Although the clathrin-independent kiss and run mode has been proposed as a potential mechanism for the fast retrieval in ribbon synapses, there is until now no evidence for this (LoGiudice and Matthews, 2007). The molecular mechanisms for fast endocytosis at synaptic ribbons are unclear.

Slow endocytosis ( $\tau \sim 10-30$  seconds) in bipolar cells on the other hand is clathrin- and dynamin-dependent but  $\text{Ca}^{2+}$  independent (Jokusch et al., 2005).

Several studies indicate that synaptic ribbons are involved in endocytotic membrane traffic. Electron microscopic tracer analyses showed that ribbons are associated with tubular invaginations of the presynaptic plasma membranes and other membrane compartments of endosomal origin (Lenzi et al., 1999, 2002; Paillart et al., 2003). Endocytotic mutant fish with a defect in synaptojanin, a polyphosphoinositide phosphatase important for endocytosis and for the organization of the actin cytoskeleton, show unanchored ribbons and strongly disturbed membrane trafficking (van Epps et al., 2004). These findings indicate that normal endocytic activity is important for ribbon anchoring.

### 1.5.2.1. Clathrin-mediated endocytosis

Clathrin-mediated endocytosis is the uptake of material into the cell from the surface using clathrin-coated vesicles. Endocytosis requires the coordinated assembly of a large number of proteins at the plasma membrane, the timing and composition of which are very regular (Kaksonen et al., 2005; Taylor et al., 2011). The pathway itself is versatile, as different cargoes can be packaged using a range of accessory adaptor proteins. Clathrin-mediated endocytosis is used by all known eukaryotic cells (McMahon and Boucrot, 2011).

In general clathrin coated vesicle formation has been subdivided into 5 different steps: initiation/nucleation, cargo selection, coat assembly, scission and uncoating (Figure 6).

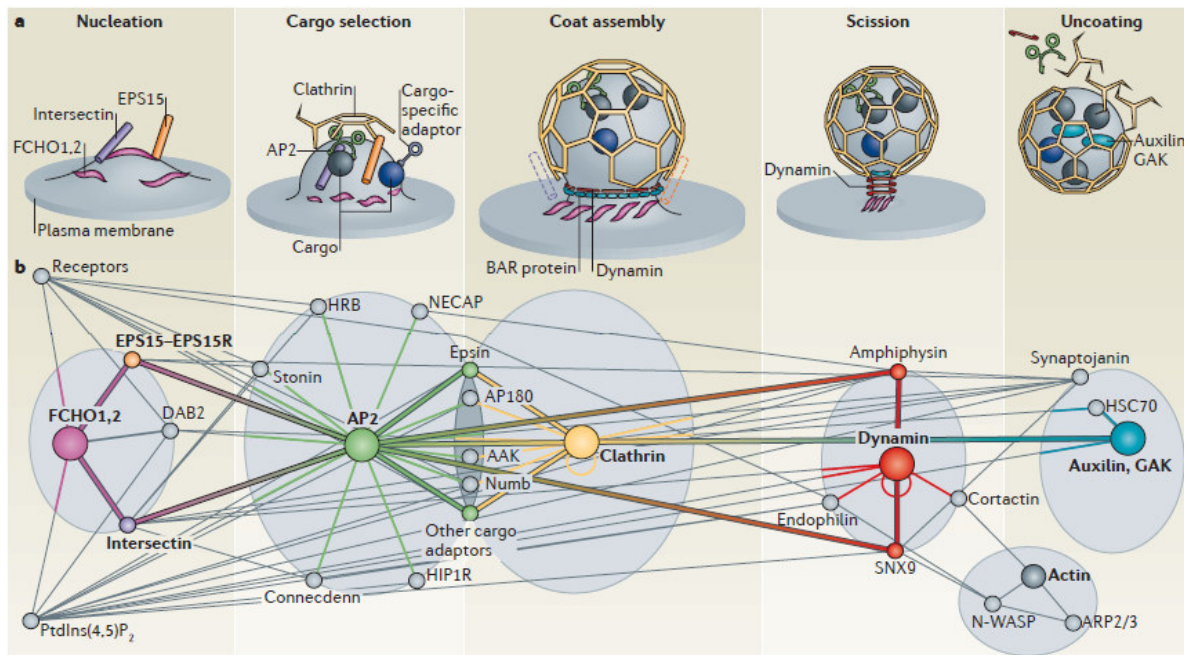


**Figure 6 The clathrin-coated vesicle cycle. A.** The proposed five steps of clathrin-coated vesicle formation. Nucleation: FCH domain only (FCHO) proteins bind phosphatidylinositol-4,5-bisphosphate (PtdIns(4,5)P<sub>2</sub>)-rich zones of the plasma membrane and recruit EPS15–EPS15R (EGFR pathway substrate 15–EPS15-related) and intersectins to initiate clathrin-coated pit formation by recruiting adaptor protein 2 (AP2). Cargo selection: AP2 recruits several classes of receptors directly through its  $\mu$ -subunit and  $\sigma$ -subunit. Cargo-specific adaptors (for example, stonin, HRB and Numb) bind to AP2 appendage domains and recruit specific receptors to the AP2 hub. Coat assembly: clathrin triskelia are recruited by the AP2 hub and polymerize in hexagons and pentagons to form the clathrin coat around the nascent pit. Scission: the GTPase dynamin is recruited at the neck of the forming vesicle by BAR domain-containing proteins, where it self-polymerizes and, upon GTP hydrolysis, induces membrane scission. The actin machinery module can be added at this stage for actin polymerization at the neck of the pit, which can aid in vesicle production (not shown). Uncoating: auxilin or cyclin G-associated kinase (GAK) recruit the ATPase heat shock cognate 70 (HSC70) to disassemble the clathrin coat and produce an endocytic vesicle containing the cargo molecules. Synaptojanin probably facilitates this by releasing adaptor

proteins from the vesicle membrane through its PtdIns lipid phosphatase activity. The components of the clathrin machinery are then freed and become available for another round of clathrin-coated vesicle formation. **B. The clathrin network.** The protein–protein interactions underlying the different stages of vesicle progression are shown. Major hubs are obvious because of their central location in the network and the large number of interacting molecules. They are essential for pathway progression and are denoted by the central coloured circles. Possible pathways of progression between hubs are shown with thicker lines. (McMahon and Boucrot, 2011)

Many endocytosis-related proteins are recruited to form complexes on the retrieved pits at each step including clathrin, AP2, AP180, dynamin, amphiphysin, endophilin, synaptojanin, intersectin, syndapin, auxilin, HSC70 ATPase and so on (Cousin and Robinson, 2001). In this work I focussed on clathrin, dynamin1, amphiphysin, endophilin, synaptojanin, syndapin and calcineurin.

Clathrin is a self-assembling protein that is recruited to membranes from the cytoplasm of eukaryotic cells to form a protein coat. The function of this coat is to sort proteins in the membrane and to contribute to membrane deformation. The clathrin coat is composed of two layers: an inner layer of adaptors and an outer clathrin layer.

The clathrin protein is composed of three trimerized heavy chain subunits that can self-assemble into a polyhedral, clathrate (latticed) array on membranes, inspiring its name (Pearse 1976; for review see Brodsky 2012). The most well characterized form of clathrin has bound light chain subunits (CLCs). Clathrin heavy chains (CHCs) are present in all analyzed eukaryotes (Wakeham et al., 2005). With the emergence of vertebrates, separate gene duplications gave rise to two CHCs and two CLCs. The two CHCs, now named for their encoding human chromosomes (17 and 22), form the basis of two distinct clathrins, both of which contribute to protein sorting into coated membrane vesicles or domains at different intracellular locations. The well-characterized isoform CHC17 clathrin is involved in many intracellular membrane traffic pathways including receptor-mediated endocytosis, lysosome biogenesis, and endosomal sorting. CHC17 is expressed ubiquitously in all tissues. Human CHC22 clathrin, in contrast, mediates a much more defined step in retrograde transport from endosomes to the *trans*-Golgi network (TGN). In muscle, in which its expression is highest, CHC22 controls transport pathways that influence targeting of the GLUT4 glucose transporter. The same role applies in fat tissue (Vassilopoulos et al., 2009). The low level of CHC22 in other tissues also contributes to intracellular retrograde transport (Esk et al., 2010). While CHC22 clathrin fills a special, species restricted

niche in humans, it is a pseudogene in mice, lost in both laboratory and wild mouse strains (Wakeman et al., 2005).

The two vertebrate genes encoding CLCs produce CLCa and CLCb (formerly called LCa and LCb in the literature), both are characterized by neuronal splicing variants. In cells, CLCa and CLCb associate exclusively with CHC17 and are involved in its function and stability, and they do not bind CHC22 clathrin (Liu et al., 2001).

The two CHCs are 85% identical in their protein sequence and comprise two structural elements that have been suggested as shared features of membrane associated proteins in eukaryotic cells: a long  $\alpha$ -solenoid region and a single  $\beta$ -propeller domain. Other coat proteins and some nuclear pore complex proteins comprise different combinations of these two structural domains (Field et al., 2011). The CHC17  $\alpha$ -solenoid region consists of eight repeats of a structural motif of 10 helices of 10–12 residues connected by loops (Ybe et al., 1999). The motif is designated as a clathrin heavy chain repeat (CHCR) and a recent alignment of CHCRs in bovine clathrin heavy chain is available in the online supplement to Wilbur et al. (2010). The CHCRs form the ankle, distal leg, and proximal leg segments, and the C-terminal end of CHCR7 contributes to trimerization (Ybe et al., 2007).

The trimerization domain also comprises a helical tripod that extends from CHCR7 below the triskelion vertex toward the cell membrane (Fotin et al., 2004). The vertex itself is puckered, which gives the CHC17 triskelion a characteristic orientation. The terminal domain (TD) of CHC17 is a seven-bladed  $\beta$ -propeller, connected to CHCR0 of the ankle, by a linker region (Figure 7). Recently, Lemmon & Traub (2012) comprehensively reviewed the interactions between the TD and clathrin-binding proteins, including descriptions of structural details and binding motifs. The main partners for the TD are adaptors and accessory proteins, which interact with four different sites on the TD.

Clathrin (CHC 17) is able to form several types of structures, at the plasma membrane it builds classic coated pits and budded coated vesicles with diameters of 80–200 nm as well as flat lattices (sometimes called “plaques”). The latter are observed on the basal surface of an attached cell (Saffarian et al., 2009) at sites of integrin-substrate interaction (De Deyne et al., 1998), and can be induced by immobilization of ligands for receptors that are normally internalized in clathrin coated vesicles (Takemura et al. 1986). Clathrin itself is unable to bind directly to the membrane or to cargo receptors and thus relies on adaptor proteins and complexes

(for example adaptor protein 2 (AP2)) and accessory proteins (for example AP180 and epsin) to be recruited to the plasma membrane during the initiation/nucleation and cargo selection process. The adaptor proteins determine the location of clathrin assembly and the type of cargo that is accumulated in the clathrin-coated structures formed. The formation of endocytic coated vesicles relies on the membrane recruitment of AP2 and its interaction with PtdIns(4,5)P<sub>2</sub>, which induces a conformational change in AP2 to promote cargo binding (Antonescu et al., 2011; Cocucci et al., 2012; Kelly & Owen, 2011). Single-molecule imaging suggests this interaction has to be accompanied by clathrin recruitment, such that successful coat formation is a cooperative process (Cocucci et al., 2012). A successful clathrin coat forms by cooperation between adaptors and clathrin at the outset, enhanced by cargo (for review see Brodsky et al., 2012).

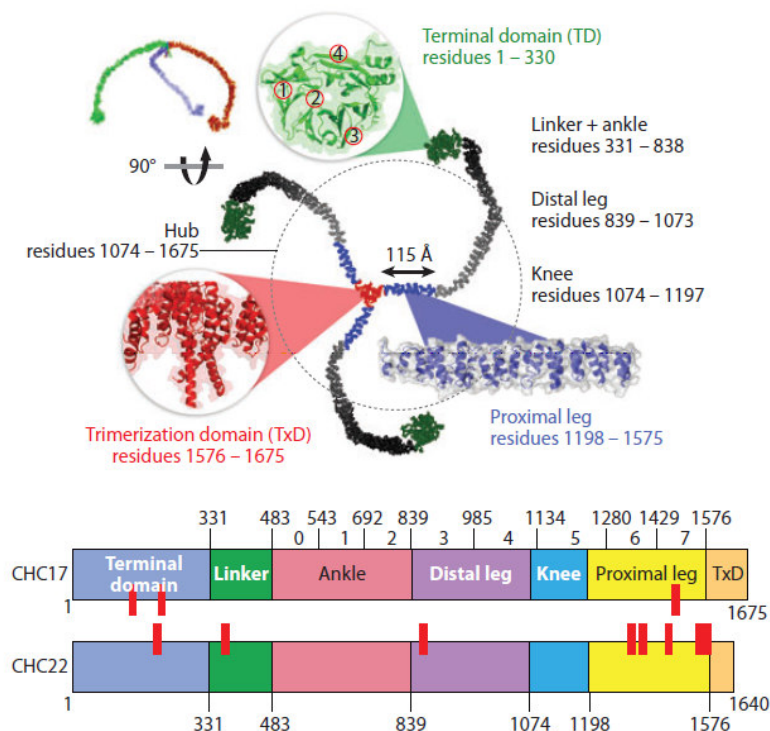


**Figure 7 Structural features of clathrin heavy chains.** The domain structures and amino acid boundaries are indicated for functional domains of CHC17. The structures reproduced are from PyMol (triskelion-accession number 3IYV; trimerization domain-accession number 3LVH; terminal domain-accession number 2XZG; proximal leg-accession number 1B89) and are based on Fotin et al. (2004b), ter Haar et al. (1998), and Ybe et al. (1999). The four numbered sites on the terminal domain structure represent binding sites for interacting proteins based on Lemmon & Traub (2012). At the bottom, the predicted domain structure of CHC22 is aligned with CHC17, and the amino acid boundaries of the eight clathrin heavy chain repeats (CHCR 0–7) in CHC17 are delineated. The red marks highlight conserved differences between the CHC17 and CHC22 protein families determined by DIVERGE analysis, adapted from Wakeham et al. (2005).

The vesicle scission depends on the mechanochemical enzyme dynamin. It is recruited by BAR domain-containing proteins, which have a preference for the curvature of the vesicle neck and are likely to help form the neck in the initiation step (Wigge et al., 1995; Ferguson et al., 2009; Sundborger et al., 2011).

Mammalian genomes contain 3 dynamin genes. The proteins encoded by these genes share the same domain organization and an overall 80% homology, but have distinct expression patterns. Dynamin 1 is selectively expressed at high levels in neurons and is generally not present in non-neuronal tissues, although it can be detected in many cultured cell lines. Dynamin 2 is expressed ubiquitously. Dynamin 3 is found predominantly in the brain (at much lower levels than dynamin 1) and testis, and at lower levels in some tissues such as the lung. Dynamin diversity is compounded by the existence of multiple splice variants for each of the three dynamins (for review see Ferguson and Camilli, 2012).

Dynamin 1 has been typically described as comprising: an N-terminal GTPase or G domain; a 'middle' or 'stalk' region; a pleckstrin homology (PH) domain; a GED domain, so called because its interactions with the GTPase domain had suggested a function as a GTPase effector domain; and a proline-rich C-terminal region, typically referred to as the proline-rich domain (PRD, Figure 8a).

-Introduction-

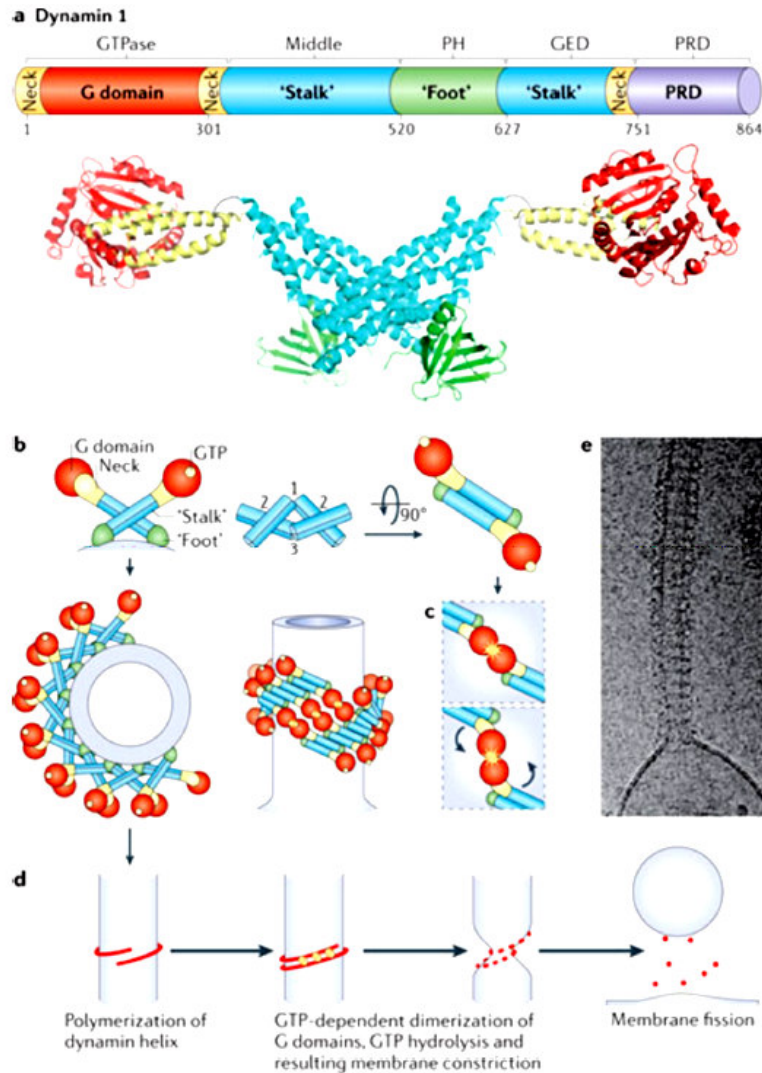


**Figure 8 Structure of dynamin and putative mechanism of dynamin-mediated membrane fission.**

**A. Top:** Linear representation of the domain organization of dynamin based on its 3D structure as revealed by crystallographic studies (numbers indicate amino acid position within the primary sequence of human dynamin 1, xa splice variant). Regions that belong to the same folded module are shown in the same color. Bottom: crystal structure of a dynamin dimer (color coded to match the linear representation). Molecular graphics were created with Pymol, PDB code 3SNH 42). **B.** Schematic representation of dynamin dimers and of helical dynamin polymers around a tubular template in two different orientations (90 degrees rotation). The colour-coding of the domains matches the colors of panel (a). The approximate location of the bound nucleotide is highlighted in yellow. Dynamin polymerization occurs as a result of interactions between the stalks of dynamin monomers (interface 2) and between stalk dimers (interfaces 1 and 3). The GTP-dependent dimerization of G domains between adjacent rungs of the dynamin helix (highlighted in yellow stars, longitudinal view of the helix), is thought to promote assembly-stimulated GTPase activity, resulting in membrane constriction and ultimately fission. **D.** Proposed GTP hydrolysis-dependent lever-like movement of dynamin's neck (BSE) relative to the Gdomain. (e) Schematic view of the key steps leading to dynamin-mediated membrane fission. **E.** Cryo-EM image showing a helical polymer of purified dynamin that has driven the formation of a tubule from a liposome. Image kindly provided by Adam Frost and Vincenz Unger (University of Utah and Northwestern University respectively). Ferguson and De Camilli, 2012

The PRD contains an array of PxxP amino acid motifs that interact with many SH3 domain containing proteins to localize dynamin at endocytic sites and coordinate dynamin's function with these other factors during endocytosis (Grabs et al., 1997; Lundmark and Carlson, 2004; Shpetner, Herskovitis and Vallee, 1996). The PRDSH3 interactions are typically of moderate affinity but the presence of multiple SH3-binding motifs in the PRD and multiple SH3-domain-containing proteins at endocytic sites, and the polymeric state of these proteins results in a significant avidity effect that enhances the ability of such interactions to concentrate dynamin. At least some interactions of the dynamin PRD are regulated by phosphorylation (Grabs et al., 1997). Purified dynamin spontaneously polymerizes into rings and helices when incubated in low ionic strength solutions (Hinshaw and Schmid, 1995) or in the presence of narrow negatively charged tubular templates (such as membrane tubules, microtubules or actin bundles) (Mooren et al., 2009; Roux et al., 2010).

During the synaptic vesicle scission Dynamin assembles at the neck of a budded endocytic clathrin-coated-vesicle and the hydrolysis of GTP induces a conformational change who leads to a constriction or stretching to promote vesicle scission (Figure 8b).

One of the dynamin recruiting BAR-domain containing proteins is amphiphysin I. It is an acidic, hydrophilic protein that is abundant in the nervous system and concentrated in presynaptic terminals. Until now amphiphysin I is known to have 6 splice variants, one brain amphiphysin I (695aa), one neuronal amphiphysin I (653aa with a deletion of amino acids 425-466) (Floyd et al., 1998), and 4 retina-specific amphiphysin Irs (Terada et al., 2002). Amphiphysin Ir is specifically expressed in the retina and it has been shown to be specifically expressed in rat ribbon synapses (Hosoya et al., 2004).

Amphiphysin I is a modular protein with a  $\alpha$ -helix, a BAR domain, a proline-rich domain (PRD), a CLAP domain (clathrin, AP2-binding domain), and a C-terminal SH3 domain (Figure 9).

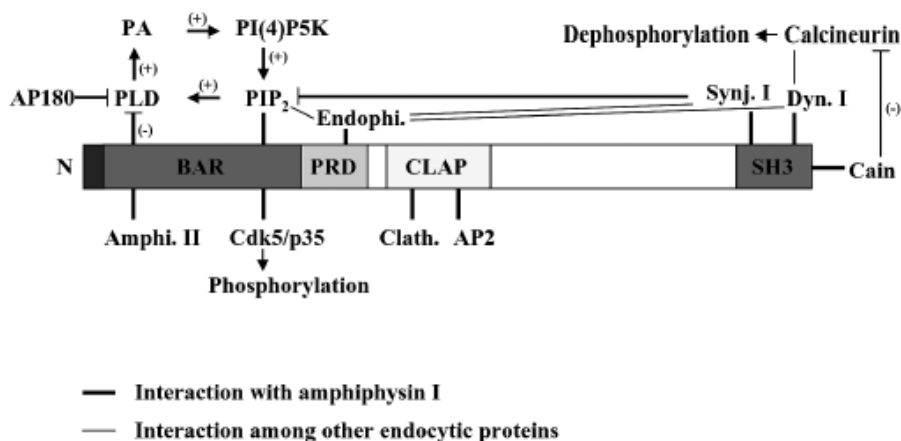


**Figure 9 Interactions between amphiphysin I and other endocytic components during clathrin mediated SVE.** Amphiphysin I is a multilinker protein. It interacts with amphiphysin II (amphi. II), lipid membrane (PI(4, 5)P<sub>2</sub>), cdk5p35 complex, and PLD (phospholipase D) at the N-terminus concluding BAR domain, with endophilin (endophi.) at the PRD domain, with clathrin (clath.) and AP2 at the CLAP domain, and with dynamin 1 (dyn. I), synaptojanin 1 (synj. I), and cain at the C-terminal SH3 domain. There is a positive feedback between PLD and PIP<sub>2</sub>:PLD will increase PIP<sub>2</sub> production by hydrolyzing PC to PA. PA activates PI(4)P5K activity, then PIP<sub>2</sub> will be produced from PI(4)P by PI(4)P5K activity, while at the same time PIP<sub>2</sub> activates PLD. Amphiphysin I (1–373aa) has been reported to bind PLD and to inhibit PLD activity. The interaction between amphiphysin I and PLD will regulate PIP<sub>2</sub> production, at the same time AP180 and synj. I also have an inhibiting effect at PLD activity and thus regulate PIP<sub>2</sub> dependent clathrin complex formation. On the other hand, amphiphysin I can regulate CME by recruiting cain (calcineurin inhibitor). Calcineurin binds dynamitin and is recruited to the endocytic zone by amphiphysin I to execute its dephosphorylation effect on endocytic proteins, which is essential for CME induction. But its activity will be downregulated by its inhibitor, cain. This may promote cdk5 dependent rephosphorylation and dissociation of endocytic protein. Besides the association with amphiphysin I, the schematic figure also shows the interactions among other endocytic proteins (thin line).

Amphiphysin I interacts with a lot of other endocytic components during synaptic vesicle endocytosis including interactions with PIP<sub>2</sub> of the plasma membrane, PLD, the cdk5/p35 complex and amphiphysin II at its N-terminal region; interactions with endophilin by the PRD domain; interactions with AP2 and clathrin by the CLAP domain; and interactions with dynamitin I, synaptojanin and cain by the C-terminal SH3 domain (Figure 9; for review see Wu et al., 2009).

Amphiphysin I is suggested to be colocalized with dynamitin I on the collar of the retrieved pits (Wigge et al., 1998). It senses and facilitates membrane curvature (Mc Mahon et al., 1997) and stimulates the GTPase activity of dynamitin in presence of lipid membrane (Yoshida et al., 2009), and thus is involved in the invagination and fission steps of clathrin mediated synaptic vesicle endocytosis.

Another BAR domain containing proteins which interacts with dynamitin is syndapin

(also known as Pacsin). It occurs as three genes, producing three primary protein isoforms in mammals. All the three isoforms show high conservation of their domain structure and sequence homology, except for the variable region (Kessel and Qualmann, 2004) (Figure 10).

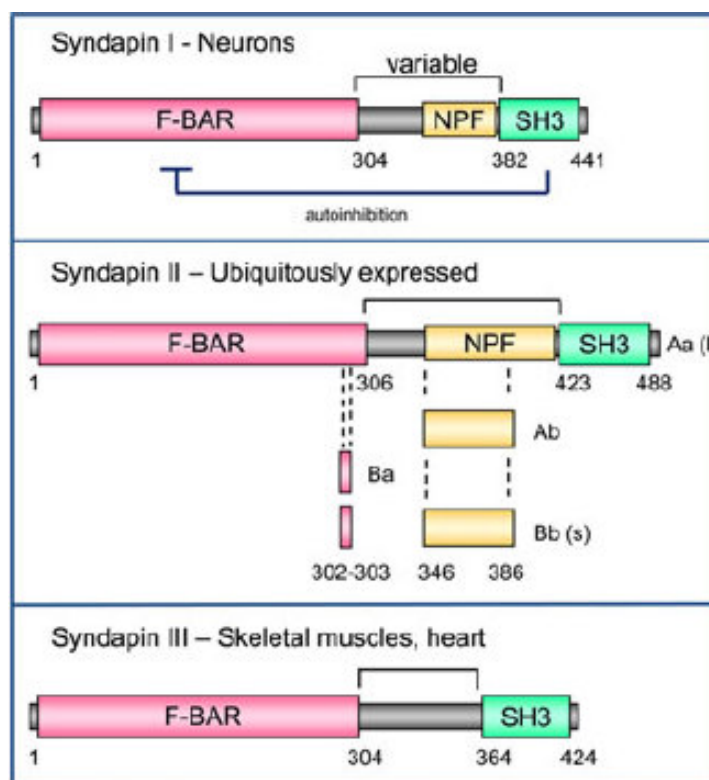


**Figure 10 Domain organization and structure of syndapin isoforms.** Schematic representation of the domain structure of the three syndapin isoforms and splice variants. Syndapin II splice variants Aa (l) long variant; Ab; Ba; and Bb (s) short variant have the indicated dotted labelled regions spliced from the Aa (l) variant. Syndapin I is expressed mainly in neurones, whereas syndapin II is ubiquitously expressed in all tissues, and syndapin III is expressed mainly in skeletal muscle and the heart. All three isoforms contain an N-terminal F-BAR domain and a C-terminal SH3 domain. The two domains are connected by a long variable linker region, which includes multiple Asn-Pro-Phe (NPF) sequence motifs for only syndapin I and II. Syndapin I is autoinhibited, whereby the SH3 domain associates with the F-BAR domain, reducing its membrane tubulating activity.

Syndapin I is the neuronal-specific isoform (Paulsson et al., 1998; Qualmann et al., 1999), syndapin II is ubiquitously expressed in all examined tissues (Ritter et al., 1999) and syndapin III is expressed mainly in skeletal muscles and heart (Modregger et al., 2000; Sumoy et al., 2001).

All three isoforms are members of the F-BAR domain subfamily (Paulsson et al., 1998; Qualmann et al., 1999) and the protein sequences for their N-terminal F-BAR domains are highly conserved. They all contain a C-terminal Src-homology 3 (SH3)

domain for autoinhibition and to mediate protein–protein interactions. The primary proteins that interact at this SH3 domain are common to the three forms and include dynamin, synaptojanin, synapsin and neural Wiskott–Aldrich syndrome protein (N-WASP) (Qualmann et al., 1999; Modregger et al., 2000; Qualmann and Kelly, 2000). The two major domains in the three syndapins are connected by a long variable linker region. In this regard, syndapin I and II differ from syndapin III by the presence in the linker of multiple asparagineproline-phenylalanine (NPF) amino acid sequence motifs. Such motifs are known to bind Eps15 homology-domain (EHD)-containing proteins such as EHD1, which are typically involved in vesicle recycling (Braun et al., 2005) (Figure 10). Syndapin I has a role in activity-dependent bulk endocytosis (ADBE) in neurones; syndapin II in clathrin-mediated endocytosis, caveolae formation, Golgi traffic and endosome recycling; and syndapin III in glucose transporter trafficking. Both, syndapin I and II, interact with several endocytic key proteins such as dynamin, synaptojanin and synapsin.

The syndapin I – dynamin I interaction is the best understood interaction in central nerve terminals. Its binding is inhibited by dynamin I phosphorylation at the two main phosphosites Ser774 and Ser778; thus it preferentially interacts with the dephosphorylated form of dynamin (Anggono et al., 2006). Their interaction is necessary for SVE, as well as for secretory fusion and pore formation in chromaffin cells (Anggono et al., 2006; Samasilp et al., 2012). Syndapin binding to dynamin involves not only dephosphorylation at Ser774 and Ser778, but also requires two sequence elements in the region 772-RRSPTSSPTPQRRAPAVPPARPGSR-796 of the dynamin I proline-rich domain (PRD). First, it utilizes a single PxxP core motif common to almost all SH3 domain interactions. Second, it requires an adjacent non-PxxP N-terminally anchored extension that bridges the phosphobox (a region encompassing residues 772–781 of the dynamin I PRD). The latter is an unusual feature not known to be involved in most other SH3 domain interactions and may contribute to binding specificity and high affinity (Anggono and Robinson, 2007).

Also essential for the clathrin-mediated endocytosis is the BAR-domain containing protein endophilin. Two subfamilies of endophilin are reported endophilins A (Chen and Antonarakis, 1997; Micheva et al., 1997) and endophilins B (Huttner and Schmidt, 2000).

All endophilins consist of an N-terminal BAR domain, a variable middle region and a C-terminal SH3 domain. BAR domains are dimerization domains that are able to

induce and stabilize membrane curvature and to “sense” (i.e., bind selectively to) already curved membrane. The endophilin BAR domain (henceforth the endoBAR) forms a crescent-shaped dimer, with each monomer made up of three kinked, antiparallel  $\alpha$  helices (Gallop et al., 2006; Massuda et al., 2006; Weissenhorn et al., 2005). The endoBAR belongs to the N-BAR class, implying that an amphipathic helix, Helix 0 (H0), is apposed to the N-terminus of the actual BAR domain. The endoBAR also has an insert in Helix 1, the most N-terminal of the three  $\alpha$  helices. The Helix 1 insert (H1I, residues 60 to 88 in mammalian endophilin A1) protrudes from the concave endoBAR surface and establishes a second amphipathic helix in addition to Helix 0. This helix is also named the central amphipathic helix. The higher-order structure of the central variable region is unknown. However, it is known that the variable region is important in determining whether endophilin promotes or inhibits receptor-mediated endocytosis (Sugiura et al., 2004). It contains several phosphoresidues, implying that it has a role in the post-translational regulation of endophilin activity. It also harbors a calcium channel binding site (Chen et al., 2004). SH3 domains are common protein-recognition modules (for review see Kaneko, Li and Li, 2008). The structure of the rat endophilin A2 SH3 domain has been solved by X-ray crystallography (Loll et al., 2004). It adopts the  $\beta$ -barrel core typical of SH3 domains, with a hydrophobic groove that accommodates proline-rich peptide sequences present in binding partners. It is highly similar to the NMR structure of the human endophilin A1 and A3 SH3 (Gao et al., 2004). Despite this high degree of structural similarity, the SH3 domains of the three paralogs can exhibit specificity in their interaction with binding partners (see, for example Yam et al., 2004).

## -Introduction-

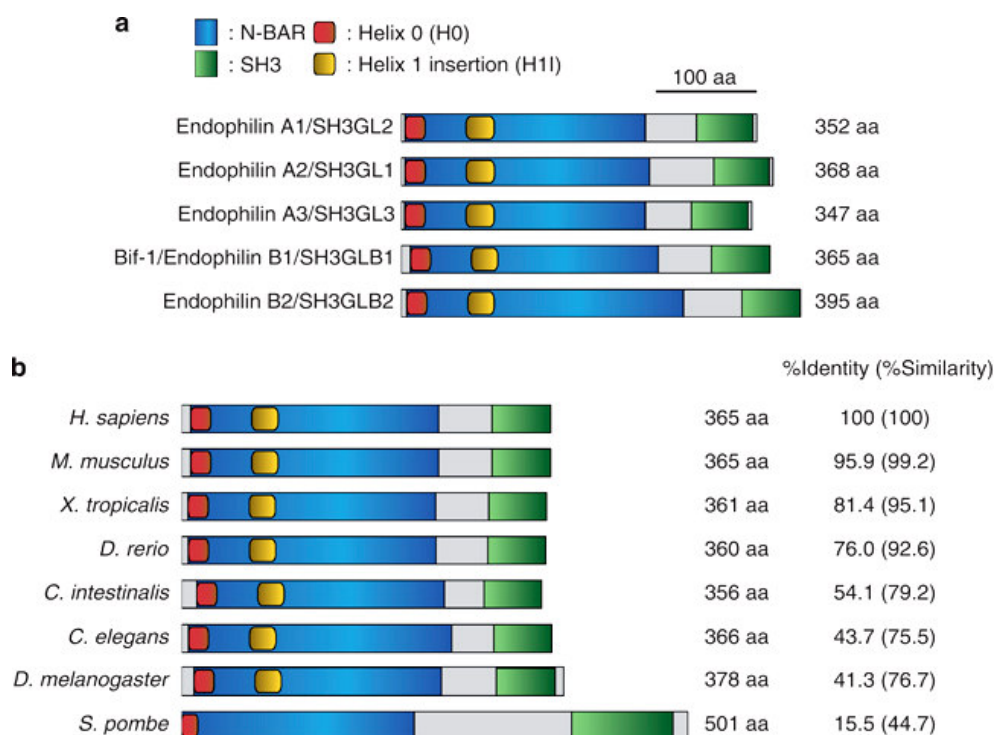


**Figure 11 The domain structure of the endophilin protein family.** Schematic representation of human Endophilin A and B proteins, all endophilins are composed of an N-terminal N-BAR domain and a C-terminal SH3 domain. The helix 0 (HO) and helix 1 insertion (H1I) regions located in the N-BAR domain are well conserved between the endophilin A and B families (Takahashi, Meyerkord and Wang, 2014).

Endophilin A is reported to be linked to synaptic vesicle endocytosis and to bind synaptojanin and dynamin1 (Ringstad, Nemoto and De Camilli, 1997). Endophilin A is concentrated in presynaptic nerve terminals, and strongly overlaps in distribution with dynamin I, synaptojanin and amphiphysin I (Ringstad, Nemoto and De Camilli, 1997). It is thought to coordinate curvature acquisition with both fission and uncoating of clathrin-coated vesicles via the interaction of its carboxy-terminal SH3 domain with dynamin and the PI(4,5)P2 phosphatase synaptojanin (Ringstad et al. 2001). Endophilin was proposed to start acting at early stages of clathrin-mediated budding, based on antibody-microinjection experiments in giant lamprey axons (Ringstad et al. 1999). However, more recent imaging studies (Perera et al. 2006; Ferguson et al. 2009; Taylor et al. 2011) and genetic studies in *Drosophila*, *C. elegans*, and mice, favor late actions (Schuske et al. 2003; Verstreken et al. 2003; Dickman et al. 2005; Milosevic et al. 2011), primarily in uncoating via endophilin's property to recruit synaptojanin.

Synaptojanin is a PI(4,5)P2 phosphatase that can dephosphorylate both the 4- and 5-position of inositol rings. Its proline-rich C-terminus interacts with the SH3-domain

of endophilin and other BAR proteins (McPherson et al., 1996; Guo et al., 1999; Ringstad et al., 2001) (Figure 12). Therefore synaptojanin is primarily recruited by endophilin at the necks of clathrin-coated pits just before fission and one of its main functions is to couple the fission reaction of endocytosis to the shedding of the adaptors during uncoating (Cremona and De Camilli, 2001; Milosevic et al., 2011). It has also been proposed that the PI(4,5)P<sub>2</sub> phosphatase activity of synaptojanin may have a direct action in fission by creating a lipid-phase-boundary, and thus an interfacial force, between a PI(4,5)P<sub>2</sub>-depleted bud and the PI(4,5)P<sub>2</sub>-rich plasma membrane (Liu et al., 2009), or by promoting the dissociation of dynamin after constriction of the dynamin collar (Chang-Ileto et al., 2010). However, genetic studies in mice support a primary uncoating function of synaptojanin, although they do not rule out other roles (Cremona et al., 1999; Hayashi et al., 2008; Milosevic et al., 2011). The zebrafish *nrc* mutant is characterized by a defect in the synaptojanin (van Epps and others 2004; Mani and others 2007). In this mutant, synaptic ribbons are unanchored, and membrane trafficking is strongly disturbed as judged by the ultrastructural appearance of abnormal membrane profiles and reduced number of synaptic vesicles. The disturbance in synaptic transmission between photoreceptors (cones) and bipolar cells can lead to blindness.

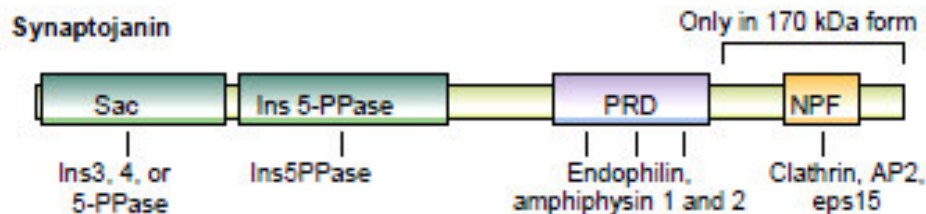


**Figure 12 Schematic domain structure of synaptojanin:** Synaptojanin contains two domains that dephosphorylate phosphatidylinositol polyphosphates (PtdInsPs): Sac and Ins 5-PPase. It has a PRD that binds many SH3 domain-containing proteins and an alternatively spliced isoform (170 kDa) that has three C-terminal NPF repeats that bind clathrin, eps15 and AP2.

The structure of synaptojanin shows in general an N-terminal Sac-domain (Figure 12), homologous to the yeast protein Sac1, which has been genetically implicated in the regulation of phospholipid metabolism (De Camilli et al., 1996). Its central region represents its 5-phosphatase activity directed towards a variety of soluble inositol polyphosphates and inositol phospholipids (McPherson et al., 1996; Woscholski et

al., 1997; Chung et al., 1997; Sakisaka et al., 1997). Phosphoinositides function in regulating a number of important proteins involved in synaptic vesicle endocytosis including the clathrin adaptors AP2 and AP180 (Gaidarov et al. 1996; Hao et al., 1997), dynamin (Zheng et al., 1996; Salim et al., 1996; Lin and Gillmann, 1996) and synaptotagmin (Fukuda et al. 1995). The C-terminus of synaptojanin, which is proline-rich, contains several SH3-domain consensus-binding sites and in fact, amphiphysin I and II interact *in vitro* with synaptojanin through distinct SH3 binding sequences (Micheva et al., 1997) (Figure 12), as well as endophilin. Furthermore synaptojanin has three NPF repeats at its C-Terminus through which clathrin, eps 15 and AP2 bind to synaptojanin.

Also important for the clathrin coated vesicle cycle is the  $Ca^{2+}$ -dependent phosphatase calcineurin. Clathrin-mediated endocytosis is regulated by the phosphorylation and dephosphorylation of endocytic proteins. When nerve terminals in the brain are stimulated, a group of phosphoproteins (called dephosphins, including dynamin I, amphiphysin I and II, synaptojanin, epsin, eps15 and AP180) are coordinately dephosphorylated by calcineurin (Cousin and Robinson, 2001; Figure 13). The switching from the phosphorylated state of endocytic proteins to the dephosphorylated state after nerve terminal depolarization is essential for triggering clathrin mediated endocytosis.

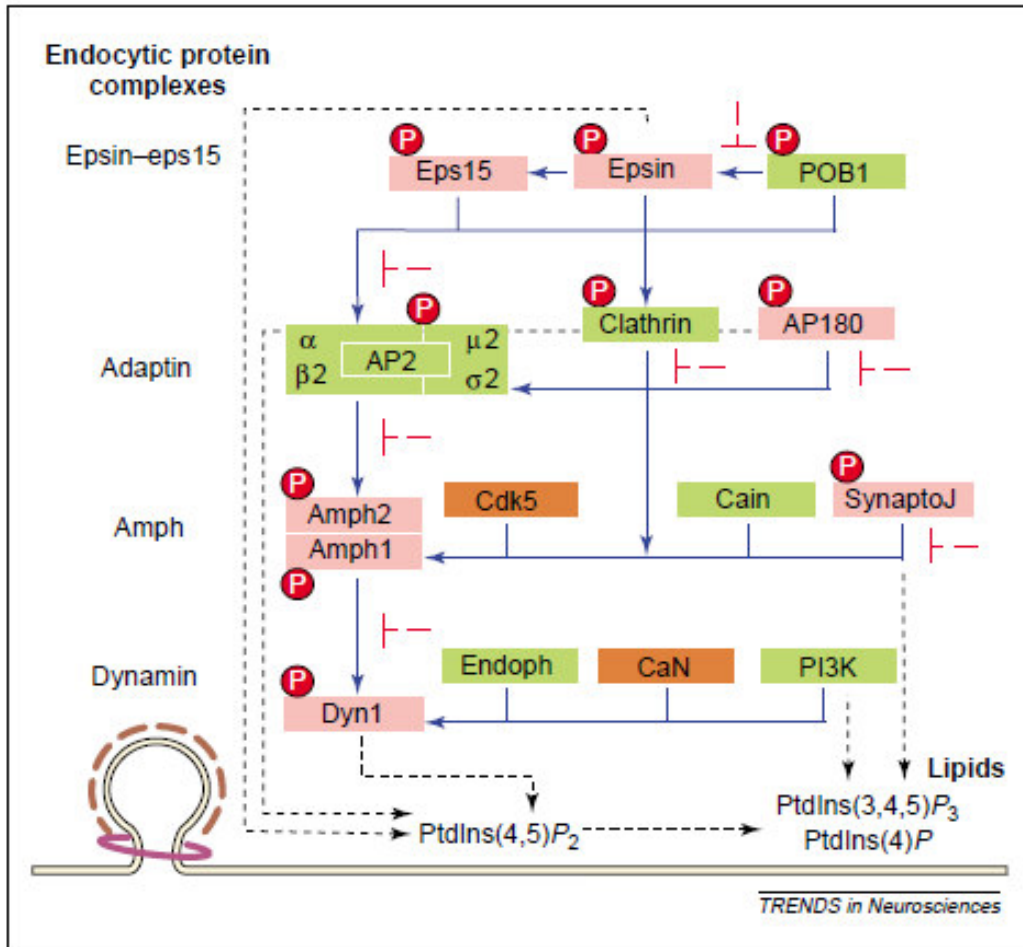


**Figure 13 The phosphorylation cycle of the dephosphins regulates protein–protein interactions and protein–lipid interactions.** In a resting nerve terminal a pool of the dephosphins (pink) are phosphorylated and predominantly in the cytosol. On stimulation, Ca<sup>2+</sup> influx activates calcineurin (CaN), which dephosphorylates the dephosphins. This stimulates interactions between the dephosphins and other endocytosis proteins (green), which form essential endocytic protein complexes at different stages of the pathway (based on dynamin, amphiphysin, adaptin and epsin or eps15). For the sake of clarity, most other interactions not related to phosphorylation are omitted. Dephosphorylation also stimulates interactions between the different complexes, which links the different stages of endocytosis. The blue arrows indicate essential protein interactions and the broken red bars indicate the interactions known to be inhibited by protein phosphorylation. Essential interactions of the dephosphins with membrane lipids are indicated by the broken black lines and arrows. Many of the cytosolic dephosphins are recruited to the plasma membrane via interactions with membrane lipids, which provides a mechanism of recruitment to sites of endocytosis. At least one dephosphin in each protein complex associates with membrane lipids. For dynamin 1, dephosphorylation stimulates interaction with membranes. Abbreviations: Amph, amphiphysin; CaN, calcineurin; Dyn1, dynamin 1; Endoph, endophilin; PI3K, phosphatidylinositol 3 kinase; POB1, partner of Ral-binding protein 1; SynaptoJ, synaptojanin (Cousin and Robinson, 2001; Trends in Neurosciences)

Clathrin-mediated endocytosis has a range of different functions, including regulating the surface expression of proteins, sampling the cell's environment for growth and

guidance cues, bringing nutrients into cells, controlling the activation of signalling pathways, retrieving proteins deposited after vesicle fusion and turning over membrane components by sending these components for degradation in lysosomes. In neuronal synapses clathrin-mediated endocytosis is coupled to the exocytic activity and is essential for the synaptic vesicle recycling to maintain the pool of synaptic vesicles. It has also an integral role in regulating the size (Nonet et al., 1999) and composition of synaptic vesicles (Takamori et al., 2006).

#### **1.5.2.2. Clathrin-independent endocytosis**

Clathrin-independent endocytosis is the uptake of material into the cell from the surface without any coating and seems to have no mechanism for selection of cargo proteins. Cells can have several forms of clathrin-independent endocytic mechanisms and they can be responsible for the major fraction of membrane and fluid taken into the cell. The vesicular uptake can be associated with for instance RhoA, Rac, Cdc42, Arf6, caveolae and macropinocytosis. Importantly, lipid modification, BAR-proteins and insertion of proteins into the plasma membrane help to create invaginations that facilitate vesicle formation, in some cases even without dynamin (Roberts-Galbraith et al. 2010; Graham et al., 2010; for review see Sandvig et al., 2011). Important players in vesicle formation are actin and actin-associated proteins (Rohn et al., 2010), as well as a member of the sorting nexin family, nexin 9 (van Weering et al. 2010).

Several clathrin-independent endocytic mechanisms are found in all cells studied so far, but their location, their capacity, properties and functions can be cell-type and context dependent. As already described under 1.5.2 the molecular mechanisms for clathrin-independent endocytosis at synaptic ribbons are unclear.

#### **1.6. Working hypothesis**

The continuous exocytosis at the ribbon synapse needs to be balanced by compensatory endocytosis to replenish vesicle pools. The rate of vesicle replenishment is an important factor in the signalling at photoreceptor ribbon synapses (Jackman et al., 2009; Babai et al., 2010). Recent analyses indicated that synaptic ribbons have an important role in the resupply of release-ready synaptic

-Introduction-

vesicles (Spassova et al., 2004; Griesinger et al., 2005; Jackman et al., 2009; Frank et al., 2010; Babai et al., 2010; Schnee et al., 2011; Snellman et al., 2011; Tian et al., 2012). How vesicle replenishment is organized and accomplished in the ribbon synapse is still largely unclear. In this work I applied super-resolution structured illumination microscopy (SR-SIM) and immunogold electron microscopy to localize key proteins of the recycling endocytic machinery in photoreceptor ribbon synapses. I found a local endocytic machinery highly enriched at the peri-active zone in close vicinity to the synaptic ribbon complex. This local endocytic machinery is ideally suited to “reload” empty vesicle sites at the active zone and/or the synaptic ribbon and therefore to contribute to signalling at the ribbon synapse.

## **2. Material and Methods**

### **2.1. Materials**

#### **2.1.1. Antibodies**

##### **Primary antibodies:**

*Anti-RIBEYE(B)-domain/CtBP2* (U2656; Schmitz et al., 2000) polyclonal rabbit antiserum against RIBEYE(B)-domain. It was used for immunofluorescence labelling in a 1:2,000 dilution and for western blotting in a 1:10,000 dilution (if not denoted otherwise).

*Anti-CtBP2* (BD Transduction Laboratories, #612044) mouse monoclonal antibody raised against the carboxyterminal amino acids (aa) 361-445 of CtBP2. This antibody detects RIBEYE (i.e. RIBEYE(B)-domain/CtBP2) in western blotting analyses and labels synaptic ribbons in immunofluorescence labelling analyses (e.g. Schwarz et al., 2011). This antibody was used for immunofluorescence labelling at a 1:500 dilution.

*Anti-dynamin* (hudy-1, upstate/Millipore [order number #05-319]). For the detection of dynamin, we used a well characterized protein G-purified monoclonal mouse antibody generated against a peptide (aa822-aa838, SPDPFGPPPQVPSRPNR) in the proline-rich, carboxy-terminal region of dynamin-1 (Warnock et al., 1995; Takei et al., 1995; Hinshaw and Schmid, 1995). Dynamin-1 is the predominant neuron-specific form of dynamin expressed in brain (e.g. Raimondi et al., 2011; for review, see Ferguson and de Camilli, 2012). The amino acid sequence of this peptide used for immunization is highly conserved between species in dynamin-1 (e.g. 100% amino acid (aa) identity in man, mouse, pig, cow and horse). The amino acid sequence of this peptide stretch is also conserved in dynamin-2, the ubiquitous, non-neuronal form of dynamin (70% aa identity) and also in dynamin-3 (77% aa identity). Dynamin-3 is also preferentially expressed in brain (as dynamin-1) but at much lower levels (Raimondi et al., 2011; for review, see Ferguson and De Camilli, 2012). The hudy-1 monoclonal antibody was denoted as “anti-dynamin” antibody in the result section. The corresponding blocking peptide was synthesized by Dr. Martin Jung (Saarland University; Dept. of Biochemistry and Molecular Biology) and used for pre-absorption control experiments. The hudy-1 monoclonal antibody was applied for western blotting and immunogold electron

microscopy in a 1:1,000 dilution and for immunostaining in a 1:500 dilution (if not denoted otherwise).

*Anti-syndapin/pacsin* (Synaptic Systems, Göttingen, Germany, product number 196002) polyclonal antiserum against syndapin-1/pacsin-1. The antiserum was used for immunofluorescence microscopy at a 1:250 dilution, for western blotting in a 1:1,000 dilution. The syndapin peptide was purchased from Synaptic Systems (196-0P) for pre-absorption control experiments.

*Anti-amphiphysin* (Synaptic Systems, Göttingen, Germany, product number 120002) was raised against a synthetic peptide (aa2-aa15; ADIKTGIFAKNVQK) of amphiphysin 1. The antiserum was used for western blotting in a 1:1,000 dilution and for immunostaining in a 1:250 dilution. The blocking peptide was purchased from Synaptic Systems (120-OP) for pre-absorption control experiments.

*Anti-endophilin1* (Synaptic Systems, Göttingen, Germany, product number 159002) is a polyclonal antiserum raised against a synthetic peptide coding for aa256-aa276 of mouse endophilin 1 (QPKPRMSLEFATGDSTQ). For immunostaining the antiserum was diluted 1:250 and for western-blotting 1:1,000. The endophilin peptide was also obtained from Synaptic Systems (Synaptic Systems, 159-OP) for pre-absorption (blocking) control experiments.

*Anti-pan-calcineurin A* antibody is an affinity-purified rabbit polyclonal antibody raised against a carboxyterminal peptide of calcineurin A (antibody from Cell Signaling [via NEB, New England Biolabs]; order number #2614). The antibody is purified by both protein A- and peptide-affinity chromatography. It was used for immunofluorescence microscopy in a 1:100 dilution and for western blotting in a 1:1,000 dilution.

*Anti-clathrin heavy chain* (abcam; ab21679), a polyclonal rabbit antibody raised against a peptide in the carboxyterminus of human clathrin heavy chain. The blocking peptide (for pre-absorption control experiments) was also obtained from abcam (ab23440). This antibody detects clathrin heavy chain, variant 1 (CHC-V1) (see text) and was used for immunofluorescence microscopy and western blotting in a 1:1,000 dilution; for postembedding immunogold electron microscopy it was diluted 1:250.

*Anti-clathrin heavy chain* (Cell Signaling/NEB; order number: P1663), an affinity-purified rabbit antibody against a carboxyterminal peptide of human clathrin heavy chain. This antibody detects clathrin heavy chain, variant 1 (CHC-V1) (see

text) and was used at a 1:250 dilution for immunofluorescence microscopy. The immunolabelling data on CHC-V1 presented were obtained by immunolabelling with the above mentioned antibody from abcam (abcam21679) against CHC-V1; but qualitatively identical immunolabelling results were obtained also with the anti-CHC-V1 antibody from Cell Signaling (P1663) (data not shown).

*Anti-clathrin heavy chain* (Abcam/ab59710) is a polyclonal rabbit antiserum which was raised against aa619-638 (KAGLLQRALEHFTDLYDIKR) of rat clathrin heavy chain (100% identical with mouse, highly conserved). For western blotting, the antibody was diluted 1:1,000 and for immunofluorescence labelling 1:500. This antibody detects clathrin heavy chain, variant 2 (CHC-V2) (see text).

*Anti-clathrin heavy chain* (X22 mouse monoclonal antibody raised against clathrin heavy chain; obtained from Abcam). This antibody was raised against clathrin heavy chain purified from human brain (Brodsky, 1985). The antibody was used for immunofluorescence microscopy in a 1:100 dilution. This antibody detects clathrin heavy chain, variant 2 (CHC-V2) (see text).

*Anti-panSV2*, a monoclonal antibody against the synaptic vesicle protein SV2 (panSV2 monoclonal antibody, raised against all SV2 variants (Buckley and Kelly, 1985) was used to label the synaptic vesicle-containing presynaptic terminals. The supernatant was collected from cultured hybridoma cells (obtained from the Developmental Studies Hybridoma Bank (DSHB), University of Iowa) and used at a 1:20 dilution.

*Anti-VGLUT1* (NeuroMAB, UC Davis; clone N28/9), a mouse monoclonal antibody, raised against fusion protein encoding aa493-560 of the rat vesicular glutamate transporter 1 (VGLUT1). The antibody was used for immunofluorescence microscopy in a 1:500 dilution. VGLUT1 is a marker protein of glutamatergic synaptic vesicles (Wojcik et al., 2004).

*Anti-VGLUT1* (Synaptic Systems, Göttingen; order number: 135302). This rabbit polyclonal antibody was raised against aa456-560 of rat vesicular glutamate transporter 1 (vglut1) and used for immunofluorescence microscopy at a 1:500 dilution.

*Anti-PSD-95* (NeuroMAB, UC Davis; clone K28/43), a mouse monoclonal antibody raised against fusion protein encoding aa77-299 of human PSD-95. This antibody was used at a 1:500 dilution for immunofluorescence microscopy.

*Anti-PSD-95* (L667), a rabbit polyclonal antibody against rat PSD-95 (Irie et

al., 1997). This antibody was a kind gift of Prof. Dr. Thomas C. Südhof (Stanford University) and used at a 1:1,000 dilution for immunofluorescence microscopy.

*Anti-Bassoon* (Stressgen, VAM-PS003), a mouse monoclonal antibody raised against fusion protein encoding aa738-103 of rat bassoon. This antibody was used at a 1:100 dilution for immunofluorescence microscopy.

*Anti-Bassoon* (Synaptic Systems, Göttingen; order number: 141002) is a polyclonal rabbit antibody raised against a fusion protein encoding the carboxyterminal 330 amino acids of rat bassoon. The antibody was used for immunofluorescence in a 1:100 dilution.

### **2.1.2. Secondary antibodies**

The following secondary antibodies were used: chicken anti-mouse-Alexa488; donkey anti-rabbit-Alexa568; goat anti-mouse Cy5; goat anti-mouse-Alexa488. All fluorophore-conjugated secondary antibodies were purchased from Molecular Probes/Invitrogen and used at a 1:1,000 dilution for 1hr at room temperature (RT) for immunolabelling experiments.

For western blot analysis two antibodies, conjugated with horseradish peroxidase, from Sigma Aldrich were used: one anti mouse (IgG) and one anti rabbit (IgG) antibody, both raised in goat.

For immogold labellings a goat anti-mouse or a goat anti-rabbit secondary antibody conjugated to 10nm gold particles (Sigma) were used.

### **2.1.3. Animal tissue**

For all experiments done with mouse retinas adult mice of either sex were used. Mice were sacrificed in the early afternoon. Eyes were collected at environmental daylight conditions (luminance of  $\approx 2 \text{ cd/m}^2$ ). Similar data as shown for the mouse retina were also obtained with the bovine retina (of either sexes; data not shown). Bovine retina was isolated out of bovine eyes, received from slaughterhouse.

**2.1.4. Buffers and Media**

ECL-solution	<p>ECL-I:                      Tris 1M, pH 8.5, 10 ml                      Luminol stock 1 ml                      Para-hydroxy Coumarin Acid (PCA)                      440 µl.                      Make up to 100 ml with dd H<sub>2</sub>O</p> <p>ECL-II :                      Tris 1M, pH 8.5, 10 ml                      H<sub>2</sub>O<sub>2</sub> 64µl                      Make up to 100 ml with dd H<sub>2</sub>O</p>
5x PBS	<p>40g NaCl                      1g KCl                      7.2g Na<sub>2</sub>HPO<sub>4</sub>                      1.2g KH<sub>2</sub>PO<sub>4</sub>                      Make up to 1 liter with dd H<sub>2</sub>O</p>
Ponceau S-stain	<p>30g Trichloroaceticacid                      5g Ponceau S                      Make up to 1 liter with dd H<sub>2</sub>O</p>
SDS-PAGE-Electrophoresis buffer	<p>3.03g Tris                      14.4g Glycine                      1.0g SDS                      Make up to 1 liter with dd H<sub>2</sub>O</p>
SDS-loading buffer 4 x	<p>1,6g SDS                      4ml β-Mercaptoethanol                      2ml Glycerol                      2ml 1M Tris pH 7                      4mg Bromo phenol blue                      2ml of ddH<sub>2</sub>O</p>

Transfer Buffer (Western Blot)	Tris 15.125g Glycine 72.05g Methanol 1 liter Make up to 5 liters with dd H <sub>2</sub> O
--------------------------------	--

## **2.2, Methods**

### **2.2.1. Immunofluorescence microscopy**

#### **2.2.1.1. Immunolabeling of cryo-sections**

Freshly isolated, chemically unfixed mouse retina was flash-frozen in liquid nitrogen-cooled isopentane. From these samples, 10 µm cryostat sections were cut with a Leica cryostat and heatfixed for 15 min at 60° Celsius. After heat-fixation sections were washed with PBS for 5min. Afterwards sections were incubated with the respective primary and secondary antibodies as described (Schmitz et al., 2000; Alpadi et al., 2008),

#### **2.2.1.2. Immunolabelling of 0.5µm-thin resin sections:**

##### **Embedding procedure**

The preparation procedure for sample embedding into epon resin is a modification from the procedure described by Drenckhahn and Franz (1986). In brief, tissue was flash-frozen in liquid nitrogen-cooled isopentane. Then, as a modification of the original procedure, lyophilization of the tissue was performed while the tissue was continuously cooled by liquid nitrogen. Lyophilization of the samples was typically performed at a vacuum of  $\approx 10^{-7}$  mbar ( $10^{-5}$  Pa) using a TCP270 turbomolecular pump (Arthur-Pfeiffer-Vacuumtechnik, Wetzlar/ABlar, Germany) controlled by a PKG020 Pirani-gold cathode gauge control unit and an oil diffusion pump as pre-pumping unit (type DUO 004B; Arthur-Pfeiffer-Vacuumtechnik, Wetzlar/ABlar, Germany). Samples were lyophilized in liquid nitrogen for  $\approx 24$ hrs. Afterwards, samples were equilibrated to room temperature, infiltrated with Epon resin and degassed for 24hrs to ensure complete penetration with Epon. Curing of

the resin-embedded samples was done at 60°C for ≈24hrs.

#### **2.2.1.3. Immunolabelling procedure for use with 0.5µm-thin resin sections**

Immunofluorescence labelling experiments were performed with semithin sections (thickness of approx. 0.5µm) to obtain optimal resolution. The usefulness of semithin sections to obtain images with nanoscale resolution has been previously demonstrated by Punge et al. (2008). From the tissue blocks, 0.5µm -thin sections were cut with a Reichert ultramicrotome. Epon was removed by the procedure of Major et al (1961) with slight modifications. In brief, Epon was removed by incubating the sections in the following solutions: sodium methanolate (30% solution in methanol; MERCK) (10min); 1:1 mixture of xylol/methanol (10min); acetone (2x10min), H<sub>2</sub>O (10min), PBS (10min). Afterwards sections were incubated with the respective primary and secondary antibodies as described (Schmitz et al., 2000; Alpadi et al., 2008),

#### **2.2.1.4. Control incubations**

Control incubations for immunolabelling experiments were done by omitting the primary antibody followed incubating with secondary antibody only. No immunofluorescent signal was observed in photoreceptor synapses in these control incubations. In further control experiments, primary antibodies were pre-absorbed with the respective antigen as described below and processed for immunolabelling.

#### **2.2.1.5. Direct-Labeling of primary antibodies (mouse anti-CtBP2) with fluorophores (DyLight 488/DyLight650)**

For triple immunolabelling experiments, purified anti-CtBP2 mouse monoclonal antibody was conjugated with DyLight488 (or DyLight650) amine-reactive dye with the Thermo Scientific DyLight 488 Amine Reactive Dye Kit (Thermo Scientific #5302)/Thermo Scientific DyLight650 Microscale Antibody Labeling Kit (Thermo Scientific #84536) according to the manufacturer's instructions. 25µg of purified antibody (in a volume of 100µl) were dialyzed against a large volume of PBS in a Slide-A-Lyzer Mini Dialysis Units Plus Float kit (Thermo Scientific #66576).

Afterwards, the antibody was coupled with the NHS-activated DyLight488/DyLight650 compound exactly according to the manufacturer's instructions. DyLight488-conjugated primary antibody against CtBP2 was used in a 1:20 dilution for immunolabelling. DyLight650-conjugated primary antibody against CtBP2 was used in a 1:30 dilution for immunolabelling.

#### **2.2.1.6. Triple immunolabelling for super-resolution structured illumination microscopy (SR-SIM)**

For triple-immunolabelling, we used a directly labelled mouse monoclonal antibody (CtBP2 antibody conjugated with either DyLight488 or DyLight650, as indicated in the respective experiments) and two other primary antibodies (one from mouse, the second from rabbit [as indicated in the respective experiments], which were not directly fluorophore-labelled. First, sections were incubated with the two unlabelled primary antibodies at the same time overnight (at the dilutions given above). On the next day, sections were washed 3 times with PBS and afterwards incubated with the respective secondary antibodies (goat anti-mouse-Cy5; and donkey anti-rabbit-Alexa568 or donkey anti-rabbit Alexa568 and chicken anti-mouse Alexa488). After 1hr incubation, sections were washed again 3 times with PBS and finally incubated with the directly DyLight488/ DyLight650-labelled CtBP2 primary antibody (in the dilutions summarized above) overnight at 4°C. After overnight incubation, sections were washed 3 times with PBS and embedded with anti-fade solution containing n-propyl gallate (NPG) as previously described (Schmitz et al., 2000).

#### **2.2.1.7. Blocking of antibodies: Preabsorption experiments**

For preabsorption blocking experiments, antisera were diluted to their indicated respective working concentrations. To these antibody working dilutions either the specific blocking peptide (20µg) or an unrelated peptide (same amount) were added. These mixtures were incubated overnight on a turning wheel at 4°C and used on the other day for immunolabelling experiments as described below.

### **2.2.1.8. Super-resolution structured illumination microscopy (SR-SIM)**

In order to further improve the spatial resolution of our immunolabelling data we applied multicolour super-resolution (SR) 3D-SIM analyses (Schemmelleh et al., 2008). The resolution of normal microscopy is limited to approximately 200 nm in lateral (XY) and 500nm in axial (Z) direction. Super-resolution microscopy gives the possibility to exceed this diffraction limit. SR-SIM increases the normal lateral resolution by factor two and 3D- super-resolution structured illumination microscopy (3D-SIM) provides the same increase in axial direction. Another advantage of the SR-SIM is the possibility to use standard dyes and staining protocols (for review, see Schemmelleh et al., 2010). For structured illumination microscopy, the ELYRA PS1 setup (as well as a precursor prototype) from Zeiss was used. Images were taken with a 63x Plan-Apochromat (NA=1.4) with excitation light of 488, 561 and 635 nm wavelengths and then processed for structured illumination microscopy to obtain higher resolutions (Gustafsson et al., 2008; for review, see Schemmelleh et al., 2010). Z stacks with an interval of 150nm were used to scan the whole retina section for 3D- super-resolution structural illumination microscopy (3D-SIM) (Schemmelleh et al., 2008; for review, see Schemmelleh et al., 2010). For acquisition and processing as well as for 3-D reconstruction and maximum projection the Zen2010 software (ZEISS) was used. For imaging analysis, sections were oversampled to exclude signal loss; for 3D-reconstruction only relevant image planes were used. For the 3-D reconstruction the transparent mode was applied.

In general, there is a potential risk of projection artefacts using SR-SIM e.g. due to chromatic aberration (Schemmelleh et al., 2008). The employed ZEISS setup is corrected for chromatic aberration in X-/Y- and Z-direction using multicolour beads and all taken images were examined considering this problem. Identical imaging results were obtained if different fluorophores were used for imaging.

### **2.2.2. Postembedding immunogold electron microscopy:**

#### **Tissue embedding and immunogold labelling procedure**

Tissue embedding and immunogold labelling was done as previously described (Schmitz et al., 2000) with some modifications. In brief, freshly isolated mouse retinas were fixed in 0.05% glutaraldehyde, 2% freshly depolymerized paraformaldehyde in PBS, pH 7.4, for 2hrs at 4°C. After several washes with PBS,

followed by H<sub>2</sub>O, samples were treated with tannic acid (0.1% (w/v) in H<sub>2</sub>O) for 1hr at 4°C. Samples were washed with H<sub>2</sub>O and incubated for 2hrs in 1% uranyl acetate (in H<sub>2</sub>O). Subsequently, probes were dehydrated in an ascending concentration of ethanol. At 30% ethanol, samples were transferred from 4°C to -20°C to minimize extraction of lipids and were kept at -20°C during the entire embedding procedure. Dehydration was performed in steps of 30%, 50%, 70%, 80% 90% and 98% ethanol (each for ≈30 mins). Afterwards, samples were infiltrated with London Resin (LR)-Gold (Electron Microscopic Sciences, EMS) to which 2% of H<sub>2</sub>O (v/v) had been added. LR-Gold solution was changed thrice and finally replaced by LR-Gold/2% H<sub>2</sub>O resin solution that contained 0.1% benzil as polymerization catalyst. Polymerization was performed at -20°C with UV light (for ≈24hrs). For immunolabelling, ultrathin sections (50-80nm in thickness) were first treated with 0.5% bovine serum albumine (BSA) in PBS for 45 mins at RT to block non-specific protein binding sites. Then, primary antibodies (dynamin [hudy-1] or clathrin [clhc-V1; ab21679] were applied overnight at a 1:250 dilution in 0.5% BSA/PBS. After several washes with PBS, binding of the primary antibody was detected with goat anti-mouse/goat anti-rabbit secondary antibody conjugated to 10nm gold particles (Sigma). Afterwards, immune complexes were fixed with 2.5% glutaraldehyde in PBS for 15mins at RT. Sections were contrasted with 2% uranylacetate in H<sub>2</sub>O and analyzed with a Tecnai Biotwin digital transmission electron microscope. As negative controls, either primary antibodies were omitted and/or unrelated antibodies were used.

### **2.2.3. SDS-PAGE**

SDS PAGE was done as described by Maniatis *et al*, 2005. One dimensional gel electrophoresis separates proteins according to their molecular size in the presence of 0.1% SDS. The polyacrylamide gel is casted as a separating gel topped by a stacking gel. Sample proteins were solubilised by boiling in 4X SDS loading buffer.

### **2.2.4. Western blots**

Western blot analyses were performed as previously described (Schmitz *et al.*, 2000) using the indicated antibodies at the indicated dilutions. Binding of the primary

antibodies were detected with secondary antibodies conjugated with horseradish peroxidase and enhanced chemiluminescence (ECL). ECL signals of the antibody-incubated western blots were scanned and documented with a BioRad gelDoc Chemiluminescence detection system. As molecular weight standards for sodium dodecyl sulfate polyacrylamide gel electrophoresis (SDS-PAGE), we used a prestained protein ladder (Thermo; order number 26616), the Roti-Mark Standard molecular weight markers (Roth, Germany; T851); and erythrocyte ghost membranes (Bennett, 1983).

### **2.2.5. Isolation of photoreceptors from the mature mouse retina**

(Done by Rashmi Katiyar)

Photoreceptor cells from the mature retina were isolated by gentle enzymatic digestion with papain largely as previously described (Townes-Anderson et al., 1985, 1988; Rebrik and Korenbrot, 2004). In brief, retinas were isolated from adult mice within 5mins post mortem (in ambient light). The enucleated eyes were bisected at the equatorial plane and the posterior eye cup transferred into ice-cold low  $\text{Ca}^{2+}$ -containing saline solution (abbreviated as LCS solution; containing 132mM NaCl, 3mM KCl, 1mM  $\text{MgCl}_2 \cdot 6\text{H}_2\text{O}$ , 0.5mM  $\text{CaCl}_2$ , 10mM sodium pyruvate, 10mM glucose, 10mM HEPES, pH 7.4,  $\approx 300\text{mOsm/L}$ ). LCS was saturated with 5%  $\text{CO}_2/95\% \text{O}_2$  prior to use. From the posterior eyecup, the neural retina was gently peeled off from the pigment epithelium and incubated in 1ml of cysteine-activated papain solution (containing 9U/ml of papain [Sigma, #76220-25G], 2.7mM L-cysteine [Roth, #1693.1] in LCS) for 20 min (at  $25^\circ\text{C}$ ). After removing the papain solution, the retina was gently washed three times with 1mL of LCS solution containing 2% FCS and 0.01mg/ml DNase (Sigma, #DN25-110MG). To dissociate photoreceptor cells, papain-treated retina was gently triturated (3-4 times) with a wide-bore plastic pasteur pipette. The resulting cell suspension was plated on concanavalin A (Sigma, #C7275-250mg)-coated coverslips. For coating of 25mm round coverslips,  $\approx 200\mu\text{l}$  of 1mg/ml concanavalin A (in LCS solution) were added for 1hr at RT. Unbound concanavalin A was removed by several washes with LCS prior to the experiments. Cells were allowed to settle on the coverslips for 30mins at  $37^\circ\text{C}$  for tight attachment. For immunocytochemistry, cells were washed once with LCS and fixed with 4% paraformaldehyde in PBS for 15mins at RT. Fixed cells were washed 3 times with PBS and then permeabilized with 0.1% saponin (S4521-10G, Sigma) in PBS for

15min at RT. After permeabilization, cells were treated with 1% BSA in PBS for 45mins and were incubated with primary antibodies, i.e. hudy-1 (1:250) and U2656 (1:1,000) for overnight at 4°C. After 3 times washing with PBS, the cells were incubated for 1hr at RT with secondary antibodies, goat anti-mouse-Alexa488 and goat anti-rabbit-Alexa 568. After three washes with PBS, coverslips were mounted on glass cover slides with anti-fade solution and sealed with nail polish.

### **2.2.6. Analysis of synaptic ribbon-associated endocytic activity in synaptic terminals of isolated mouse photoreceptors**

(Done by Rashmi Katiyar)

Isolated mouse photoreceptors, prepared as described above, were incubated for 2 min at room temperature with 1µM of Texas Red-hydrazide (Molecular Probes; T6256), a paraformaldehyde (PFA)-fixable analog of sulforhodamine 101 (SR101) (Nimmerjahn et al., 2004; Euler et al., 2009). Texas Red-hydrazide/SR101 was dissolved in LCS to which 2mM Ca<sup>2+</sup> were added. Texas Red-hydrazide- and SR101-loading experiments resulted in very similar labelling patterns in isolated mouse photoreceptors (Fig. 20 and data not shown). After labelling, photoreceptors were rinsed 3 times with LCS. To test for the importance of dynamin in ribbon-associated endocytosis, photoreceptors were incubated for 30 min at 37°C with 100µM dynasore, a specific blocker of dynamin activity (Macia et al., 2006; Kirchhausen et al., 2008; van Hook and Thoreson, 2012), before incubation with sulforhodamine/Texas Red-hadrazide. After labelling and three short washes with LCS, photoreceptors were fixed with 4%PFA for 15 min at RT and processed as described above.

### **3. Results**

#### **3.1. Testing of antibodies**

In order to localize key proteins of the recycling endocytic machinery in photoreceptor ribbon synapses, I used different antibodies against known key proteins of synaptic vesicle endocytosis. First the different antibodies were tested for their specificity on mouse retina lysate. For this purpose, I performed western blot analysis of the indicated antibodies using crude retina lysate (Figure 14).

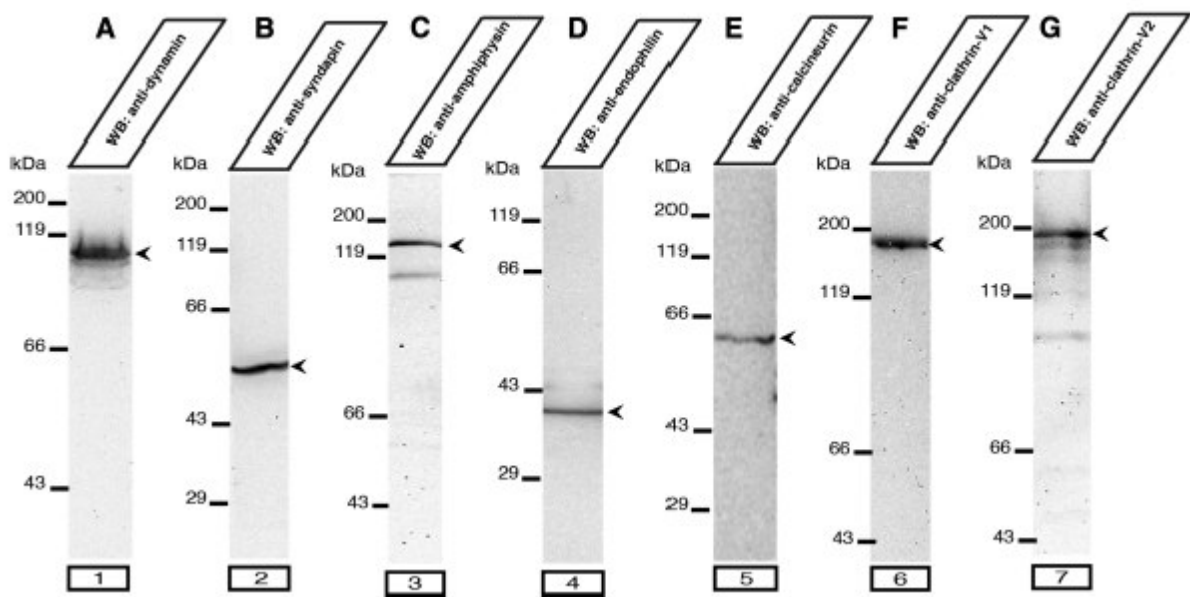


**Figure 14 Expression of endocytic proteins in the mouse retina.** (A-G) Expression of endocytic proteins in extracts of the mouse retina as judged by western blot analyses. All antibodies detect their respective antigen at the expected running position (indicated by arrowheads). In (A-E), proteins were separated by 10% acrylamide SDS-PAGE; in (F-G) by 8% acrylamide SDS-PAGE. Arrowheads indicate predicted running position of respective proteins.

All tested antibodies detected their respective antigen at the expected running position (Figure 14).

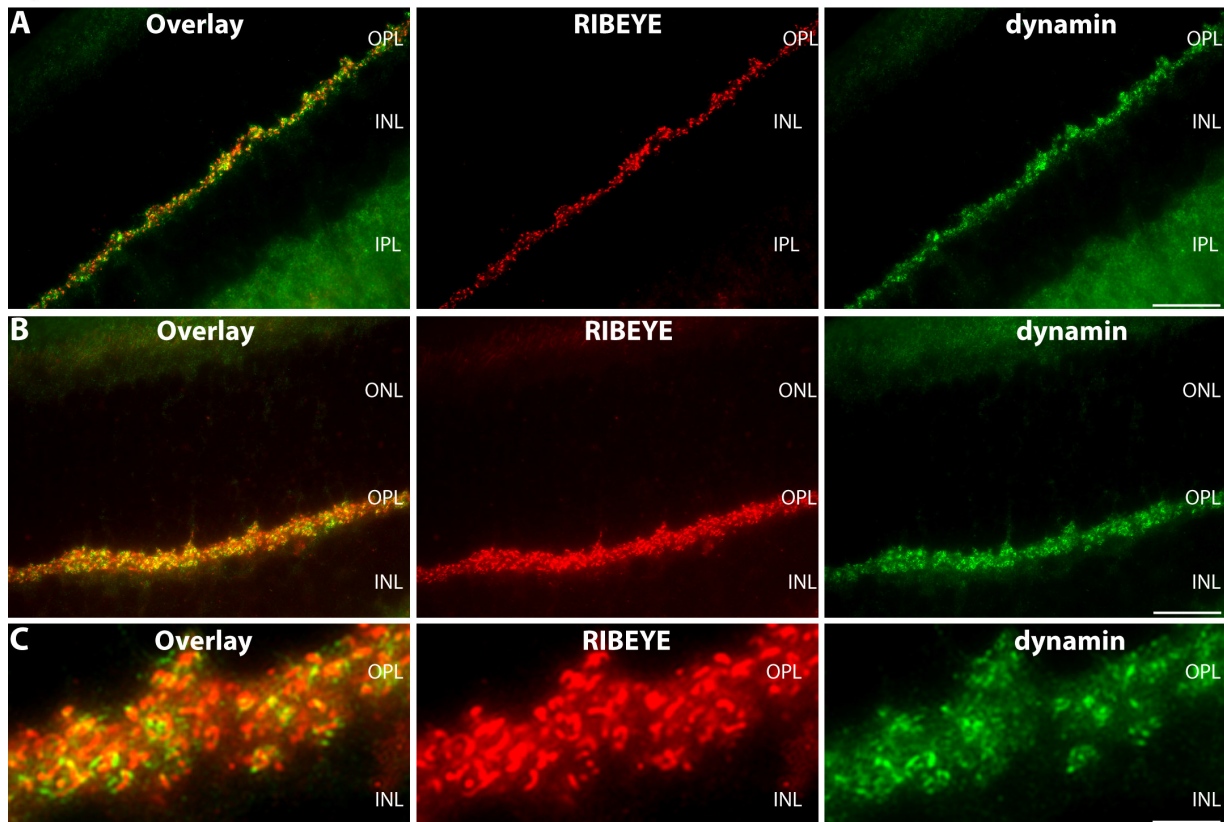
#### **3.2. Localisation of dynamin**

After that, I first focused on dynamin, a mechano-enzyme that is essential for many forms of endocytosis (Praefcke and McMahon, 2004; Ferguson et al., 2007; Heymann and Hinshaw, 2009; Schmid and Frolov, 2011; Ferguson and de Camilli, 2012). Dynamin has well defined functional domains, including an aminoterminal

GTPase-domain (G-domain), a central lipid-binding PH-domain, a bipartite stalk region, a GTPase effector domain and a proline-rich carboxyterminal region to which SH3-containing proteins can dock in a differential manner (for review, see Clayton and Cousin, 2009; Ferguson and de Camilli, 2012; Yamashita, 2012). For immunolabelling of dynamin, I used a well characterized mouse monoclonal antibody against dynamin (Warnock et al., 1995; Takei et al., 1995; Hinshaw and Schmid, 1995) on conventional cryostat sections of mouse eyes (Figure 15 A-C) and 0.5  $\mu$ m-thin resin sections for immunolabelling analyses to obtain better resolution (Figure 15 D-E). Using the described immunolabelling techniques, I found dynamin highly enriched in both synaptic layers of the retina, the outer and inner plexiform layer (OPL and IPL, respectively; Figure 15).

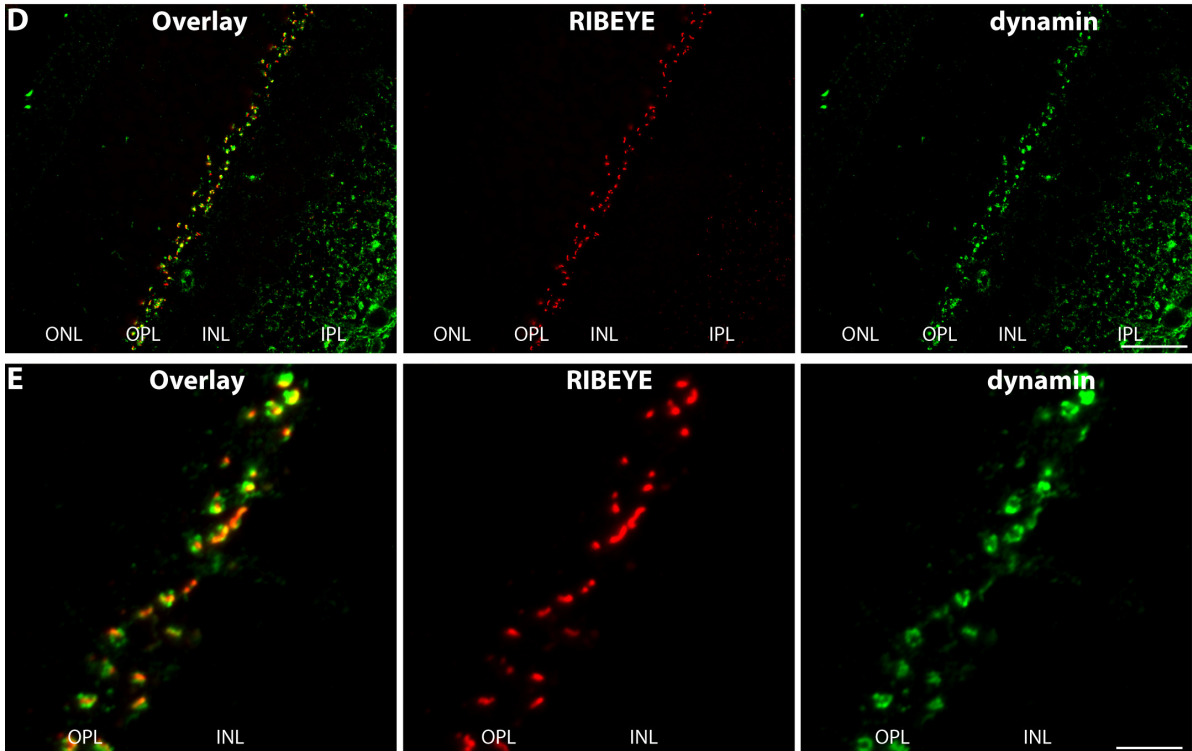
In comparison to conventional cryostat sections (Figure 15 A-C), 0.5  $\mu$ m-thin resin sections (Figure 15 D, E) show less background and a much better resolution. Therefore, I proceeded from this point on with immunolabelling of 0.5  $\mu$ m resin sections to obtain optimal resolution of the immunolocalized proteins.

Figure 15  
cryostat section



(legend see next page)

semithin section



**Figure 15 Comparisons of low-magnification micrographs of cryostat (A-C) and semithin sections (D-E) of the mouse retina double-immunolabelled with polyclonal antibodies against RIBEYE (U2656) and monoclonal against dynamin (hudy-1).**

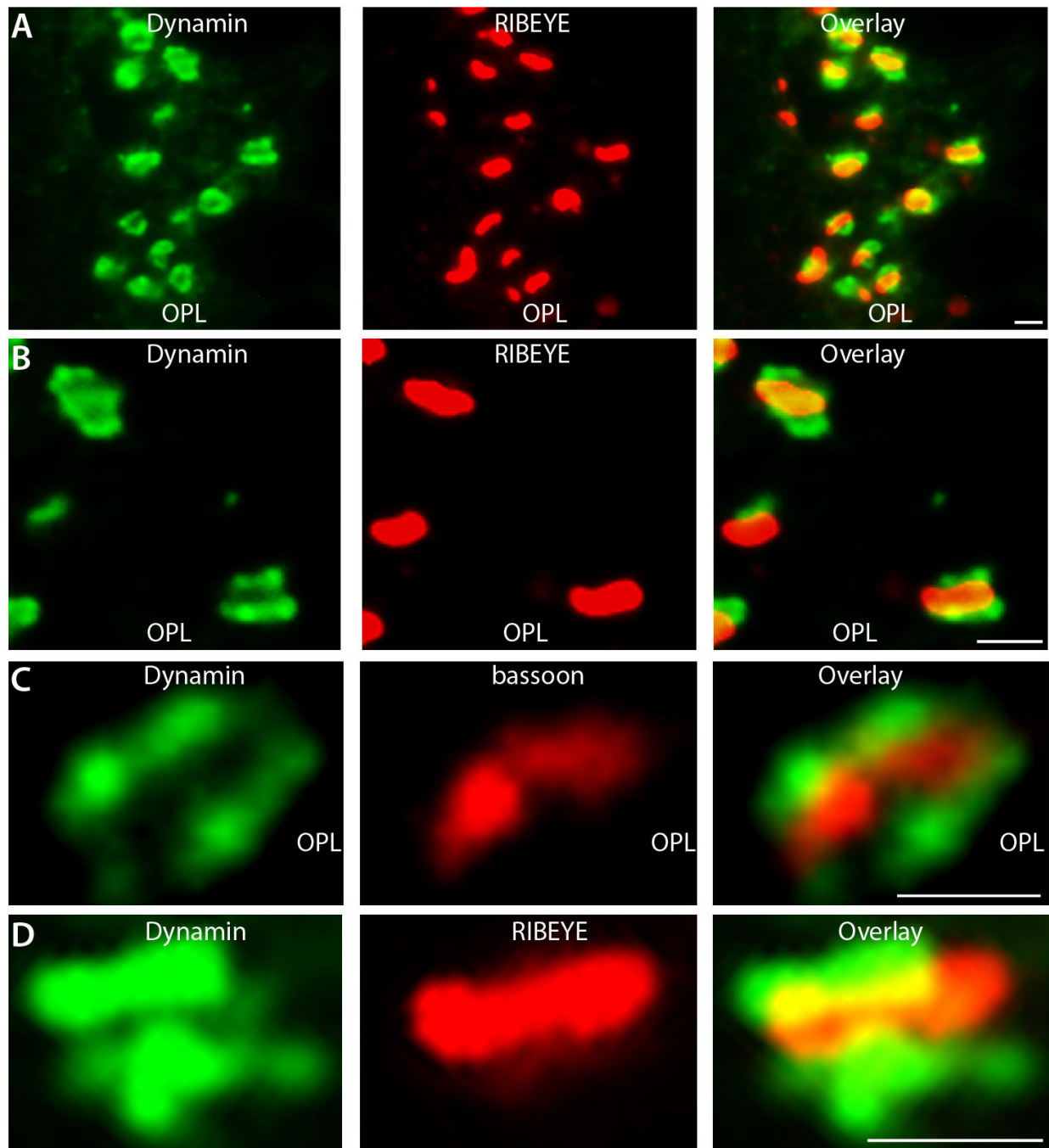
Dynamin is highly enriched in the synaptic layers of the retina, the OPL and IPL, in a punctate manner. Synaptic ribbons were immunolabelled with polyclonal antibodies against RIBEYE and showed a close association with the dynamin immunolabel in the OPL. In comparison to cryostat sections (A-C) semithin sections (D-E) show a clearer signal with higher resolution and less background. Abbreviations: ONL, outer nuclear layer; OPL, outer plexiform layer; INL, inner nuclear layer; IPL, inner plexiform layer. Scale bars: 35  $\mu\text{m}$  (A,B, D), 10  $\mu\text{m}$  (C,E).

The outer plexiform layer, that contains the photoreceptor ribbon synapses, showed a particularly strong dynamin immunosignal (Figure 15, 16). High magnification/resolution analyses demonstrated that this dynamin immunosignal in photoreceptor synapses is present in a discrete manner and highly enriched around the synaptic ribbon that was immunolabelled with antibodies against RIBEYE (Figure 16 A, B). Furthermore, dynamin was found in close proximity to the active zone protein bassoon (Figure 16 C).

Bassoon is localized at the base of the synaptic ribbon (tom Dieck et al., 2005). Super-resolution structured-illumination microscopy (SR-SIM) showed a ring of dynamin immunoreactivity surrounding the synaptic ribbon in close proximity, i.e. less than 250nm (Figure 16 E, F). The optical resolution obtained by SR-SIM analyses clearly exceeded the resolution that could be obtained by conventional imaging as

judged by a comparative imaging analysis of the same incubations either by conventional (D) or SR-SIM imaging (E) at identical magnifications.

Figure 16



(legend see next page)

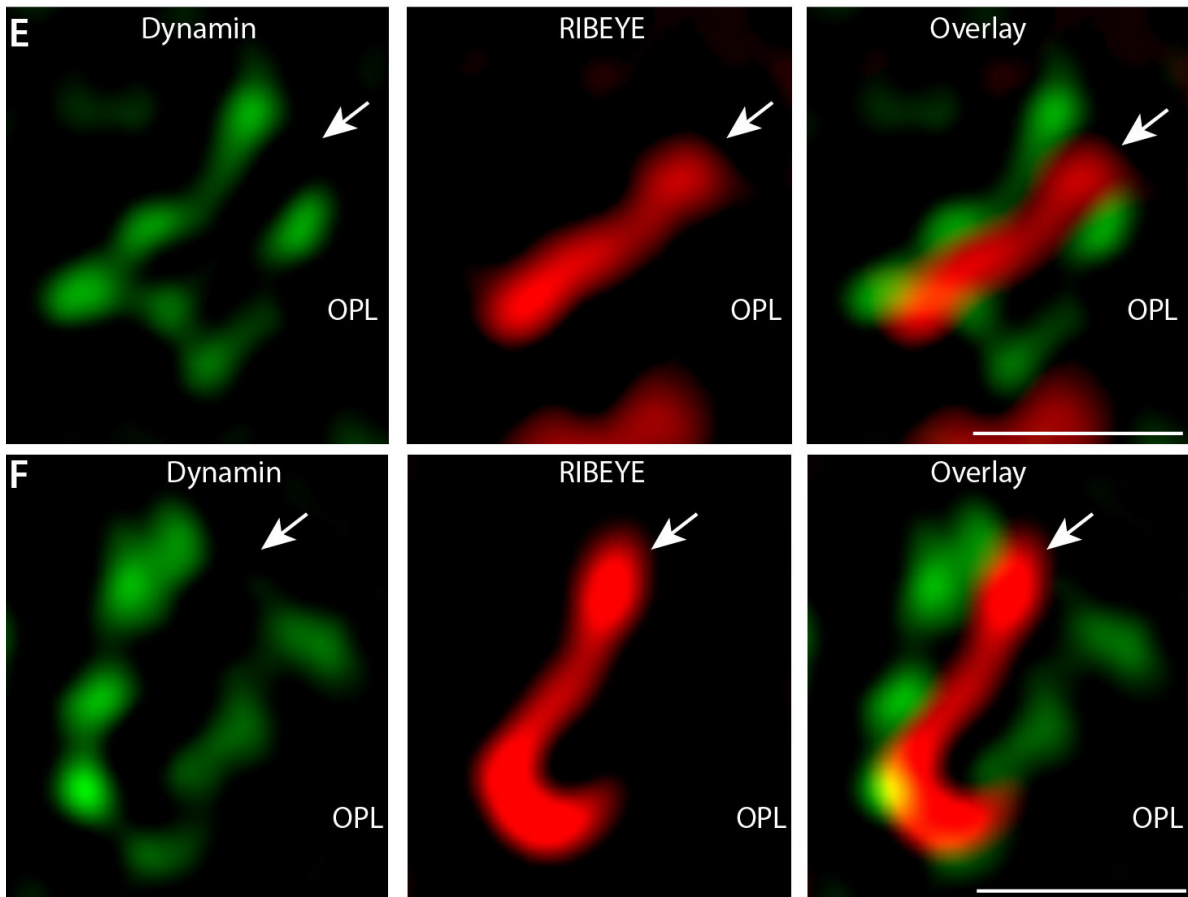
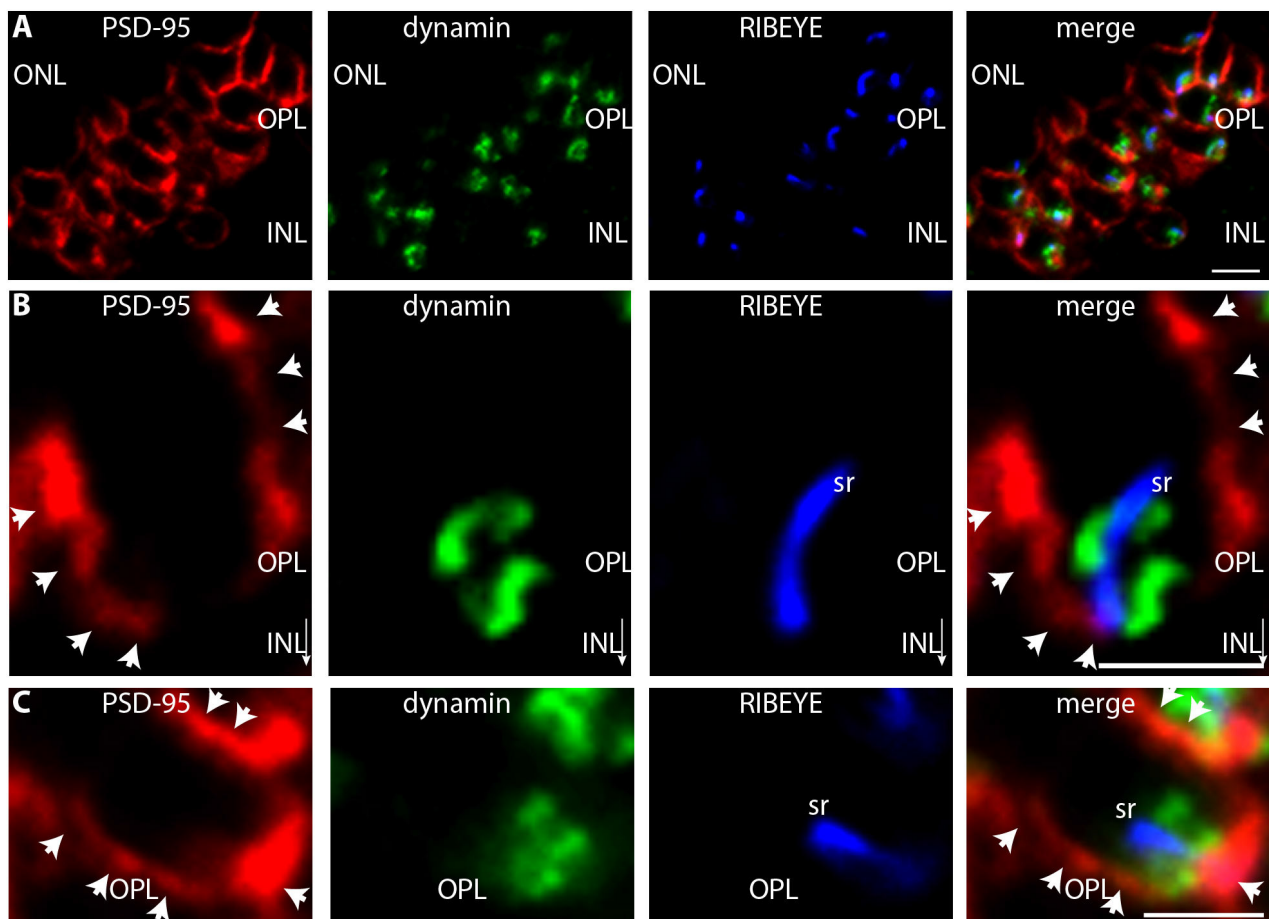


**Figure 16 Distribution of dynamin in photoreceptor ribbon synapses at high resolution (immunolabelling of 0.5 $\mu$ m-thin sections).** (A-B) Conventional imaging of 0.5  $\mu$ m-thin sections of the mouse retina double-immunolabelled with polyclonal antibodies against RIBEYE (U2656) and mouse monoclonal antibodies against dynamin (hudy-1). (C) Conventional imaging of 0.5 $\mu$ m-thin sections of the mouse retina double-immunolabelled with polyclonal antibodies against bassoon and mouse monoclonal antibodies against dynamin (hudy-1). (D) shows at the same magnification as in (E-F) - but without SR-SIM imaging - mouse retina double-immunolabelled with polyclonal antibodies against RIBEYE (U2656) and mouse monoclonal antibodies against dynamin (hudy-1). (E-F) 2D-super-resolution structured illumination microscopy (2D SR-SIM) pictures of 0.5 $\mu$ m-thin sections from the mouse retina double-immunolabelled with rabbit polyclonal antibodies against RIBEYE (U2656) and mouse monoclonal antibodies against dynamin (hudy-1). The dynamin immunosignal is highly enriched around the synaptic ribbon (arrow). Abbreviations: OPL, outer plexiform layer. Scale bars: 1 $\mu$ m (A-E).

The observation of dynamin being located in close vicinity to the synaptic ribbon was further corroborated with triple immunolabelling experiments. With these triple immunolabelling experiments, I correlated the localization of dynamin to other proteins of the presynaptic photoreceptor terminal (Figure 17). I used antibodies against PSD-95 to label the presynaptic plasma membrane of photoreceptor terminals (Koulen et al., 1998; Aartsen et al., 2009). In contrast to other synapses, PSD-95 is located presynaptically in photoreceptor ribbon synapses and antibodies

against PSD-95 nicely demarcate the outline of the presynaptic terminal (Figure 17 A-C). Antibodies against the vesicular transporter 1 (VGLUT1) were used to label the glutamatergic synaptic vesicles in the photoreceptor presynaptic terminals (Wojcik et al., 2004) (Figure 17 D, E). Similar to the previously described immunolabelling data, I observed RIBEYE and dynamin located close to each other at the distal portion of the presynaptic terminal that faces the INL (Figure 17 A-E). Quantitative distance measurements of nearest distance indicated that dynamin puncta are located in about  $\approx 125\text{nm}$  ( $\pm \approx 50\text{nm}$  s.d.; 100 synapses analyzed) away from RIBEYE-puncta and  $\approx 120\text{nm}$  ( $\pm 40\text{nm}$  s.d.; 100 synapses analyzed) away from the bassoon puncta in retinal sections.

Figure 17



(legend see next page)

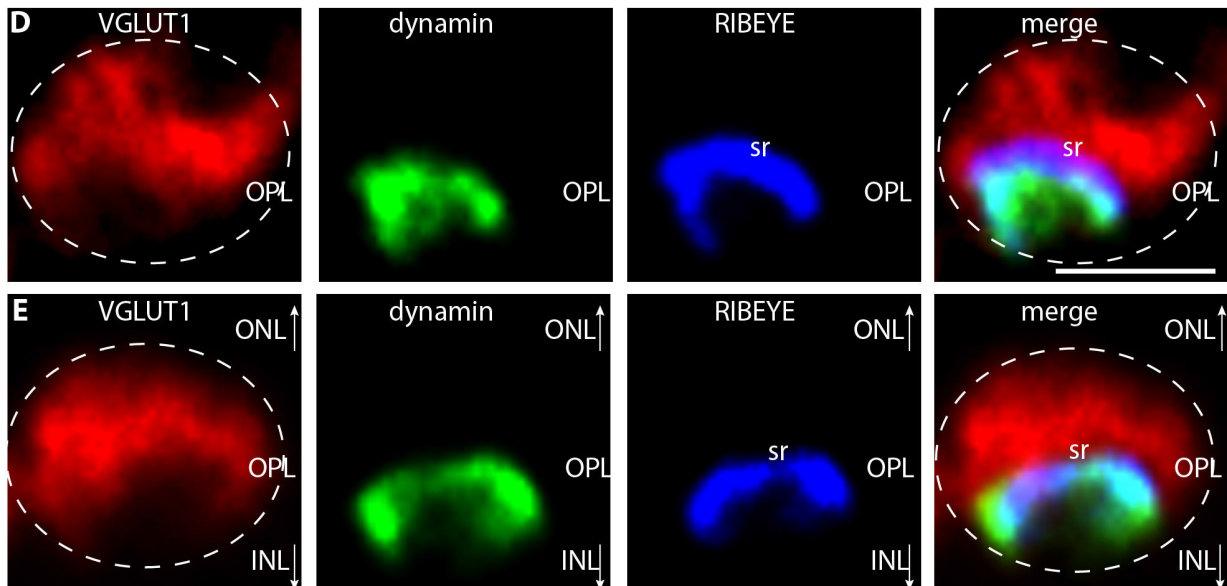


**Figure 17 Localization of dynamin in relation to other synaptic proteins of the presynaptic photoreceptor terminal.** 0.5 $\mu$ m-thin sections from mouse retina were triple-immunolabelled with rabbit polyclonal antibodies against PSD-95 (L667) (**A-C**)/ or VGLUT1 (**D-E**), mouse monoclonal antibodies against dynamin (hudy-1) (**A-E**) and DyLight650-direct labelled primary antibodies against RIBEYE(B)/CtBP2 (**A-E**). In (**A-C**), the PSD-95 immunosignals label the presynaptic plasma membrane of the presynaptic terminals (Koulen et al., 1998; Aartsen et al., 2009) thus demarcating the extension of a single presynaptic terminal (arrowheads in (**B-C**)). RIBEYE and dynamin are located close to each other at the distal end of the photoreceptor terminal that is facing the INL (**A-C**). In (**D-E**), presynaptic terminals were immunolabelled with antibodies against the vesicular transporter VGLUT1, a marker protein of glutamatergic synaptic vesicles. Single photoreceptor presynaptic terminals are indicated by the white, dashed circles in (**D-E**). Similar as in (**A-C**), RIBEYE and dynamin are located close to each other at the distal border of the the immunolabeled glutamatergic vesicles of the presynaptic terminal that face the INL. Abbreviations: OPL, outer plexiform layer; ONL, outer nuclear layer; INL, inner nuclear layer; sr, synaptic ribbon. Scale bars: 1 $\mu$ m (**A-E**).

Also isolated mouse photoreceptors, that display the typical ultrastructural morphology of photoreceptor synaptic terminals (Figure 18 E), showed a similar immunolabelling pattern. Similar to the observations in the intact retina, a focal enrichment of dynamin was observed in close vicinity to the synaptic ribbon in isolated photoreceptors (Figure 18 A-D).

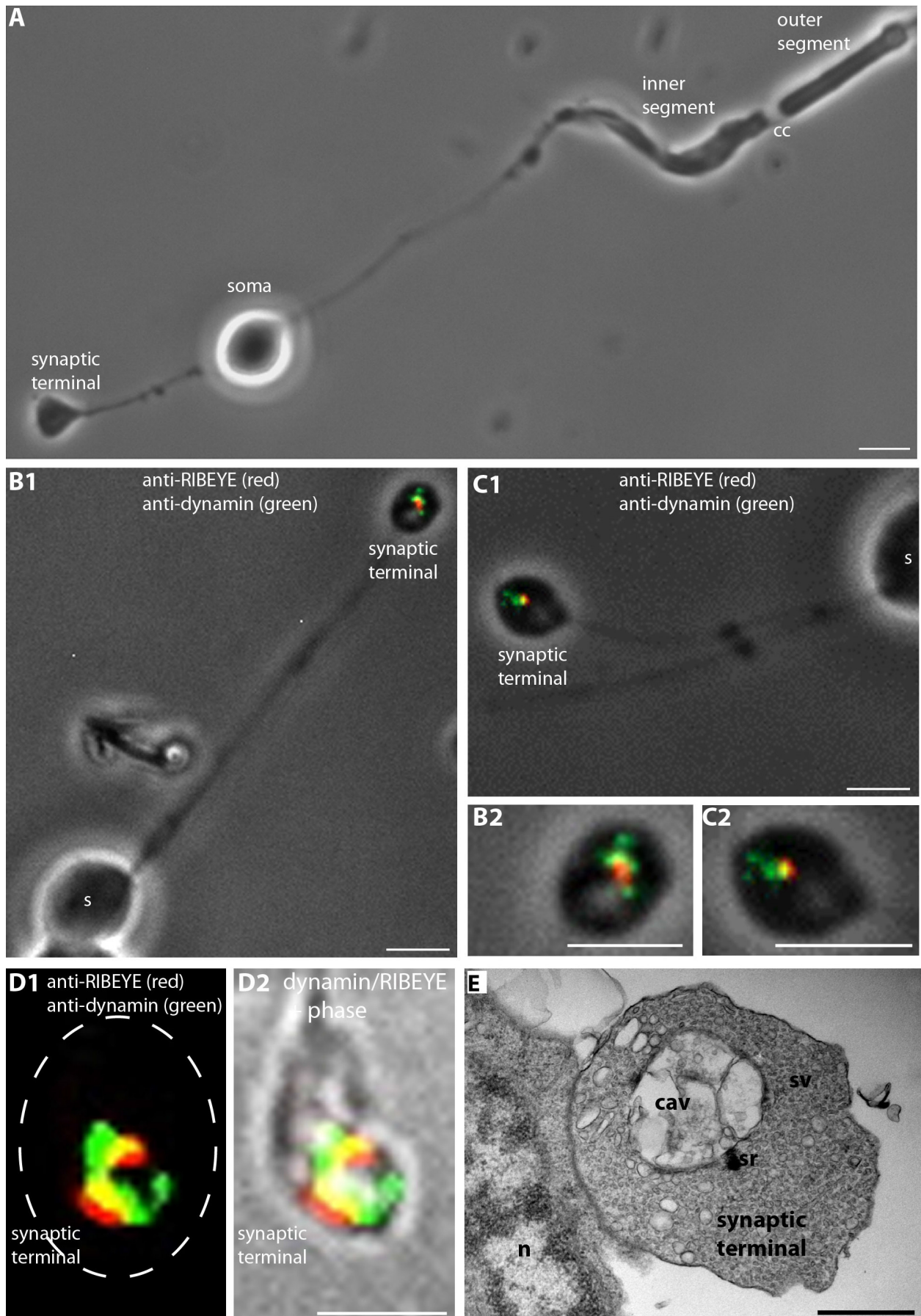


**Figure 18** Dynamin is highly enriched at the synaptic ribbons in presynaptic terminals of isolated photoreceptors from the mouse retina. Isolated photoreceptors from the

mouse retina were double-immunolabelled with mouse monoclonal antibodies against dynamin and rabbit polyclonal antibodies against RIBEYE (**A-D**). Dynamin is highly enriched in close vicinity to the synaptic ribbon. (**E**) shows the ultrastructural morphology of a synaptic terminal from isolated mouse photoreceptors. The typical large presynaptic terminal with large numbers of synaptic vesicles together with a synaptic ribbon anchored to the active zone are visible. In (**E**), the center of the presynaptic terminals contains the postsynaptic cavity (cav) with tips of the postsynaptic dendrites from horizontal and bipolar cells. These are separated from the soma of the postsynaptic cells during the isolation procedure. Abbreviations: s, soma of an isolated photoreceptor cell; cc, connecting cilium; n, nucleus of an isolated photoreceptor cell; cav, synaptic invagination of the photoreceptor synaptic complex that contains the tips of the postsynaptic dendrites from bipolar and horizontal cells. Scale bars: 1µm (**A-D**); 500nm (**E**). [experiment was done by Rashmi Katiyar]

Finally, I performed postembedding electron microscopy with antibodies against dynamin to determine at the ultrastructural level where exactly dynamin is located in the distal portion of the presynaptic terminal. Postembedding immunogold electron microscopy demonstrated that dynamin is strongly enriched at the presynaptic plasma membrane in close vicinity to the synaptic ribbon (Figure 19). This area is denoted as peri-active zone in the text because it is located directly lateral to the active zone of exocytosis where the synaptic ribbons are anchored and where exocytosis occurs (for review, see Mercer and Thoreson, 2011; Schmitz et al., 2012). These ultrastructural immunolocalization data support the described light microscopical immunolabelling data which demonstrated that dynamin is located about 120nm distant from the synaptic ribbon. Dynamin was found predominantly, though not exclusively, at the presynaptic plasma membrane in close vicinity to the synaptic ribbon (less than 200nm distance from the base of the synaptic ribbon). Some dynamin immunolabel was also present at the presynaptic plasma membrane in some distance from the ribbon (more than 200nm distance from the ribbon). There was very little, if any, dynamin at the extrasynaptic plasma membrane outside of the synaptic cavity (Figure 19).

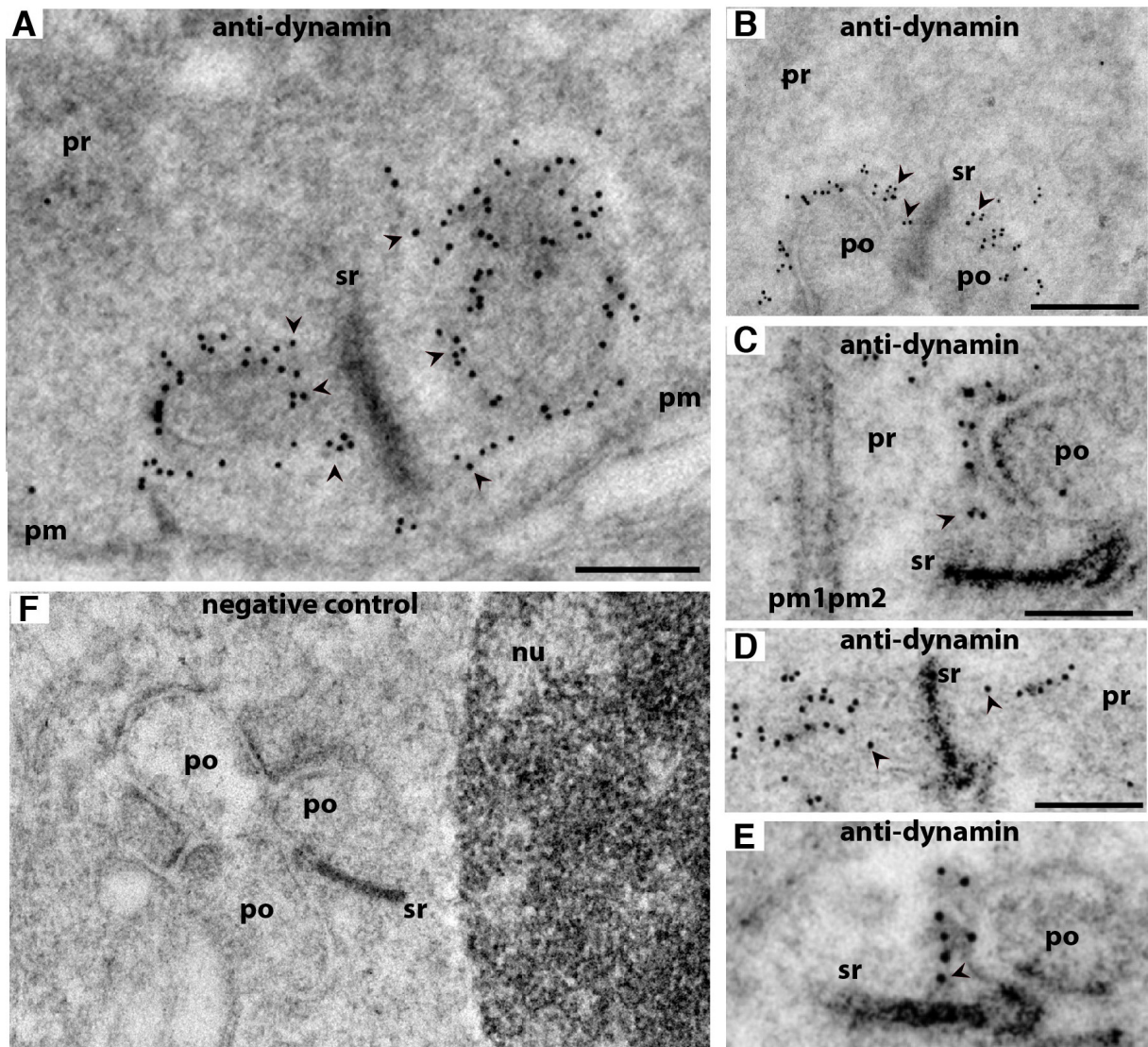


**Figure 19 Postembedding immunogold labelling of photoreceptor synapses of the mouse retina with dynamin antibodies.** (A-E) Ultrathin sections immunolabelled with mouse monoclonal antibodies against dynamin (hudy-1). Binding of the primary antibodies was detected with goat anti-mouse antibodies conjugated to 10nm gold particles. The dynamin immunogoldlabel is highly enriched around the synaptic ribbon (arrowheads). The dynamin immunogold label was found at the presynaptic membrane in close vicinity to the synaptic ribbon. (F) is a control incubation where only secondary antibody (but no primary antibody) were used. No immunosignal was observed under these incubation conditions further stressing the specificity of the immunolabelling results. Please note that a postembedding protocol was used. In postembedding protocols no osmium tetroxide can be used. Therefore, lipid-rich membrane compartments i.e. synaptic vesicles, remain invisible with that method. Abbreviations: pr, presynaptic terminal; po, postsynaptic dendrite; sr, synaptic ribbon; pm, extrasynaptic plasma membrane (outside of the presynaptic plasma membrane invagination); pm1, pm2, extrasynaptic plasma membrane of two neighboring synapses; nu, nucleus. Black arrowheads point to dynamin immunogold particles close to the synaptic ribbons. Scale bars: 400nm (A), 300nm (B, F); 250nm (C, D); 200nm (E).

### **3.3. Localization of Dynamin interacting-proteins**

It was already shown that dynamin is typically recruited to membranes via SH3 domain-containing proteins such as syndapin/pacsin and amphiphysin (Di Paolo et al., 2002; Yoshida et al., 2004; Wu et al., 2009a; Koch et al., 2011). I localized these proteins in the retina and in photoreceptor ribbon synapses to determine their localization in comparison to localization of dynamin and the synaptic ribbon.

I found that the dynamin-interacting proteins syndapin and amphiphysin showed a very similar distribution as dynamin (Figs. 20, 21). Both syndapin and amphiphysin were highly enriched in the synaptic layers of the retina, particularly in the OPL, and showed a highly discrete, punctate distribution pattern at these sites (Figure 20, 21). Syndapin and amphiphysin were particularly enriched in close proximity to the synaptic ribbon that was visualized with antibodies against RIBEYE (Figure 20, 21). Amphiphysin and syndapin were highly clustered around the synaptic ribbon as judged by SR-SIM immunolabelling analyses of semithin retinal sections using double-immunolabelling experiments with antibodies against RIBEYE and amphiphysin or syndapin (Figures 20 C, 21 C, next page).

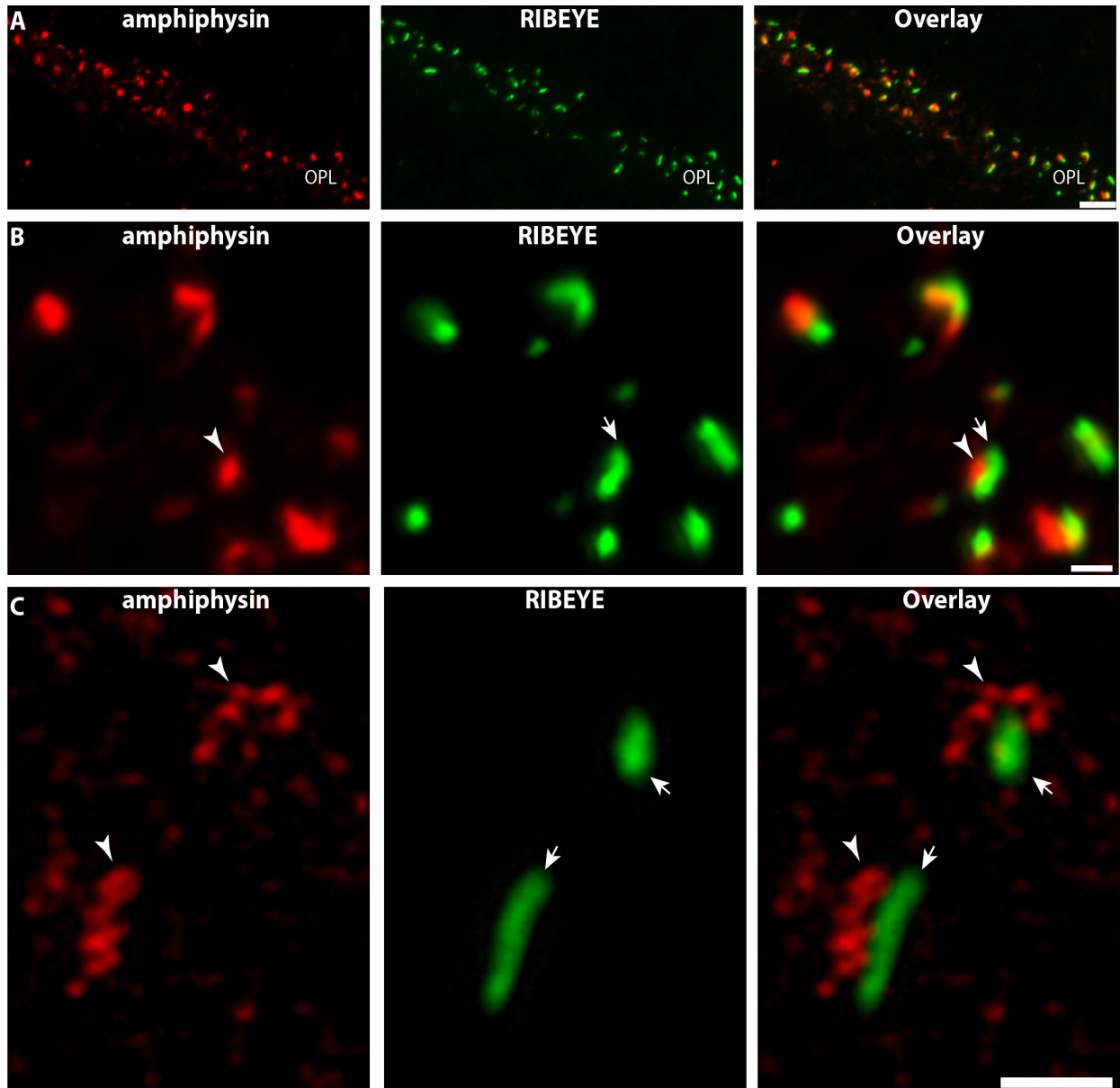


**Figure 20 Distribution of amphiphysin in photoreceptor ribbon synapses at high resolution.** 0.5 $\mu$ m-thin sections of the mouse retina double-immunolabelled with polyclonal antibodies against amphiphysin and mouse monoclonal antibodies against RIBEYE (B)-domain/CtBP2. Arrows point to immunolabelled synaptic ribbons. (**A**, **B**) represent micrographs obtained by conventional imaging; (**C**) is a super-resolution 2D-SIM micrograph (maximum projection of z-stacks). Abbreviations: OPL, outer plexiform layer. Scale bars: 1  $\mu$ m (A-C). Arrowheads point to amphiphysin in the vicinity of synaptic ribbons.

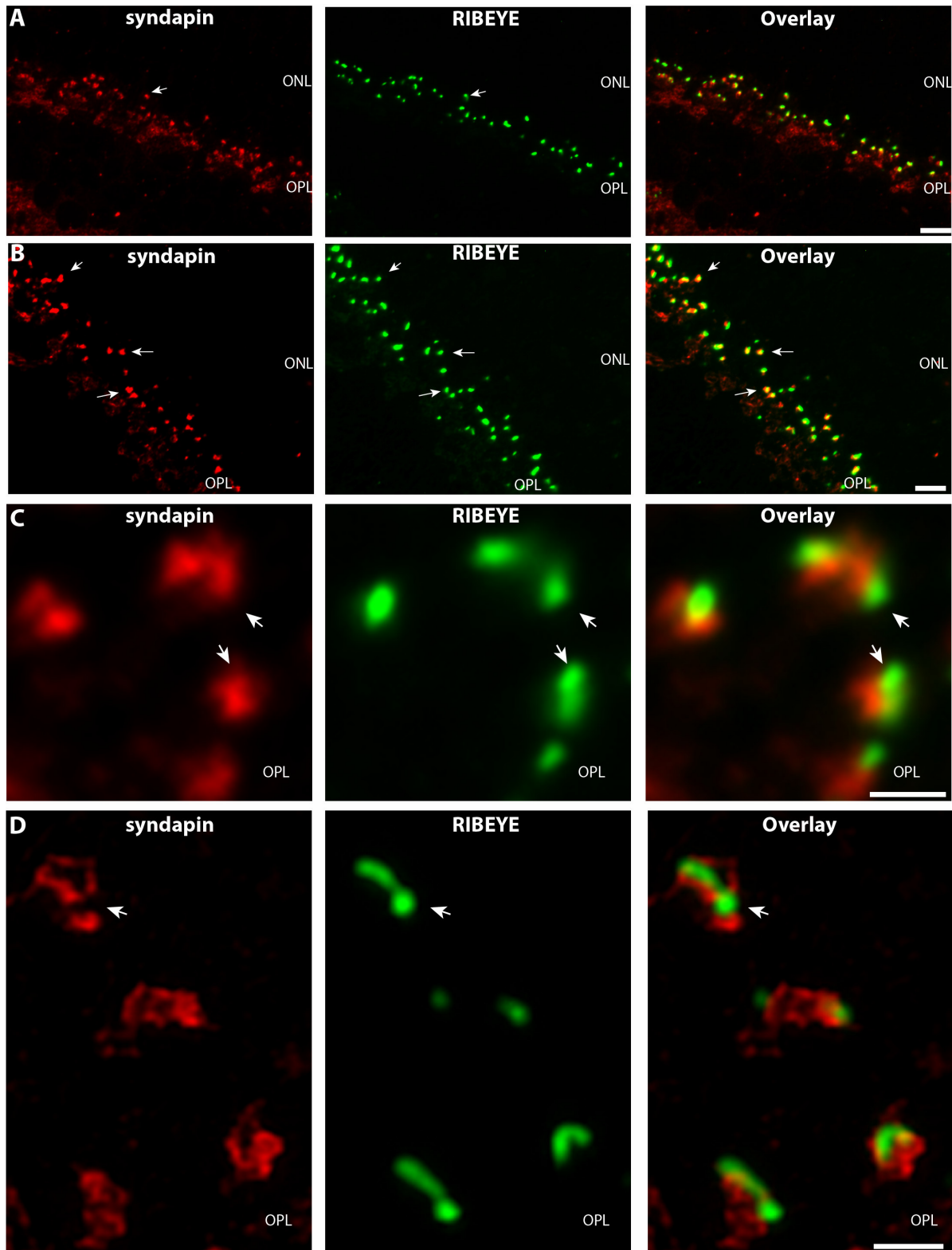
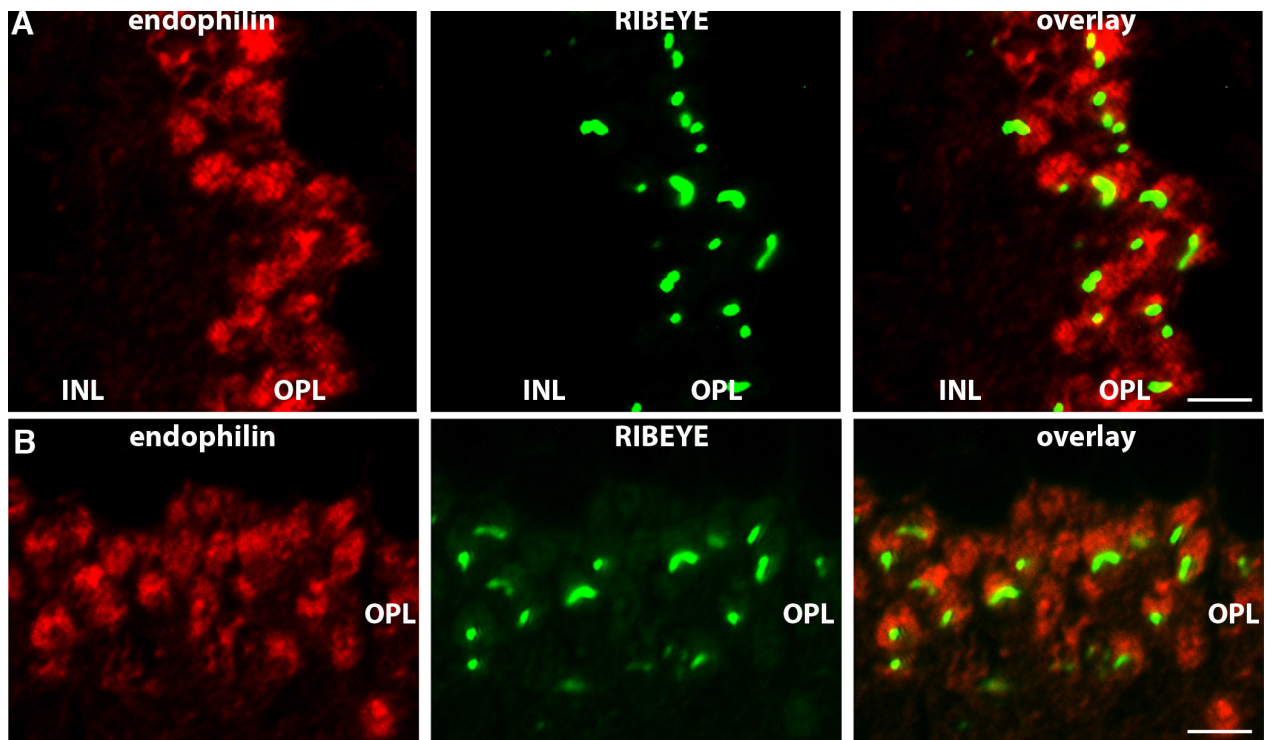


**Figure 21 Distribution of syndapin in photoreceptor ribbon synapses.** (A,B) low magnification micrographs of 0.5 $\mu$ m-thin sections of the mouse retina double-immunolabelled with rabbit polyclonal antibodies against syndapin and mouse monoclonal antibodies against RIBEYE(B)-domain/CtBP2. (C,D) high magnification micrographs, either obtained by conventional imaging (C) or by super-resolution 2D-SIM-imaging (D). (D) is a maximum projection of the respective z-stacks. Abbreviations: ONL, outer nuclear layer; OPL, outer plexiform layer. Arrows point to anti-RIBEYE-immunolabelled synaptic ribbons. Scale bars: 20 $\mu$ m (A), 10 $\mu$ m (B), 1 $\mu$ m (C,D)

Endophilin is another SH3-containing protein that can interact with dynamin (Mizuno et al., 2010; Llobet et al., 2011; Milosevic et al., 2011). In contrast to syndapin and amphiphysin (Figure 20, 21), endophilin was neither enriched around the synaptic ribbon (Figure 22A, B) nor restricted to the dynamin immunosignal around the synaptic ribbon (Figure 22 C) but was diffusely distributed throughout the entire presynaptic terminal (Figure 22 A-F). In these experiments the extension of the presynaptic terminal was immunolabelled with antibodies against the synaptic vesicle protein 2 (panSV2; Figure 22 D-E) or with antibodies against the vesicular glutamate transporter 1 (VGLUT1) both with identical results (Figure 22 D-F).

Figure 22



(legend see next page)

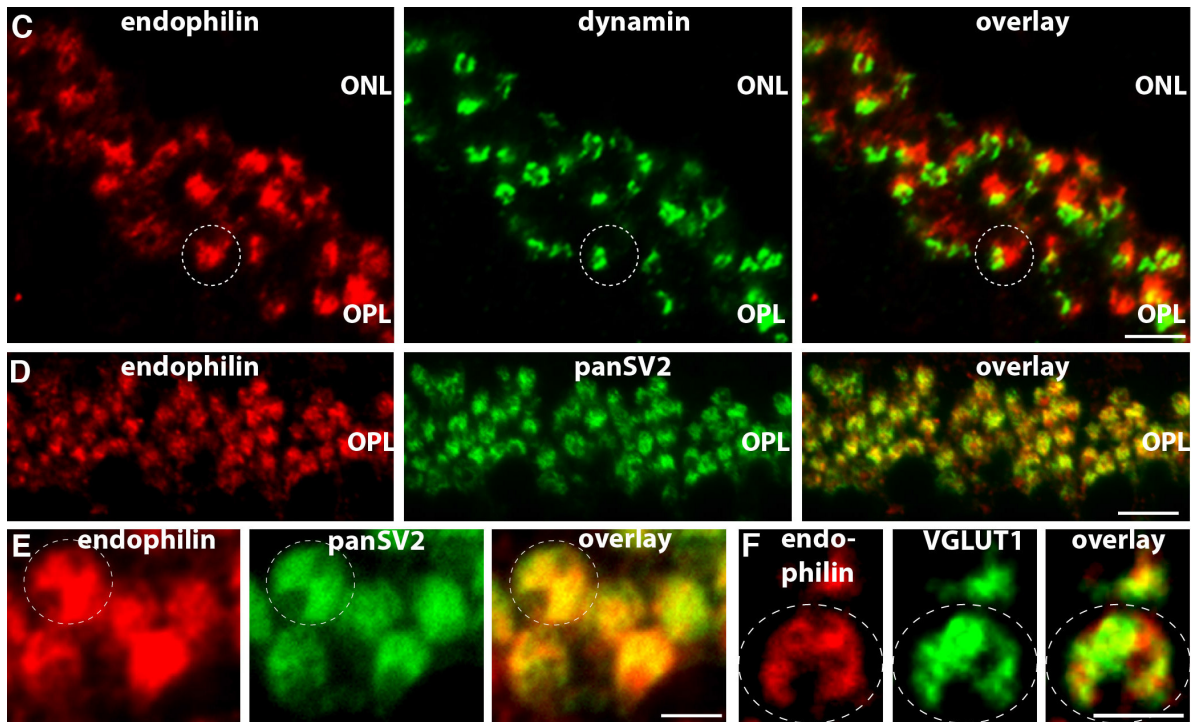
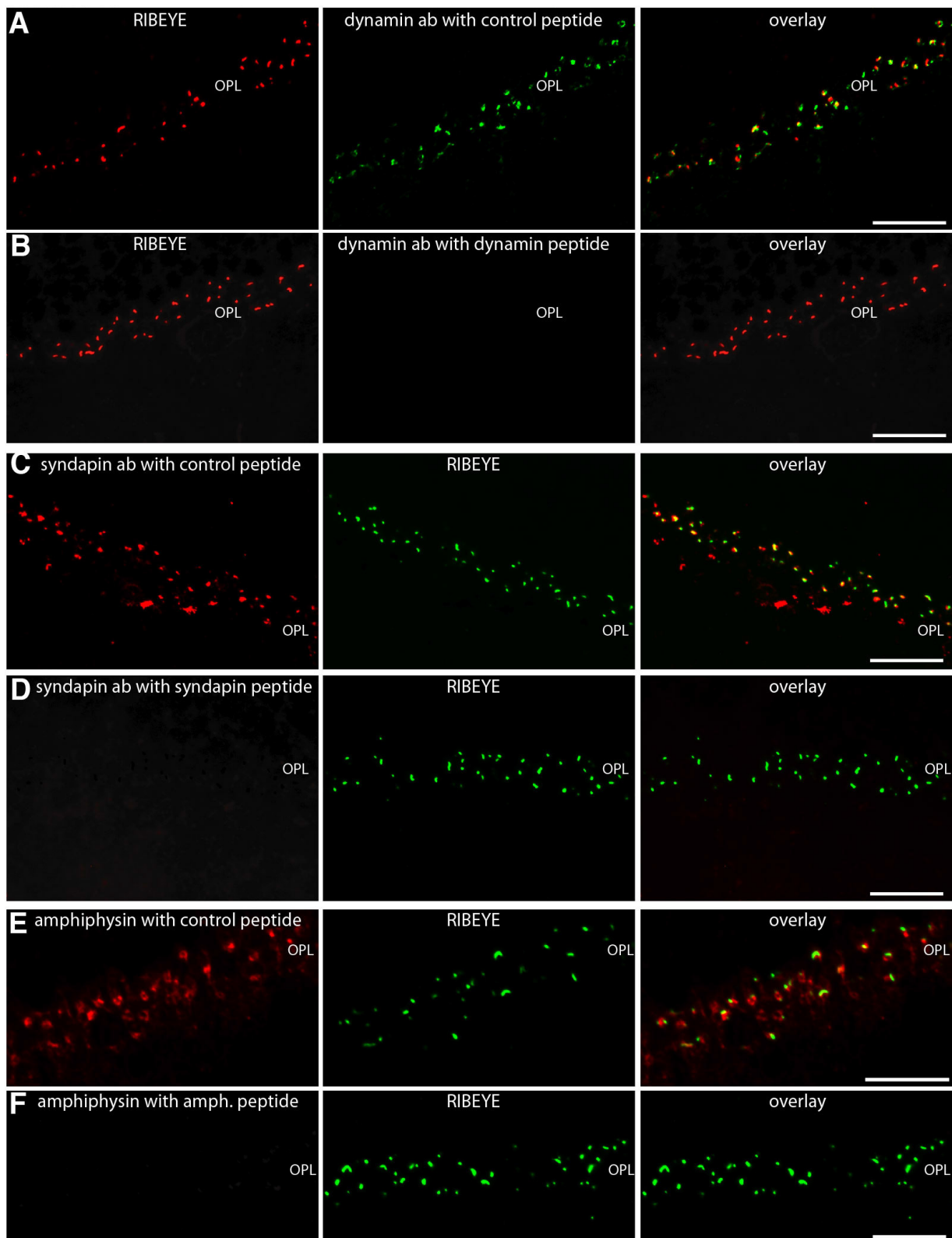


**Figure 22 Localization of endophilin in photoreceptor synapses of the mouse retina.** (A-B) 0.5 $\mu$ m-thin sections of the mouse retina double- immunolabelled with rabbit polyclonal antibodies against endophilin and mouse monoclonal antibodies against RIBEYE (B)-domain/CtBP2. (C) 0.5 $\mu$ m-thin sections of the mouse retina double- immunolabelled with rabbit polyclonal antibodies against endophilin and mouse monoclonal antibodies against dynamin. (D,E) 0.5 $\mu$ m-thin sections of the mouse retina double- immunolabelled with rabbit polyclonal antibodies against endophilin and mouse monoclonal antibodies against the synaptic vesicle protein 2 (SV2; detecting all SV2 isoforms). (F) 0.5 $\mu$ m-thin sections of the mouse retina double- immunolabelled with rabbit polyclonal antibodies against endophilin and mouse monoclonal antibodies against VGLUT1. Dashed circles in (C, E, F) denote single presynaptic photoreceptor terminals. Endophilin is diffusely distributed throughout the presynaptic terminal and is not particularly enriched at the synaptic ribbon. All micrographs were obtained by conventional imaging. Abbreviations: INL, inner nuclear layer; OPL, outer plexiform layer; ONL, outer nuclear layer. Scale bars: 10 $\mu$ m (A), 5 $\mu$ m (B, C), 12 $\mu$ m (D), 2 $\mu$ m (E).

### **3.4. Proof of specificity**

To test whether the received immunosignals are real or not, I performed blocking experiments (see material and methods) with the respective antigens and an unrelated control antigen. The blocking experiments show that all the described immunolabelling experiments could be specifically blocked with the respective antigens used for immunization (Figure 23) but not with irrelevant peptides demonstrating the specificity of the immunolabelling analyses.

Figure 23



(legend see next page)

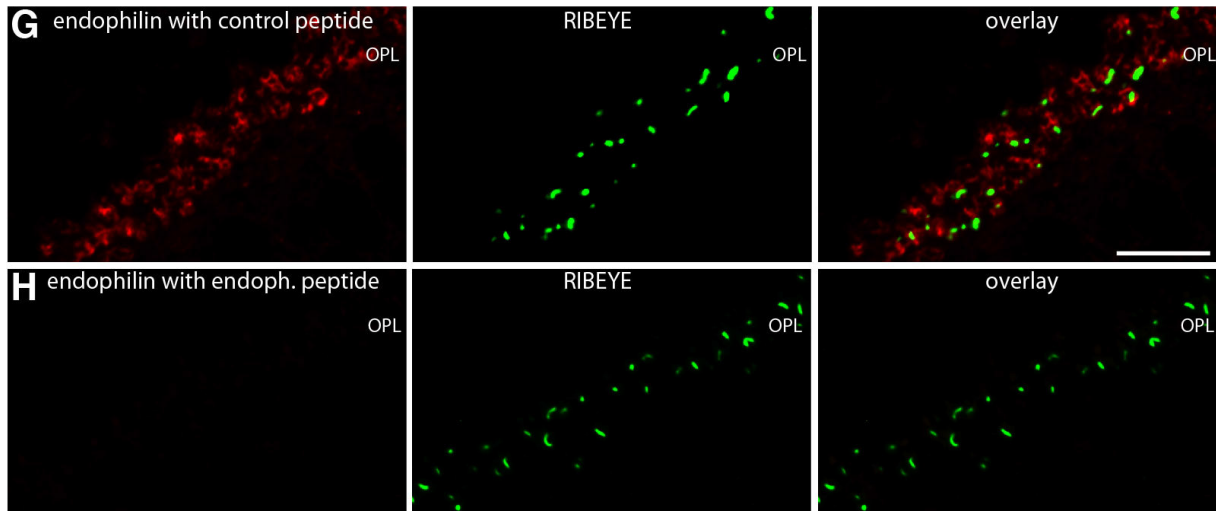


**Figure 23 Pre-absorption control experiments for the immunolabelling analyses.** Double-immunolabelling of 0.5nm-thin mouse retinal sections with the indicated antibodies pre-absorbed with either their specific peptide used for immunization (**B,D,F,H**) or with an unrelated control peptide (**A,C,E,G**). To visualize ribbon synapses, sections were co-immunolabelled with either rabbit polyclonal antibodies against RIBEYE (U2656 in A,B) or mouse monoclonal antibodies against RIBEYE(B)-domain/CtBP2. The specific peptides completely blocked the respective immunosignals at the synaptic ribbon (**B,D,F,H**) whereas the control peptide had no influence of the immunosignals (**A,C,E,G**) showing the specificity of the immunolabelling signals. Abbreviations: OPL, outer plexiform layer. Scale bars: 35 $\mu$ m.

### **3.5. Hight resolution analysis**

The antibodies against amphiphysin/syndapin did not work for postembedding immunogold labelling in my hands. Therefore, I applied SR-SIM (as triple-labelling) to define their position in the presynaptic terminal as precise as possible at the light microscopic level. I performed triple immunolabelling experiments to further characterize the spatial relation of syndapin/amphiphysin to synaptic ribbons and dynamin. Using two-dimensional (2D)-super-resolution structured illumination microscopy (2D-SR-SIM), I found that both amphiphysin as well as syndapin are typically localized and strongly enriched around the synaptic ribbon (Figure 24). The impression was confirmed using 3D-super-resolution structured illumination microscopy (3D-SR-SIM; Figure 25). Both 2D- and 3D-SR-SIM results showed a tubulo-/vesicular-like distribution pattern of syndapin and amphiphysin around the synaptic ribbon (Figures 24, 25).

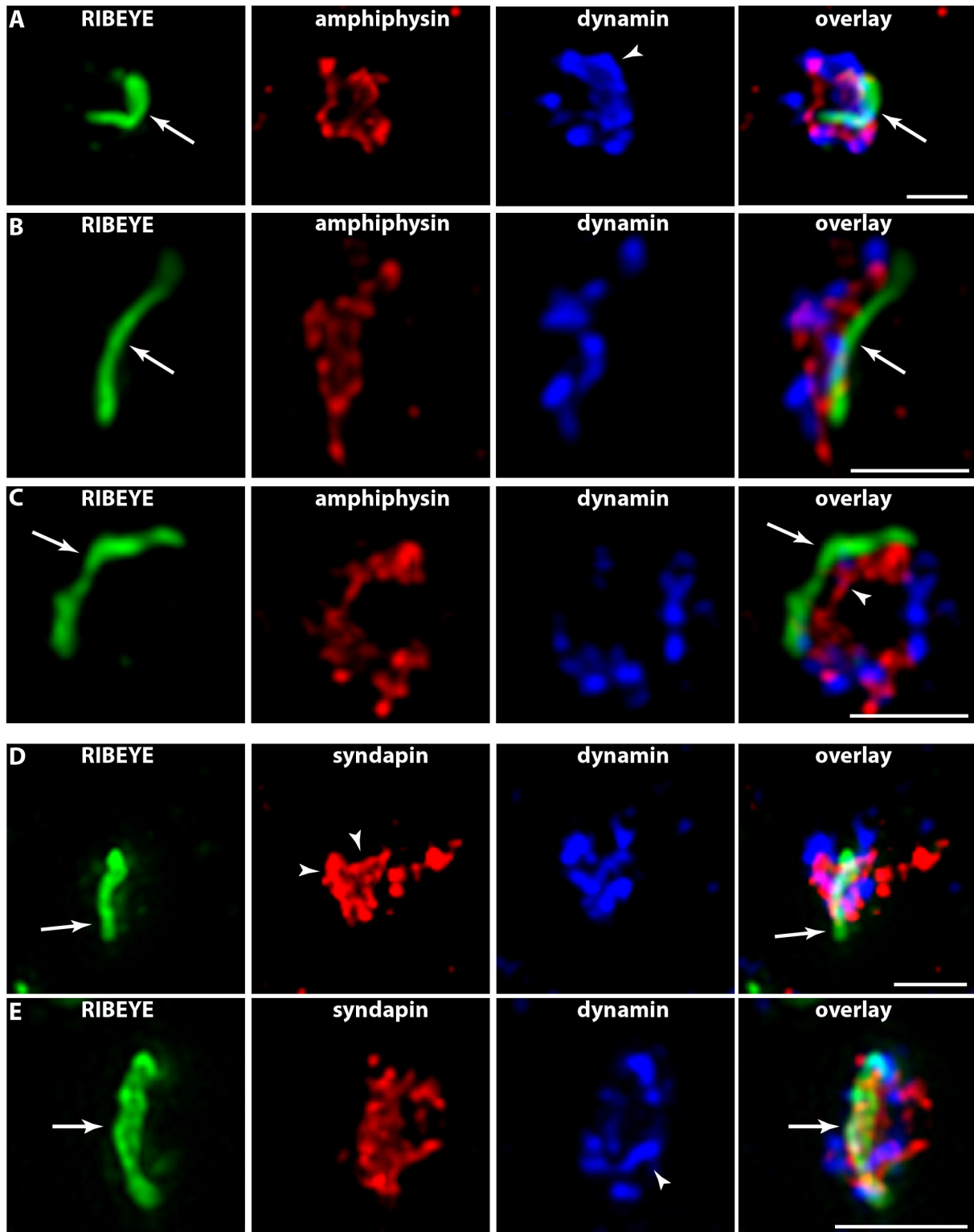


**Figure 24 Multicolor, high resolution 2D-super-resolution SIM images.** 2D super-resolution SIM analyses of thin sections of the mouse retina triple-immunolabelled with directly labelled mouse monoclonal antibody against RIBEYE(B)-domain/CtBP2, rabbit polyclonal antibody against amphiphysin (A-C) or syndapin (D-E) and mouse monoclonal antibody against dynamin. The rabbit primary antibody was detected with donkey anti-rabbit secondary antibody conjugated to Alexa568; binding of the mouse monoclonal antibody was detected with donkey anti-mouse antibodies conjugated to Alexa648. Arrows denote immunolabelled synaptic ribbon; arrowheads to tubulovesicular-like labelling pattern of syndapin-/amphiphysin- immunoreactivity around the synaptic ribbon. Scale bars: 1 $\mu$ m

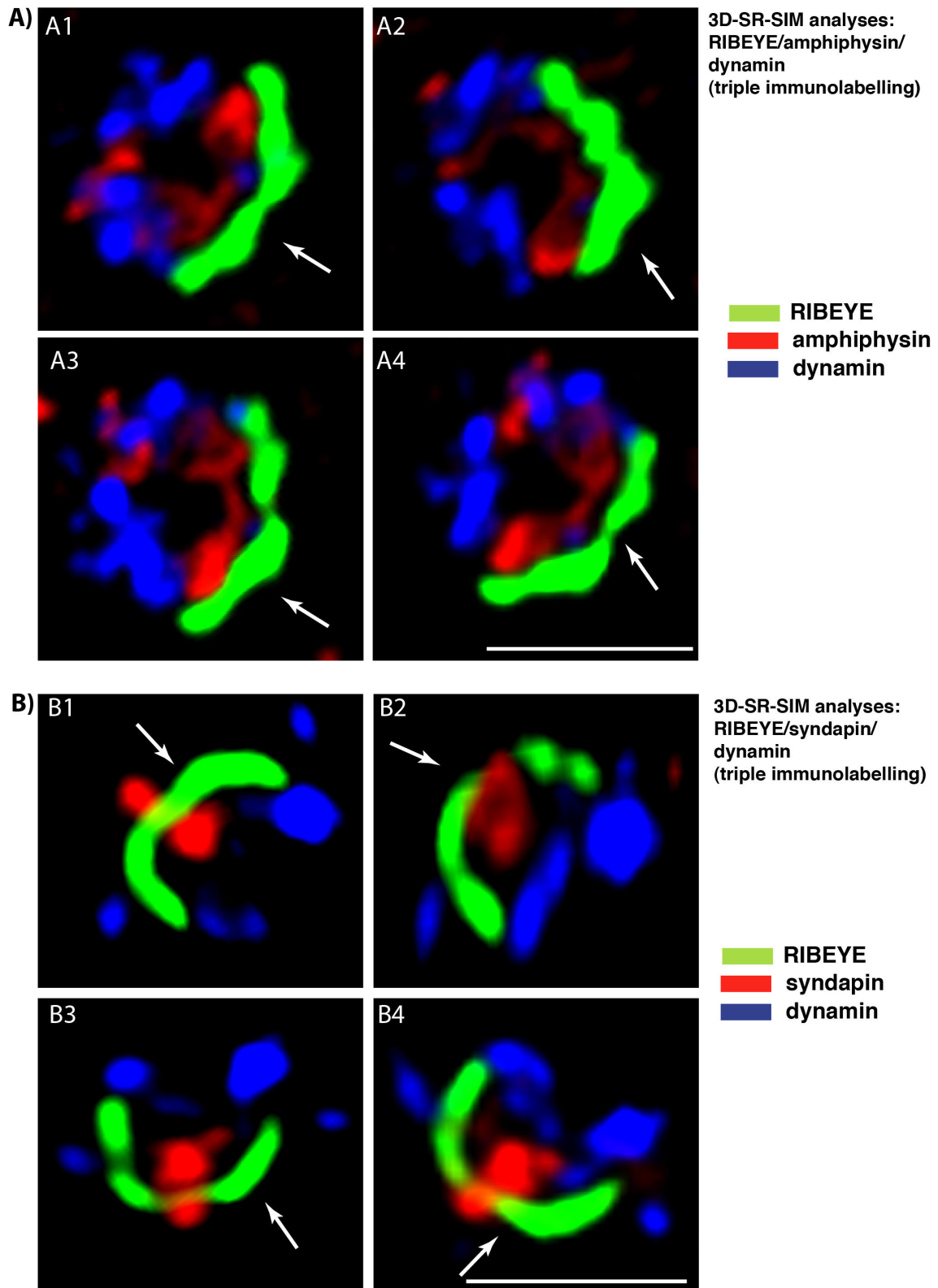


**Figure 25 Multicolor, high-resolution 3D-super-resolution SIM analyses of RIBEYE, dynamin and syndapin/amphiphysin in the active zone of a single photoreceptor synapse.** In (A) triple immunolabellings were performed with antibodies against RIBEYE, dynamin and amphiphysin; in (B) with antibodies against RIBEYE, dynamin and syndapin. (A1-A4 and B1-B4, respectively) denote different views of the same immunolabelled synaptic ribbons in a photoreceptor synapse as analyzed by super-resolution 3D-structured illumination microscopy (SR-3D-SIM). Arrows denote immunolabelled synaptic ribbon. Scale bars: 1  $\mu$ m (A, B).

### **3.6. Localisation of other endocytic proteins**

Interestingly, calcineurin, a  $\text{Ca}^{2+}$ -sensing phosphatase involved in coupling  $\text{Ca}^{2+}$ -dependent activity and endocytosis (for review, see Clayton and Cousin, 2009), is also highly enriched at the synaptic ribbon complex (Figure 26). Thus, influx of  $\text{Ca}^{2+}$  through voltage-gated calcium channels could mediate activity-dependent endocytosis at the synaptic ribbon through such a mechanism (see discussion).

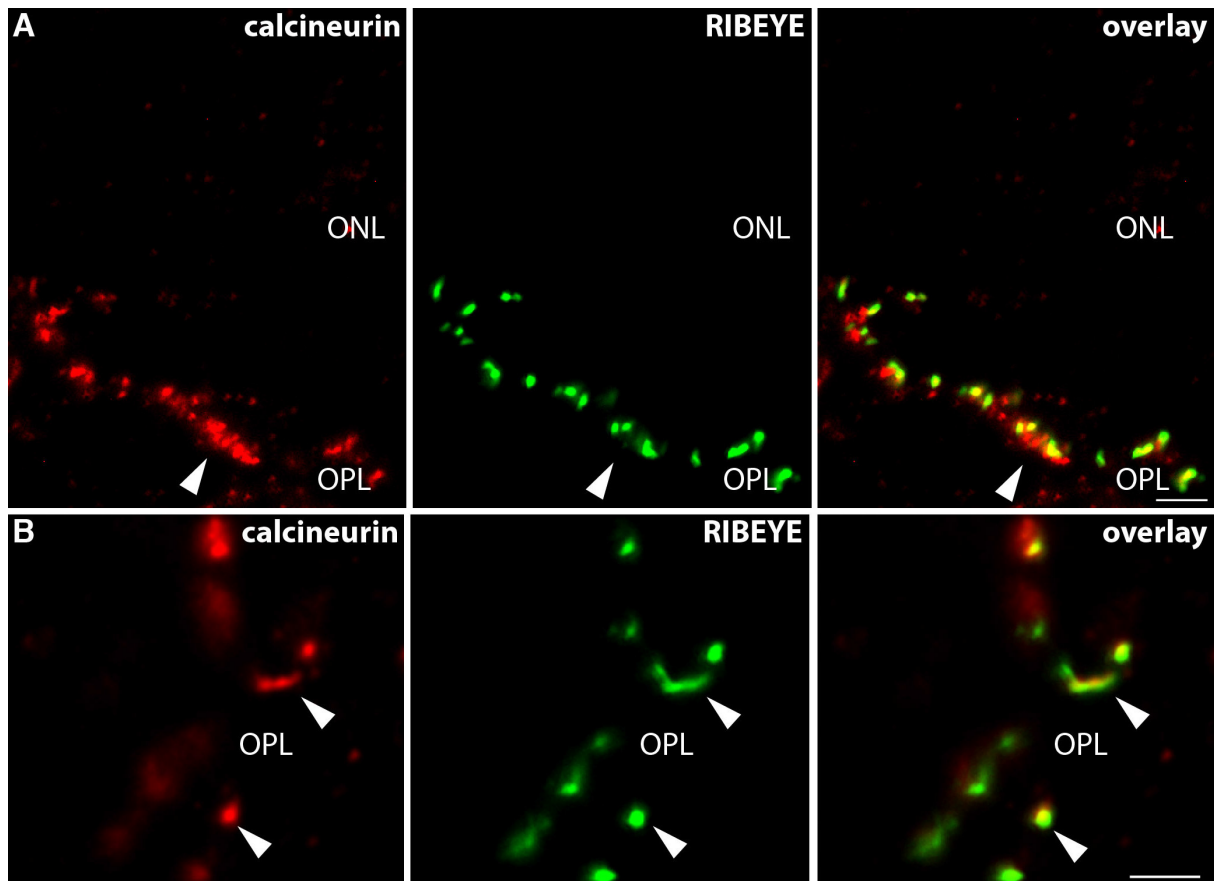
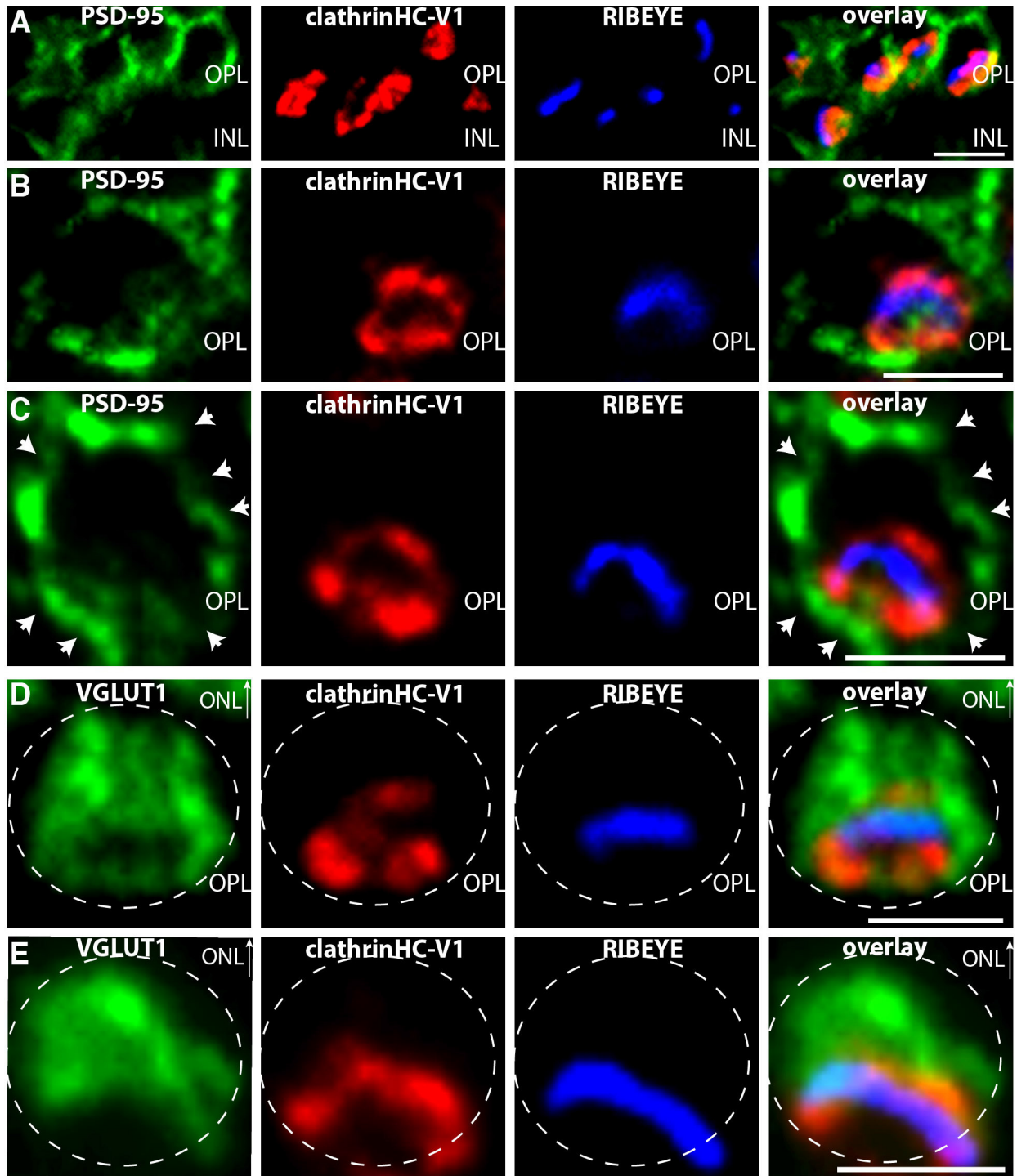


**Figure 26** The  $\text{Ca}^{2+}$ -binding phosphatase calcineurin, a  $\text{Ca}^{2+}$ -sensor of endocytosis, is enriched at the synaptic ribbon. 0.5 $\mu\text{m}$ -thin section of the mouse retina double-immunolabelled with affinity-purified rabbit polyclonal antibodies against calcineurin and mouse monoclonal antibodies against RIBEYE (B)domain/CtBP2 (conventional imaging). Calcineurin is highly enriched at the synaptic ribbons (arrowheads). Abbreviations: ONL, outer nuclear layer; OPL, outer plexiform layer. Scale bars: 10 $\mu\text{m}$

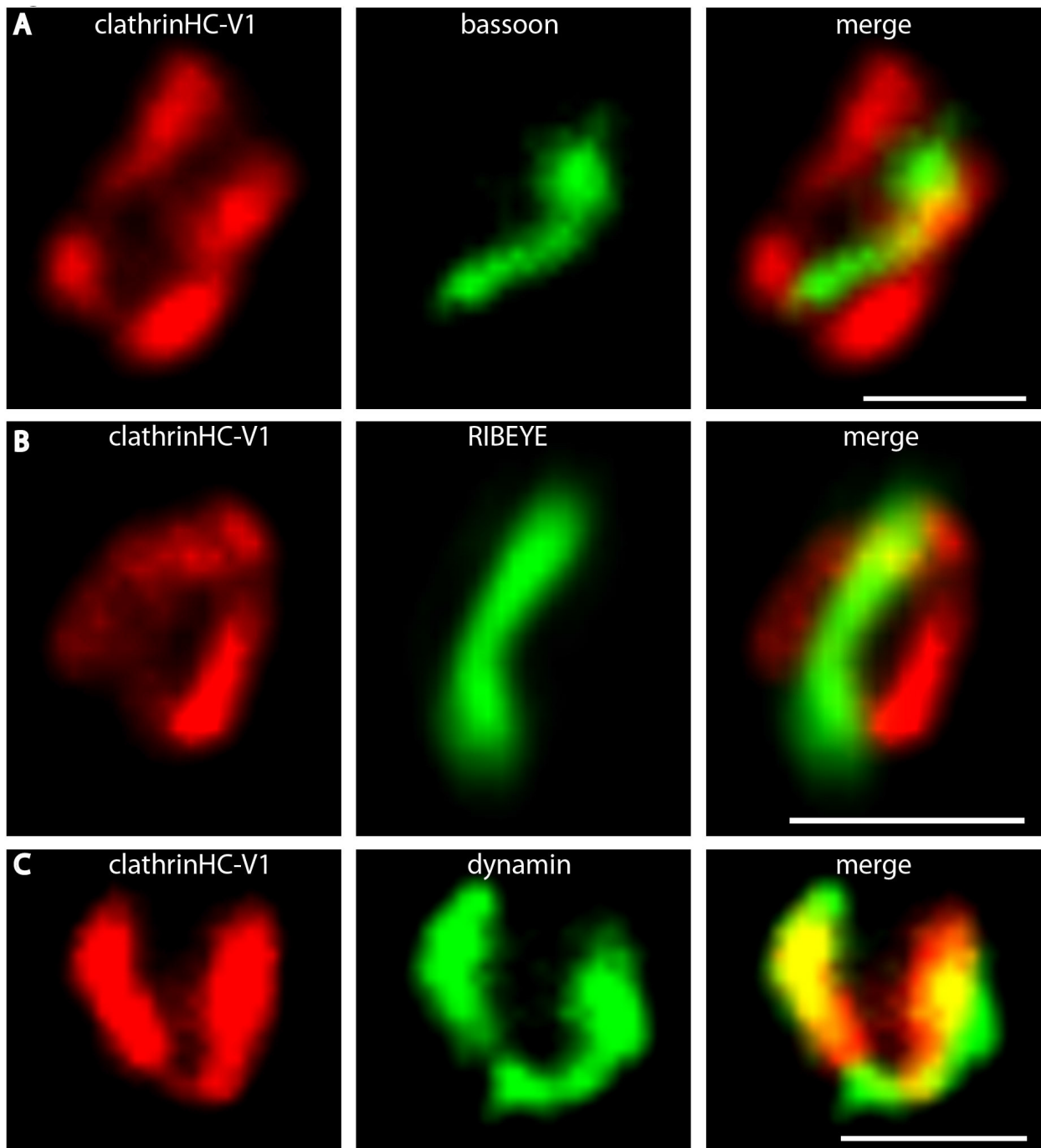
Finally, I analyzed the distribution pattern of clathrin. Clathrin is instrumental for many, though not all, forms of synaptic vesicle endocytosis (for review, see Murthy and de Camilli, 2003; Wilbur et al., 2005; Brodsky, 2012). To analyze the distribution of clathrin in photoreceptor presynaptic terminals, I used four different antibodies against different epitopes of clathrin heavy chain. In humans, two clathrin heavy chain genes (CHC17 and CHC22) are present (for review, see Brodsky, 2012). In the

mouse genome, there is only one active clathrin heavy gene that corresponds to human CHC17. A second clathrin gene in the mouse genome is a non-active pseudogene (Wakeham et al., 2005; for review, see Brodsky, 2012).

Using two different antibodies raised against the carboxyterminus of clathrin heavy chain (abcam; ab21679, Cell Signaling; P1663) I observed a strong clathrin signal in close vicinity of the RIBEYE-immunolabelled synaptic ribbon (Figures 27-29). The clathrin immunosignal was surrounding the synaptic ribbon (Figure 27A, B) that was immunolabelled with antibodies against RIBEYE (Figure 27A, B). The signal is similar to the synaptic ribbon- localized in the distal portion of the synaptic terminal that faces the inner nuclear layer (INL) (Figure 27). The borders of the presynaptic terminal were either marked with antibodies against-PSD-95 that labels the presynaptic plasma membrane of photoreceptor terminals (Figure 27 A-C) or with antibodies against the vesicular glutamate transporter 1 (VGLUT1) (Figure 27 D-E), a component of the presynaptic glutamatergic vesicles. The clathrin variant, detected by these antibodies, is denoted as clathrin heavy chain-variant 1 (CHC-V1) in the following text. CHC-V1 runs at the expected molecular weight of clathrin heavy chain in western blotting analyses (Figure 14F, Figure 31A, lane 1) and the immunosignals could be blocked with the respective immunization peptides (Figure 31 B,D) but not with control peptides (Figure 31C, E) demonstrating the specificity of the immunolabelling data. Clathrin heavy chain variant 1 (CHC-V1) is located and enriched in close vicinity to RIBEYE and bassoon as judged by high resolution immunofluorescence microscopy (Figure 28A, B). The CHC-V1-immunosignal overlapped to a large extent with the dynamin immunosignal (Figure 28C).

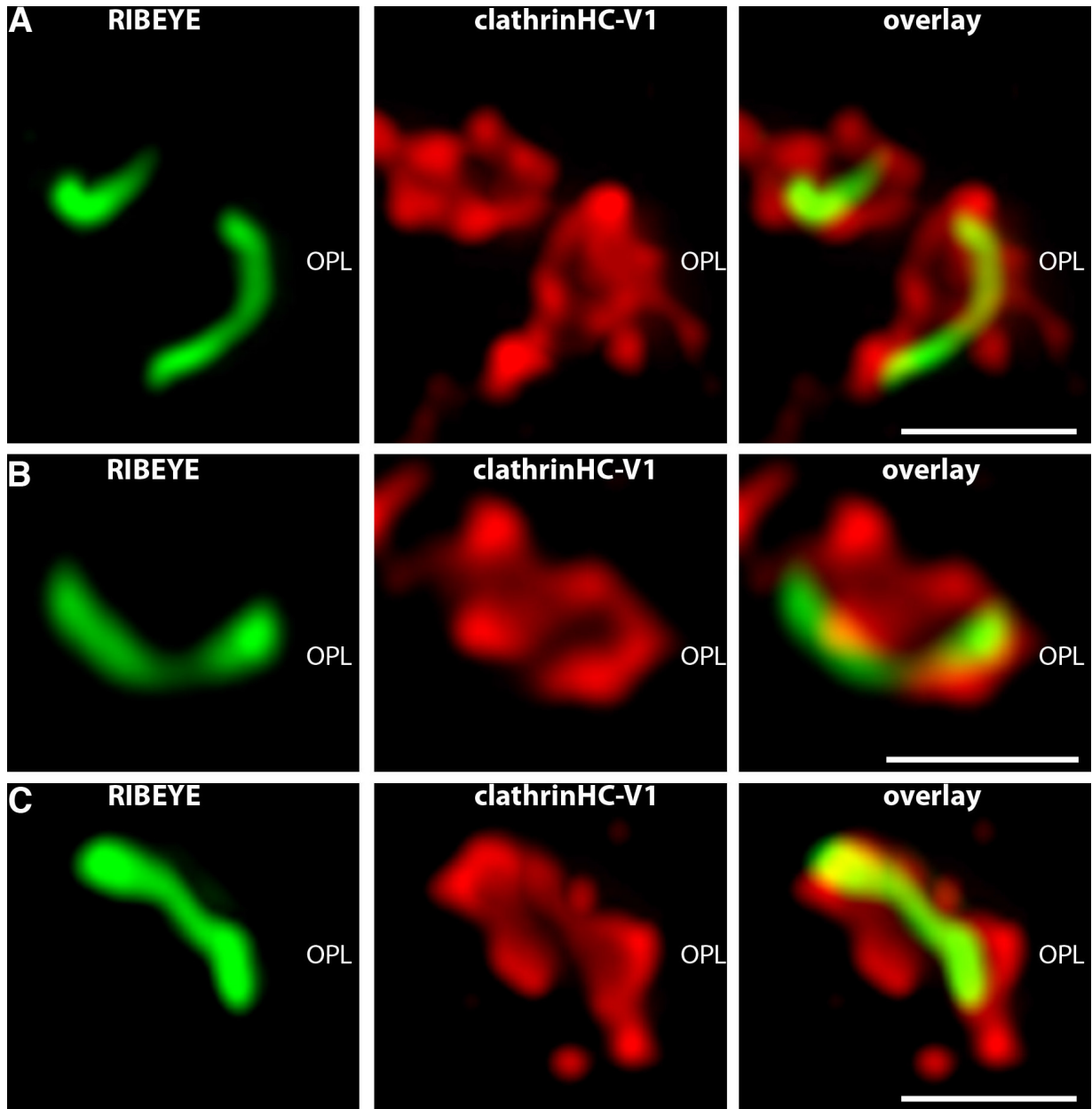


**Figure 27 Localization of clathrin heavy chain (variant 1) in the presynaptic photoreceptor terminal.** 0.5 $\mu$ m-thin sections from mouse retina were triple-immunolabelled with mouse monoclonal antibodies against PSD-95 (A-C)/ or VGLUT1 (D-E), rabbit polyclonal antibodies against clathrin heavy chain (variant-1, abcam) (A-E) and DyLight650-direct labelled primary antibodies against RIBEYE(B)/CtBP2 (A-E). The PSD-95 immunosignals in (A-C) demarcate the plasma membrane of the presynaptic terminals in the OPL (arrowheads in C). In (D-E), presynaptic terminals were immunolabelled with antibodies against the vesicular transporter VGLUT1, a marker protein of glutamatergic synaptic vesicles. Dashed circles in (D, E) denote single presynaptic photoreceptor terminals. RIBEYE and dynamin are located close to each other at the distal end of the photoreceptor terminal that is facing the INL (A-C). Abbreviations: OPL, outer plexiform layer; ONL, outer nuclear layer; INL, inner nuclear layer. Scale bars: 1 $\mu$ m (A-E).



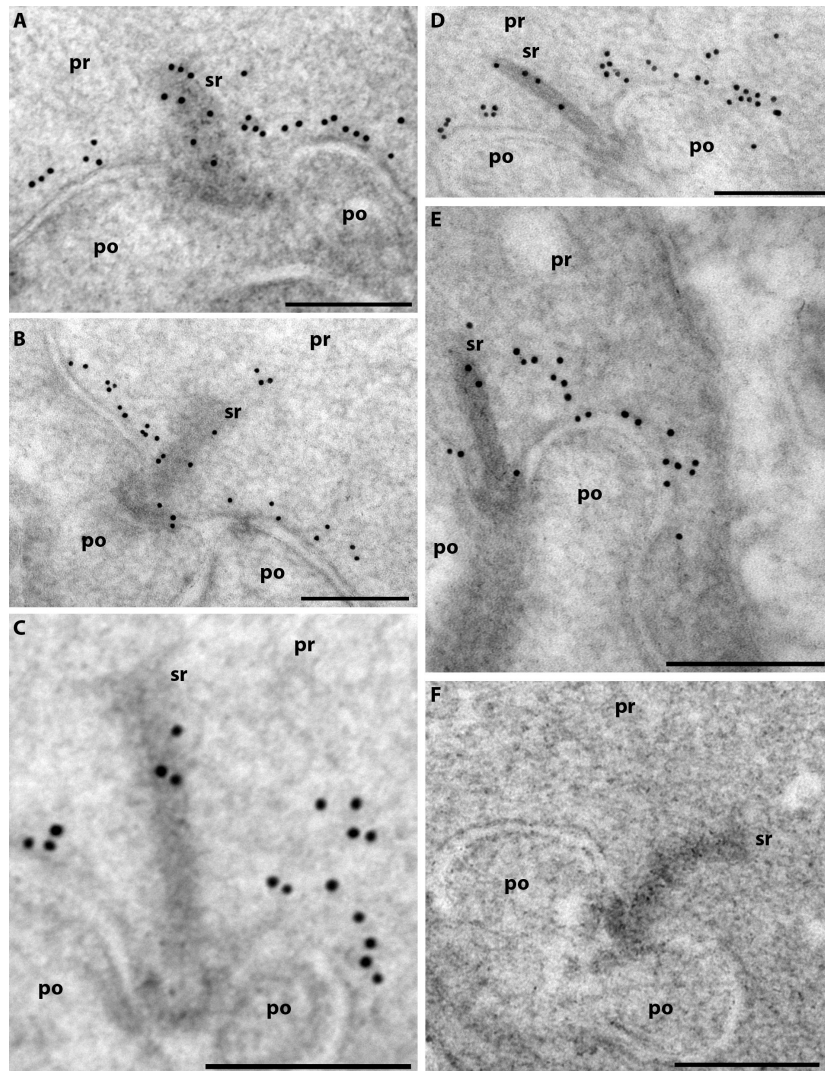
**Figure 28 High magnification analyses of clathrin heavy chain (variant 1) in relation to bassoon, RIBEYE and dynamin in single photoreceptor synapses.** 0.5 $\mu$ m-thin section of the mouse retina double-immunolabelled with rabbit polyclonal antibodies against clathrin heavy chain (variant 1) and mouse monoclonal antibodies against bassoon in (A); In (B) sections were double-immunolabelled with rabbit polyclonal antibodies against clathrin heavy chain (variant 1) and mouse monoclonal antibodies against RIBEYE(B)-domain/CtBP2; In (C) sections were double-immunolabelled with rabbit polyclonal antibodies against clathrin heavy chain (variant 1) and mouse monoclonal antibodies against dynamin. Clathrin heavy chain (variant 1) is located very close to both RIBEYE and bassoon but does not overlap with the respective immunosignals in double immunolabelling experiments. In contrast, the clathrin heavy chain (variant 1) immunosignals overlaps with the dynamin immunosignal at the active zone of photoreceptor ribbon synapses to a large extent. All images were obtained by conventional imaging. Abbreviations: OPL, outer plexiform layer. Scale bars: 1 $\mu$ m (A-C).

Figure 29 shows super-resolution structured-illumination microscopy of thin-sectioned mouse photoreceptor synapses, double-immunolabelled with antibodies against RIBEYE and CHC-V1 further demonstrating a close spatial correlation of these proteins at the synaptic ribbon complex. As shown also before, the CHC-V1 immunosignal surrounded the RIBEYE-labelled synaptic ribbon typically in a distance less than 250nm as judged by SR-SIM analyses.



**Figure 29 Multicolor, high resolution 2D-super-resolution SIM analyses of clathrin heavy chain (variant 1) in relation to synaptic ribbons (maximum projections).** 2D super-resolution SIM analyses of thin sections of mouse retina double-immunolabelled with mouse monoclonal antibody against RIBEYE(B)-domain/CtBP2 and rabbit polyclonal antibody against clathrin heavy chain, variant 1 (CHC-V1) (A-C). Clathrin heavy chain (variant 1) is located in close proximity to the RIBEYE-labelled synaptic ribbon. Abbreviations: OPL, outer plexiform layer. Scale bars: 1 $\mu$ m (A-C).

Finally, postembedding immunogold electron microscopy with antibodies against CHC-V1 demonstrated that the strongest CHC-V1 immunosignal was found actually at the presynaptic plasma membrane in close proximity (less than 200nm) of the synaptic ribbons (Figure 30). These ultrastructural data completely confirm and extend the light microscopic CHC-V1 immunolabelling data and show the localization of CHC-V1 in the peri-active zone (Figure 30) similar as shown above for dynamin (Figure 19).



**Figure 30 Postembedding immunogold labelling of photoreceptor synapses from the mouse retina with antibodies against clathrin heavy chain (variant 1).** (A-E) Ultrathin sections immunolabelled with mouse monoclonal antibodies against clathrin heavy chain (clhc-V1; abcam). Binding of the primary antibodies was detected with goat anti-rabbit antibodies conjugated to 10nm gold particles. A strong clathrin-hc-V1 immunogold label could be observed at the plasma membrane in close proximity to the synaptic ribbon (sr). The immunogold labelling experiments confirm the previously shown immunofluorescence labelling data and demonstrate the enrichment of clathrin heavy chain variant 1 (clhc-V1) in the peri-active zone of the photoreceptor ribbon synapse. (F) is a negative control in which the primary antibody was omitted. Abbreviations: pr, presynaptic photoreceptor terminal; po, postsynaptic dendrites of the photoreceptor synaptic complex; sr, synaptic ribbon. Scale bars: 250nm (A-F).

Furthermore, I found evidence for a second clathrin-containing compartment that is not spatially related to the synaptic ribbon. This clathrin-containing compartment was labelled by two different antibodies directed against epitopes in the central region of clathrin heavy chain (Abcam/ab59710; X22/Abcam). This clathrin heavy chain variant detected by these latter antibodies is denoted as clathrin heavy chain variant 2 (CHC-V2) in the following text. CHC-V2 migrates slightly slower than CHC-V1 at a slightly higher molecular weight position (Figure 31A). This becomes obvious if low percentage (5%) acrylamide SDS-PAGE gels (Figure 31A) were used (instead of 8% acrylamide running gels; Figure 14G).

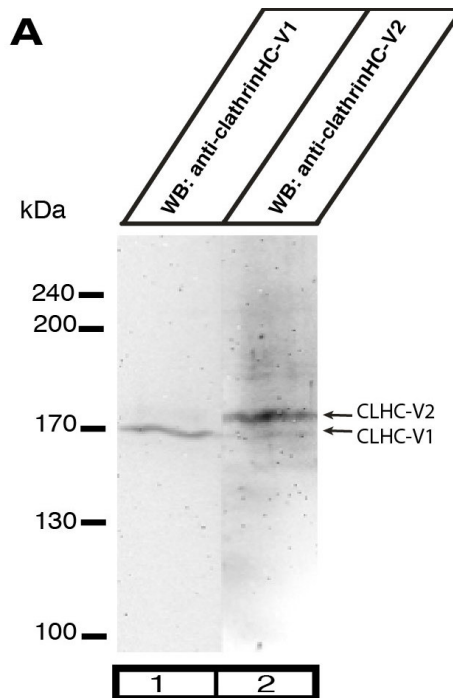


**Figure 31 (A) Western blot analyses of clathrin heavy chain, variant 1 and variant 2 (after separation in 5% acrylamide running gels).** The running position of the immunoreactive bands detected by the different antibodies against the clathrin heavy chain variant 1 (lane 1) and antibodies against clathrin heavy chain variant 2 (lane 2) differ slightly. Clathrin heavy chain variant 1 shows a slightly lower running position than variant 2.

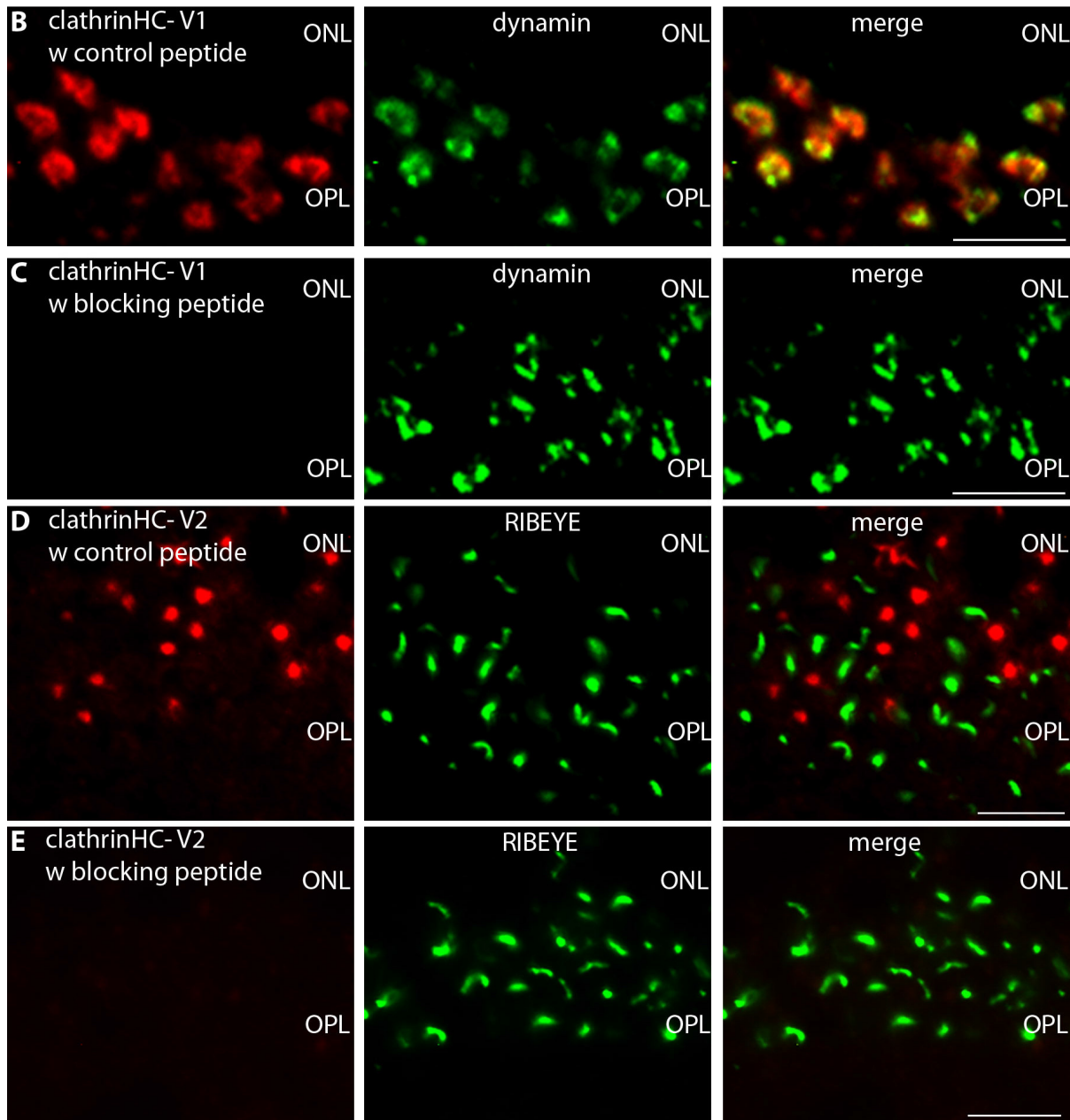
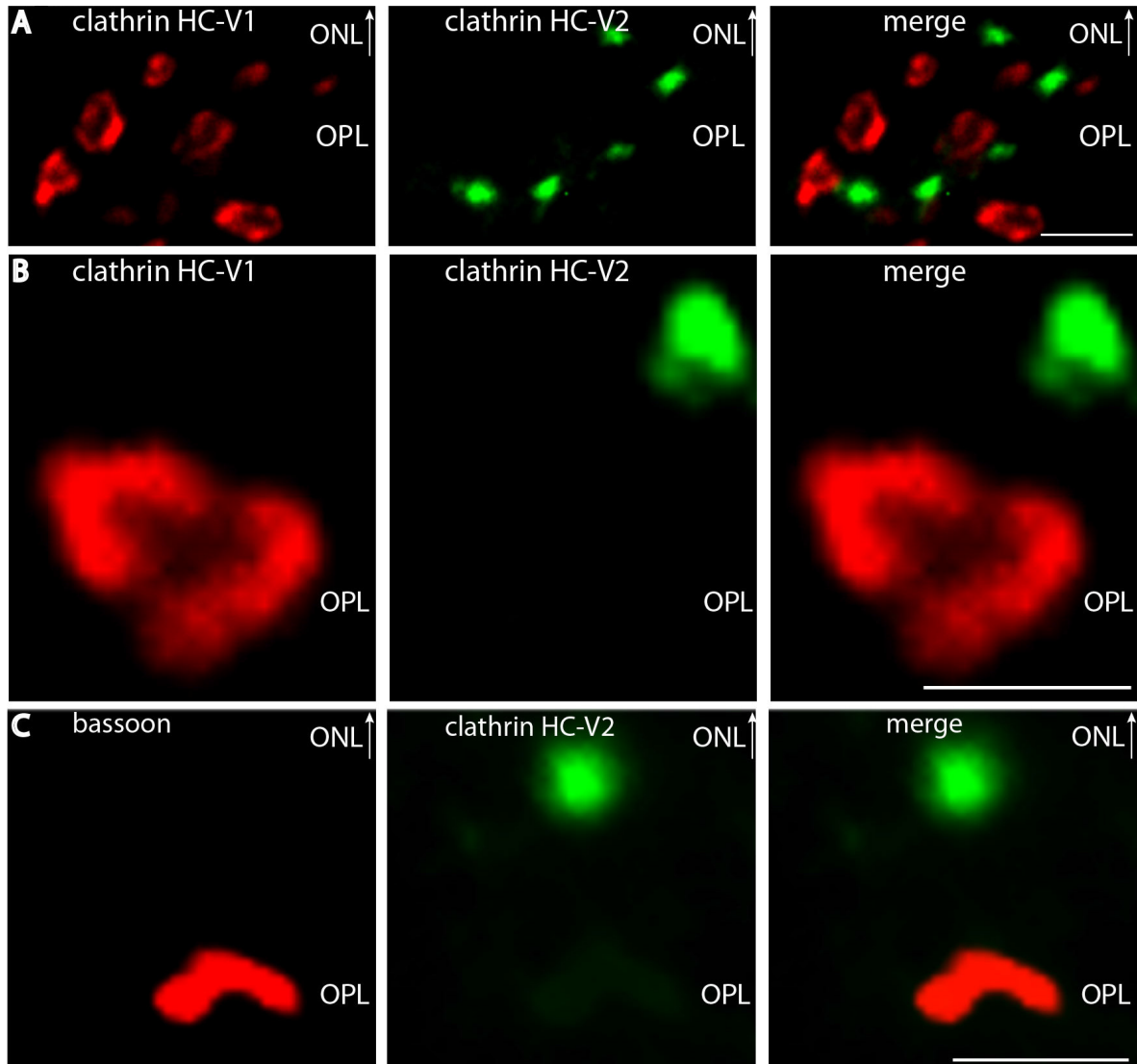


**Figure 31 (B-E) Pre-absorption control experiments for the antibodies against clathrin heavy chain variants 1 and 2 (immunolabelling analyses).** Double-immunolabelling of 0.5 $\mu$ m-thin mouse retinal sections with the indicated antibodies pre-absorbed with either their specific peptide used for immunization (**C, E**) or with an unrelated control peptide (**B, D**). In parallel, sections were incubated with monoclonal anti-dynamin antibodies (**B, C**) or RIBEYE (**D, E**) as labelling positive controls. The specific peptides completely blocked the respective clathrin heavy chain immunosignals (**C, E**) whereas the control peptide had no influence of the clathrin heavy chain immunosignals (**B, D**) showing the specificity of the immunolabelling signals. Abbreviations: OPL, outer plexiform layer; ONL, outer nuclear layer. Scale bars: 5 $\mu$ m (B-E).

In immunolabelling analyses, CHC-V2 is located in a large distance from both RIBEYE and the active zone protein bassoon as judged by high resolution double-immunolabelling analyses (Figure 32). The mean distance of CHC-V2 from RIBEYE- and bassoon puncta (nearest, mean distance) is  $\approx$ 580nm ( $\pm$ 210nm s.d., 100

synapses analyzed) for CHC-V2-RIBEYE and  $\approx 750\text{nm}$  ( $\pm \approx 200\text{nm}$  s.d.; 100 synapses analyzed).

Figure 32



(legend see next page)

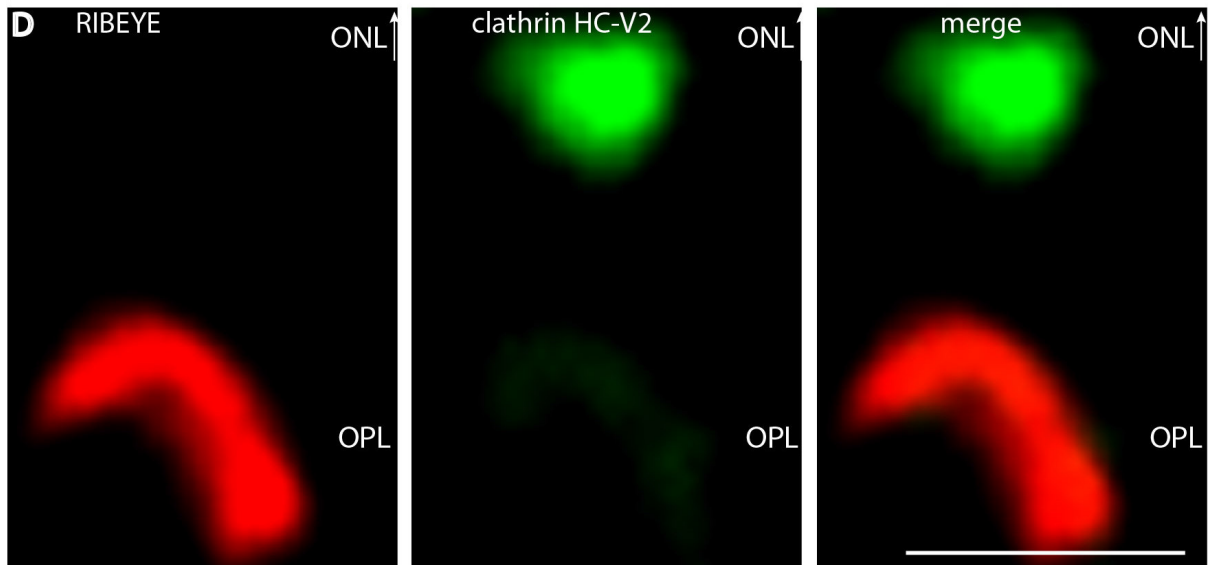


**Figure 32 Two different clathrin heavy chain variants are found in photoreceptor terminals at different locations (immunolabelling analyses).** 0.5 $\mu$ m-thin section of the mouse retina double-immunolabelled with rabbit polyclonal antibodies against clathrin heavy chain (variant 1; A-B) and mouse monoclonal antibodies against clathrin heavy chain (variant 2; A-D). The immunosignals for the two variants of clathrin heavy chain do not overlap and are located in a large distance from each other. In (C-D), sections were double-immunolabeled with antibodies against bassoon and RIBEYE to relate the localization of clathrin heavy chain, variant 2, to the localization of these proteins in the presynaptic terminal. Also bassoon and RIBEYE are localized in a large distance from immunolabelled clathrin heavy chain, variant 2. For further localization data of clathrin heavy chain, variant 2, in relation to other proteins of the presynaptic terminal, see also Fig. 19. Abbreviations: OPL, outer plexiform layer; ONL, outer nuclear layer. Scale bars: 1 $\mu$ m (A-D).

Despite the large distance of CHC-V2 from the synaptic ribbon, CHC-V2 is still located in the presynaptic terminal as judged by triple-immunolabelling experiments with antibodies against PSD-95/ VGLUT1, RIBEYE and anti-CHC-V2 (Figure 33). But, in contrast to CHC-V1, CHC-V2 is located in the proximal portion of the presynaptic terminal, which is separated from the synaptic ribbon by the bulk of glutamatergic synaptic vesicles (Figure 33 C, D). The antibodies against CHC-V2 did not work in postembedding immunogold electron microscopy in my hands. But since this clathrin variant is clearly not associated with the synaptic ribbon complex the identification of the underlying organelle, though principally important, is of minor relevance for the present study which is concerned with vesicle retrieval in the perisynaptic zone surrounding the synaptic ribbon complex (see also discussion).

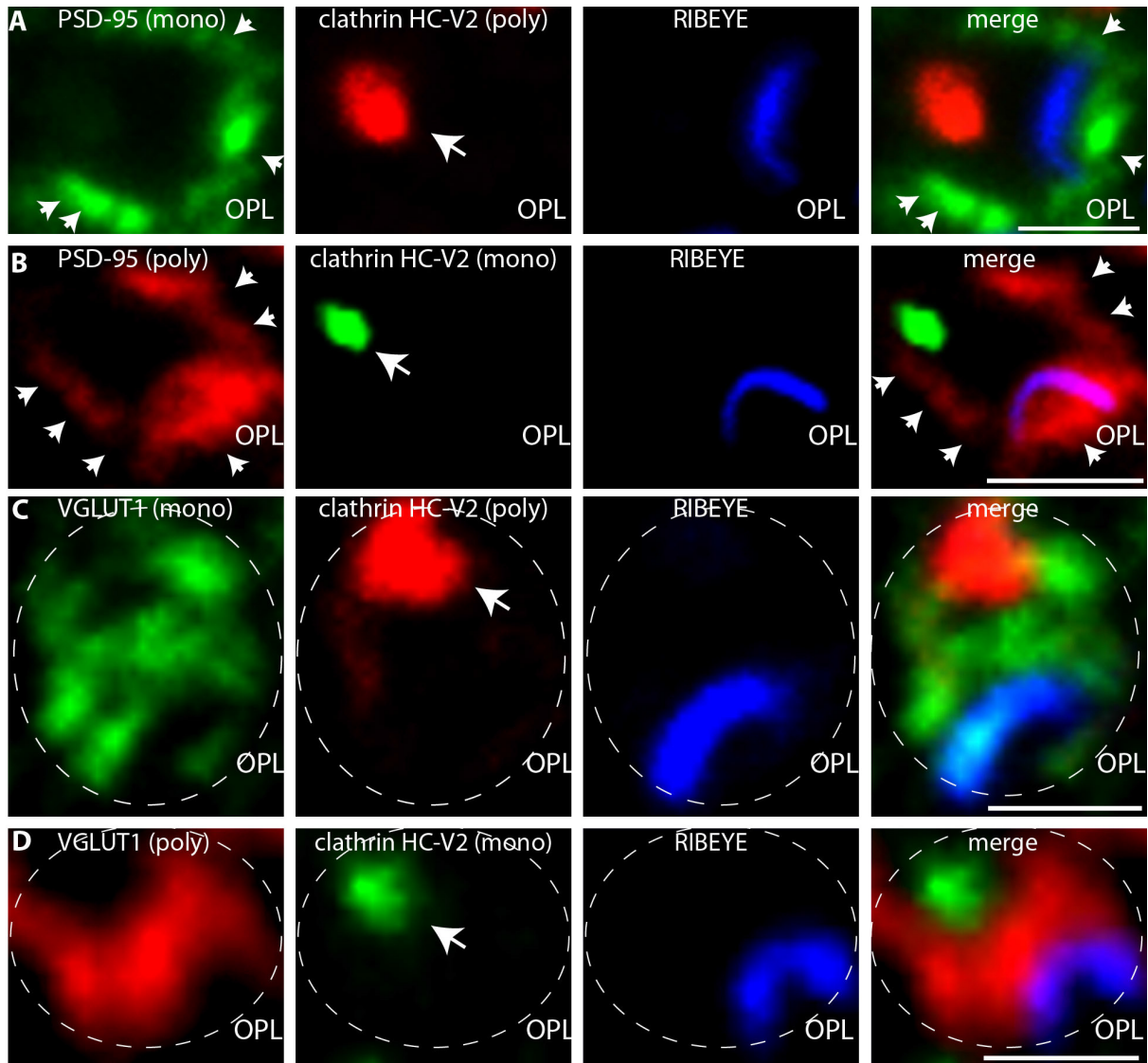
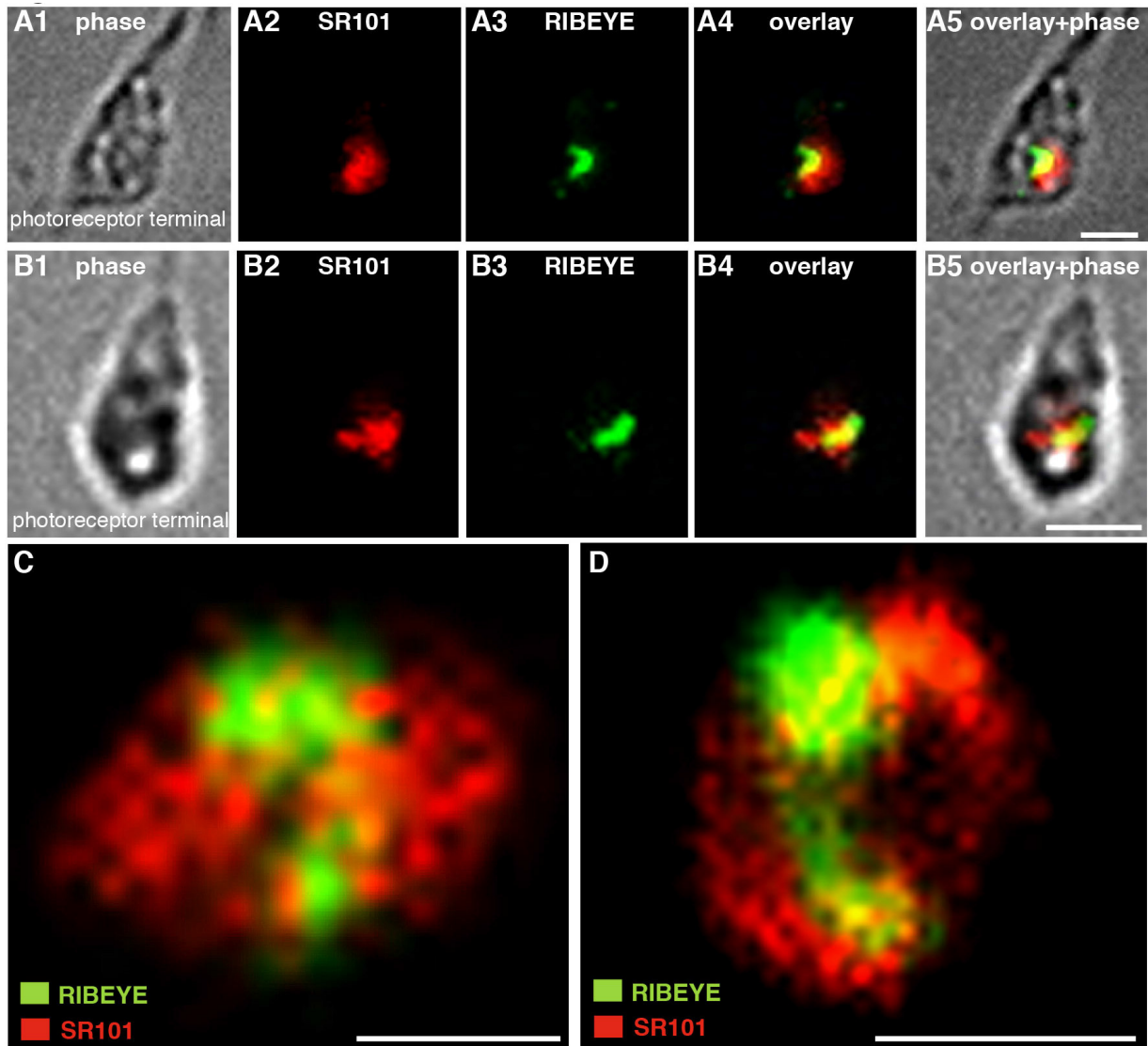


**Figure 33 Two clathrin heavy chain variants are differentially localized in photoreceptor presynaptic terminals (further immunolabelling analyses).** In (A,C) 0.5 $\mu$ m-thin section of the mouse retina triple-immunolabelled with rabbit polyclonal antibodies against clathrin heavy chain (variant 2; A-B) and mouse monoclonal antibodies against either PSD-95 (A) or VGLUT1 (C). The synaptic ribbon was visualized with a DyLight650-labelled primary antibody against RIBEYE(B)-domain/CtBP2. The PSD-95 immunolabel demarcates the plasma membrane of the entire photoreceptor presynaptic terminal (small arrows). The clathrin variant 2 antibody labelled a spot-like structure (big arrows) in the presynaptic terminal that, in contrast to clathrin heavy chain variant 1, was localized in a large distance from the synaptic ribbon. A virtually identical immunolabelling pattern was obtained if the sections were triple-immunolabelled with a monoclonal antibody against clathrin heavy chain, variant 2, a rabbit polyclonal antibody against PSD-95 and the DyLight650 directly-labelled antibody against RIBEYE(B)-domain/CtBP2 (B). In (D), presynaptic vesicles were immunolabelled with antibodies against VGLUT1. Similarly to the previously shown data, the clathrin heavy chain variant 2 was located at the entry of the presynaptic terminal separated from the synaptic ribbon by the bulk of glutamatergic synaptic vesicles. This distribution of clathrin heavy chain variant 2 is in contrast to the distribution of clathrin heavy chain, variant 2 which is located at the synaptic ribbon at the same end of the presynaptic terminal (compare Fig. 13D, E). Dashed circles in (D, E) denote single presynaptic photoreceptor terminals. Abbreviations: OPL, outer plexiform layer. Scale bars: 1  $\mu$ m (A-D).

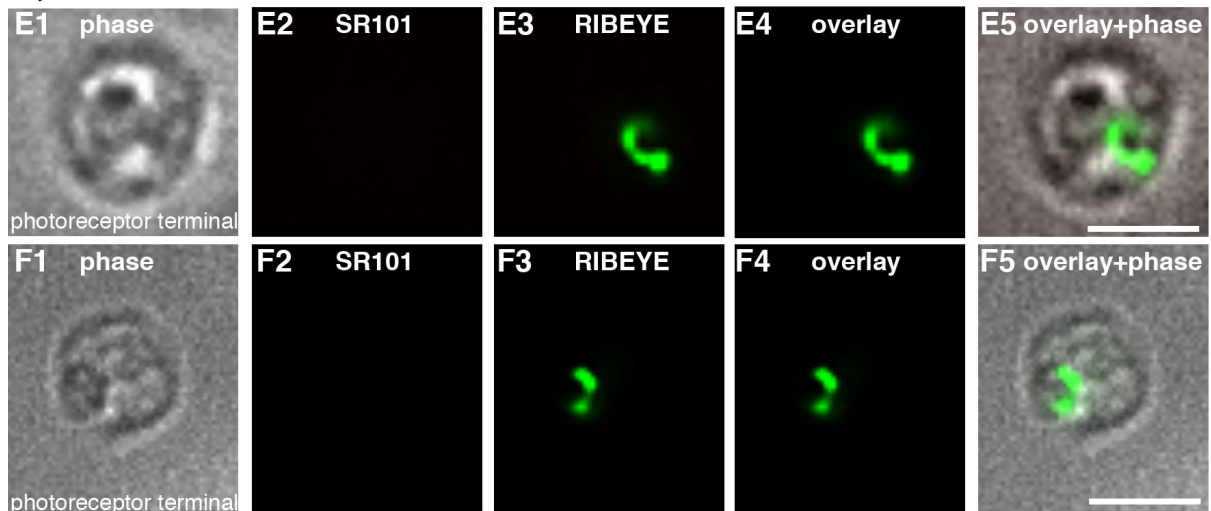
Finally, together with Rashmi Katiyar, I demonstrate that also functionally the synaptic ribbon complex is a hotspot of endocytic activity. If isolated mouse photoreceptors were loaded with a short pulse of the fluid-phase marker sulforhodamine (SR101), SR101 was predominantly taken up in immediate vicinity to the synaptic ribbon (Figure 34). The synaptic ribbon was immunolabelled by antibodies against RIBEYE in these experiments. The uptake of SR101 was dependent upon dynamin activity because SR101 uptake was completely blocked in the presence of dynasore, a specific inhibitor of dynamin activity (Figure 34 E-F). We obtained the same result using the FM1-43 Dye (data not shown).

Figure 34



(legend see next page)

Dynasore-treated



**Figure 34 Imaging of synaptic ribbon-associated endocytosis in isolated mouse photoreceptors.** Isolated mouse photoreceptors were incubated for 2min with sulforhodamine (SR101), which is taken up by fluid phase endocytosis. SR101-loaded photoreceptors were fixed and immunolabelled with antibodies against RIBEYE(B)-domain/CtBP2. A hot-spot of SR101 uptake is found in close association to the synaptic ribbon (**A-E**). (A, B) were obtained by conventional imaging; (C, D) by maximum projections of z-stacks from confocal images. In (E, F), isolated photoreceptors were pre-incubated with dynasore, a specific inhibitor of dynamin: Pre-treatment with dynasore (100mM) completely inhibits the synaptic ribbon-associated uptake of SR101. Scale bars: 1 $\mu$ m (A-F). [experiment was done together with Rashmi Katiyar]

## **4. Discussion**

In the present study, I analyzed the endocytic machinery of photoreceptor synapses with high-resolution immunolabelling techniques and found a strong enrichment of major endocytic proteins in the area surrounding the active zone and the synaptic ribbon (for working hypothesis see Figure 35). In agreement with the focal enrichment of endocytic proteins, I observed a preferential uptake of sulforhodamine (SR101), a fluid phase endocytosis marker, in close vicinity to the synaptic ribbon in mouse photoreceptor terminals (same results were obtained with FM1-43/ data not shown). Thus, the local enrichment of endocytic proteins around the synaptic ribbon correlates also with the respective functional endocytic activity at that site. These data suggest that the peri-active zone region surrounding of the synaptic ribbon in photoreceptor synapses is a hotspot of endocytic vesicle retrieval. Dynamin plays an essential role to peri-active zone endocytosis around the synaptic ribbon because dynasore, a specific inhibitor of dynamin activity, completely inhibited ribbon complex-associated uptake of SR101. Visualization of peri-active zone endocytosis in photoreceptor terminals was achieved by short loading pulses with sulforhodamine (SR101). Longer tracer loading times generate a more diffuse labelling pattern of the presynaptic terminal (data not shown) similar to HRP-uptake experiments in previous EM studies (Ripps et al., 1976; Schacher et al., 1976; Schaeffer and Raviola, 1978; Cooper and McLaughlin, 1983).

The peri-active zone vesicle retrieval at the synaptic ribbon could promote rapid and efficient retrieval of synaptic vesicle components, which is particularly important for the tonically active ribbon synapses. The proposal of ribbon-associated vesicle retrieval is in line with recent findings that supported a major role of synaptic ribbons for replenishment of release-ready synaptic vesicles (Jackman et al., 2009; Babai et al., 2010). Focal, peri-active zone endocytosis around the photoreceptor active zone appears conceptionally similar to peri-active zone endocytosis previously found also in other synapses with different properties, e.g. in lamprey neurons, neuromuscular junction and hippocampal synapses (for review, see Shupliakov, 2009; Haucke et al., 2011; Yamashita, 2012; Saheki and DeCamilli, 2012). Consequently, tuning and regulation of peri-active zone endocytosis can be expected to differ strongly in these different types of tonic and non-tonic synapses.

In general, different forms of endocytosis involve different sets of proteins (for review, see Wu et al., 2007; Doherty and McMahon, 2009; Dittman and Ryan, 2009; Donaldson et al., 2009; Scita and Di Fiori, 2010; Sandvig et al., 2011; Saheki and De Camilli, 2012). I found dynamin as well as the dynamin-associated proteins syndapin/pacsin and amphiphysin highly enriched in close vicinity to the synaptic ribbons. In agreement with the light microscopic immunolabelling data, dynamin was found preferentially localized to the presynaptic plasma membrane next to the synaptic ribbon, as judged by postembedding immunogold electron microscopy. These ultrastructural data further support the concept of peri-active zone endocytosis in ribbon synapses. Endophilin was also found at the synaptic ribbon but predominantly diffusely throughout the entire presynaptic terminal. In conventional synapses, endophilin is also distributed diffusely in the entire synaptic vesicle pool although endophilin acts at the plasma membrane (Bai et al., 2010). Also, the peri-active zone component intersectin is known to cycle between different locations in the synapse (for review, see Shupliakov, 2009; Pechstein et al., 2010; Haucke et al., 2011). Remarkably, I detected two immunologically distinct forms of clathrin heavy chain in the presynaptic photoreceptor terminal, CHC-V1 and CHC-V2. CHC-V1 was associated with the synaptic ribbon complex, as judged by immunolabelling with two different antibodies against CHC-V1, whereas CHC-V2 was not localized at synaptic ribbons. The identity and function of this CHC-V2-containing organelle needs to be analyzed in detail by future investigations. In contrast, clathrin heavy chain-variant 1 is present at the synaptic ribbon complex, where it overlaps with dynamin immunoreactivity. In support of these light microscopic data, I showed by postembedding immunogold electron microscopy that CHC-V1 is preferentially localized at the presynaptic plasma membrane in close vicinity to the active zone and synaptic ribbon. The antibodies against CHC-V2 did not work for postembedding immunogold electron microscopy in my hands. But the CHC-V2 immunosignals were clearly localized in a large distance ( $\approx 580\text{nm}$ ) from the bassoon-labelled active zone in the proximal part of the presynaptic terminal.

The reason for these two completely different located clathrin immunosignals might be the effect of different splice variants of the clathrin gene. It was already shown that due to gene duplication two different CHCs, CHC 17 and CHC22, exist. Both CHCs are 85% identical in their protein sequence, but the remaining 25% could perhaps lead to a different localisation. Lemmon and Traub (2012) reviewed recently the

interaction between the terminal domain of clathrin and clathrin-binding proteins. In this domain also a difference between CHC17 and CHC22 (see Figure 7) was shown. This could be the explanation why CHC-V2 is not located close to the typical „neighbor” proteins like Dynamin1. On the other hand I focused on mouse retinal tissue in this work, in mice CHC22 is only a pseudogene (Wakeman et al.), therefore it should not be expressed. Another explanation could be that CHC-V2 is another structural form of CHC17. As Brodsky (2012) reviewed, CHC17 can form several types of structures such as budded coated vesicles. The identity of this CHC-V2-containing compartment in the photoreceptor terminal needs to be revealed by future investigations.

My proposal of peri-active zone endocytosis in photoreceptor synapses is in agreement with electron microscopic data that demonstrated coated buds and -vesicles at the presynaptic plasma membrane lateral to the synaptic ribbon (e.g. Gray and Pease, 1971). These coated membranes were located in pouches of the presynaptic terminals located lateral to the synaptic ribbon and opposite to the dendritic tips of horizontal cells. These are exactly the sites where I found enrichment of dynamin and a clathrin (CHC-V1) using postembedding immunogold electron microscopy.

Previous analyses, mostly obtained from electrophysiological analyses of retinal bipolar cells and inner ear hair cells, revealed at least two distinct modes of endocytosis in ribbon synapses: a fast phase and a slow phase of endocytosis (with time constants of about  $\approx 1$ s and of  $\approx 15$ -30s; e.g. Neves and Lagnado, 1999; Moser and Beutner, 2000; Beutner and Moser, 2001; for review, LoGiudice and Matthews, 2007; Wu et al., 2007; Smith et al., 2008; Schmitz, 2009; Royle and Lagnado, 2010). In terms of its localization close to the active zone, the ribbon complex-associated endocytic machinery would be ideally suited to serve fast endocytosis in photoreceptors. On the other hand, in retinal bipolar cells fast endocytosis was found to be clathrin-independent though (Jokusch et al., 2005).

The local peri-active zone endocytic machinery in photoreceptor synapses will be exposed to fluctuations of presynaptic  $[Ca^{2+}]_i$  that results from  $Ca^{2+}$ -influx through voltage-gated  $Ca^{2+}$ -channels at the active zone. The role of  $Ca^{2+}$  for various forms of endocytosis is not yet completely understood (for review, see Smith et al., 2008; Shupliakov, 2009; Yamashita, 2012). But many recent studies demonstrated that increases of  $[Ca^{2+}]_i$  can promote and activate endocytosis (Neves and Lagnado,

1999; Neves et al., 2001; Beutner et al., 2001; Wu et al., 2005, 2007, 2009b; Hosoi et al., 2009; Kim and von Gersdorff, 2009; Babai et al., 2010; Schnee et al., 2011). Recent analyses of vesicle retrieval suggested that vesicle replenishment at the photoreceptor ribbon synapse occurs close to presynaptic voltage-gated  $\text{Ca}^{2+}$ -channels and could be stimulated by increases of presynaptic  $\text{Ca}^{2+}$  (Babai et al., 2010).

I found calcineurin, a  $\text{Ca}^{2+}$ -activated, calmodulin-dependent phosphatase localized in close vicinity to the synaptic ribbon. In conventional synapses, calcineurin is a  $\text{Ca}^{2+}$ -dependent regulator of endocytosis that adjusts activity-dependent endocytosis by dephosphorylating endocytic proteins, e.g. dynamin. By this way, calcineurin can control functionally important protein-protein interactions and endocytic networks (for review, see Cousin and Robinson, 2001, Clayton and Cousin, 2009; Yamashita, 2012). Thus, calcineurin is a potential  $\text{Ca}^{2+}$ -sensor that could adjust local, ribbon-associated endocytosis to different levels of synaptic activity also in photoreceptor ribbon synapses. Calcineurin specifically binds to the dynamin-1Xb splice isoform of dynamin-1 (Xue et al., 2011; Bodmer et al., 2011) predicting that this dynamin splice variant is present at synaptic ribbons of photoreceptor synapses. Clearly, also other possibilities could apply. In conventional synapses various mechanisms are known to be installed that regulate endocytosis (for review, see Südhof, 2004, 2012; Shupliakov, 2009; Koch and Holt, 2012, Yao et al., 2012; Yamashita, 2012).

Recently, it was demonstrated that CtBP proteins perform an important role in mediating certain aspects of endocytosis (Bonazzi et al., 2005; Amstutz et al., 2008; Liberali et al., 2008; for review, see Hansen and Nichols, 2009). RIBEYE is also a member of the CtBP protein family and could possibly fulfill a similar role in the ribbon synapse. Recently, RIBEYE(B)-domain was demonstrated to be an LPA-acyltransferase that generates phosphatidic acid (PA) at the synaptic ribbon (Schwarz et al., 2011). Phosphatidic acid (PA) is a phospholipid with a highly negative curvature and can favor vesicle budding and fission (Jenkins and Frohman, 2005; Yang et al., 2008; Roth, 2008). Bioactive lipids, such as PA, cholesterol and sphingolipids, have been proposed to play a role in distinct forms of endocytotic membrane retrieval (Donaldson, 2009; Fine et al., 2011; Campelo and Malhotra, 2011, 2012; Lariccia et al., 2011). PA also favors binding of dynamin to membranes (Burger et al., 2000; Andresen et al., 2002; Roth, 2008).

Currently, I can only speculate how the endocytic machinery is anchored at the synaptic ribbon complex of photoreceptor synapses. The protein Munc119 is recruited to synaptic ribbon via interaction with RIBEYE (Alpadi et al., 2008). Interestingly, in T-lymphocytes, Munc119 was found in a protein complex with dynamin and shown to regulate dynamin function (Karim et al., 2010). Therefore, Munc119 might perform a similar role in photoreceptor ribbon synapses by anchoring the endocytic machinery to synaptic ribbons and/or regulating its activity.  $\beta$ -subunits of voltage-gated  $\text{Ca}^{2+}$ -channels also bind dynamin (Gonzalez-Gutierrez et al., 2007; Miranda-Laferte et al., 2011; Xue et al., 2011; Neely A and Hidalgo P, 2014). Thus, presynaptic the  $\text{Ca}^{2+}$ -channels of the active zone could also be involved in recruiting the endocytotic machinery. It needs to be kept in mind that endocytic retrieval might differ in different types of ribbon synapses. For example, bulk membrane retrieval (Cousin, 2009) is an important mechanism of membrane retrieval in retinal bipolar cells (Holt et al., 2003; Paillart et al., 2003) but absent in photoreceptor ribbon terminals (Rea et al., 2004). Furthermore, multiple modes of endocytosis could co-exist in a single synapse (Holt et al., 2003; Paillart et al., 2003; LoGiudice et al., 2009).

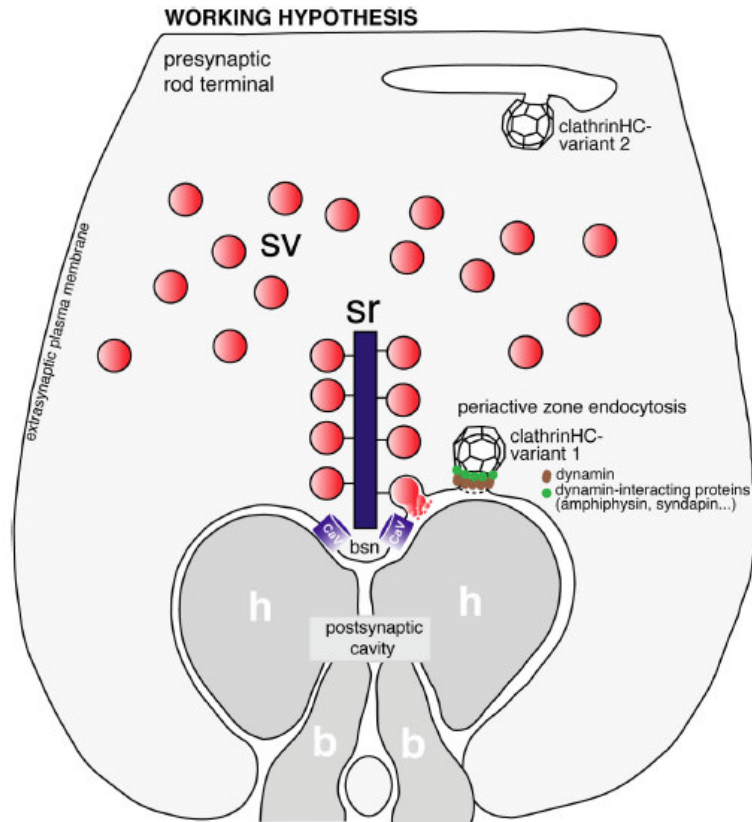


**Figure 35 Simplified, schematic summary of the immunolocalization data presented in this thesis.** Key players of endocytic membrane traffic, including dynamin, dynamin-binding proteins, and CHC-V1, are enriched in a peri-active zone of photoreceptor synapses. Besides CHC-V1, CHC-V2 is also present in the presynaptic photoreceptor terminal. In contrast to CHC-V1, CHC-V2 is located a large distance from the peri-active zone, possibly on an endosomal compartment in the proximal region of the presynaptic terminal. Endosomal-like membrane compartments have been previously observed by transmission electron microscopy in this part of the photoreceptor terminal (Ripps et al., 1976; Schacher et al., 1976; Schaeffer and Raviola, 1978; Cooper and McLaughlin, 1983). The drawing of the photoreceptor terminal is modified based on a drawing of Gray and Pease (1971). sr, Synaptic ribbon;sv, synaptic vesicles; clathrinHC-V1, clathrin heavy chain variant 1, CHC-V1; clathrinHC-V2, CHC-V2; CaV, voltage-gated calcium channels of the photoreceptor active zone; h, postsynaptic dendritic tip of a horizontal cell; b, postsynaptic dendritic tip of an invaginating bipolar cell; bsn, bassoon.

## **5. Further projects**

All the data presented in this thesis is already published in Wahl et al., "A local peri-active zone endocytic machinery at photoreceptor synapses in close vicinity to synaptic ribbons" at the Journal of Neuroscience (J. of Neuroscience, June 2013, 19; 33(25):10278-300). In my second project I worked on the localisation of the tubby like 1 protein (Tulp1), which is implicated in the genetic origin of human Retinitis pigmentosa 14 (RP-14), a heterogeneous group of inherited retinal diseases in which the rod and cone photoreceptor cells degenerate, leading to blindness (Hagstrom *et al.*, 1998). I found Tulp1 located in the peri-active zone of the synaptic ribbon complex co-located with the plasma membrane protein PIP2. By investigation of Tulp1 knock-out mice, I found strong evidences for an involvement of Tulp1 in the endocytic cycle at the synaptic ribbon (Wahl, Magupalli et al.; manuscript in preparation).

## **6. References**

- Aartsen WM, Arsanto JP, Chauvin JP, Vos RM, Versteeg I, Cardozo BN, Bivic AL, Wijnholds J (2009): PSD95beta regulates plasma membrane Ca<sup>2+</sup>-pump localization at the photoreceptor synapse. *Mol Cell Neurosci* 41: 156–165.
- Alpadi K, Magupalli VG, Käppel S, Köblitz L, Schwarz K, Seigel GM, Sung CH, Schmitz F (2008): RIBEYE recruits Munc119, the mammalian ortholog of the *Caenorhabditis elegans* protein unc119, to synaptic ribbons of photoreceptor synapses. *J Biol Chem* 283:26461–26467.
- Amstutz B, Castaldelli M, Kalin S, Imelli N, Boucke K, Wandeler E, Mercer J, Hemmi S, Greber UF (2008): Subversion of CtBP1-controlled macropinocytosis by human adenovirus serotype3. *EMBO J* 27:956–969.
- Andresen BT, Rizzo MA, Shome K, Romero G (2002): The role of phosphatidic acid in the regulation of the Ras/MEK/Erk signalling cascade. *FEBS Lett* 531:65–68.
- Anggono V, Smillie KJ, Graham ME, Valova VA, Cousin MA & Robinson PJ (2006): Syndapin I is the phosphorylation-regulated dynamin I partner in synaptic vesicle endocytosis. *Nat Neurosci* 9(6):752-60.
- Anggono V & Robinson PJ (2007): Syndapin I and endophilin I bind to overlapping proline-rich regions of dynamin I: role in synaptic vesicle endocytosis. *J Neurochem* 102(3):931-43
- Babai N, Bartoletti TM, Thoreson WB (2010): Calcium regulates vesicle replenishment at the cone ribbon synapse. *J Neurosci* 30:15866–15877.
- Bai J, Hu Z, Dittman JS, Pym ECG, Kaplan JM (2010): Endophilin functions as a membrane-binding molecule and is delivered to endocytic zones by exocytosis. *Cell* 143:430–441.
- Bennett V (1983): Proteins involved in membrane-cytoskeleton association in human erythrocytes spectrin, ankyrin and band 3. *Methods Enzymol* 96:313–324.
- Beutner D, Voets T, Neher E, Moser T (2001): Calcium dependence of exocytosis and endocytosis at the cochlear inner hair cell afferent synapse. *Neuron* 29:681–690.
- Bodmer D, Ascano M, Kuruvilla R (2011): Isoform specific dephosphorylation of dynamin1 by calcineurin couples neurotrophin receptor endocytosis to axonal growth. *Neuron* 70:1085–1099.

- References -

- Bonazzi M, Spano S, Turacchio G, Cericola C, Valente C, Colanzi A, Kweon HS, Hsu VW, Polishchuck EV, Polishchuck RS, Sallesse M, Pulvirenti T, Corda D, Luini A (2005): CtPB3/BARS drives membrane fission in dynamin-independent transport pathways. *Nature Cell Biol* 7:570–580.
- Braun A, Pinyol R, Dahlhaus R, Koch D, Fonarev P, Grant BD, Kessels MM & Qualmann B (2005): EHD proteins associate with syndapin I and II and such interactions play a crucial role in endosomal recycling. *Mol Biol Cell* 16(8):3642-58.
- Brodsky FM. (1985): Clathrin structure characterized with monoclonal antibodies. I. Analysis of multiple antigenic sites. *J Cell Biol* 101:2047–2054.
- Brodsky FM (2012): Diversity of clathrin function: new tricks for an old protein. *Ann Rev Cell Dev Biol* 28:309–336.
- Buckley K, Kelly RB (1985): Identification of a transmembrane glycoprotein specific for secretory vesicles of neuronal and endocrine cells. *J Cell Biol* 100:1284–1294.
- Burger KN, Demel RA, Schmid SL, de Kruijff B (2000): Dynamin is membrane-active: lipid insertion is induced by phosphoinositides and phosphatidic acid. *Biochem* 39:12485–12493.
- Campelo F, Malhotra V (2011): PKD regulates membrane fission to generate TGN to cell surface transport carriers. *Cold Spring Harbor Perspect* 1;3(2). pii: a005280.
- Campelo F, Malhotra V (2012): Membrane fission: the biogenesis of transport vesicles. *Ann Rev Biochem* 81:407– 427.
- Chang-Ileto B, Frere SG, Chan RB, Voronov SV, Roux A, Di Paolo G (2011): Synaptojanin 1-mediated PI(4,5)P<sub>2</sub> hydrolysis is modulated by membrane curvature and facilitates membrane fission. *Dev. Cell* 15; 20(2):206-18.
- Chen H & Antonarakis S E (1997): The SH3D1A gene maps to human chromosome 21q22.1→ q22.2. *Cytogenetics and Cell Genetics* 78(3-4):213-5.
- Chen Y, Deng L, Maeno-Hikichi Y, Lai M, Chang S, Chen G (2003): Formation of an endophilin-Ca<sup>2+</sup> channel complex is critical for clathrin-mediated synaptic vesicle endocytosis. *Cell* 115(1):37-48.
- Chung J-K, Sekiya F, Kang H-S, Lee C, Han J-S, Kim SR, Bae YS, Morris AJ and Rhee SG (1997): Synaptojanin inhibition of phospholipase D activity by hydrolysis of phosphatidylinositol 4,5-bisphosphate. *J Biol Chem* 272(25):15980-5

- References -

- Clayton EL, Cousin MA (2009): The molecular physiology of activity-dependent bulk endocytosis of synaptic vesicles. *J Neurochem* 111:901–914.
- Cooper NGF, McLaughlin BJ (1983): Tracer uptake by photoreceptor synaptic terminals. *J Ultrastruct* 84:252–267.
- Corda D, Colanzi A, Luini A (2006): The multiple activities of CtBP/BARS proteins: the Golgi view. *Trends Cell Biol* 16(3):167-73.
- Cousin MA, Robinson PJ (2001): The dephosphins: dephosphorylation by calcineurin triggers synaptic vesicle endocytosis. *Trends Neurosci* 24(11):659-65
- Cousin MA (2009): Activity-dependent bulk synaptic vesicle endocytosis-a fast, high capacity membrane retrieval mechanism. *Mol Neurobiol* 39:185–189.
- Cremona O, Di Paolo G, Wenk MR, Luthi A, Kim WT, Takei K, Daniell L, Nemoto Y, Shears SB, Flavell RA (1999): Essential role of phosphoinositide metabolism in synaptic vesicle recycling. *Cell* 15; 99(2):179-88.
- Cremona O, De Camilli P (2001): Phosphoinositides in membrane traffic at the synapse. *J Cell Sci* 114(Pt 6):1041-52.
- De Camilli P, Emr SD, McPherson PS and Novick P (1996): Phosphoinositides as regulators in membrane traffic. *Science* 15; 271(5255):1533-9.
- De Deyne PG, O'Neill A, Resneck WG, Dmytrenko GM, Pumplun DW, Bloch RJ (1998): The vitronectin receptor associates with clathrin-coated membrane domains via the cytoplasmic domain of its  $\beta 5$  subunit. *J Cell Sci* 111 (Pt 18):2729-40.
- Dickman DK, Horne JA, Meinertzhagen IA, Schwarz TL (2005): A slowed classical pathway rather than kiss-and run mediates endocytosis at synapses lacking synaptojanin and endophilin. *Cell* 4; 123(3):521-33.
- Di Paolo G, Sankaranarayanan S, Wenk MR, Daniell L, Perucco E, Caldarone BJ, Flavell R, Picciotto MR, Ryan TA, Cremona O, De Camilli P (2002): Decreased synaptic vesicle recycling efficiency and cognitive defects in amphiphysin 1 knockout mice. *Neuron* 33:789–804.
- Dittman J, Ryan TA (2009): Molecular circuitry of endocytosis at nerve terminals. *Ann Rev Cell Dev Biol* 25: 133–160.

- References -

- Doherty GJ, McMahon HT (2009): Mechanisms of endocytosis. *Ann Rev Biochem* 78:857–902.
- Donaldson JG (2009): Phospholipase D in endocytosis and endosomal recycling pathways. *Biochim Biophys Acta* 1791:845– 849.
- Donaldson JG, Porat-Shliom N, Cohen LA (2009): Clathrin-independent endocytosis: a unique platform for cell signalling and PM remodelling. *Cell Signal* 21: 1– 6.
- Dowling JE (1987): The retina: An Approachable Part of the Brain. Cambridge, MA. *Harvard University Press*
- Drenckhahn D, Franz H (1986): Identification of actin-, a-actinin-, and viculin-containing plaques at the lateral membrane of epithelial cells. *J Cell Biol* 102:1843–1852.
- Euler T, Hausselt SE, Margolis DJ, Breuninger T, Castell X, Detwiler PB, Denk W (2009): Eyecup scope—optical recordings of light stimulus-evoked fluorescence signals in the retina. *Pfugers Arch* 457:1393–1414.
- Esk C, Chen CY, Johannes L, Brodsky FM (2010): The clathrin heavy chain isoform CHC22 functions in a novel endosomal sorting step. *J Cell Biol* 11 ; 188(1):131-44.
- Ferguson SM, Brasnjo G, Hayashi M, Wölfel M, Collesi C, Giovedi S, Raimondi A, Gong LW, Ariel P, Paradise S, O’Toole E, Flavell R, Cremona O, Miesenböck G, Ryan TA, De Camilli P (2007): A selective activity-dependent requirement for dynamin 1 in synaptic vesicle endocytosis. *Science* 27; 316(5824):570-4.
- Ferguson SM, Raimondi A, Paradise S, Shen H, Mesaki K, Ferguson A, Destaing O, Ko G, Takasaki J, Cremona OEOT, Camilli P (2009): Coordinated actions of actin and BAR proteins upstream of dynamin at endocytic clathrin-coated pits. *Dev Cell* 17(6):811-22.
- Ferguson SM, De Camilli P (2012): Dynamin, a membrane remodelling GTPase. *Nature Rev Mol Cell Biol* 13:75– 88.
- Field MC, Sali A, Rout MP (2011): On a bender—BARs, ESCRTs, COPs, and finally getting your coat. *J Cell Biol* 13; 193(6):963-72.
- Fine M, Llaguno MC, Laricchia V, Lin M-J, Yaradanakul A, Hilgeman DW (2011): Massive endocytosis driven by lipidic forces originating in the outer

plasmalemmal monolayer: a new approach to membrane recycling and lipid domains. *J Gen Physiol* 137:137–154.

- Fotin A, Cheng Y, Grigorieff N, Walz T, Harrison SC, Kirchhausen T (2004a): Structure of an auxilin-bound clathrin coat and its implications for the mechanism of uncoating. *Nature* 2; 432(7017):649-53.
- Fotin A, Cheng Y, Sliz P, Grigorieff N, Harrison SC, Kirchhausen T, Walz T (2004b): Molecular model for a complete clathrin lattice from electron cryomicroscopy. *Nature* 2; 432(7017):573-9.
- Frank T, Rutherford MA, Strenzke N, Neef A, Pangrsic T, Khimich D, Fejtova A, Gundelfinger ED, Liberman MC, Harke B, Bryan KE, Lee A, Egner A, Riedel D, Moser T (2010): Bassoon and the synaptic ribbon organize Ca<sup>2+</sup>-channels and vesicles to add release sites and promote refilling. *Neuron* 68:724 –738.
- Fuchs PA (2005): Time and intensity coding at the hair cell's ribbon synapse. *J Physiol* 1; 566(Pt 1):7-12.
- Fukuda M, Moreira JE, Lewis SM, Sugimori M, Ninobe M, Mikoshiba K and Llinas R (1995): Role of the C2B domain of synaptotagmin in vesicular release and recycling as determined by specific antibody injection into the squid giant synapse preterminal. *Proc Natl Acad Sci USA* 7; 92(23):10708-12.
- Gaidarov I, Chen Q, Falck JR, Redy KK and Keen JH (1996): A functional phosphatidylinositol 3,4,5-trisphosphate/phosphoinositide binding domain in the clathrin adaptor AP-2 alpha subunit. Implications for the endocytic pathway. *J Biol Chem* 23; 271(34):20922-9.
- Gallop JL, Jao CC, Kent HM, Butler PJ, Evans PR, Langen R (2006): Mechanism of endophilin N-BAR domain-mediated membrane curvature. *EMBO Journal* 21; 25(12):2898-910.
- Gao YG, Yan XZ, Song AX, Chang YG, Gao XC, Jiang N, Zhang Q, Hu HY: (2006): Structural insights into the specific binding of huntingtin proline-rich region with the SH3 and WW domains. *Structure* 14(12):1755-65.
- Gonzalez-Gutierrez G, Miranda-Laferte E, Neely A, Hidalgo P (2007): The src homology 3 domain of the beta-subunit of voltage-gated calcium channels promotes endocytosis via dynamin interactions. *J Biol Chem* 282:2156–2162.
- Grabs D (1997): The SH3 domain of amphiphysin binds the proline-rich domain of dynamin at a single site that defines a new SH3 binding consensus sequence. *The Journal of biological chemistry* 16; 272(20):13419-25.
- Graham TR (2004): Flippases and vesicle-mediated protein transport. *Trends Cell Biol* 14(12):670-7.

- Gray EG, Pease HL (1971): On understanding the organization of the retinal receptor synapses. *Brain Res* 10;35(1):1-15
- Griesinger CB, Richards CD, Ashmore JF (2005): Fast vesicle replenishment allows indefatigable signalling at the first auditory synapse. *Nature* 12; 435(7039):212-5.
- Guo S, Stolz LE, Lemrow SM, York JD (1999): SAC1-like domains of yeast SAC1, INP52, and INP53 and of human synaptojanin encode polyphosphoinositide phosphatases. *J Biol Chem* 7; 274(19):12990-5.
- Gustafsson MG, Shao L, Carlton PM, Wang CJ, Golubovskaya IN, Cande WZ, Agard WA, Sedat JW (2008): Three-dimensional resolution doubling in wide-field fluorescence microscopy by structured illumination. *Biophys J* 94(12):4957-70.
- Hagstrom SA, North MA, Nishina PM, Berson EL, and Dryja TP (1998): Recessive mutations in the gene encoding tubby-like protein TULP1 in patients with retinitis pigmentosa. *Nature Genetics*. 18, 174-176.
- Hao W, Tan Z, Prasad K, Reddy KK, Chen J, Prestwich GD, Falck JR, Shears SB and Lafer EM (1997): Regulation of AP-3 function by inositides. Identification of phosphatidylinositol 3, 4, 5-trisphosphate as a potent ligand. *J Biol Chem* 7; 272(10):6393-8.
- Hansen CG, Nichols BJ (2009): Molecular mechanisms of clathrin-independent endocytosis. *J Cell Sci* 122:1713–1721.
- Haucke V, Neher E, Sigrist SJ (2011): Protein scaffolds in the coupling of synaptic exocytosis and endocytosis. *Nature Rev Neurosci* 12:127–138.
- Hayashi M, Raimondi A, O'Toole E, Paradise S, Collesi C, Cremona O, Ferguson SM, De Camilli P (2008): Cell- and stimulus-dependent heterogeneity of synaptic vesicle endocytic recycling mechanisms revealed by studies of dynamin 1-null neurons. *Proc Natl Acad Sci* 12; 105(6):2175-80.
- Heidelberger R, Thoreson WB, Witkovsky P (2005): Synaptic transmission at retinal ribbon synapses. *Prog Retin Eye Res* 24:682–720.
- Heymann JAW, Hinshaw JE (2009): Dynamins at a glance. *J Cell Sci* 122:3427–3431.
- Hinshaw JE, Schmid SL (1995): Dynamin self-assembles into rings suggesting a mechanism for coated vesicle budding. *Nature* 374:190 –192.
- Holt M, Cooke A, Wu MM, Lagnado L (2003): Bulk membrane retrieval in the synaptic terminal of retinal bipolar cells. *J Neurosci* 23: 1329 –1339.

- Hosoi N, Holt M, Sakaba T (2009): Calcium dependence of exo- and endocytic coupling at a glutamatergic synapse. *Neuron* 63:216–229.
- Hua Y, Sinha R, Thiel CS, Schmidt R, Huve J, Martens H, Hell SW, Egner A, Klingauf J (2011): A readily retrievable pool of synaptic vesicles. *Nat Neurosci* 14:833–839.
- Huttner WB & Schmidt A (2000): Lipids, lipid modification and lipid-protein interaction in membrane budding and fission—insights from the roles of endophilin A1 and synaptophysin in synaptic vesicle endocytosis. *Current Opinion in Neurobiology* 10(5):543-51.
- Irie M, Hata Y, Takeuchi M, Ichtchenko K, Toyoda A, Hirao K, Takai Y, Rosahl TW, Südhof TC (1997): Binding of neuroligins to PSD-95. *Science* 277:1511–1515.
- Jackman SL, Choi SY, Thoreson WB, Rabl K, Bartoletti TM, Kramer RH (2009): Role of the synaptic ribbon in transmitting the cone light response. *Nature Neurosci.* 12:303–310.
- Jenkins GM, Frohman MA (2005): Phospholipase D a lipid centric review. *Cell Mol Life Sci* 62:2305–2316.
- Johnson SL, Forge A, Knipper M, Münkner S, Marcotti W (2008): Tonotopic variation in the calcium dependence of neurotransmitter release and vesicle pool replenishment at mammalian auditory ribbon synapses. *J Neurosci* 23; 28(30):7670-8.
- Jokusch WJ, Praefcke GJ, McMahon HT, Lagnado L (2005): Clathrin-dependent and clathrin-independent retrieval of synaptic vesicles in retinal bipolar cells. *Neuron* 46:869–878.
- Kaksonen M, Toret CP, Drubin DG (2005): A modular design for the clathrin- and actin-mediated endocytosis machinery. *Cell* 121; 123(2):305-20.
- Kaneko T, Li L & Li SS (2008): The SH3 domain—a family of versatile peptide- and protein-recognition module. *Front Bioscience* 13; 13:4938-52.
- Katsanis N, Fisher EM (1998): A novel C-terminal binding protein (CTBP2) is closely related to CTBP1, an adenovirus E1A-binding protein, and maps to human chromosome 21q21.3. *Genomics* 15; 47(2):294-9.
- Karim Z, Vepachedu R, Gorska M, Alam R (2010): UNC119 inhibits dynamin and dynamin-dependent endocytic processes. *Cell Signal* 22:128–137.
- Keifer J, Vyas D, Houk JC (1992): Sulforhodamine labelling of neural circuits engaged in motor pattern generation in the in vitro turtle brainstem cerebellum. *J Neurosci* 12:3187–3199.

- References -

- Kessels MM & Qualmann B (2004): The syndapin protein family: linking membrane trafficking with the cytoskeleton. *J Cell Sci* 1; 117(Pt 15):3077-86.
- Kim JH, von Gersdorff H (2009): Traffic jams during vesicle cycling lead to synaptic depression. *Neuron* 30; 63(2):143-5.
- Kirchhausen T, Macia E, Pelish HE (2008): Use of dynasore, the small molecule inhibitor of dynamin, in the regulation of endocytosis. *Methods Enzymol* 488:77–93.
- Koch D, Spiwox-Becker I, Sabanov V, Sinning A, Dugladze T, Stellmacher A, Ahuja R, Grimm J, Schuler S, Müller A, Angenstein F, Ahmed T, Diesler A, Moser M, tom Dieck S, Spessert R, Boeckers TM, Fässler R, Hübner CA, Balschun D, Gloveli T, Kessels MM, Qualmann B (2011): Proper synaptic vesicle formation and neuronal network activity critically rely on syndapin I. *EMBO J* 30:4955– 4969.
- Koch M, Holt M (2012): Coupling exo- and endocytosis: an essential role for PIP2 at the synapse. *Biochim Biophys Acta* 1821:1114 –1132.
- Koulen P, Fletcher EL, Craven SE, Bredt DS, Wässle H (1998): Immunocytochemical localization of the postsynaptic density protein PSD-95 in the mammalian retina. *J Neurosci* 18: 10136 –10149.
- Lariccia V, Fine M, Magi S, Lin MJ, Yaradanakul A, Llaguno MC, Hilgeman DW (2011): Massive calcium-activated endocytosis without involvement of classical endocytic proteins. *J Gen Physiol* 137:111–132.
- Lenzi D, Crum J, Ellisman MH, Roberts WM (2002): Depolarization redistributes synaptic membrane and creates a gradient of vesicles on the synaptic body of a ribbon synapse. *Neuron* 14;36(4):649-59.
- Lenzi D, Runyeon JW, Crum J, Ellisman MH, Roberts WM (1999): Synaptic vesicle populations in saccular hair cells reconstructed by electron tomography. *J Neurosci* 1; 19(1):119-32.
- Liberali P, Kakkonen E, Turacchio G, Valente C, Spaar A, Perinetti G, Böckmann RA, Corda D, Colanzi A, Marjomaki V, Luini A (2008): The closure of Pak1-dependent macropinosomes requires the phosphorylation of CtBP1/BARS. *EMBO J* 27:970 –981.
- Lichtman JW, Wilkinson RS, Rich MM (1985): Multiple innervation of tonic endplates revealed by activity-dependent uptake of fluorescent probes. *Nature* 314:357–359.
- Lin HC and Gilman AG (1996): Regulation of dynamin I GTPase activity by G protein betagamma subunits and phosphatidylinositol 4,5-bisphosphate. *J Biol Chem* 8;271(45):27979-82.

- References -

- Liu AP, Aguet F, Danuser G, and Schmid SL (2010): Local clustering of transferrin receptors promotes clathrin-coated pit initiation. *J Cell Biol* 27; 191(7):1381-93.
- Liu SH, Towler MC, Chen E, Chen CY, Song W, Apodaca G, Brodsky FM (2001): A novel clathrin homolog that co-distributes with cytoskeletal components functions in the trans-Golgi network. *EMBO J* 15; 20(1-2):272-84.
- Llobet A, Gallop JL, Burden JJ, Camdere G, Chandra P, Vallis Y, Hopkins CR, Lagnado L, Mc Mahon HT (2011): Endophilin drives the fast mode of vesicle retrieval in a ribbon synapse. *J Neurosci* 31:8512– 8519.
- LoGiudice L, Matthews G (2007): Endocytosis at ribbon synapses. *Traffic* 8:1123–1128.
- LoGiudice L, Sterling P, Matthews G (2009): Vesicle recycling at ribbon synapses in the finely branched axon terminals of mouse retinal bipolar neurons. *Neurosci* 164:1546 –1556.
- Loll PJ, Swain E, Chen Y, Turner BT, & Zhang JF (2008): Structure of the SH3 domain of rat endophilin A2. *Acta Crystallographica. Section F, Structural Biology and Crystallization Communications* 1; 64(Pt 4):243-6.
- Lundmark R, Carlsson SR (2004): Regulated membrane recruitment of dynamin-2 mediated by sortingnexin 9. *The Journal of biological chemistry* 8;279(41):42694-702.
- Macia E, Ehrlich M, Massol R, Boucrot E, Brunner C, Kirchhausen T (2006): Dynasore, a cell-permeable inhibitor of dynamin. *Dev Cell* 10:839–850.
- Magupalli V, Schwarz K, Alpadi K, Natarajan S, Seigel GM, Schmitz F (2008): Multiple RIBEYE-RIBEYE interactions create a dynamic scaffold for the formation of synaptic ribbons. *J Neurosci* 6; 28(32):7954-67.
- Malhotra V, Campelo F (2011): PKD regulates membrane fission to generate TGN to cell surface transport carriers. *Cold Spring Harb Perspect Biol* 3:a005280.
- Major HD, Hampton JC, Rosario B (1961): A simple method for removing the resin from epoxy-embedded tissue. *J Biophys Biochem Cytol* 9:909–910.
- Masuda M, Takeda S, Sone M, Ohki T, Mori H, Kamioka Y (2006): Endophilin BAR domain drives membrane curvature by two newly identified structure-based mechanisms. *EMBO Journal* 21; 25(12):2889-97.
- McMahan HT, Boucrot E (2011): Molecular mechanism and physiological functions of clathrin-mediated endocytosis. *Nat Rev Cell Mol Biol* 22; 12(8):517-33.

- References -

- McPherson PS, Garcia E, Slepnev VI, David C, Zhang X, Grabs D, Sossin W S, Bauerfeind R, Nemoto Y and De Camilli P (1996): A presynaptic inositol-5-phosphatase. *Nature* 25; 379(6563):353-7.
- Micheva KD, Kay BK, & McPherson PS (1997): Synaptojanin forms two separate complexes in the nerve terminal. Interactions with endophilin and amphiphysin. *The Journal of Biological Chemistry* 24; 272(43):27239-45.
- Mercer AJ, Thoreson WB (2011): The dynamic architecture of photoreceptor ribbon synapses: cytoskeletal, extracellular matrix, and intramembrane proteins. *Vis Neurosci* 28:453– 471.
- Midorikawa M, Tsukamoto Y, Berglund K, Ishii M, Tachibana M (2007): Different roles of ribbon-associated and ribbon-free active zones in retinal bipolar cells. *Nat Neurosci* 10:1268 –1276.
- Milosevic I, Giovedi S, Lou X, Raimondi A, Collesi C, Shen H, Paradise S, O’Toole E, Ferguson S, Cremona O, De Camilli P (2011): Recruitment of endophilin to clathrin-coated pit necks is required for efficient vesicle uncoating after fission. *Neuron* 72:587– 601.
- Miranda-Laferte E, Gonzalez-Gutierrez G, Schmidt S, Zeug A, Ponimaskin E, Neely A, Hidalgo P (2011): Homodimerization of the src homology 3 domain of the calcium channel beta-subunit drives dynamin-dependent endocytosis. *J Biol Chem* 286:22203–22210.
- Mizuno N, Jao CC, Langen R, Steven AC (2010): Multiple modes of endophilin-mediated conversion of lipid vesicles into coated tubes: implications for synaptic vesicle endocytosis. *J Biol Chem* 285:23351–23358.
- Modregger J, Ritter B, Witter B, Paulsson M & Plomann M (2000): All three PACSIN isoforms bind to endocytic proteins and inhibit endocytosis. *J Cell Sci* 113 Pt 24:4511-21.
- Mooren OL, Kotova TI, Moore AJ, Schafer DA (2009): Dynamin2 GTPase and cortactin remodel actin filaments. *J Biol Chem* 4; 284(36):23995-4005.
- Moser T, Beutner D (2000): Kinetics of exocytosis and endocytosis at the cochlear inner hair cell afferent synapse of the mouse. *Proc Natl Acad Sci USA* 97:883– 888.
- Moser T, Brandt A, Lysakowski A (2006): Hair cell ribbon synapses. *Cell Tissue Res* 326:347–359.
- Murthy VN, de Camilli P (2003): Cell biology of the presynaptic terminal. *Ann Rev Neurosci* 26:701–728.
- Neves G, Lagnado L (1999): The kinetics of exocytosis and endocytosis in the synaptic terminal of goldfish retinal bipolar cells. *J Physiol* 515:181–202.

- Neves G, Gomis A, Lagnado L (2001): Calcium influx selects the fast mode of endocytosis in the synaptic terminal of retinal bipolar cells. *Proc Natl Acad Sci USA* 98:15282–15287.
- Neely A, Hidalgo P (2014): Structure-function of proteins interacting with the  $\alpha 1$  pore-forming subunit of high-voltage-activated calcium channels. *Front Physiol* 3;5:209.
- Nimmerjahn A, Kirchhoff F, Kerr JN, Helmchen F (2004): Sulforhodamine 101 as a specific marker of astroglia in the neocortex in vivo. *Nature Meth* 1:31–37.
- Nonet ML, Holgado AM, Brewer F, Serpe CJ, Norbeck BA, Holleran J, Wei L, Hartweg E, Jorgensen EM, Alfonso A (1999): UNC-11, a *Caenorhabditis elegans* AP180 homologue, regulates the size and protein composition of synaptic vesicles. *Mol Biol Cell* 10(7):2343-60
- Paillart C, Li J, Matthews G, Sterling P (2003): Endocytosis and vesicle recycling at a ribbon synapse. *J Neurosci* 23:4092– 4099.
- Parsons TD and Sterling P (2003): Synaptic Ribbon: conveyor belt or safety belt? *Neuron* 6; 37(3):379-82.
- Pearse BM (1976): Clathrin: a unique protein associated with intracellular transfer of membrane by coated vesicles. *Proc Natl Acad Sci USA* 73(4):1255-9.
- Pechstein A, Shupliakov O, Haucke V (2010): Intersectin 1: a versatile actor in the synaptic vesicle cycle. *Biochem Soc Trans* 38:181–186.
- Perera RM, Zoncu R, Lucast L, De Camilli P, Toomre D (2006): Two synaptojanin 1 isoforms are recruited to clathrin- coated pits at different stages. *Proc Natl Acad Sci* 19; 103(51):19332-7.
- Plomann M, Lange R, Vopper G, Cremer H, Heinlein UA, Scheff S, Baldwin SA, Leitges M, Cramer M, Paulsson M (1998): PACSIN, a brain protein that is upregulated upon differentiation into neuronal cells. *Eur J Biochem* 15; 256(1):201-11.
- Punge A, Rizzoli SO, Jahn R, Wildanger JD, Meyer L, Schönle A, Kastrop L, Hell SW (2008): 3D reconstruction of high-resolution STED microscope images. *Microsc Res Tech* 71:644–650.
- Praefcke GK, McMahon HT (2004): The dynamin superfamily: universal membrane tubulation and fission molecules? *Nature Rev Mol Cell Biol* 5:133–147
- Qualmann B, Roos J, DiGregorio PJ & Kelly RB (1999): Syndapin I, a synaptic dynamin-binding protein that associates with the neural Wiskott–Aldrichsyndrome protein. *Mol Biol Cell* 10(2):501-13.

- References -

- Qualmann B & Kelly RB (2000): Syndapin isoforms participate in receptor-mediated endocytosis and actin organization. *J Cell Biol* 6; 148(5):1047-62.
- Rabl K, Cadetti L, Thoreson WB (2005): Kinetics of exocytosis is faster in cones than in rods. *J Neurosci* 4; 25(18):4633-40.
- Raimondi A, Ferguson SM, Lou X, Armbruster M, Paradise S, Giovedi S, Messa M, Kono N, Takasaki J, Cappello V, O'Toole E, Ryan TA, De Camilli P (2011): Overlapping role of dynamin isoforms in synaptic vesicle endocytosis. *Neuron* 70:1100–1114.
- Rea R, Li J, Dharia A, Levitan ES, Sterling P, Kramer RH (2004): Streamlined synaptic vesicle cycle in cone photoreceptor terminals. *Neuron* 41:755–766
- Rebrik TI, Korenbrot J (2004): In intact mammalian photoreceptors, Ca<sup>2+</sup>-dependent modulation of cGMP-gated ion channels is detectable in cones but not in rods. *J Gen Physiol* 123:63–75.
- Ringstad N, Nemoto Y, & De Camilli P (1997): The SH3p4/Sh3p8/SH3p13 protein family: Binding partners for synaptojanin and dynamin via a Grb2-like Src homology 3 domain. *Proceedings of the National Academy of Sciences of the United States of America* 5; 94(16):8569-74.
- Ringstad N, Gad H, Low P, Di Paolo G, Brodin L, Shupliakov O, De Camilli P (1999): Endophilin/SH3p4 is required for the transition from early to late stages in clathrin-mediated synaptic vesicle endocytosis. *Neuron* 24(1):143-54.
- Ringstad N, Nemoto Y, De Camilli P (2001): Differential expression of endophilin 1 and 2 dimers at central nervous system synapses. *J Biol Chem* 2; 276(44):40424-30.
- Ripps H, Shakib M, MacDonald ED (1976): Peroxidase uptake by photoreceptor terminals of the skate retina. *J Cell Biol* 70(1):86-96.
- Ritter B, Modregger J, Paulsson M & Plomann M (1999): PACSIN 2, a novel member of the PACSIN family of cytoplasmic adapter proteins. *FEBS Lett* 9; 454(3):356-62.
- Roberts-Galbraith RH, Gould KL (2010): Setting the F-BAR: functions and regulation of the F-BAR protein family. *Cell Cycle* 15; 9(20):4091-7.
- Rohn JL, Baum B (2010): Actin and cellular architecture at a glance. *J. Cell Sci* 15; 123(Pt 2):155-8.
- Roth MG (2008): Molecular mechanisms of PLD function in membrane traffic. *Traffic* 9(8):1233-9.
- Roux A (2010): Membrane curvature controls dynamin polymerization. *Proceedings of the National Academy of Sciences of the United States of America* 2; 107(9):4141-6.

- Royle SJ, Lagnado L (2010): Clathrin-mediated endocytosis at the synaptic terminal: bridging the gap between physiology and molecules. *Traffic* 11(12):1489-97.
- Saffarian S, Cocucci E, Kirchhausen T (2009): Distinct dynamics of endocytic clathrin-coated pits and coated plaques. *PLoS Biol* 7(9):e1000191.
- Sakisaka T, Itoh T, Miura K and Takenawa T (1997): Phosphatidylinositol 4, 5 bisphosphate phosphatase regulates the rearrangement of actin filaments. *Mol Biol Cell* 17(7):3841-9.
- Saheki Y, De Camilli P (2012): Synaptic vesicle endocytosis. *Cold Spring Harbor Persp Biol* 4:a005645.
- Salim K, Bottonley MJ, Querfurth E, Zvelebil MJ, Gout I, Scaife R, Margolis RL, Gigg R, Driscoll PC, Waterfield MD and Panayotou G (1996): Distinct specificity in the recognition of phosphoinositides by the pleckstrin homology domains of dynamin and Bruton's tyrosine kinase. *EMBO J* 15; 15(22):6241-50.
- Samasilp P, Chan SA & Smith C (2012): Activity dependent fusion pore expansion regulated by a calcineurin-dependent dynamin-syndapin pathway in mouse adrenal chromaffin cells. *J Neurosci* 25; 32(30):10438-47.
- Sandvig K, Pust S, Skotland T, van Deurs B (2011): Clathrin-independent endocytosis: mechanisms and function. *Curr Opin Cell Biol* 23:413– 420.
- Schacher S, Holtzman E, Hood DC (1976): Synaptic activity of frog photoreceptors: a peroxidase uptake study. *J Cell Biol* 70:178 –192.
- Schaeffer SF, Raviola E (1978): Membrane recycling in the cone cell endings of the turtle retina. *J Cell Biol* 79:802– 825.
- Schaeper U, Boyd JM, Verma S, Uhlmann E, Subramanian T, and Chinnadurai G (1995): Molecular cloning and characterization of a cellular phosphoprotein that interacts with a conserved Cterminal domain of adenovirus E1A involved in negative modulation of oncogenic transformation. *Proc Natl Acad Sci USA* 7;92(23):10467-71.
- Schermelleh L, Carlton PM, Haase S, Shao L, Winoto L, Kner P, Burke B, Cardoso MC, Agard DA, Gustafsson MG, Leonhardt H, Sedat JW (2008): Subdiffraction multicolor imaging of the nuclear periphery with 3D structured illumination microscopy. *Science* 320:1332–1336.
- Schermelleh L, Heintzmann R, Leonhardt H (2010): A guide to super-resolution fluorescence microscopy. *J Cell Biol* 90:165–175.
- Schmid SL, Frolov VA: Dynamin (2011): Fundamental design of a membrane fission catalyst. *Ann Rev Cell Dev Biol* 27:79 –105.

- References -

- Schmitz F (2009): The making of synaptic ribbons: how they are built and what they do. *Neuroscientist* 15:611– 624.
- Schmitz F, Königstorfer A, Südhof TC (2000): RIBEYE, a protein's journey through evolution provides insights into synaptic ribbon function. *Neuron* 28:857– 872.
- Schmitz F, Natarajan S, Venkatesan JK, Wahl S, Schwarz K, Grabner CP (2012): EF-hand – mediated  $Ca^{2+}$ - and cGMP-signaling in photoreceptor presynaptic terminals. *Front Mol Neurosci* 5:26.
- Schnee ME, Santos-Sacchi J, Castellano-Munoz M, Kong J-H, Ricci AJ (2011): Calcium-dependent synaptic vesicle trafficking underlies indefatigable release of the hair cell afferent fiber synapse. *Neuron* 70:326 –338.
- Schoch S, Gundelfinger ED (2006): Molecular organization of the presynaptic active zone. *Cell Tissue Res* 326:379 –391.
- Schoch S, Mittelstaedt T, Kaeser PS, Padgett D, Feldmann N, Chevaleyre V, Castillo PE, Hammer RE, Han W, Schmitz F, Lin W, Südhof TC (2006): Redundant functions of RIM1alpha and RIM2alpha in  $Ca^{2+}$ -triggered neurotransmitter release. *EMBO J* 25:5852–5863.
- Schuske KR, Richmond JE, Matthies DS, Davis WS, Runz S, Rube DA, van der Bliek AM, Jorgensen EM (2003): Endophilin is required for synaptic vesicle endocytosis by localizing synaptojanin. *Neuron* 13;40(4):749-62.
- Schwarz K, Natarajan S, Kassas N, Vitale N, Schmitz F (2011): The synaptic ribbon is a site of phosphatidic acid generation in ribbon synapses. *J Neurosci* 31:15996 –16011.
- Schweizer FE, Ryan TA (2006): The synaptic vesicle: cycle of exocytosis and endocytosis. *Curr Opin Neurobiol* 16(3):298-304.
- Scita G, Di Fiori PP (2010): The endocytic matrix. *Nature* 463:464–473.
- Sheng Z, Choi SY, Dharia A, Li J, Sterling P, Kramer RH (2007): Synaptic  $Ca^{2+}$  in darkness is lower in rods than cones causing slower tonic release of vesicles. *J Neurosci* 9; 27(19):5033-42.
- Shpetner HS, Herskovits JS, Vallee RB (1996): A binding site for SH3 domains targets dynamin to coated pits. *The Journal of biological chemistry* 5; 271(1):13-6.
- Shupliakov O (2009): The synaptic vesicle cluster: a source of endocytic proteins during neurotransmitter release. *Neurosci* 158:204 –210.
- Smith SM, Renden R, von Gersdorff H (2008): Synaptic vesicle endocytosis: fast and slow modes of membrane retrieval. *Trends Neurosci* 31:559 –568.

- Snellman J, Mehta B, Babai N, Bartoletti TM, Akmentin W, Francis A, Matthews G, Thoreson WB, Zenisek D (2011): Acute destruction of the synaptic ribbon reveals a role for the ribbon in vesicle priming. *Nature Neurosci* 14:1135–1141.
- Spassova MA, Avissar M, Furman AC, Crumling MA, Saunders JC, Parsons TD (2004): Evidence that rapid replenishment of the synaptic ribbon mediates recovery from short-term adaptation at the hair cell afferent synapse. *J Assoc Res Otolaryngol* 5:376–390
- Sjöstrand FS (1953): The ultrastructure of the outer segments of rods and cones of the eye as revealed by the electron microscope. *J Cell Physiol* 42(1):15-44.
- Sterling P (1998): The retina. In *The Synaptic Organization of the Brain*. Fourth Edition, G.Shepherd, ed. *New York: Oxford University Press*
- Sterling P and Matthews G (2005): Structure and function of ribbon synapses. *Trends Neurosci* 28(1):20-9.
- Südhof TC (2004): The synaptic vesicle cycle. *Ann Rev Neurosci* 27:509–547.
- Südhof TC, Rothman JE (2009): Membrane fusion: grappling with SNARE and SM proteins. *Science* 323(5913):474-7.
- Südhof TC (2012): Calcium control of neurotransmitter release. *Cold Spring Harbor Perspec Biol* 4:a011353.
- Sugiura H, Iwata K, Matsuoka M, Hayashi H, Takemiya T, Yasuda S, Ichikawa M, Yamauchi T, Mehlen P, Haga T, Yamagata K (2004): Inhibitory role of endophilin 3 in receptor-mediated endocytosis. *The Journal of Biological Chemistry* 28; 279(22):23343-8.
- Sumoy L, Pluvinet R, Andreu N, Estivill X & Escarceller M (2001): PACSIN 3 is a novel SH3 domain cytoplasmic adapter protein of the pacsin-syndapin FAP52 gene family. *Gene* 10; 262(1-2):199-205.
- Takamori S, Holt M, Stenius K, Lemke EA, Gronborg M, Riedel D, Urlaub H, Schenck S, Brugger B, Ringler P (2006): Molecular anatomy of a trafficking organelle. *Cell* 17; 127(4):831-46.
- Takei K, McPherson PS, Schmid SL, de Camilli P (1995): Tubular membrane invaginations coated by dynamin rings are induced by GTP- $\gamma$ -S in nerve terminals. *Nature* 374:186–190.
- Takemura R, Stenberg PE, Bainton DF, Werb Z (1986): Rapid redistribution of clathrin onto macrophage plasma membranes in response to Fc receptor-ligand interaction during frustrated phagocytosis. *J Cell Biol* 102(1):55-69.

- Taylor MJ, Perrais D, Merrifield CJ (2011): A high precision survey of the molecular dynamics of mammalian clathrin-mediated endocytosis. *PLoS Biol* 9(3):e1000604.
- Teng H, Cole JC, Roberts RL, Wilkinson RS (1999): Endocytic active zones: hot spots for endocytosis in vertebrate neuromuscular terminals. *J Neurosci* 19:4855– 4866.
- Thoreson WB (2007): Kinetics of synaptic transmission at ribbon synapses of rods and cones. *Mol Neurobiol* 36(3):205-23.
- Thoreson WB, Rabl K, Townes-Anderson E, Heidelberger R (2004): A highly Ca<sup>2+</sup>-sensitive pool of vesicles contributes to linearity at the rod photoreceptor ribbon synapse. *Neuron* 27;42(4):595-605.
- Tian M, Xu CS, Montpetit R, Kramer RH (2012): Rab3A mediates vesicle delivery at photoreceptor ribbon synapses. *J Neurosci* 32:6931– 6936.
- tom Dieck S, Altmann WD, Kessels MM, Qualmann B, Regus H, Brauner D, Jejtova A, Bracko O, Gundelfinger ED, Brandstätter JH *Biol* (2005): Molecular dissection of the photoreceptor ribbon synapse: physical interaction of Bassoon and RIBEYE is essential for the assembly of the ribbon complex. *J Cell* 168:825– 836.
- tom Dieck S, Brandstätter JH (2006): Ribbon synapses of the retina. *Cell Tissue Res* 326:339 –346.
- Townes-Anderson E, MacLeish PR, Raviola E (1985): Solitary rod photoreceptors from mature salamander retina: ultrastructure and uptake of horseradish peroxidase. *J Cell Biol* 100:175–188.
- Townes-Anderson E, Dacheux RF, Raviola E (1988): Rod photoreceptors dissociated from the adult rabbit retina. *J Neurosci* 8:320 –331.
- Van Epps HA, Hayashi M, Lucast L, Stearns L, Stearns GW, Hurley JB, and others (2004): The zebrafish nrc mutant reveals a role for the polyphosphoinositide phosphatase synaptojanin 1 in cone photoreceptor ribbon anchoring. *J Neurosci* 6; 24(40):8641-50.
- Van Hook MJ, Thoreson WB (2012): Rapid synaptic vesicle endocytosis in cone photoreceptors of salamander retina. *J Neurosci* 32:18112–18123.
- van Weering JR, Brown E, Sharp TH, Mantell J, Cullen PJ, Verkade P (2010): Intracellular membrane traffic at high resolution. *Methods Cell Biol* 96:619-48. doi: 10.1016/S0091-679X(10)96026-3.
- Vassilopoulos S, Esk C, Hoshino S, Funke BH, Chen CY, Plocik AM, Wright WE, Kucherlapati R, Brodsky FM (2009): A role for the CHC22 clathrin heavy-chain isoform in human glucose metabolism. *Science* 29; 324(5931):1192-6.

- References -

- Verstreken P, Koh TW, Schulze KL, Zhai RG, Hiesinger PR, Zhou Y, Mehta SQ, Cao Y, Roos J, Bellen HJ (2003): Synaptojanin is recruited by endophilin to promote synaptic vesicle uncoating. *Neuron* 13; 40(4):733-48.
- Wan L, Almers W, Chen W (2005): Two ribeye genes in teleosts: the role of Ribeye in ribbon formation and bipolar cell development. *J Neurosci* 26; 25(4):941-9.
- Wässle (2004): Parallel processing in the mammalian retina. *Nature Reviews Neuroscience* 5(10):747-57.
- Wakeham DE, Abi-Rached L, Towler MC, Wilbur JD, Parham P, Brodsky FM (2005): Clathrin heavy and light chain isoforms originated by independent mechanisms of gene duplication during chordate evolution. *Proc Natl Acad Sci USA* 102:7209 –7214.
- Warnock DE, Terlecky LJ, Schmid SL (1995): Dynamin GTPase is stimulated by crosslinking through the c-terminal proline-rich domain. *EMBO J* 14:1322–1328.
- Weissenhorn W (2005): Crystal structure of the endophilin-A1 BAR domain. *Journal of Molecular Biology* 19; 351(3):653-61.
- Wilbur JD, Hwang PK, Brodsky FM (2005): New faces of the familiar clathrin lattice. *Traffic* 6:346 –350.
- Woscholski R, Finan PM, Radley E, Totty NF, Sterling AE, Hsuan JJ, Waterfield MD and Parker PJ (1997): Synaptojanin is the major constitutively active phosphatidylinositol-3,4,5-trisphosphate 5-phosphatase in rodent brain. *J. Biol. Chem* 11; 272(15):9625-8.
- Wojcik SM, Rhee JS, Herzog E, Sigler A, Jahn R, Takamori S, Brose N, Rosenmund C (2004): An essential role for vesicular glutamate transporter 1 (VGLUT1) in postnatal development and control of quantal size. *Proc Natl Acad Sci USA* 101:7158 –7163.
- Wu LG, Ryan TA, Lagnado L (2007): Modes of vesicle retrieval at ribbon synapses, calyx-type synapses and small central synapses. *J Neurosci* 27: 11793–11802.
- Wu W, Xu J, Wu XS, Wu LG (2005): Activity-dependent acceleration of endocytosis at a central synapse. *J Neurosci* 25:11676 –11683.
- Wu Y, Matsui H, Tomizawa K (2009a): Amphiphysin I and regulation of synaptic vesicle endocytosis. *Acta Med Okayama* 63:305–323.
- Wu XS, McNeil BD, Xu J, Fan J, Xue I, Melicoff E, Adachi R, Bai L, Wu LG (2009b):  $Ca^{2+}$  and calmodulin initiate all forms of endocytosis during depolarization of a nerve terminal. *Nature Neurosci* 12:1003–1010.

- References -

- Xue J, Graham ME, Novelle AE, Sue N, Gray N, McNiven MA, Smilley KJ, Cousin MA, Robinson PJ (2011): Calcineurin selectively docks with the dynamin1xb splice variant to regulate activity-dependent bulk endocytosis. *J Biol Chem* 286:30295–30303.
- Yamashita T (2012): Ca<sup>2+</sup>-dependent regulation of synaptic vesicle endocytosis. *Neurosci Res* 73:1–7.
- Yam JW, Jin DY, So CW, & Chan LC (2004): Identification and characterization of EBP, a novel EEN binding protein that inhibits Ras signaling and is recruited into the nucleus by the MLL-EEN fusion protein. *Blood* 15; 103(4):1445-53.
- Yang J-S, Gad H, Lee SY, Mironov A, Zhang L, Beznoussenko GV, Valente C, Turacchio G, Bonsra AN, Du G, Baldanzi G, Graziani A, Bourgoïn S, Frohman MA, Luini A, Hsu VW (2008): A role for phosphatidic acid in COPI vesicle fission yields insights into Golgi maintenance. *Nature Cell Biol* 10:1146 –1153.
- Yao LH, Rao Y, Varga K, Wang C-Y, Xiao P, Lindau M, Gong L-W (2012): Synaptotagmin-1 is necessary for the Ca<sup>2+</sup>-dependence of clathrin-mediated endocytosis. *J Neurosci* 32:3778 –3785.
- Ybe JA, Brodsky FM, Hofmann K, Lin K, Liu S-H, et al (1999): Clathrin self-assembly is mediated by a tandemly repeated superhelix. *Nature* 27; 399(6734):371-5.
- Yoshida Y, Kinuta M, Abe T, Liang S, Araki K, Cremona O, Di Paolo G, Moriyama Y, Yasuda T, De Camilli P, Takei K (2004): The stimulatory action of amphiphysin on dynamin function is dependent on lipid bilayer curvature. *EMBO J* 23:3483–3491.
- Zanazzi G, Matthews G (2009): The molecular architecture of ribbon presynaptic terminals. *Mol Neurobiol* 39(2):130-48.
- Zheng J, Cahill SM, Lemmon MA, Fushman D, Schlessinger J and Cowburn D (1996): Identification of the binding site for acidic phospholipids on the pH domain of dynamin: implications for stimulation of GTPase activity. *J Mol Biol* 12; 255(1):14-21.
- Zenisek D, Steyer JA, Almers W (2000): Transport, capture and exocytosis of single synaptic vesicles at active zones. *Nature* 105:4922– 4927.
- Zenisek D, Steyer JA, Feldman ME, Almers W (2002): A membrane marker leaves synaptic vesicles in milliseconds after exocytosis in retinal bipolar cells. *Neuron* 406:849–854.

## **7. List of Abbreviations**

1 <sup>st</sup>	First
2 <sup>nd</sup>	Second
µg	microgram
µl	microlitre
µM	micromolar
A	Amacrine cell
Aa	Amino acid
Ab	Antibody
AP	Adaptor protein
BC	Bipolar cell
BD	Binding Domain
bp	base pair
BAR-domain	Bin–Amphiphysin–Rvs domain
BSA	Bovine serum albumin
°C	Celsius
Ca <sup>2+</sup>	Calcium-ion
CHC	Clathrin heavy chain
CLC	Clathrin light chain
CHC-V1	Clathrin heavy chains variant 1
CHC-V2	Clathrin heavy chains variant 2
CLAP domain	Clathrin AP2-binding domain
C-terminal	Carboxy-terminal
CB	cone bipolar cell
CME	clathrin mediated endocytosis
CNS	Central nervous system
CtBP1	C-terminal Binding Protein 1
Cy5	Cyanine5
E1A-protein	Adenovirus early region 1A protein
Eps	Epsin
ECL	Enhanced chemoluminescence
EM	Electron microscopy
FM1-43	N-(3-Triethylammoniumpropyl)-4-(4-(Dibutylamino)

- Abbreviations -

	Styryl) Pyridinium Dibromide)
GTP	guanosine triphosphate
GCL	Ganglion cell layer
GTPase	Family of hydrolase enzymes that bind and hydrolyze guanosine triphosphate (GTP)
G-domain	GTPase-domain
GED-domain	GTPase-effector domain
H	Horizontal cell
HC	Horizontal cell
hrs	hours
INL	Inner nuclear layer
IPL	Inner plexiform layer
IS	Inner segments
kb	Kilobases
kDa	kilo Dalton
LCS	low $Ca^{2+}$ -containing saline solution
LR-Gold	London Resin Gold
mbar	millibar
mg	milligramm
min	minute
ml	milliliter
mono	monoclonal
MW	Molecular weight
NADH	reduced Nicotinamide adenine dinucleotide
ng	nanogram
nm	nanometer
NPG	N-propyl gallate
NPF-repeats	Asparagine, proline, phenylalanin repeats
N-terminal	Amino-terminal
ONL	Outer nuclear layer
OPL	Outer plexiform layer
OS	Outer segments
Pa	Pascal
PA	Phosphatidic acid

- Abbreviations -

PBS	Phosphate Buffered Saline
PFA	Paraformaldehyde
PE	Retinal pigment epithelium
PH-domain	Pleckstrin homology domain
PIP2	Phosphatidylinositol 4,5-bisphosphate or PtdIns(4,5)P <sub>2</sub>
PLD	Phospholipase D
poly	polyclonal
PR	Photoreceptor
pr	Presynaptic terminal
po	postsynaptic dendrite
pm	extrasynaptic plasma membrane
PRD	Proline-rich domain
PSD-95	Postsynaptic density protein-95
RB	Rod bipolar cell
RT	Room temperature
SDS	Sodiumdodecylsulfate
SDS-PAGE	SDS Polyacrylamide gel electrophoresis
SH3-domain	SRC Homology 3-Domain
SR	Synaptic ribbon
SR101	sulforhodamine
SR-SIM	Super-resolution structured illumination microscopy
SV	Synaptic vesicle
SV2	Synaptic vesicle protein 2
TD	Terminal domain
TIRF	Total Internal Reflection Fluorescence Microscopy
TNG	Trans-Golgi network
VGLUT1	vesicular glutamate transporter 1

## **8. List of figures**

<b>Figure 1:</b> (A) Section through the adult human eye (B) Schematic representation of main retinal neurons	<b>12</b>
<b>Figure 2:</b> Schematic overview of the mammalian retina.	<b>13</b>
<b>Figure 3:</b> Schematic diagramme of photoreceptor ribbon synapses.	<b>15</b>
<b>Figure 4:</b> Ultrastructure model for assembly of synaptic ribbon.	<b>15</b>
<b>Figure 5:</b> RIBEYE is the main structural element of synaptic ribbons.	<b>17</b>
<b>Figure 6:</b> The clathrin-coated vesicle cycle.	<b>21</b>
<b>Figure 7:</b> Structural features of clathrin heavy chains.	<b>24</b>
<b>Figure 8:</b> Structure of dynamin and putative mechanism of dynamin-mediated membrane fission.	<b>26</b>
<b>Figure 9:</b> Interactions between amphiphysin I and other endocytic components during clathrin mediated SVE.	<b>28</b>
<b>Figure 10:</b> Domain organization and structure of syndapin isoforms.	<b>29</b>
<b>Figure 11:</b> The domain structure of the endophilin protein family.	<b>32</b>
<b>Figure 12:</b> Schematic domain structure of synaptojanin.	<b>33</b>
<b>Figure 13:</b> The phosphorylation cycle of the dephosphins regulates protein–protein interactions and protein–lipid interactions.	<b>35</b>
<b>Figure 14:</b> Expression of endocytic proteins in the mouse retina.	<b>50</b>
<b>Figure 15:</b> Comparisons of low-magnification micrographs of cryostat (A-C) and semithin sections (D-E) of the mouse retina double-immunolabelled with polyclonal antibodies against RIBEYE (U2656) and monoclonal against dynamin (hudy-1).	<b>51/52</b>
<b>Figure 16:</b> Distribution of dynamin in photoreceptor ribbon synapses at high resolution (immunolabelling of 0.5µm-thin sections).	<b>53/54</b>
<b>Figure 17:</b> Localization of dynamin in relation to other synaptic proteins of the presynaptic photoreceptor terminal.	<b>55/56</b>
<b>Figure 18:</b> Dynamin is highly enriched at the synaptic ribbons in presynaptic terminals of isolated photoreceptors from the mouse retina.	<b>57</b>
<b>Figure 19:</b> Postembedding immunogold labelling of photoreceptor synapses of the mouse retina with dynamin antibodies.	<b>59</b>
<b>Figure 20:</b> Distribution of amphiphysin in photoreceptor ribbon synapses at high resolution.	<b>61</b>

<b>Figure 21:</b> Distribution of syndapin in photoreceptor ribbon synapses.	<b>62</b>
<b>Figure 22:</b> Localization of endophilin in photoreceptor synapses of the mouse retina.	<b>63/64</b>
<b>Figure 23:</b> Pre-absorption control experiments for the immunolabelling analyses.	<b>65/66</b>
<b>Figure 24:</b> Multicolor, high resolution 2D-super-resolution SIM images.	<b>67</b>
<b>Figure 25:</b> Multicolor, high-resolution 3D-super-resolution SIM analyses of RIBEYE, dynamin and syndapin/amphiphysin in the active zone of a single photoreceptor synapse.	<b>68</b>
<b>Figure 26:</b> The Ca <sup>2+</sup> -binding phosphatase calcineurin, a Ca <sup>2+</sup> -sensor of endocytosis, is enriched at the synaptic ribbon.	<b>69</b>
<b>Figure 27:</b> Localization of clathrin heavy chain (variant 1) in the presynaptic photoreceptor terminal.	<b>71</b>
<b>Figure 28:</b> High magnification analyses of clathrin heavy chain (variant 1) in relation to bassoon, RIBEYE and dynamin in single photoreceptor synapses.	<b>72</b>
<b>Figure 29:</b> Multicolor, high resolution 2D-super-resolution SIM analyses of clathrin heavy chain (variant 1) in relation to synaptic ribbons (maximum projections).	<b>73</b>
<b>Figure 30:</b> Postembedding immunogold labelling of photoreceptor synapses from the mouse retina with antibodies against clathrin heavy chain (variant 1).	<b>74</b>
<b>Figure 31:</b> (A) Western blot analyses of clathrin heavy chain, variant 1 and variant 2 (after separation in 5% acrylamide running gels). (B-E) Pre-absorption control experiments for the antibodies against clathrin heavy chain variants 1 and 2 (immunilabeling analyses).	<b>75/76</b>
<b>Figure 32:</b> Two different clathrin heavy chain variants are found in photoreceptor terminals at different locations (immunilabeling analyses).	<b>77/78</b>
<b>Figure 33:</b> Two clathrin heavy chain variants are differentially localized in photoreceptor presynaptic terminals (further immunolabelling analyses).	<b>79</b>
<b>Figure 34:</b> Imaging of synaptic ribbon-associated endocytosis in isolated mouse photoreceptors.	<b>80/81</b>
<b>Figure 35:</b> Simplified, schematic summary of the immunolocalization data presented in this thesis.	<b>87</b>

## **9. Acknowledgement**

I would like to express my deep and sincere gratitude to my supervisor Prof. Frank Schmitz, for his inspiring and expert guidance in carrying out this PhD thesis work. I always remember his everlasting enthusiasm, enlivening discussion and timeless support.

I also would like to thank Dr. Karin Schwarz for proofreading, timeless support, good advices and her friendship.

I would like to express my thanks also to Sylvia Brundaler for her great help, having always an „open ear” and her friendship.

My warm thanks also to my former colleagues Dr. Venkat Giri Magupalli and especially to Dr. Sivaraman Natarajan and Dr. Jagadish Kumar Venkatesan for their help, support and being my big „ PhD-brothers”, also after leaving. I miss you.

I am also deeply thankful to my colleagues and co-authors, Rashmi Katiyar and Mayur Dembla, for their help, discussions and knowledge exchange all over the time.

I would also like to thank Gabi Kiefer, Birgit Leist, Gerlinde Kühnreich, Jennifer Barthels and Tamara Paul for the excellent technical support.

On the whole I would like all of my co-workers over the years, also the unmentioned ones, for creating a friendly and happy atmosphere in the laboratory.

Especially I am endlessly grateful for everything to my parents, Reimund and Eveline Wahl, who always supported patiently my education and interests.

I can't end this acknowledgement without thanking my great family, especially grandparents and godparents, and friends, especially Milica, Nadine and Nathalie for their constant encouragement, support and love all the time.

## **10. Curriculum vitae**

**Personal informations:** place of birth: Neunkirchen  
date of birth: 27.09.1982

### **School education:**

1989-1992 Elementary school Illingen  
1992-2002 Illtal-Gymnasium Illingen, A-level (final grade: 2,4)

### **Education:**

Okt. 2002- May 2009 Studies of human and molecular biology  
Saarland University

*Master Thesis:* „Charakterisierung eines rekonstituierten  
Envelope-Proteins eines HERV-W Elementes bei  
Chromosom Xq22.3“

*Degree:* Diploma biologist, focus on  
human and molecular biology (final grade: 2,1)

May 2009- today Scientific employee, Anatomiy Homburg,  
Saarland University, AG Prof. Schmitz

### **Practical course:**

04. – 08. Sept. 2006 Institute of forensic medicine, Saarland University,  
DNA lab

## **11. Publications:**

Ruprecht K, Ferreira H, Flockerzi A, **Wahl S**, Sauter M, Mayer J, Mueller-Lantzsch N. (2008, Oct): Human endogenous retrovirus family HERV-K (HML-2) RNA transcripts are selectively packaged into retroviral particles produced by the human germ cell tumor line Tera-1 and originate mainly from a provirus on chromosome 22q11.21. *J Virol.* 82(20):10008-16.

Roebke C<sup>1</sup>, **Wahl S**<sup>1</sup>, Laufer G, Stadelmann C, Sauter M, Mueller-Lantzsch N, Mayer J, Ruprecht K (2010, Aug): An N-terminally truncated envelope protein encoded by a human endogenous retrovirus W locus on chromosome Xq22.3.. *Retrovirology.* 24;7:69. 1: both authors contributed equally

Schmitz F, Natarajan S, Venkatesan JK, **Wahl S**, Schwarz K, Grabner CP. *Front Mol Neurosci.* (2012, Feb): EF hand-mediated Ca- and cGMP-signaling in photoreceptor synaptic terminals. 29; 5:26.

**Wahl S**, Katiyar R, Schmitz F. (2013, Jun): A local, peri-active zone endocytic machinery at photoreceptor synapses in close vicinity to synaptic ribbons. *J Neurosci.* 19; 33(25):10278-300.

Dembla M, **Wahl S**, Katiyar R, Schmitz F (2014, Apr): ArfGAP3 is a component of the photoreceptor synaptic ribbon complex and forms an NAD(H)-regulated, redox-sensitive complex with RIBEYE that is important for endocytosis. *J Neurosci.* 9;34(15):5245-60.

# A Local, Periaxial Zone Endocytic Machinery at Photoreceptor Synapses in Close Vicinity to Synaptic Ribbons

Silke Wahl, Rashmi Katiyar, and Frank Schmitz

Saarland University, Institute of Anatomy and Cell Biology, Department Neuroanatomy, 66421 Homburg, Saar, Germany

Photoreceptor ribbon synapses are continuously active synapses with large active zones that contain synaptic ribbons. Synaptic ribbons are anchored to the active zones and are associated with large numbers of synaptic vesicles. The base of the ribbon that is located close to L-type voltage-gated  $Ca^{2+}$  channels is a hotspot of exocytosis. The continuous exocytosis at the ribbon synapse needs to be balanced by compensatory endocytosis. Recent analyses indicated that vesicle recycling at the synaptic ribbon is also an important determinant of synaptic signaling at the photoreceptor synapse. To get insights into mechanisms of vesicle recycling at the photoreceptor ribbon synapse, we performed super-resolution structured illumination microscopy and immunogold electron microscopy to localize major components of the endocytotic membrane retrieval machinery in the photoreceptor synapse of the mouse retina. We found dynamin, syndapin, amphiphysin, and calcineurin, a regulator of activity-dependent endocytosis, to be highly enriched around the active zone and the synaptic ribbon. We present evidence for two clathrin heavy chain variants in the photoreceptor terminal; one is enriched around the synaptic ribbon, whereas the other is localized in the entry region of the terminal. The focal enrichment of endocytic proteins around the synaptic ribbon is consistent with a focal uptake of endocytic markers at that site. This endocytic activity functionally depends on dynamin. These data propose that the presynaptic periaxial zone surrounding the synaptic ribbon complex is a hotspot of endocytosis in photoreceptor ribbon synapses.

## Introduction

Ribbon synapses are continuously active chemical synapses that are found, for example, in retinal photoreceptors and bipolar cells as well as in hair cells of the inner ear (for review, see Moser et al., 2006; Schmitz, 2009; Mercer and Thoreson, 2011). They differ from “conventional” synapses in several aspects. Ribbon synapses transmit graded changes of membrane potential into modulations of continuous, tonic exocytosis of synaptic vesicles (for review, see Heidelberger et al., 2005; Jackman et al., 2009; Mercer and Thoreson, 2011). To maintain synaptic transmission, ribbon synapses possess structural and functional specializations. The most prominent structural specialization is the synaptic ribbon, a large electron-dense presynaptic structure associated with large numbers of synaptic vesicles. In cross sections, ribbons usually appear bar shaped; three-dimensional representations reveal the plate-like, horseshoe-shaped structure of synaptic ribbons. RIBEYE is the only known protein specific to synaptic ribbons

and most likely is a major component of these structures (Schmitz et al., 2000, 2012). It belongs to the CtBP protein family. RIBEYE consists of a large unique N-terminal domain, the A domain, and a smaller C-terminal domain, the B domain, which is identical to CtBP2 (C-terminal binding-protein 2) except for the first 20 aa (Schmitz et al., 2000; for review, see Schmitz, 2009).

Photoreceptor synapses are located in the outer plexiform layer (OPL) of the retina. Rod photoreceptors contain single, large active zones with a single synaptic ribbon; cone synapses contain multiple active zones with multiple synaptic ribbons. The basal end of the synaptic ribbon is anchored to the active zone where synaptic vesicle exocytosis occurs (Zenisek et al., 2000). The active zone includes an electron-dense structure, the arciform density, which contains the active zone protein bassoon, as well as presynaptic L-type voltage-gated calcium channels (Schoch and Gundelfinger, 2006; for review, see tom Dieck and Brandstätter, 2006). Lateral to the presynaptic release sites, the periaxial zone forms membrane pouches generated by invaginations of the dendritic tips of postsynaptic horizontal cells (for review, see Gray and Pease, 1971; Schmitz et al., 2012).

The continuous exocytosis at the ribbon synapse needs to be balanced by compensatory endocytosis to replenish vesicle pools. The rate of vesicle recycling is an important factor in the signaling at photoreceptor ribbon synapses (Jackman et al., 2009; Babai et al., 2010). Recent analyses indicated that synaptic ribbons have an important role in the resupply of release-ready synaptic vesicles (Spasova et al., 2004; Griesinger et al., 2005; Jackman et al., 2009; Babai et al., 2010; Frank et al., 2010; Schnee et al., 2011; Snellman

Received Oct. 29, 2012; revised May 10, 2013; accepted May 14, 2013.

Author contributions: F.S. designed research; S.W., R.K., and F.S. performed research; S.W., R.K., and F.S. analyzed data; F.S. wrote the paper.

This work was supported by research Grants SFB894, TPA7, and GRK1326 from the German Research Community. We thank PD Dr. Elmar Krause for help with the SIM microscope (SFB894 platform project P1), PD Dr. Martin Jung (SFB894 platform project P3) for peptide synthesis, Dr. Jutta Schmitz-Kraemer for critically reading the manuscript, and Gabi Kiefer for excellent technical assistance.

Correspondence should be addressed to Dr. Frank Schmitz, Saarland University, Institute of Anatomy and Cell Biology, Department of Neuroanatomy, 66421 Homburg/Saar, Germany. E-mail: frank.schmitz@uks.eu.

DOI:10.1523/JNEUROSCI.5048-12.2013

Copyright © 2013 the authors 0270-6474/13/3310278-23\$15.00/0

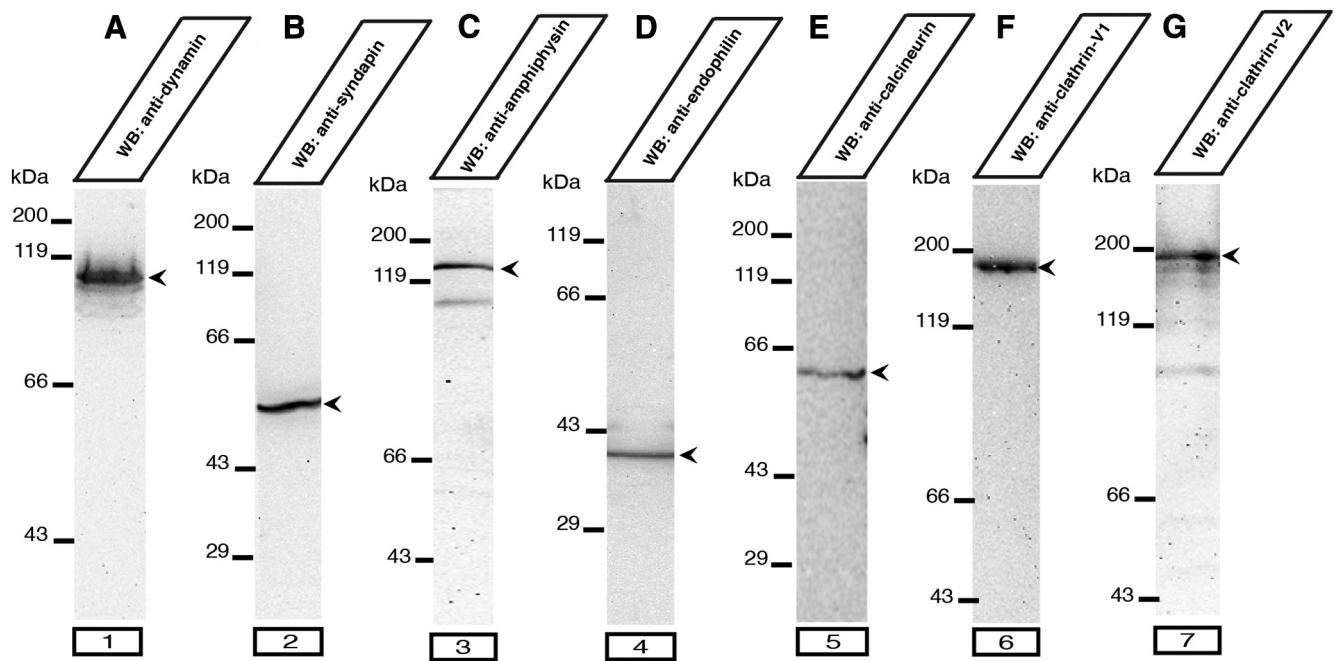


**Figure 1.** Expression of endocytic proteins in the mouse retina. **A–G**, Expression of endocytic proteins in extracts of the mouse retina as judged by Western blot analyses. All antibodies detect their respective antigen at the expected running position (indicated by arrowheads). In **A–E**, proteins were separated by 10% acrylamide SDS-PAGE; in **F–G**, by 8% acrylamide SDS-PAGE.

et al., 2011; Tian et al., 2012). How vesicle recycling is organized and accomplished in the ribbon synapse is still largely unclear. We applied super-resolution structured illumination microscopy (SR-SIM) and immunogold electron microscopy to localize key proteins of the recycling endocytic machinery in photoreceptor ribbon synapses. We found a local endocytic machinery highly enriched at the periaxial zone in close vicinity to the synaptic ribbon. This periaxial zone endocytic machinery is ideally placed to replenish the exocytotic machinery of the continuously active photoreceptor ribbon synapse.

## Materials and Methods

### Antibodies

#### Primary antibodies

Anti-RIBEYE(B)-domain/CtBP2 (U 2656) (Schmitz et al., 2000) polyclonal rabbit antiserum against RIBEYE(B)-domain was used for immunofluorescence staining in a 1:2000 dilution and for Western blotting in a 1:10,000 dilution (if not denoted otherwise).

Anti-CtBP2 (catalog #612044, BD Transduction Laboratories) mouse monoclonal antibody raised against the C-terminal amino acids 361–445 of CtBP2. This antibody detects RIBEYE [i.e., RIBEYE(B)-domain/CtBP2] in Western blotting analyses and labels synaptic ribbons in immunofluorescence labeling analyses (Schwarz et al., 2011). This antibody was used for immunofluorescence labeling in a 1:500 dilution.

For the detection of dynamin, we used a well characterized protein G-purified monoclonal mouse antibody, anti-dynamin (hudy-1; Upstate antibodies, order #05-319, Millipore) generated against a peptide (amino acids 822–838, SPDPFGPPPQVPSRPNR) in the proline-rich, C-terminal region of dynamin-1 (Hinshaw and Schmid, 1995; Takei et al., 1995; Warnock et al., 1995). Dynamin-1 is the predominant neuron-specific form of dynamin expressed in brain (Raimondi et al., 2011; for review, see Ferguson and De Camilli, 2012). The amino acid sequence of this peptide used for immunization is highly conserved between species in dynamin-1 (e.g., 100% amino acid identity in man, mouse, pig, cow, and horse). The amino acid sequence of this peptide stretch is also conserved in dynamin-2, the ubiquitous, non-neuronal form of dynamin (70% amino acid identity) and also in dynamin-3 (77% amino acid identity). Dynamin-3 is also preferentially expressed in brain (as dynamin-1) but at much lower levels (Raimondi et al., 2011; for review,

see Ferguson and De Camilli, 2012). The hudy-1 monoclonal antibody was denoted as an “anti-dynamin” antibody in Results. The corresponding blocking peptide was synthesized by Dr. Martin Jung (Department of Biochemistry and Molecular Biology, Saarland University, Homburg, Germany) and used for pre-absorption control experiments. The hudy-1 monoclonal antibody was applied for Western blotting and immunogold electron microscopy in a 1:1000 dilution and for immunostaining in a 1:500 dilution (if not denoted otherwise).

Anti-syndapin/pacsin (product #196002, Synaptic Systems) polyclonal antiserum against syndapin-1/pacsin-1 was used for immunofluorescence microscopy in a 1:250 dilution, and for Western blotting in a 1:1000 dilution. The syndapin peptide was purchased from Synaptic Systems (196-OP) for pre-absorption control experiments.

Anti-amphiphysin (product #120002, Synaptic Systems) was raised against a synthetic peptide (amino acids 2–15; ADIKTGIFAKNVQK) of amphiphysin-1. The antiserum was used for Western blotting in a 1:1000 dilution, and for immunostaining in a 1:250 dilution. The blocking peptide was purchased from Synaptic Systems (120-OP) for pre-absorption control experiments.

Anti-endophilin (product #159002, Synaptic Systems) is a polyclonal antiserum raised against a synthetic peptide coding for amino acids 256–276 of mouse endophilin-1 (QPKPRMSLEFATGDSTQ). For immunostaining, the antiserum was diluted 1:250, and for Western blotting, 1:1000. The endophilin peptide was also obtained from Synaptic Systems (159-OP) for pre-absorption (blocking) control experiments.

Anti-pan-calcineurin A antibody is an affinity-purified rabbit polyclonal antibody raised against a C-terminal peptide of calcineurin A (order number #2614, Cell Signaling Technology via New England Biolabs). The antibody is purified by both protein A- and peptide-affinity chromatography. It was used for immunofluorescence microscopy in a 1:100 dilution, and for Western blotting in a 1:1000 dilution.

Anti-clathrin heavy chain (ab21679, abcam) is a polyclonal rabbit antibody raised against a peptide in the C terminus of human clathrin heavy chain. The blocking peptide (for pre-absorption control experiments) was also obtained from abcam (ab23440). This antibody detects clathrin heavy chain-variant 1 (CHC-V1) (see Results section) and was used for immunofluorescence microscopy and Western blotting in a 1:1000 dilution; for postembedding immunogold electron microscopy, it was diluted 1:250.

Anti-clathrin heavy chain (order #P1663, Cell Signaling Technology via New England Biolabs), an affinity-purified rabbit antibody against a

C-terminal peptide of human clathrin heavy chain, detects CHC-V1 (see Results section) and was used in a 1:250 dilution for immunofluorescence microscopy. The immunolabeling data on CHC-V1 presented were obtained by immunolabeling with the above-mentioned antibody from abcam (abcam21679) against CHC-V1; but qualitatively identical immunolabeling results were obtained also with the anti-CHC-V1 antibody from Cell Signaling Technology (P1663) (data not shown).

Anti-clathrin heavy chain (ab59710, abcam) is a polyclonal rabbit antiserum that was raised against amino acids 619–638 (KAGLLQRALEHFTDLYDIKR) of rat clathrin heavy chain (100% identical with mouse, highly conserved). For Western blotting, the antibody was diluted 1:1000, and for immunofluorescence labeling, 1:500. This antibody detects CHC-V2 (see Results section).

Anti-clathrin heavy chain (X22 mouse monoclonal antibody raised against clathrin heavy chain; Abcam) was raised against clathrin heavy chain purified from human brain (Brody, 1985). The antibody was used for immunofluorescence microscopy in a 1:100 dilution. This antibody detects CHC-V2 (see Results section).

Anti-panSV2, a monoclonal antibody against the synaptic vesicle protein SV2 (panSV2 monoclonal antibody, raised against all SV2 variants; Buckley and Kelly, 1985) was used to label the synaptic vesicle-containing presynaptic terminals. The supernatant was collected from cultured hybridoma cells (obtained from the Developmental Studies Hybridoma Bank, University of Iowa) and used in a 1:20 dilution.

Anti-vesicular glutamate transporter 1 (VGLUT1; NeuroMAB, University of California, Davis, CA; clone N28/9), a mouse monoclonal antibody, raised against fusion protein encoding amino acids 493–560 of the rat (VGLUT1). The antibody was used for immunofluorescence microscopy in a 1:500 dilution. VGLUT1 is a marker protein of glutamatergic synaptic vesicles (Wojcik et al., 2004).

Anti-VGLUT1 (order #135302, Synaptic Systems). This rabbit polyclonal antibody was raised against amino acids 456–560 of rat VGLUT1 and was used for immunofluorescence microscopy in a 1:500 dilution.

Anti-PSD-95 (NeuroMAB, University of California, Davis, CA; clone K28/43), a mouse monoclonal antibody raised against fusion protein encoding amino acids 77–299 of human PSD-95, was used in a 1:500 dilution for immunofluorescence microscopy.

Anti-PSD-95 (L667) is a rabbit polyclonal antibody raised against rat PSD-95 (Irie et al., 1997). This antibody was a gift from Dr. Thomas C. Südhof (Stanford University, Palo Alto, CA) and used in a 1:1000 dilution for immunofluorescence microscopy.

Anti-Bassoon (VAM-PS003, Stressgen), a mouse monoclonal antibody raised against fusion protein encoding amino acids 738–103 of rat bassoon, was used in a 1:100 dilution for immunofluorescence microscopy.

Anti-Bassoon (order #141002, Synaptic Systems) is a polyclonal rabbit antibody raised against a fusion protein encoding the C-terminal 330 aa of rat bassoon. The antibody was used for immunofluorescence microscopy in a 1:100 dilution.

#### Secondary antibodies (for immunofluorescence labeling)

The following secondary antibodies were used: chicken anti-mouse-Alexa Fluor 488; donkey anti-rabbit-Alexa Fluor 568; goat anti-mouse

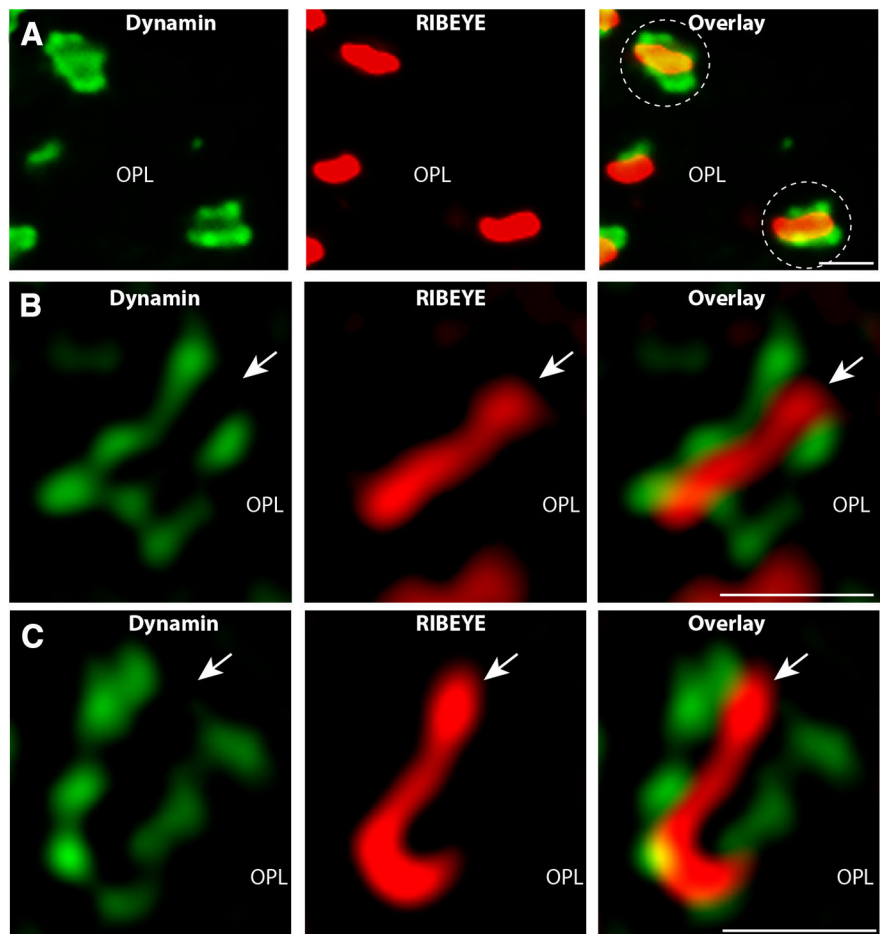


**Figure 2.** Distribution of dynamin in photoreceptor ribbon synapses at high resolution (immunolabeling of 0.5  $\mu\text{m}$  thin sections). **A**, 0.5  $\mu\text{m}$  thin sections of the mouse retina were double immunolabeled with polyclonal antibodies against RIBEYE (U2656) and mouse monoclonal antibodies against dynamin (hudy-1). Dashed circles in **A** denote single immunolabeled presynaptic photoreceptor terminals. Images shown in **A** were obtained by conventional imaging. **B**, **C**, 2D-SR-SIM images of 0.5  $\mu\text{m}$  thin sections from the mouse retina that were double immunolabeled with rabbit polyclonal antibodies against RIBEYE (U2656) and mouse monoclonal antibodies against dynamin (hudy-1). The dynamin immunosignal is highly enriched around the synaptic ribbon (arrow). OPL, Outer plexiform layer. Scale bars, 1  $\mu\text{m}$ .

Cy5; and goat anti-mouse-Alexa Fluor 488. All fluorophore-conjugated secondary antibodies were purchased from Invitrogen and were used in a 1:1000 dilution for 1 h at room temperature (RT) for immunolabeling experiments.

#### Direct labeling of primary antibodies (mouse anti-CtBP2) with fluorophores (DyLight 488/DyLight 650)

For triple-immunolabeling experiments, purified anti-CtBP2 mouse monoclonal antibody was conjugated with DyLight 488 (or DyLight 650) amine-reactive dye with the DyLight 488 Amine Reactive Dye Kit (catalog #5302, Thermo Scientific)/DyLight 650 Microscale Antibody Labeling Kit (catalog #84536, Thermo Scientific) according to the manufacturer's instructions. Twenty-five micrograms of purified antibody (in a volume of 100  $\mu\text{l}$ ) was dialyzed against a large volume of PBS in a Slide-A-Lyzer Mini Dialysis Units Plus Float kit (catalog #66576, Thermo Scientific). Afterward, the antibody was coupled with the *N*-hydroxysuccinimide-activated DyLight 488/DyLight 650 compound exactly according to the manufacturer's instructions. DyLight 488-conjugated primary antibody against CtBP2 was used in a 1:20 dilution for immunolabeling. DyLight 650-conjugated primary antibody against CtBP2 was used in a 1:30 dilution for immunolabeling.

#### Triple immunolabeling for SR-SIM

For triple immunolabeling, we used a directly labeled mouse monoclonal antibody (CtBP2 antibody conjugated with either DyLight 488 or Dy-

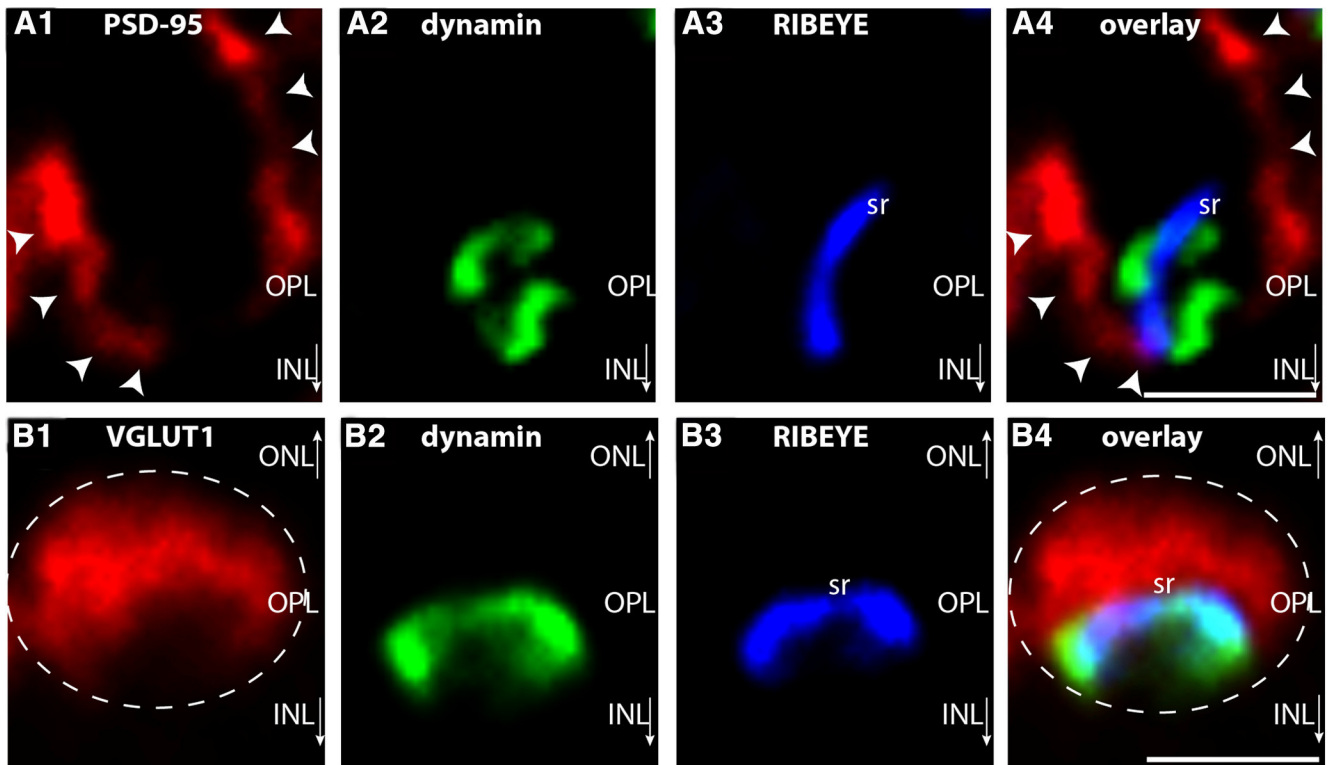


**Figure 3.** Localization of dynamin in relation to other synaptic proteins of the presynaptic photoreceptor terminal. **A, B**, The  $0.5 \mu\text{m}$  thin sections from mouse retina were triple immunolabeled with rabbit polyclonal antibodies against PSD-95 (L667) (**A**) or VGLUT1 (**B**), mouse monoclonal antibodies against dynamin (hudy-1) (**A, B**), and DyLight 650-direct labeled primary antibodies against RIBEYE(**B**)/CtBP2 (**A, B**). In **A**, the PSD-95 immunosignals label the presynaptic plasma membrane of the presynaptic terminals (Koulen et al., 1998; Aartsen et al., 2009), thus demarcating the extension of a single presynaptic terminal (arrowheads in **A**). RIBEYE and dynamin are located close to each other at the distal end of the photoreceptor terminal that is facing the INL (**A**). In **B**, presynaptic terminals were immunolabeled with antibodies against VGLUT1, a marker protein of glutamatergic synaptic vesicles. Single-photoreceptor presynaptic terminals are indicated by the white dashed circles in **B**. Similar as in **A**, RIBEYE and dynamin are located close to each other at the distal border of the immunolabeled glutamatergic vesicles of the presynaptic terminal that faces the INL. ONL, Outer nuclear layer; OPL, outer plexiform layer; INL, inner nuclear layer; sr, synaptic ribbon. Arrows next to INL and ONL point into the direction of the respective layer. Scale bars,  $1 \mu\text{m}$ .

Light 650, as indicated in the respective experiments) and two other primary antibodies (one from mouse, the second from rabbit, as indicated in the respective experiments), which were not directly fluorophore labeled. First, sections were incubated with the two unlabeled primary antibodies at the same time overnight (at the dilutions given above). On the next day, sections were washed three times with PBS and afterward were incubated with the respective secondary antibodies (goat anti-mouse-Cy5; and donkey anti-rabbit-Alexa Fluor 568 or donkey anti-rabbit Alexa Fluor 568 and chicken anti-mouse Alexa Fluor 488). After 1 h incubation, sections were washed again three times with PBS and finally incubated with the directly DyLight 488/DyLight 650-labeled CtBP2 primary antibody (in the dilutions summarized above) overnight at  $4^{\circ}\text{C}$ . After overnight incubation, sections were washed three times with PBS and embedded with antifade solution containing *n*-propyl gallate, as previously described (Schmitz et al., 2000).

#### Blocking of antibodies: preabsorption experiments

For pre-absorption blocking experiments, antisera were diluted to their indicated respective working concentrations. To these antibody dilutions either the specific blocking peptide ( $20 \mu\text{g}$ ) or an unrelated peptide (same amount) was added. These mixtures were incubated overnight on a turning wheel and were used on the other day for immunolabeling experiments, as described below.

All experiments were performed with mouse retinas of either sexes. Mice were killed in the early afternoon. Eyes were collected at environmental daylight conditions (luminance of  $\approx 2 \text{ cd/m}^2$ ). Data similar to those shown for the mouse retina were also obtained with the bovine retina (of either sexes; data not shown).

#### Immunofluorescence microscopy

##### Immunolabeling of $0.5 \mu\text{m}$ thin resin sections

**Embedding procedure.** The preparation procedure for sample embedding into EPON resin is a modification from the procedure described by Drenckhahn and Franz (1986). In brief, tissue was flash frozen in liquid nitrogen-cooled isopentane. Then, as a modification of the original procedure, lyophilization of the tissue was performed while the tissue was continuously cooled by liquid nitrogen. Lyophilization of the samples was typically performed in a vacuum of  $\approx 10^{-7}$  mbar ( $10^{-5}$  Pa) using a TCP270 turbomolecular pump (Arthur-Pfeiffer-Vacuumtechnik) controlled by a PKG020 Pirani-gold cathode gauge control unit and an oil diffusion pump as a pre-pumping unit (type DUO 004B, Arthur-Pfeiffer-Vacuumtechnik). Samples were lyophilized in liquid nitrogen for  $\approx 24$  h. Afterward, samples were equilibrated to room temperature, infiltrated with EPON resin and degassed for 24 h to ensure complete penetration with EPON. Curing of the resin-embedded samples was performed at  $60^{\circ}\text{C}$  for  $\approx 24$  h.

**Immunolabeling procedure for use with  $0.5 \mu\text{m}$  thin resin sections.** Immunofluorescence labeling experiments were performed with semithin sections (thickness,  $\approx 0.5 \mu\text{m}$ ) to obtain optimal resolution. The usefulness of semithin sections to obtain images with nanoscale resolution has been previously demonstrated by Punge et al. (2008). From the tissue blocks,  $0.5 \mu\text{m}$  thin sections were cut with a Reichert ultramicrotome. EPON resin was removed by the procedure of Mayor et al. (1961) with slight modifications. In brief, EPON resin was removed by incubating the sections in the following solutions: sodium methanolate [30% solution in methanol (MERCK) for 10 min]; 1:1 mixture of xylol/methanol (10 min); acetone ( $2 \times 10$  min);  $\text{H}_2\text{O}$  (10 min); and PBS (10 min). Afterward, sections were incubated with the

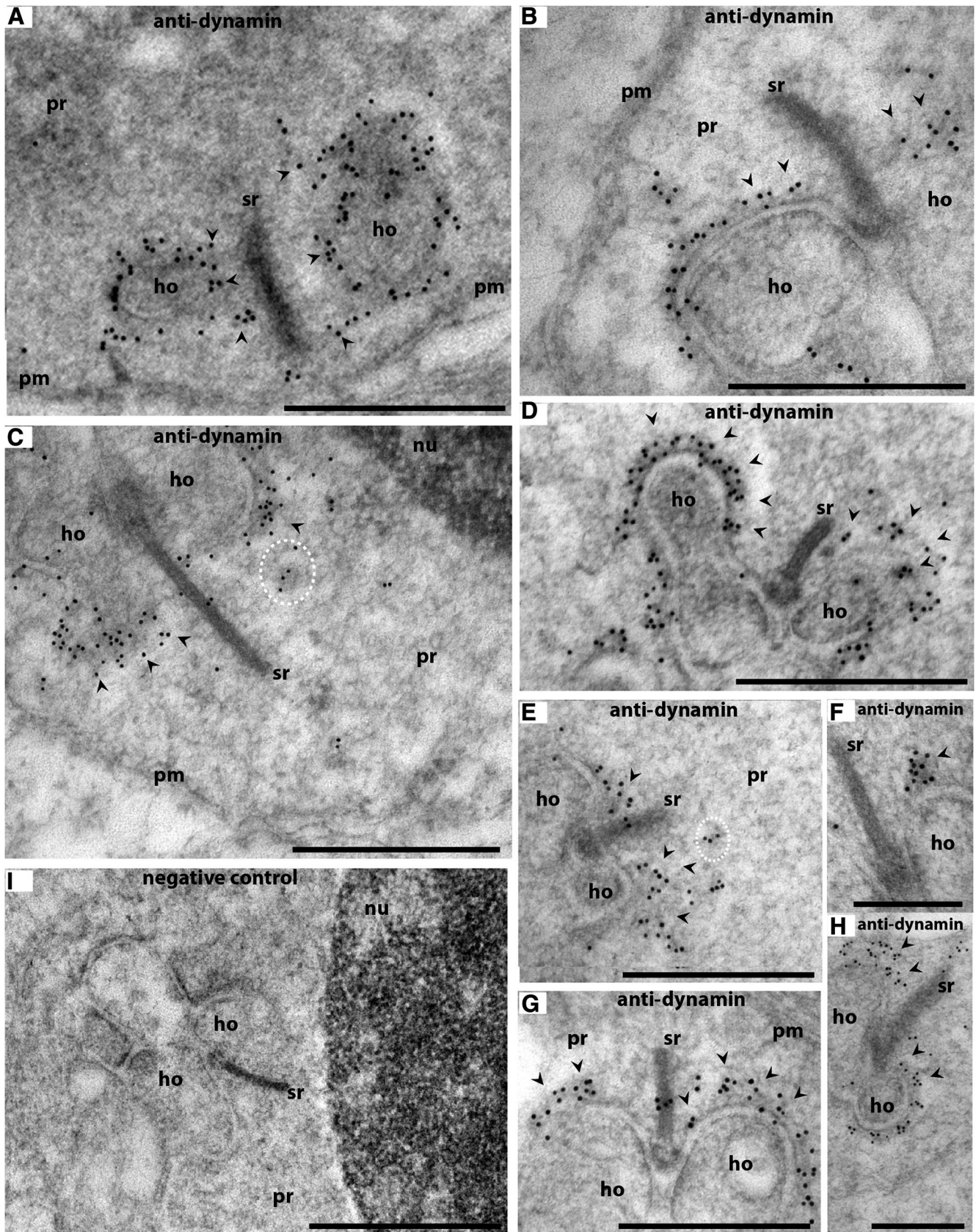


**Figure 4.** Postembedding immunogold labeling of photoreceptor synapses of the mouse retina with dynamin antibodies. *A–H*, Ultrathin sections immunolabeled with mouse monoclonal antibodies against dynamin (hudy-1). Binding of the primary antibodies was detected with goat anti-mouse antibodies conjugated to 10 nm gold particles. The dynamin immunogold label is highly enriched at the presynaptic plasma membrane surrounding the synaptic ribbon (arrowheads in *A–H*). This dynamin immunogold label at the periaxial zone was particularly strong at the lateral presynaptic plasma membrane pouches opposite to dendritic tips of postsynaptic horizontal cells (ho). *I*, A control incubation in which only secondary antibody (but no primary antibody) was applied. No immunosignal was observed under these incubations, further stressing the specificity of the immunolabeling results. A quantitative minor portion of (*Figure legend continues*.)

respective primary and secondary antibodies as described above (Schmitz et al., 2000; Alpaadi et al., 2008).

**Control incubations.** Control incubations for immunolabeling experiments were performed by omitting the primary antibody and only incubating with the secondary antibody. No immunofluorescent signal was observed in photoreceptor synapses in these control incubations. In further control experiments, antibodies were preabsorbed with the respective antigen as described below and processed for immunolabeling.

**Super-resolution structured illumination microscopy.** To further improve the spatial resolution of our immunolabeling data, we applied multicolor 3D-SR-SIM analyses (Schermelele et al., 2008). The resolution of normal microscopy is limited to  $\approx 200$  nm in lateral ( $x, y$ ) and  $\approx 500$  nm in axial ( $z$ ) direction. Super-resolution structured illumination microscopy or SR-SIM gives the possibility of exceeding this diffraction limit. SR-SIM increases the normal lateral resolution by a factor of two, and 3D-SR-SIM provides the same increase in axial direction. Another advantage of the SR-SIM is the possibility of using standard dyes and staining protocols (for review, see Schermellele et al., 2010). For structured illumination microscopy, the ELYRA PS1 setup, as well as a precursor prototype, from Zeiss were used. Images were taken with a 63 $\times$  Plan-Apochromat (numerical aperture, 1.4) with excitation light wavelengths of 488, 561, and 635 nm, and then processed for structured illumination microscopy to obtain higher resolutions (Gustafsson et al., 2008; for review, see Schermellele et al., 2010).  $Z$ -stacks with an interval of 150 nm were used to scan the whole retina section for 3D-SR-SIM (Schermelele et al., 2008; for review, see Schermellele et al., 2010). For acquisition and processing as well as for 3D reconstruction and maximum projection, the Zen2010 software (Zeiss) was used. For imaging analysis, sections were oversampled to exclude signal loss; for 3D reconstruction, only relevant image planes were used. For the 3D reconstruction, the transparent mode was applied.

In general, there is a potential risk of projection artifacts using SR-SIM due to chromatic aberration (Schermelele et al., 2008). The Zeiss setup that was used was corrected for chromatic aberration in  $x$ -,  $y$ -, and  $z$ -directions using multicolor beads, and all obtained images were examined considering this problem. Identical imaging results were obtained if different fluorophores were used for imaging.

### Postembedding immunogold electron microscopy

**Tissue embedding and immunogold labeling procedure.** Tissue embedding and immunogold labeling was performed as previously described (Schmitz et al., 2000) with some modifications. In brief, freshly isolated mouse retinas were fixed in 0.05% glutaraldehyde, 2% freshly depolymerized paraformaldehyde in PBS, pH 7.4, for 2 h at 4°C. After several washes with PBS, followed by H<sub>2</sub>O, samples were treated with tannic acid (0.1%, w/v, in H<sub>2</sub>O) for 1 h at 4°C. Samples were washed with H<sub>2</sub>O and incubated for 2 h in 1% uranyl acetate (in H<sub>2</sub>O). Subsequently, probes were dehydrated in an ascending concentration of ethanol. At 30% ethanol, samples were transferred from 4°C to  $-20^{\circ}\text{C}$  to minimize extraction of lipids and were kept at  $-20^{\circ}\text{C}$  during the entire embedding procedure. Dehydration was performed in steps of 30%, 50%, 70%, 80%, 90%, and 98% ethanol (each for  $\approx 30$  min). Afterward, samples were infiltrated with London Resin (LR)-Gold (Electron Microscopic Sciences) to which 2% of H<sub>2</sub>O (v/v) had been added. LR-gold solution was changed thrice and finally replaced by LR-gold/2% H<sub>2</sub>O resin solution that contained 0.1% benzil as a polymerization catalyst. Polymerization

was performed at  $-20^{\circ}\text{C}$  with UV light (for  $\approx 24$  h). For immunolabeling, ultrathin sections (50–80 nm in thickness) were first treated with 0.5% bovine serum albumin (BSA) in PBS for 45 min at RT to block nonspecific protein binding sites. Then, primary antibodies [dynamin (hudy-1), clathrin (CHC-V1; ab21679)] were applied overnight in a 1:250 dilution in 0.5% BSA/PBS. After several washes with PBS, binding of the primary antibody was detected with goat anti-mouse/goat anti-rabbit secondary antibody conjugated to 10 nm gold particles (Sigma). Afterward, immune complexes were fixed with 2.5% glutaraldehyde in PBS for 15 min at RT. Sections were contrasted with 2% uranylacetate in H<sub>2</sub>O and analyzed with a Tecnai Biotwin digital transmission electron microscope (FEI). As negative controls, either primary antibodies were omitted and/or unrelated antibodies were used. Please note that a postembedding protocol was used. In postembedding protocols, no osmium tetroxide can be used to enhance membrane contrast. Lipid-rich membrane compartments (i.e., synaptic vesicles) remain largely invisible with that method.

**Isolation of photoreceptors from the mature mouse retina.** Photoreceptor cells from the mature retina were isolated by gentle enzymatic digestion with papain, largely as previously described (Townes-Anderson et al., 1985, 1988; Rebrik and Korenbrot, 2004) with some modifications. In brief, retinas were isolated from adult mice within 5 min postmortem (in ambient light). The enucleated eyes were bisected at the equatorial plane, and the posterior eye cup transferred into ice-cold low-Ca<sup>2+</sup>-containing saline solution (abbreviated as “LCS” solution) containing the following: 132 mM NaCl, 3 mM KCl, 1 mM MgCl<sub>2</sub>  $\times$  6H<sub>2</sub>O, 0.5 mM CaCl<sub>2</sub>, 10 mM sodium pyruvate, 10 mM glucose, 10 mM HEPES, pH 7.4 ( $\approx 300$  mOsm/L). LCS was saturated with 5% CO<sub>2</sub>/95% O<sub>2</sub> before use. From the posterior eyecup, the neural retina was gently peeled off from the pigment epithelium and incubated in 1 ml of cysteine-activated papain solution [containing 9 U/ml papain (catalog #76220–25G, Sigma); 2.7 mM L-cysteine (catalog #1693.1, Roth) in LCS] for 20 min at 25°C. Activation of papain (9 U/ml) was done by preincubation with L-cysteine (2.7 mM in LCS) at 37°C for 20 min. After removing the papain solution, the retina was gently washed three times with 1 ml of LCS solution containing 2% FCS and 0.01 mg/ml DNase (catalog #DN25–110MG, Sigma). To dissociate photoreceptor cells, papain-treated retina was gently triturated (three to four times) with a wide-bore plastic Pasteur pipette. The resulting cell suspension was plated on concanavalin A (250 mg; catalog #C7275, Sigma)-coated coverslips. For the coating of 25 mm round coverslips,  $\approx 200$   $\mu\text{l}$  of 1 mg/ml concanavalin A (in LCS solution) was added for 1 h at RT. Unbound concanavalin A was removed by three washes with LCS before the experiments. Cells were allowed to settle on the coverslips for 30 min at 37°C for tight attachment.

For immunocytochemistry, cells were washed once with LCS and fixed with 4% paraformaldehyde in PBS for 15 min at RT. Fixed cells were washed three times with PBS and then permeabilized with 0.1% saponin (S4521–10G, Sigma) in PBS for 15 min at RT. After permeabilization, cells were treated with 1% BSA/0.1% saponin in PBS for 45 min and were incubated with primary antibodies (i.e., hudy-1, 1:250; and U2656, 1:1000) overnight at 4°C. After three washes with PBS, cells were simultaneously incubated for 1 h at RT with secondary antibodies, chicken anti-mouse-Alexa Fluor 488 and donkey anti-rabbit-Alexa Fluor 568. After washing with PBS, coverslips were mounted on glass cover slides with antifade solution and sealed with nail polish.

For conventional transmission electron microscopy, mouse photoreceptor cells isolated as described above, were processed and embedded exactly as previously described (Schoch et al., 2006). Ultrathin sections were analyzed with a Tecnai Biotwin 12 transmission electron microscope (FEI).

### Analysis of synaptic ribbon-associated endocytic activity in synaptic terminals of isolated mouse photoreceptors

Endocytic activity of isolated photoreceptors was visualized with sulforhodamine 101 (SR101) (S7635, Sigma), a fluid-phase endocytic marker (Lichtman et al., 1985; Keifer et al., 1992; Teng et al., 1999; Takahashi et al., 2002; Euler et al., 2009) or with the fixable SR101 analog Texas Red-hydrizide (T6256, Invitrogen) (Nimmerjahn et al., 2004).

←

(Figure legend continued.) dynamin immunolabel was found in a cytosolic localization within the presynaptic terminal (dashed circles in **C** and **E**). This minor portion could result from either labeling of endomembranes or tangential views of dynamin on periaxial zone of lateral pouches above the section plane. Please note that a postembedding protocol was used for immunolabeling. In postembedding protocols, no osmium tetroxide can be used. Therefore, lipid-rich membrane compartments (i.e., synaptic vesicles) remain invisible with postembedding methods. pr, Presynaptic terminal; sr, synaptic ribbon; pm, extrasynaptic plasma membrane (outside of the presynaptic plasma membrane invagination with no contact to the postsynaptic cavity; see also Fig. 17); nu, nucleus. Black arrowheads point to dynamin immunogold particles close to the synaptic ribbons. Scale bars: **A–E, G, I**, 500 nm; **F, H**, 200 nm.

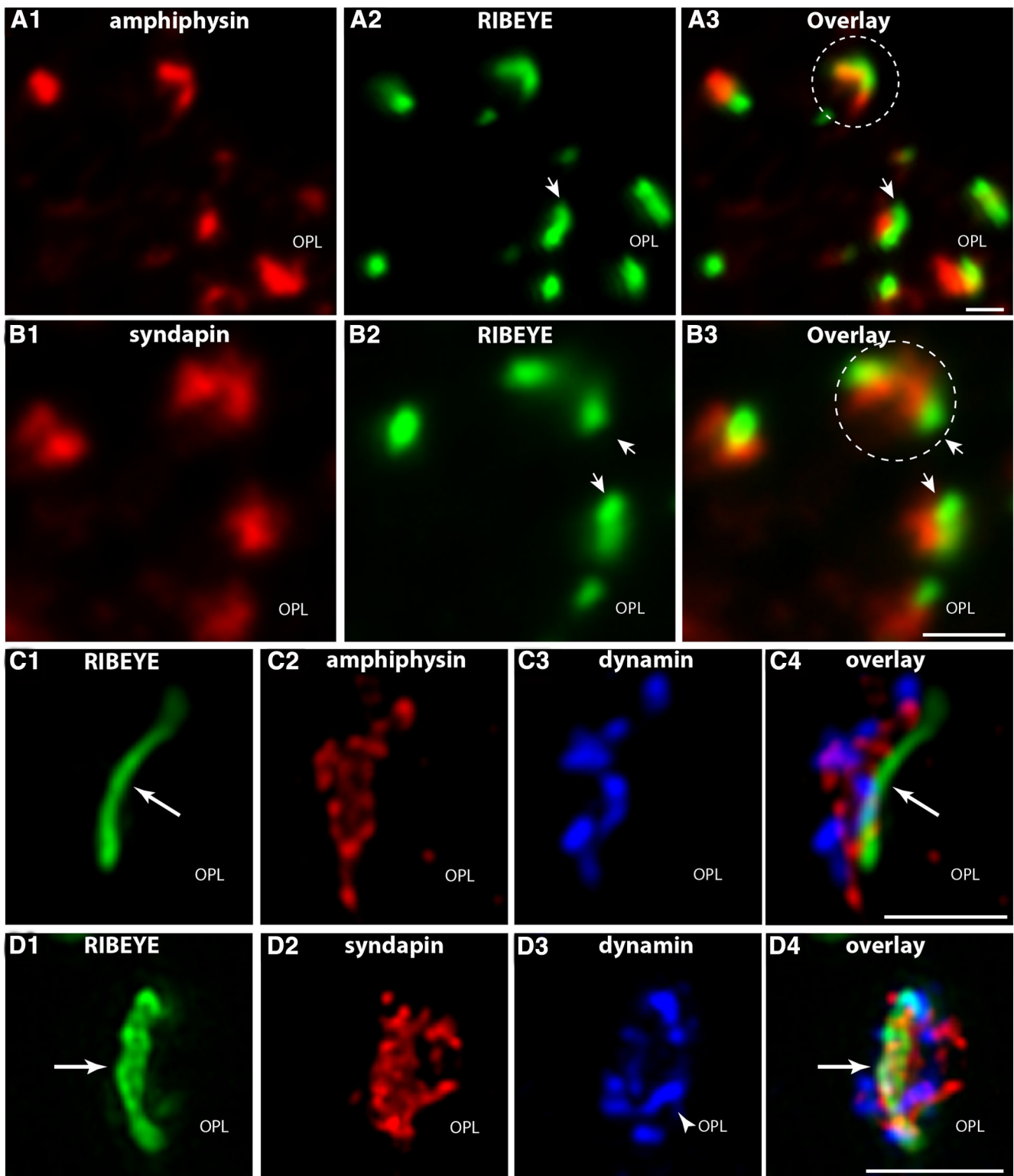


**Figure 5.** *A, B*, Distribution of amphiphysin and syndapin in photoreceptor ribbon synapses at high resolution (conventional imaging). *A, B*, The 0.5  $\mu\text{m}$  thin sections of the mouse retina were double immunolabeled with polyclonal antibodies against amphiphysin and mouse monoclonal antibodies against RIBEYE(B)-domain/CtBP2 (in *A*), and polyclonal antibodies against syndapin and mouse monoclonal antibodies against RIBEYE(B)-domain/CtBP2 (in *B*). Arrows point to immunolabeled synaptic ribbons. Dashed circles in *A* and *B* denote single-immunolabeled presynaptic terminals/synaptic ribbon complexes of rod photoreceptors. *C, D*, Multicolor, 2D-SR-SIM analyses of the distribution of amphiphysin and syndapin in photoreceptor synapses. In *C* and *D*, 0.5  $\mu\text{m}$  thin sections of the mouse retina were triple immunolabeled with Alexa Fluor 488 directly labeled mouse monoclonal antibody against RIBEYE(B)-domain/CtBP2, rabbit polyclonal antibody against amphiphysin (*C*) or syndapin (*D*) and mouse monoclonal antibody against dynamin (*C, D*). Arrows point to immunolabeled synaptic ribbons. OPL, Outer plexiform layer. Scale bars, 1  $\mu\text{m}$ .

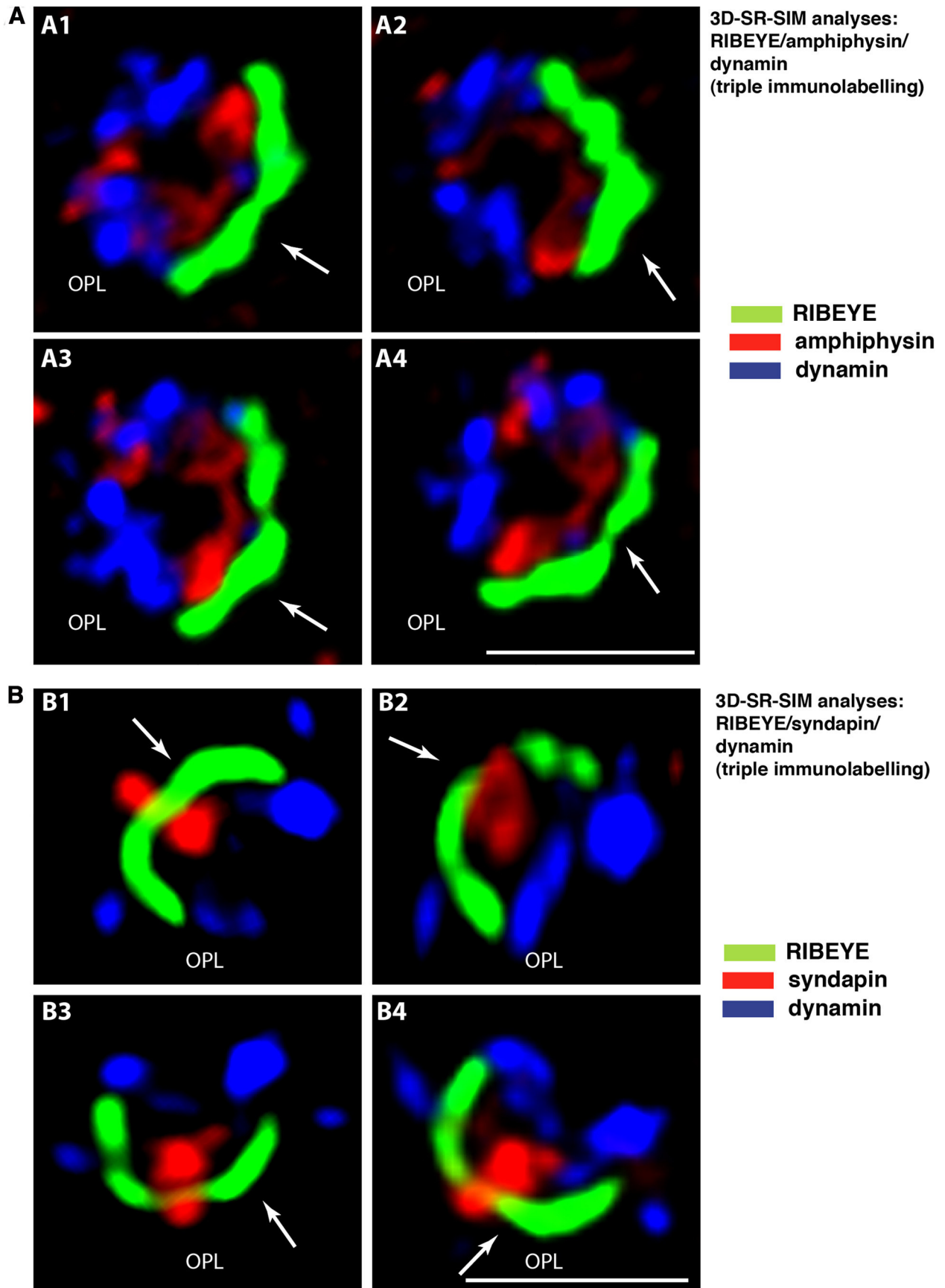


**Figure 6.** Multicolor 3D-SR-SIM of RIBEYE, dynamin, and syndapin/amphiphysin in the active zone of single rod photoreceptor synapses. In **A**, triple-immunolabeling 3D-SR-SIM analyses were performed with antibodies against RIBEYE, dynamin, and amphiphysin; in **B**, triple-immunolabeling 3D-SR-SIM analyses were performed with antibodies against RIBEYE, dynamin, and syndapin (**A1–A4** and **B1–B4**, respectively), denoting different lateral views of the same single-immunolabeled synaptic ribbon of a rod photoreceptor synapse. Arrows denote the immunolabeled synaptic ribbon. OPL, Outer plexiform layer. Scale bars, 1  $\mu$ m.

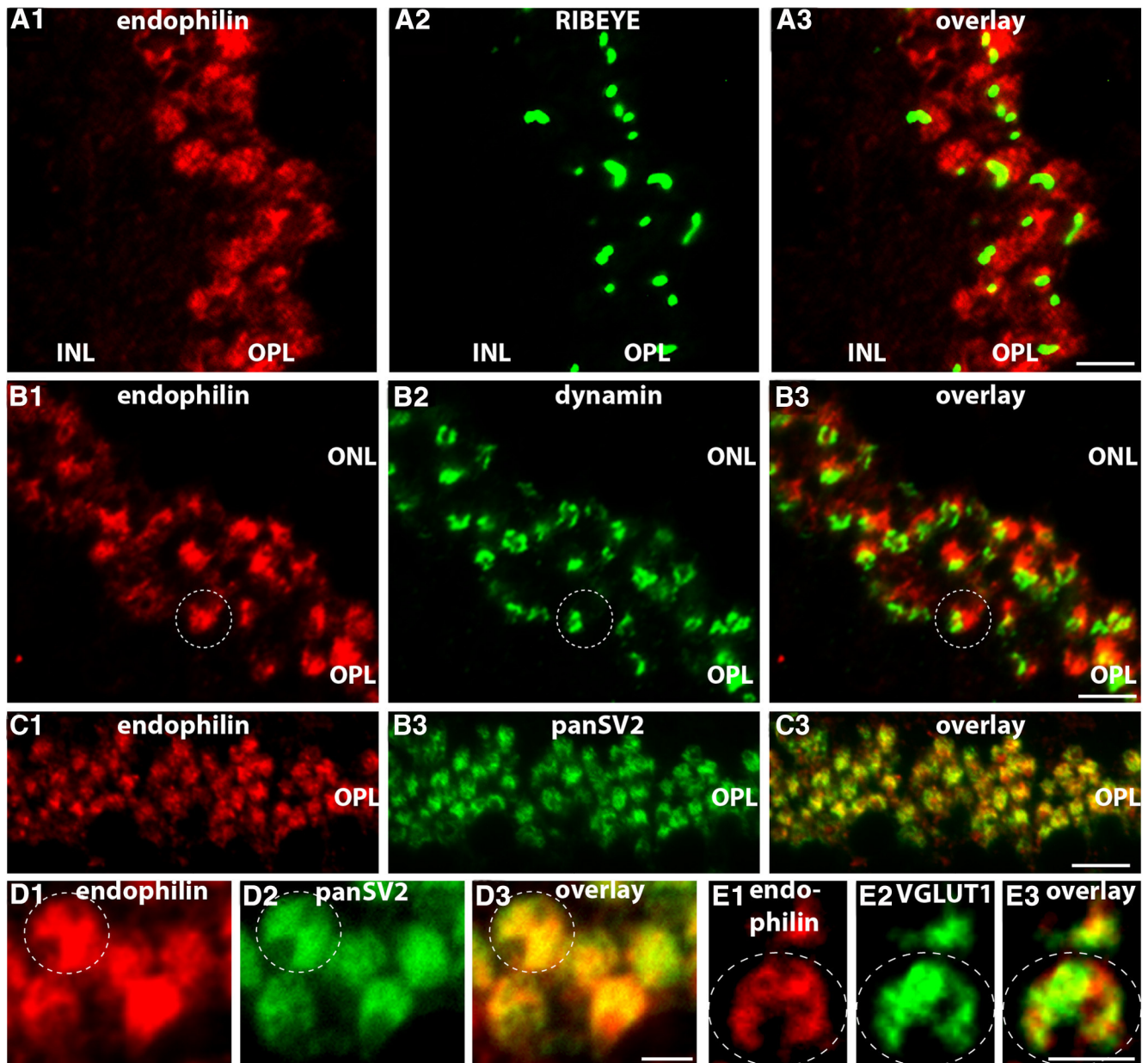


**Figure 7.** Localization of endophilin in photoreceptor synapses of the mouse retina. **A**, The 0.5  $\mu\text{m}$  thin sections of the mouse retina were double immunolabeled with rabbit polyclonal antibodies against endophilin and mouse monoclonal antibodies against RIBEYE(B)-domain/CtBP2. **B**, The 0.5  $\mu\text{m}$  thin sections of the mouse retina were double immunolabeled with rabbit polyclonal antibodies against endophilin and mouse monoclonal antibodies against dynamin. **C, D**, The 0.5  $\mu\text{m}$  thin sections of the mouse retina were double immunolabeled with rabbit polyclonal antibodies against endophilin and mouse monoclonal antibodies against the synaptic vesicle protein 2 (panSV2; detecting all SV2 isoforms). **E**, The 0.5  $\mu\text{m}$  thin sections of the mouse retina were double immunolabeled with rabbit polyclonal antibodies against endophilin and mouse monoclonal antibodies against VGLUT1. Dashed circles in **B, D**, and **E** denote single presynaptic photoreceptor terminals. Endophilin is diffusely distributed throughout the presynaptic terminal and is not particularly enriched around the synaptic ribbon. All micrographs were obtained by conventional imaging. ONL, Outer nuclear layer; OPL, outer plexiform layer; INL, inner nuclear layer. Scale bars: **A**, 10  $\mu\text{m}$ ; **B**, 5  $\mu\text{m}$ ; **C**, 12  $\mu\text{m}$ ; **D, E**, 1  $\mu\text{m}$ .

Isolated mouse photoreceptors, prepared as described above, were incubated for 2 min at room temperature with 1  $\mu\text{M}$  SR101/Texas Red-hydrazide. SR101/Texas Red-hydrazide was dissolved in LCS containing 2 mM  $\text{Ca}^{2+}$ . SR101/Texas Red-hydrazide-loading experiments resulted in virtually identical labeling results in isolated mouse photoreceptors (see Fig. 16) (data not shown). The immunolabeling results shown in Figure 16 were obtained after loading with fixable SR101 (Texas Red-hydrazide). After labeling, photoreceptors were rinsed three times with LCS. To analyze the importance of dynamin in ribbon-associated endocytosis, photoreceptors were incubated for 30 min at 37°C with 100  $\mu\text{M}$  dynasore, a specific blocker of dynamin activity (Macia et al., 2006; Kirchhausen et al., 2008; Van Hook and Thoreson, 2012), before incubation with sulforhodamine/Texas Red-

hydrazide. After labeling and three short washes with LCS, photoreceptors were fixed with 4% PFA for 15 min at RT and processed for immunolabeling as described above.

#### Western blots

Western blot analyses were performed as previously described (Schmitz et al., 2000) using the indicated antibodies at the indicated dilutions. Binding of the primary antibodies was detected with secondary antibodies conjugated with horseradish peroxidase and enhanced chemoluminescence (ECL). ECL signals of the antibody-incubated Western blots were scanned and documented with a Bio-Rad gelDoc Chemoluminescence detection system. As molecular weight standards for SDS PAGE, we used a prestained protein ladder (order #26616, Thermo Scientific),

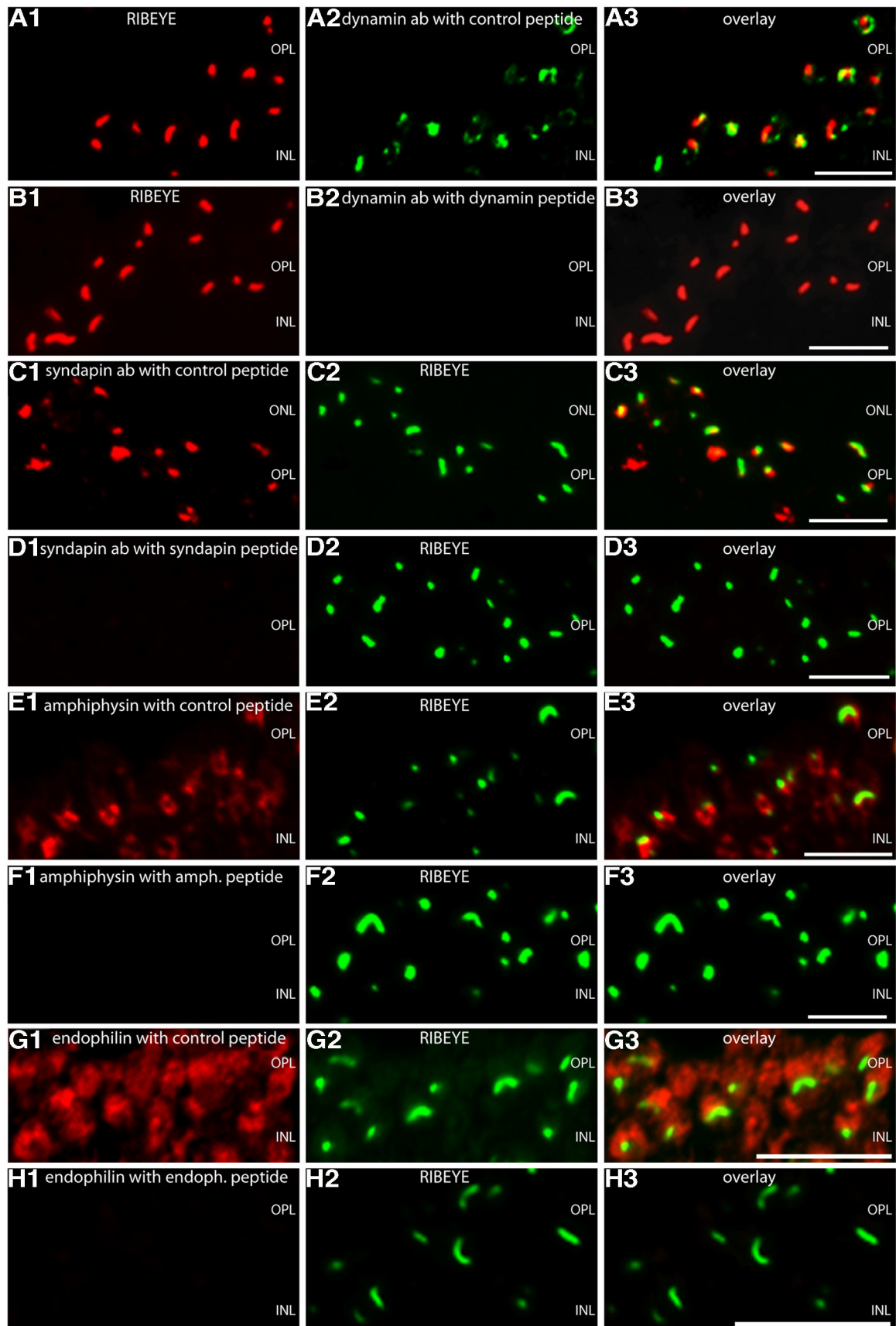


**Figure 8.** Pre-absorption control experiments for the immunolabeling analyses. **A–H**, Double immunolabeling of 0.5  $\mu\text{m}$  thin mouse retinal sections with the indicated antibodies preabsorbed with either their specific peptide used for immunization (**B, D, F, H**) or with an unrelated control peptide (**A, C, E, G**). To visualize ribbon synapses, sections were coimmunolabeled with either rabbit polyclonal antibodies against RIBEYE (U2656 in **A** and **B**) or mouse monoclonal antibodies against RIBEYE(B)-domain/CtBP2. Preabsorption with the specific peptide completely blocked the (*Figure legend continues.*)

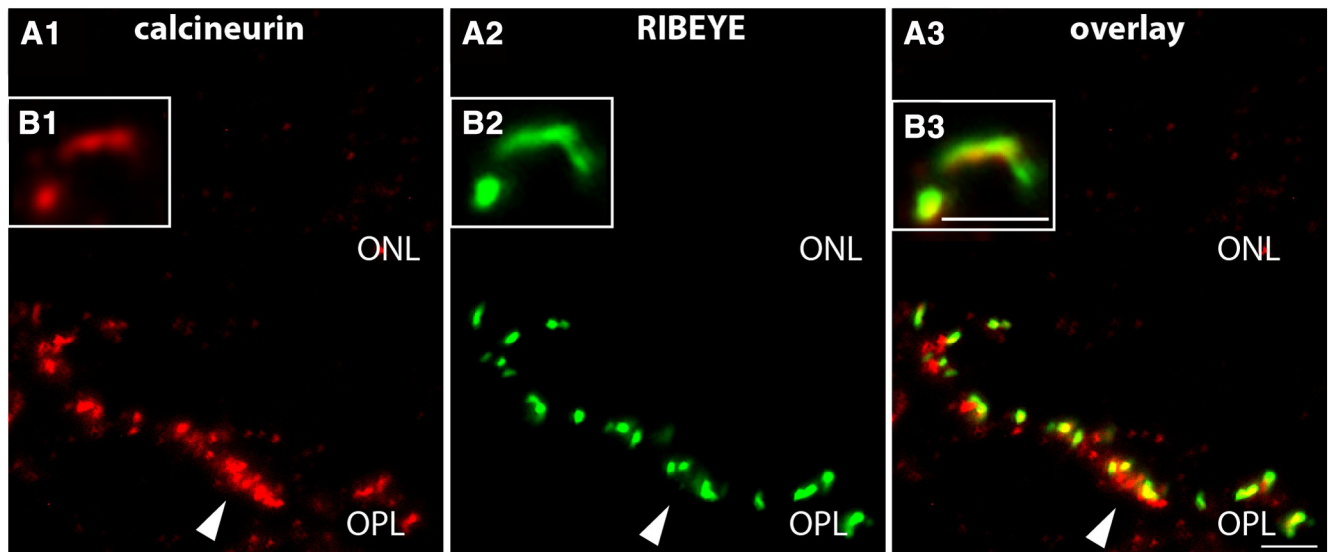


**Figure 9.** The  $\text{Ca}^{2+}$ -binding phosphatase calcineurin, a  $\text{Ca}^{2+}$  sensor of endocytosis, is enriched at the synaptic ribbon. **A**, The  $0.5 \mu\text{m}$  thin sections of the mouse retina were double immunolabeled with affinity-purified rabbit polyclonal antibodies against calcineurin and mouse monoclonal antibodies against RIBEYE(B)domain/CtBP2 (conventional imaging). Calcineurin is highly enriched at the synaptic ribbons (arrowheads in **A**). **B**, The insets show a single-immunolabeled synaptic ribbon. ONL, Outer nuclear layer; OPL, outer plexiform layer. Scale bars,  $10 \mu\text{m}$ .

the Roti-Mark Standard molecular weight markers (T851, Roth), and erythrocyte ghost membranes (Bennett, 1983).

## Results

We first focused on dynamin, a mechano-enzyme that is essential for many forms of endocytosis (Praefcke and McMahon, 2004; Ferguson et al., 2007; Heymann and Hinshaw, 2009; Schmid and Frolov, 2011; Ferguson and De Camilli, 2012). Dynamin has well defined functional domains, including an N-terminal GTPase domain, a central lipid-binding pleckstrin homology domain, a bipartite stalk region, a GTPase effector domain, and a proline-rich C-terminal region to which Src homology 3 (SH3)-containing proteins can dock in a differential manner (for review, see Clayton and Cousin, 2009; Ferguson and De Camilli, 2012; Yamashita, 2012). For immunolabeling, we used a well characterized mouse monoclonal antibody against dynamin (Hinshaw and Schmid, 1995; Takei et al., 1995; Warnock et al., 1995) and  $0.5 \mu\text{m}$  thin resin sections to obtain optimal resolution. All antibodies used in the present study for immunolabeling analyses detected their respective antigen at the expected running position in Western blot analyses (Fig. 1A–G).

### Dynamin is enriched in the periaxial zone of photoreceptor ribbon synapses

Using the described immunolabeling techniques with  $0.5 \mu\text{m}$  thin sections, we found dynamin highly enriched in both synaptic layers of the retina, the OPL and inner plexiform layer (Figs. 2, 3; data not shown). The outer plexiform layer, which contains the photoreceptor ribbon synapses, showed a particularly strong dynamin immunosignal (Figs. 2, 3). High-magnification/high-resolution analyses demonstrated that this dynamin immunosignal in photoreceptor synapses is present in a discrete manner and is highly enriched around the synaptic ribbon that

was immunolabeled with antibodies against RIBEYE (Fig. 2A). Similarly, dynamin was found in close proximity to the active zone protein bassoon (data not shown). Bassoon is localized at the base of the synaptic ribbon (tom Dieck et al., 2005). SR-SIM showed a ring of dynamin immunoreactivity closely surrounding the synaptic ribbon (i.e., within  $\approx 250 \text{ nm}$ ) (Fig. 2B, C) (data not shown). The optical resolution obtained by SR-SIM analyses exceeded the resolution that could be obtained by conventional imaging as judged by a comparative imaging analysis of the same incubations either by conventional or SR-SIM imaging at identical magnifications (data not shown). The observation of dynamin being located in close vicinity to the synaptic ribbon was further corroborated with triple-immunolabeling experiments (Fig. 3A, B). With these triple-immunolabeling experiments, we correlated the localization of dynamin to other proteins of the presynaptic photoreceptor terminal (Fig. 3A, B). We used antibodies against PSD-95 to label the presynaptic plasma membrane of photoreceptor terminals (Koulen et al., 1998; Aartsen et al., 2009). In contrast to other synapses, PSD-95 is located presynaptically in photoreceptor ribbon synapses, and antibodies against PSD-95 nicely demarcate the outline of the presynaptic terminal (Fig. 3A). Antibodies against VGLUT1 were used to label the glutamatergic synaptic vesicles in the photoreceptor presynaptic terminals (Wojcik et al., 2004) (Fig. 3B). Similar to the previously described immunolabeling data, we observed RIBEYE and dynamin located close to each other at the distal portion of the presynaptic terminal that faces the inner nuclear layer (INL) (Fig. 3A, B). Quantitative analyses of nearest distance measurements indicated that dynamin puncta are located  $\approx 125 \pm 50 \text{ nm}$  (mean  $\pm$  SD; 100 synapses analyzed) away from RIBEYE puncta and  $\approx 120 \pm 40 \text{ nm}$  (100 synapses analyzed) away from the bassoon puncta in retinal sections. Also, isolated mouse photoreceptors, which display the typical ultrastructural morphology of photoreceptor synaptic terminals (data not shown), showed a similar immunolabeling pattern of dynamin. Similar to the observations in the intact retina, a focal enrichment of dynamin was observed in close vicinity to the synaptic ribbon in isolated photoreceptors (data not shown).

(Figure legend continued.) respective immunosignals at the synaptic ribbon (B, D, F, and H), whereas the control peptide had no influence on the immunosignals (A, C, E, and G), showing the specificity of the immunolabeling results. ONL, Outer nuclear layer; OPL, outer plexiform layer; INL, inner nuclear layer. Scale bars,  $10 \mu\text{m}$ .

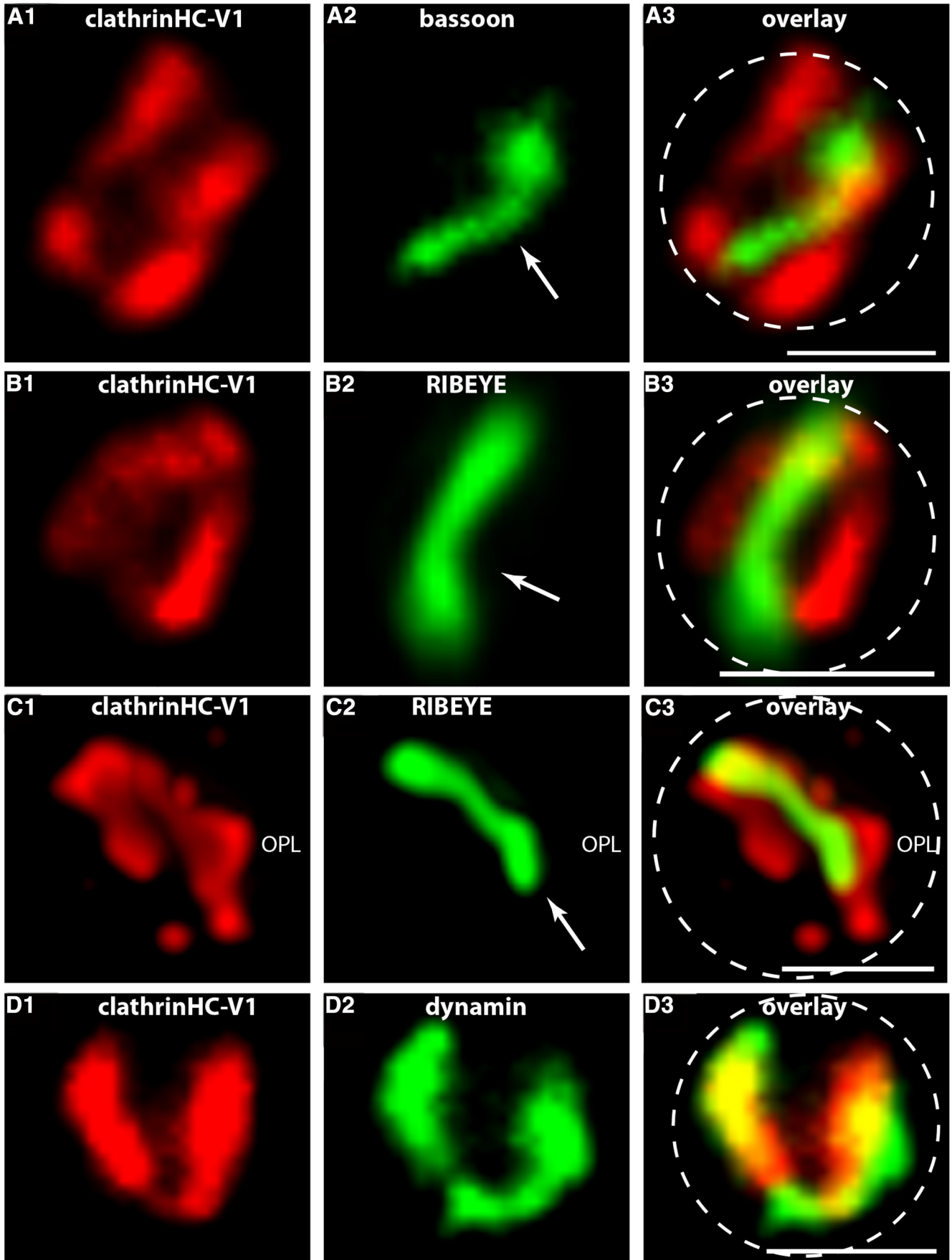


**Figure 10.** High-magnification analyses of CHC-V1 in relation to bassoon, RIBEYE, and dynamin in single-photoreceptor synapses. *A*, The 0.5  $\mu\text{m}$  thin sections of the mouse retina were double immunolabeled with rabbit polyclonal antibodies against CHC-V1 and mouse monoclonal antibodies against bassoon. In *B* and *C*, sections were double immunolabeled (*Figure legend continues.*)

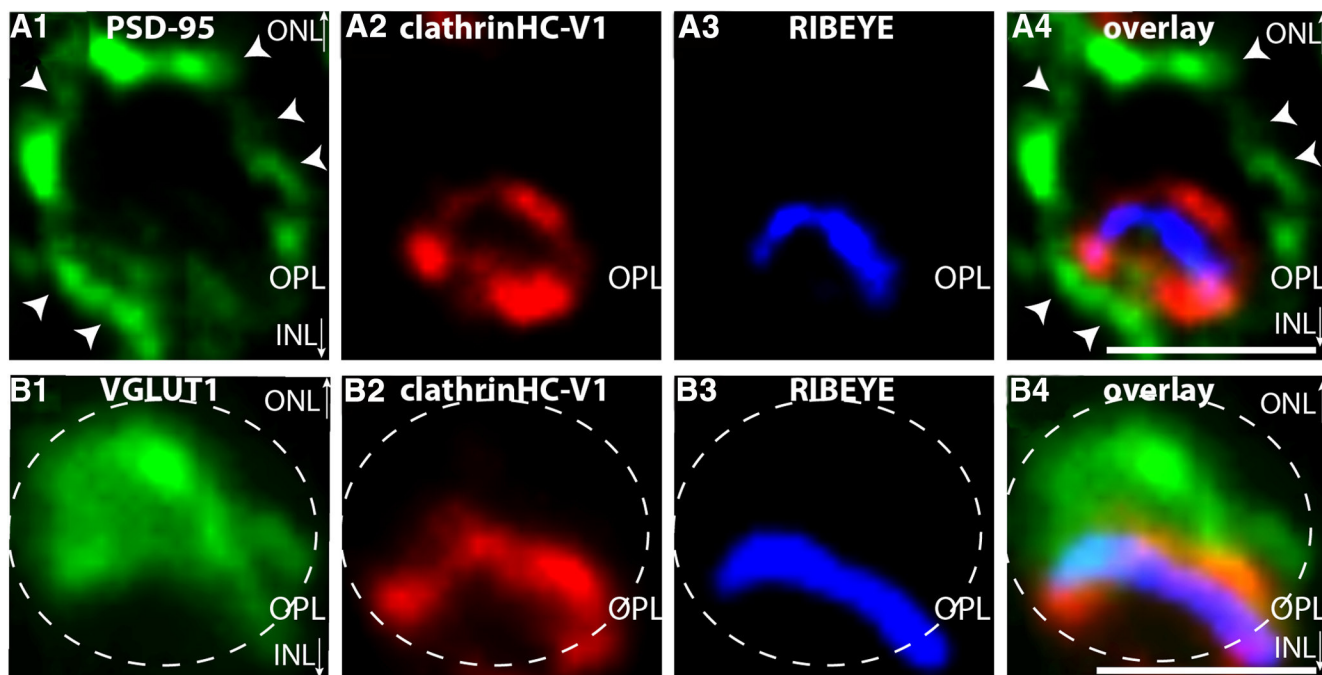


**Figure 11.** Localization of CHC-V1 in the presynaptic rod photoreceptor terminal in relation to PSD-95 and VGLUT1. **A, B**, The 0.5  $\mu\text{m}$  thin sections from mouse retina were triple immunolabeled with mouse monoclonal antibodies against PSD-95 (**A**) or VGLUT1 (**B**), rabbit polyclonal antibodies against CHC-V1 (abcam) (**A, B**) and DyLight 650 direct labeled primary antibodies against RIBEYE(B)/CtBP2 (**A, B**). The PSD-95 immunosignals in **A** demarcate the plasma membrane of photoreceptor presynaptic terminals in the OPL (**A**, arrowheads). In **B**, presynaptic terminals were immunolabeled with antibodies against the vesicular transporter VGLUT1, a marker protein of glutamatergic synaptic vesicles. The dashed circle in **B** denotes a single-immunolabeled presynaptic photoreceptor terminal. RIBEYE and CHC-V1 are located close to each other at the distal end of the photoreceptor terminal that is facing the INL (**A, B**). ONL, Outer nuclear layer; clathrinHC-V1, CHC-V1; OPL, outer plexiform layer; INL, inner plexiform layer. Scale bars, 1  $\mu\text{m}$ .

Finally, we performed postembedding electron microscopy with antibodies against dynamin to determine at the ultrastructural level where exactly dynamin is located in the distal portion of the presynaptic terminal. Postembedding immunogold electron microscopy demonstrated that dynamin is strongly enriched at the presynaptic plasma membrane in close vicinity to the synaptic ribbon (Fig. 4). This area is denoted as the periaxial zone in the text because it is located directly lateral to the active zone of exocytosis, where the synaptic ribbons are anchored and exocytosis occurs (for review, see Mercer and Thoreson, 2011; Schmitz et al., 2012). These ultrastructural immunolocalization data support the described light microscopy immunolabeling data, which demonstrated that dynamin is located  $\sim 120$  nm distant from the synaptic ribbon. Dynamin was found predominantly, though not exclusively, at the presynaptic plasma membrane in close vicinity to the synaptic ribbon (within  $\approx 250$  nm distance from the base of the synaptic ribbon). Some dynamin immunolabeling was also present at the presynaptic plasma membrane, some distance from the ribbon ( $>250$  nm away from the base of the ribbon). There was very little, if any, dynamin at the extrasynaptic outer plasma membrane of the photoreceptor presynaptic terminal,

which is not in contact with the tips of postsynaptic horizontal and bipolar cells (Fig. 4) (data not shown). The photoreceptor presynaptic terminal has a bell-shaped appearance, which is generated by the invagination of the entire postsynaptic dendritic complex into the photoreceptor presynaptic terminal (for review, see Gray and Pease, 1971; Schmitz, 2009). The outer extrasynaptic plasma membrane of this bell-shaped presynaptic terminal, which is not in contact with the dendritic complex, did not contain any dynamin immunoreactivity (Fig. 4) (data not shown). Only the inner, presynaptic plasma membrane was immunolabeled by the dynamin antibody with a strong enrichment of the dynamin immunogold label in the periaxial zones lateral to the synaptic ribbons (Fig. 4A–H) (data not shown).

#### Major SH3 domain-containing dynamin-binding proteins are also enriched at the periaxial zone in photoreceptor synapses

Dynamin is typically recruited to membranes via SH3 domain-containing proteins such as syndapin/pacsin and amphiphysin (Di Paolo et al., 2002; Yoshida et al., 2004; Wu et al., 2009b; Koch et al., 2011). We localized these proteins in the retina and in photoreceptor ribbon synapses to determine their localization, also compared with localization of dynamin and the synaptic ribbon. We found that the dynamin-interacting proteins amphiphysin and syndapin showed a very similar distribution as dynamin (Fig. 5). Both amphiphysin and syndapin were highly enriched in the synaptic layers of the retina, particularly in the OPL, and showed a highly discrete, punctate distribution pattern at these sites (Fig. 5). Amphiphysin and syndapin were particularly enriched in close proximity to the synaptic ribbon that was visualized with antibodies against RIBEYE (Fig. 5A, B).

Amphiphysin and syndapin were also highly clustered around the synaptic ribbon in these double-immunolabeling experi-

←

(Figure legend continued.) with rabbit polyclonal antibodies against CHC-V1 and mouse monoclonal antibodies against RIBEYE(B)-domain/CtBP2. In **D**, sections were double immunolabeled with rabbit polyclonal antibodies against CHC-V1 and mouse monoclonal antibodies against dynamin. CHC-V1 is located very close to both RIBEYE and bassoon but does not overlap. In contrast, the CHC-V1 immunosignals overlap with the dynamin immunosignal at the active zone of photoreceptor ribbon synapses to a large extent (**D**). **A, B**, and **D** were obtained by conventional imaging at high magnification; **C** is a maximum projection of a z-stack obtained by 2D-SR-SIM. Dashed circles in **A–D** denote single presynaptic photoreceptor terminals; clathrinHC-V1, CHC-V1; OPL, outer plexiform layer. Scale bars, 1  $\mu\text{m}$ .

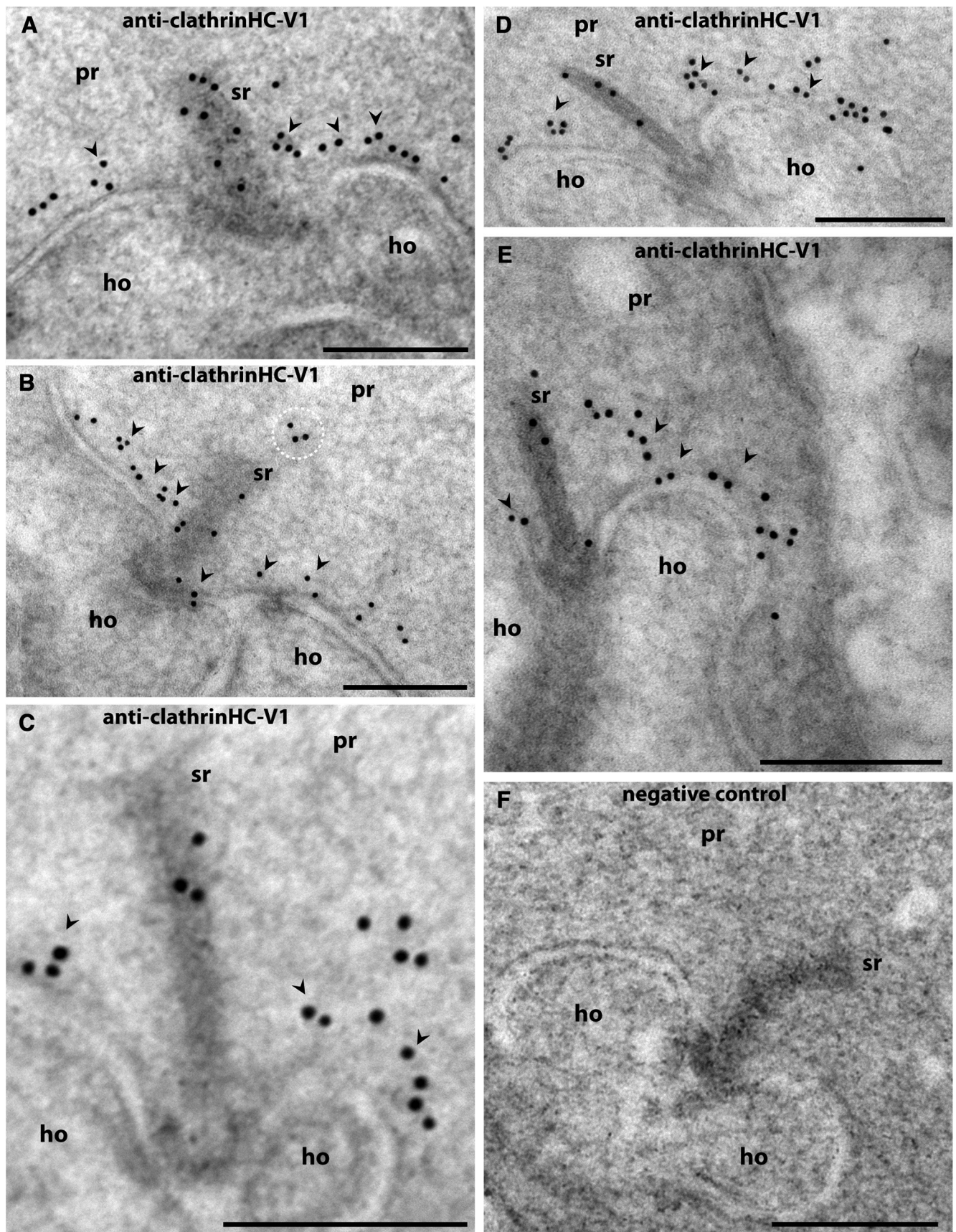


**Figure 12.** Postembedding immunogold labeling of photoreceptor synapses from the mouse retina with antibodies against CHC-V1. **A–E**, Ultrathin sections of the mouse retina were immunolabeled with mouse monoclonal antibodies against CHC-V1 (catalog #21679, abcam). Binding of the primary antibodies was detected with goat anti-rabbit antibodies conjugated to 10 nm gold particles. A strong CHC-V1 immunogold label (arrowheads) was observed at the plasma membrane in close proximity to the synaptic ribbon (sr). The immunogold labeling (*Figure legend continues.*)

ments in 2D-SR-SIM analyses (data not shown). The antibodies against amphiphysin/syndapin did not work for postembedding immunogold labeling in our hands. Therefore, we applied triple immunolabeling SR-SIM analyses to define the localization of these proteins in the presynaptic terminal as precise as possible at the light microscopic level. Using 2D-SR-SIM, we found that both amphiphysin as well as syndapin are typically localized and strongly enriched around the synaptic ribbon in these triple-immunolabeling analyses (Fig. 5C,D). The impression was confirmed by using 3D-SR-SIM of these triple-immunolabeling experiments (Fig. 6A,B). Both 2D-SR-SIM and 3D-SR-SIM results showed a tubulo-/vesicular-like distribution pattern of syndapin and amphiphysin around the synaptic ribbon (Figs. 5C,D, 6A,B).

Endophilin is another SH3-containing protein that can interact with dynamin (Mizuno et al., 2010; Llobet et al., 2011; Milosevic et al., 2011). In contrast to amphiphysin and syndapin (Figs. 5, 6), endophilin was neither enriched around the synaptic ribbon (Fig. 7A) nor restricted to the dynamin immunosignal around the synaptic ribbon (Fig. 7B). Endophilin was diffusely distributed throughout the entire presynaptic terminal (Fig. 7A–E). In these experiments, the extension of the presynaptic terminal was immunolabeled with panSV2 (Fig. 7C,D) or with antibodies against the VGLUT1 (Fig. 7E), both with identical results. All the described immunolabeling experiments could be specifically blocked with the respective antigen used for immunization (Fig. 8) (data not shown) but not with irrelevant peptides demonstrating the specificity of the immunolabeling analyses.

#### Localization of calcineurin, a putative $Ca^{2+}$ sensor of endocytosis, in photoreceptor ribbon synapses

Interestingly, calcineurin, a  $Ca^{2+}$ -sensing phosphatase involved in coupling  $Ca^{2+}$ -dependent activity and endocytosis (for review, see Clayton and Cousin, 2009), is highly enriched at the synaptic ribbon complex (Fig. 9). Thus, the influx of  $Ca^{2+}$  through voltage-gated calcium channels could mediate activity-dependent endocytosis at the synaptic ribbon through such a mechanism (see Discussion).

#### Evidence for two distinct clathrin heavy chain variants (CHC-V1 and CHC-V2) in the presynaptic photoreceptor terminal at distinct localizations

Finally, we analyzed for the distribution of clathrin. Clathrin is instrumental for many, though not all, forms of synaptic vesicle endocytosis (for review, see Murthy and de Camilli, 2003; Wilbur et al., 2005; Doherty and McMahon, 2009; Brodsky, 2012). To analyze the distribution of clathrin in photoreceptor presynaptic terminals, we used four different antibodies against different epitopes of clathrin heavy chain. In humans, two clathrin heavy chain genes (CHC17 and CHC22) are present (for review, see Brodsky, 2012). In the mouse genome, there is only one active clathrin heavy gene that corresponds to human CHC17. A second clathrin gene is a nonactive pseudogene in the mouse genome (Wakeham et al., 2005; for review, see Brodsky, 2012).

←

(Figure legend continued.) experiments confirm the previously shown immunofluorescence labeling data and demonstrate the enrichment of CHC-V1 in the periaxial zone of the photoreceptor ribbon synapse. Arrowheads indicate the CHC-V1 enrichment in the periaxial zone. Only a very minor fraction of CHC-V1 was found in the presynaptic cytosol (dashed circle). F is a negative control in which the primary antibody was omitted. clathrin-HC-V1, CHC-V1; pr, presynaptic photoreceptor terminal; ho, dendritic tips of postsynaptic horizontal cells; pm, plasma membrane. Scale bars: A–F, 250 nm.

We used two different antibodies raised against the C terminus of clathrin heavy chain (ab21679, abcam; P1663, Cell Signaling Technology) for the immunolocalization analyses. The clathrin variant, detected by these antibodies, is denoted as CHC-V1 in the following text. Using these antibodies against CHC-V1, we observed a strong clathrin signal in close vicinity to the RIBEYE-immunolabeled synaptic ribbon (Figs. 10, 11) (data not shown). The clathrin immunosignal was surrounding both the bassoon-labeled active zone (Fig. 10A) and the RIBEYE-immunolabeled synaptic ribbon (Fig. 10B). Also, SR-SIM analyses of thin-sectioned mouse photoreceptor synapses that were double immunolabeled with antibodies against RIBEYE and CHC-V1 demonstrated a close spatial correlation of these proteins. The CHC-V1 immunosignal closely surrounded the RIBEYE-labeled synaptic ribbon in these SR-SIM analyses (Fig. 10C). The CHC-V1 immunosignal overlapped to a large extent with the dynamin immunosignal (Fig. 10D).

The CHC-V1 immunosignal is, similar to the synaptic ribbon, localized in the distal portion of the synaptic terminal that faces the INL (Fig. 11). The borders of the presynaptic terminal were marked either with antibodies against PSD-95, which labels the presynaptic plasma membrane of photoreceptor terminals (Fig. 11A), or with antibodies against VGLUT1 (Fig. 11B), a component of the presynaptic glutamatergic vesicles. In Western blotting analyses, CHC-V1 migrated at the expected molecular weight position of clathrin heavy chain (Fig. 1F; see also Fig. 13A, lane 1). The CHC-V1 immunofluorescence signals could be blocked by preabsorption with the respective peptide used for immunization (see Fig. 13C) but not by preabsorption with control peptides (see Fig. 13B), demonstrating the specificity of the immunolabeling data.

Finally, postembedding immunogold electron microscopy with antibodies against CHC-V1 demonstrated that a strong CHC-V1 immunosignal was actually found at the presynaptic plasma membrane in close proximity (within  $\approx 250$  nm) from the synaptic ribbon (Fig. 12). These ultrastructural data completely confirm and extend the light microscopic CHC-V1 immunolabeling data and show the localization of CHC-V1 in the periaxial zone (Fig. 12) in a very similar position as that shown above for dynamin (Fig. 4).

We found evidence for a second clathrin-containing compartment that is not spatially related to the synaptic ribbon (see Figs. 14, 15). This clathrin-containing compartment was labeled by two different antibodies directed against epitopes in the central region of clathrin heavy chain (ab59710, Abcam; X22, abcam). This clathrin heavy chain variant detected by these latter antibodies is denoted as CHC-V2 in the following text. CHC-V2 migrates slightly slower than CHC-V1 at a slightly higher molecular weight position (Fig. 13A). This becomes obvious if low percentage (5%) acrylamide SDS-PAGE gels (Fig. 13A) were used (instead of 8% acrylamide running gels; Fig. 1G). In immunolabeling analyses, CHC-V2 is located a large distance from both RIBEYE and the active zone protein bassoon as well as CHC-V1 as judged by high-resolution double-immunolabeling analyses (Fig. 14A–C). The mean distance of CHC-V2 from RIBEYE and bassoon puncta (nearest, mean distance) is  $\approx 580 \pm 210$  nm (100 synapses analyzed) for CHC-V2-RIBEYE and  $\approx 750 \pm 200$  nm (100 synapses analyzed) for CHC-V2-bassoon. These are two large distances particularly if one considers that the diameter of a single rod photoreceptor terminal, measured as distance of the lateral PSD-95 immunosignals of a single synaptic terminal, is  $\approx 1280 \pm 330$  nm (100 synapses analyzed). Despite the large

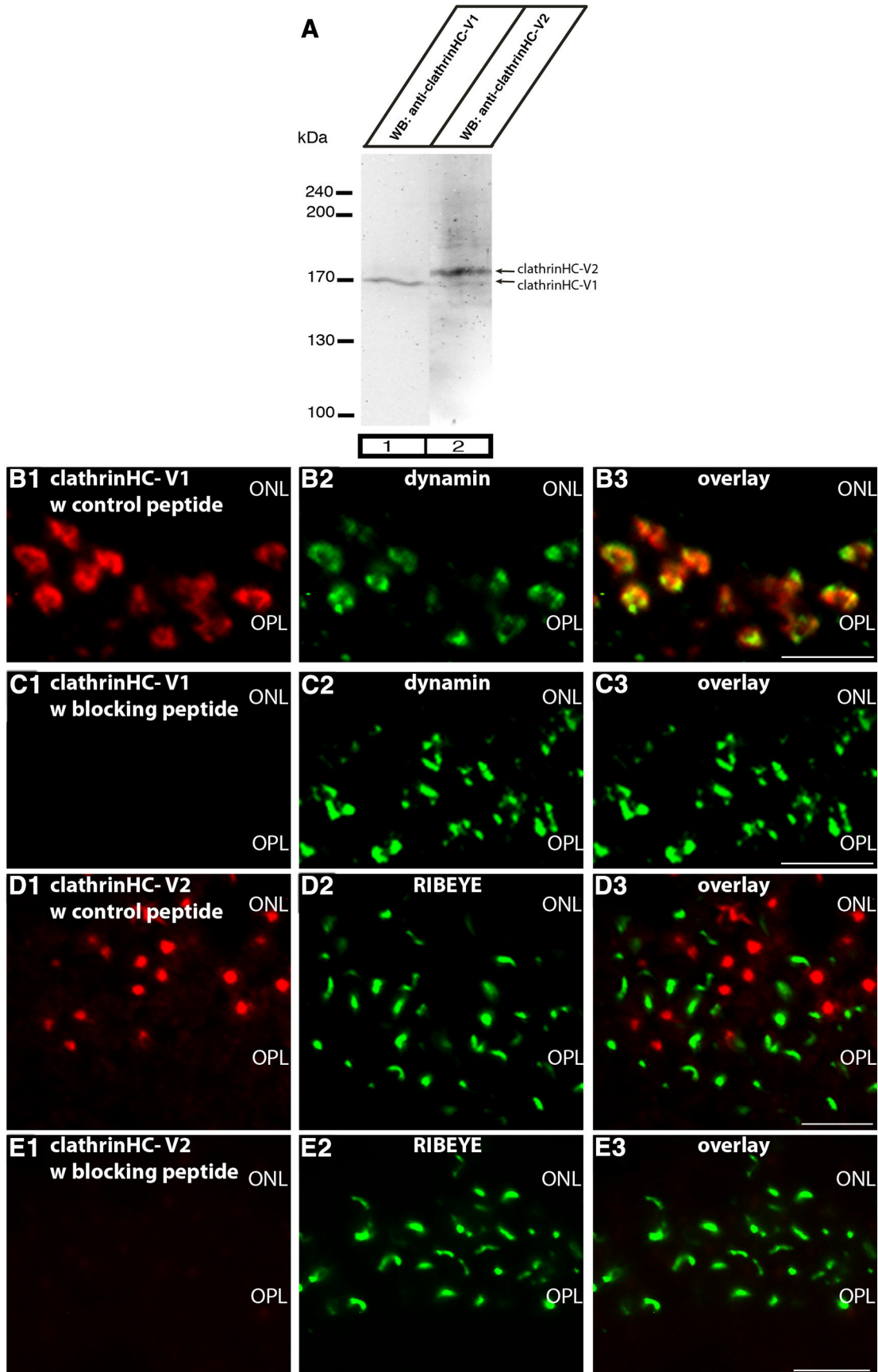


**Figure 13.** *A*, Western blot analyses of two different clathrin heavy chains, variant 1 and variant 2 (after separation in 5% acrylamide SDS-PAGE running gels). The running position of the immunoreactive bands detected by the different antibodies against the CHC-V1 (lane 1) and antibodies against clathrin heavy chain variant 2 (lane 2) differ slightly. CHC-V1 is slightly smaller than CHC-V2 in Western blot analyses (after separation in 5% acrylamide SDS-PAGE running gels). *B–E*, Pre-absorption control experiments for the antibodies against CHC-V1 (*Figure legend continues.*)

distance of CHC-V2 from the synaptic ribbon, CHC-V2 is still located in the presynaptic terminal as judged by triple-immunolabeling experiments with antibodies against PSD-95/VGLUT1, RIBEYE, and anti-CHC-V2 (Fig. 15*A,B*). But, in contrast to CHC-V1, CHC-V2 is located in the proximal portion of the presynaptic terminal, which is separated from the synaptic ribbon by the bulk of glutamatergic synaptic vesicles (Fig. 15*B*). The antibodies against CHC-V2 did not work in postembedding immunogold electron microscopy. But since this clathrin variant is clearly not associated with the synaptic ribbon complex the identification of the underlying organelle, though principally important, is of minor relevance for the present study, which is concerned with vesicle retrieval in the periaxial zone surrounding the synaptic ribbon complex (see also Discussion).

### The periaxial zone of photoreceptor ribbon synapses is a hotspot of endocytic activity

Finally, we also presented functional evidence that the synaptic ribbon complex is a hotspot of endocytic activity. If isolated mouse photoreceptors (Fig. 16*A*) were loaded with a short pulse of the fluid-phase marker SR101, SR101 was predominantly taken up in immediate vicinity to the synaptic ribbon (Fig. 16*B–D*) (data not shown). The synaptic ribbon was visualized by immunolabeling with antibodies against RIBEYE in these experiments. The uptake of SR101 was dependent upon dynamin activity because SR101 uptake was completely blocked in the presence of dynasore, a specific inhibitor of dynamin activity (Fig. 16*E*) (data not shown). Our data are schematically summarized in Figure 17.

### Discussion

In the present study, we analyzed the distribution of major proteins of the endocytic machinery in photoreceptor synapses with immunolabeling and high-resolution imaging. We found a strong enrichment of these proteins in the periaxial zone (i.e., the area that surrounds the active zone and the synaptic ribbon). In agreement with the periaxial zone enrichment, we observed a preferential uptake of sulforhodamine (SR101), a fluid-phase endocytosis marker, around synaptic

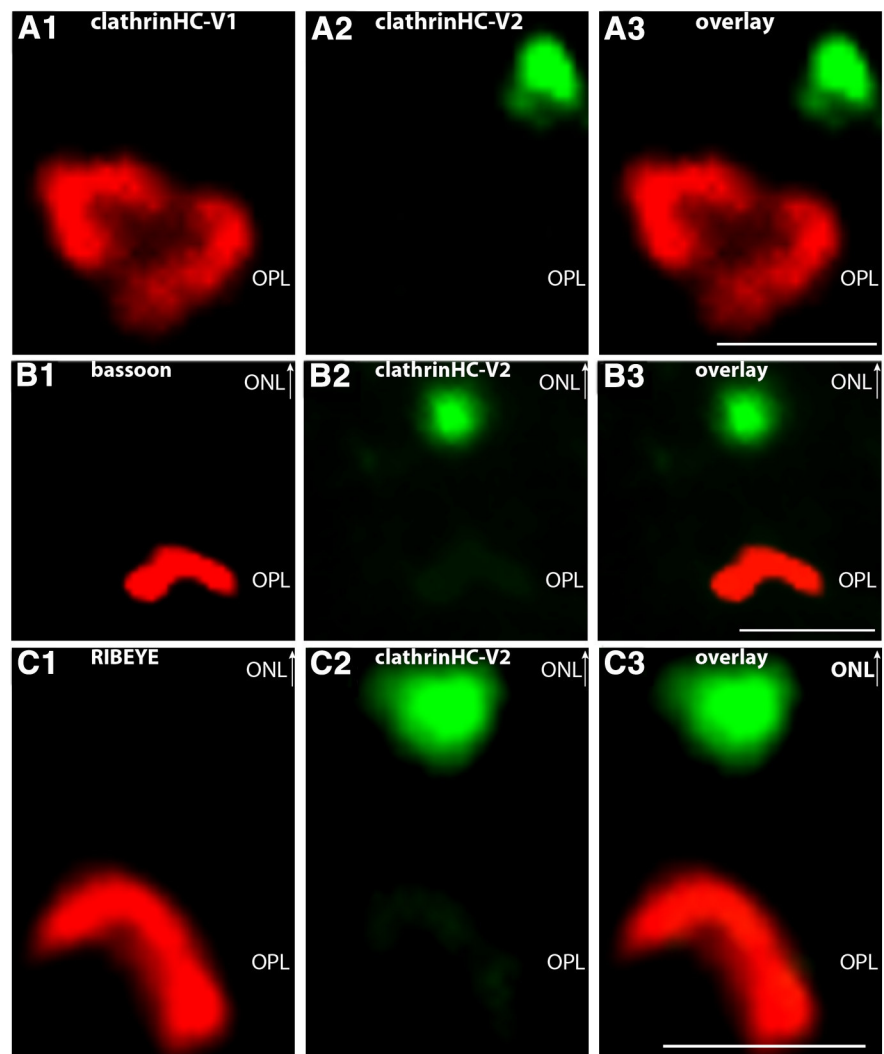


**Figure 14.** Two different clathrin heavy chain variants are found in photoreceptor terminals at different locations (immunofluorescence analyses). **A**, The 0.5  $\mu\text{m}$  thin sections of the mouse retina were double immunolabeled with rabbit polyclonal antibodies against CHC-V1 and mouse monoclonal antibodies against CHC-V2. The immunosignals for the two variants of clathrin heavy chain do not overlap and are located a large distance from each other (**A**). In **B** and **C**, sections were double immunolabeled with polyclonal antibodies against bassoon (**B**) and RIBEYE (**C**) to relate the localization of CHC-V2 to the localization of these proteins in the presynaptic photoreceptor terminal. Bassoon and RIBEYE are localized in a large distance from immunolabeled CHC-V2. For further localization data of CHC-V2 in relation to other proteins of the presynaptic terminal, see also Figure 15. ONL, Outer nuclear layer; OPL, outer plexiform layer; clathrinHC-V1, CHC-V1; clathrinHC-V2, CHC-V2. Scale bars, 1  $\mu\text{m}$ .

ribbons in mouse photoreceptors. These data suggest that the periaxial zone region in photoreceptor synapses is a hotspot of endocytic vesicle retrieval. Dynamin is likely to play an essential role in periaxial zone endocytosis because dynasore, a specific inhibitor of dynamin activity, completely inhibited ribbon complex-associated uptake of SR101. Visualization of periaxial zone endocytosis in photoreceptor terminals was achieved by short loading pulses with sulforhodamine (SR101) as an uptake marker for endocytosis. Longer tracer loading times generate a diffuse presynaptic labeling pattern (data not shown) similar to HRP uptake experiments in previous EM studies (Ripps et al., 1976; Schacher et al., 1976; Schaefer and Raviola, 1978; Cooper and McLaughlin, 1983).

The periaxial zone vesicle retrieval could promote rapid synaptic vesicle recycling, which is particularly important for the tonically active ribbon synapses. The suggested vesicle retrieval at the periaxial zone close to the synaptic ribbon is in line with recent findings that supported a major role of synaptic ribbons

(Figure legend continued.) and CHC-V2 (immunolabeling analyses). Double immunolabeling of 0.5  $\mu\text{m}$  thin mouse retinal sections with the indicated antibodies preabsorbed with either their specific peptide used for immunization (**C, E**) or with an unrelated control peptide (**B, D**). In parallel, sections were incubated with monoclonal anti-dynamin antibodies (**B, C**) or RIBEYE (**D, E**) as labeling positive controls. The specific peptides completely blocked the respective clathrin heavy chain immunosignals (**C, E**), whereas the control peptide had no influence of the clathrin heavy chain immunosignals (**B, D**) showing the specificity of the immunolabeling signals. ONL, Outer nuclear layer; OPL, outer plexiform layer; clathrinHC-V1, CHC-V1; clathrinHC-V2, CHC-V2. Scale bars: **B–E**, 5  $\mu\text{m}$ .

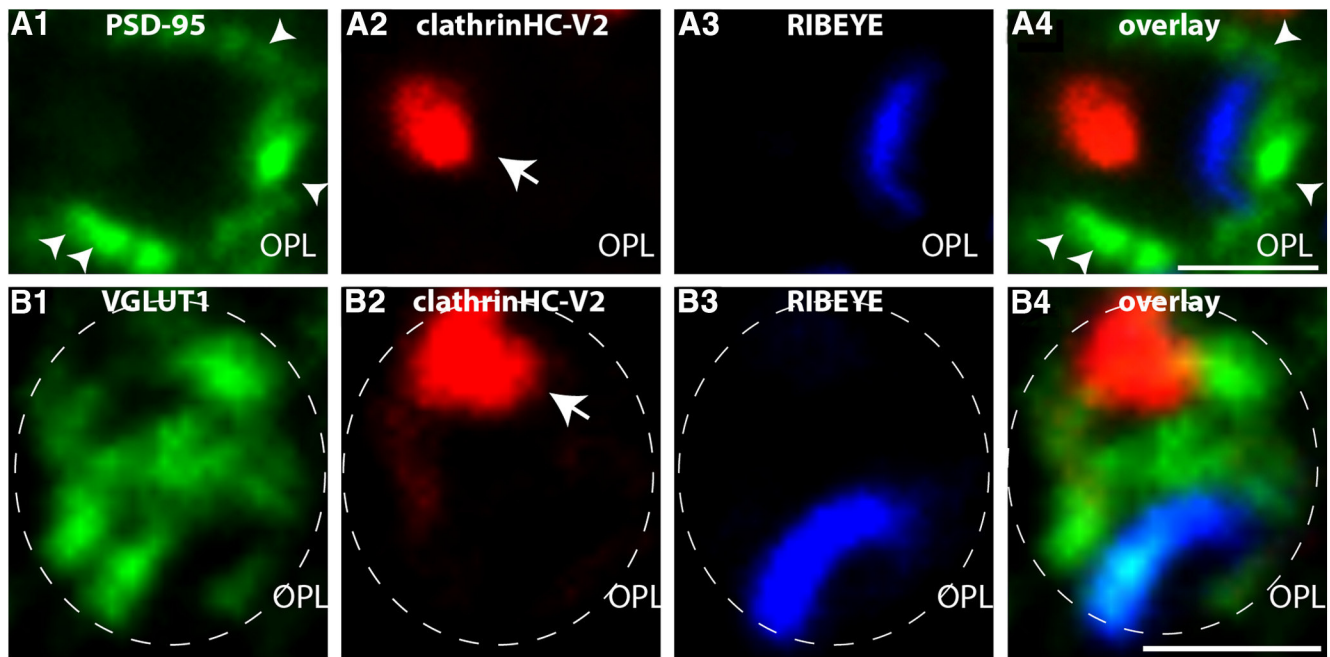


**Figure 15.** Localization of CHC-V2 (clathrinHC-V2) in the presynaptic photoreceptor terminal in relation to PSD-95 and VGLUT1. In **A** and **B**,  $0.5\ \mu\text{m}$  thin sections of the mouse retina were triple immunolabeled with rabbit polyclonal antibodies against CHC-V2 and mouse monoclonal antibodies against either PSD-95 (**A**) or VGLUT1 (**B**). The synaptic ribbon was visualized with a DyLight 650-labeled primary antibody against RIBEYE(B)-domain/CtBP2. The PSD-95 immunosignals demarcate the plasma membrane of the entire photoreceptor presynaptic terminal (arrowheads). The CHC-V2 antibody labeled a spot-like structure in the presynaptic terminal (arrows) that—in contrast to CHC-V1—was localized in a large distance from the synaptic ribbon. A virtually identical immunolabeling pattern was obtained if the sections were triple immunolabeled with a monoclonal antibody (X22, abcam) against CHC-V2, a rabbit polyclonal antibody against PSD-95, and the DyLight 650 directly labeled antibody against RIBEYE(B)-domain/CtBP2 (data not shown). Identical results were obtained if presynaptic vesicles were immunolabeled with rabbit polyclonal antibodies against VGLUT1 and if CHC-V2 was immunolabeled with the monoclonal clathrin heavy chain antibody X22 (abcam) (data not shown). Similarly, as in **A** and **B**, the localization of the synaptic ribbon was determined by DyLight 650-labeled primary antibody against RIBEYE(B)-domain/CtBP2 in these incubations (data not shown). **B**, The CHC-V2 was located in a spot-like manner (arrow in B2) at the entry of the presynaptic terminal. CHC-V2 was separated from the synaptic ribbon by the bulk of glutamatergic synaptic vesicles that were immunolabeled by VGLUT1 antibodies (**B**). This distribution of CHC-V2 is in contrast to the distribution of CHC-V1 (see Figs. 10, 11). In contrast to CHC-V2, CHC-V1 is highly enriched around the synaptic ribbon (compare with Fig. 11A,B). Dashed circles in **B** denote a single presynaptic photoreceptor terminal in the outer plexiform layer (OPL). clathrinHC-V2, CHC-V2; clathrinHC-V1, CHC-V1. Scale bars,  $1\ \mu\text{m}$ .

for recycling of release-ready synaptic vesicles (Jackman et al., 2009; Babai et al., 2010). This proposal is conceptionally similar to periactive zone endocytosis found also in other synapses (e.g., in lamprey neurons, neuromuscular junction and hippocampal synapses) (Teng et al., 1999; for review, see Shupliakov, 2009; Haucke et al., 2011; Hua et al., 2011; Saheki and De Camilli, 2012; Yamashita, 2012). It will be interesting to see how regulation of periactive zone endocytosis is accomplished in these physiologically different types of synapses.

In general, different forms of endocytosis involve different sets of proteins (for review, see Wu et al., 2007; Dittman and Ryan, 2009; Doherty and McMahon, 2009; Donaldson et al., 2009; Scita and Di Fiori, 2010; Sandvig et al., 2011; Saheki and De Camilli, 2012). We found dynamin as well as the dynamin-associated proteins syndapin/pacsin and amphiphysin highly enriched in close vicinity to the synaptic ribbons. In agreement with the light microscopic immunolabeling data, dynamin was found preferentially localized at the presynaptic plasma membrane next to the synaptic ribbon, as judged by postembedding immunogold electron microscopy. These ultrastructural data further support the concept of periactive zone endocytosis in ribbon synapses. Dynamin immunoreactivity at the plasma membrane outside of the periactive zone could support retrieval of vesicles that have been fused outside of the ribbon-associated active zone (Midorikawa et al., 2007; Zenisek, 2008). Endophilin was also found at the synaptic ribbon but predominantly diffusely distributed throughout the entire presynaptic terminal. In conventional synapses, endophilin is also distributed diffusely in the entire

synaptic vesicle pool, although endophilin acts at the plasma membrane (Bai et al., 2010). Similarly, intersectin, a periactive zone component in conventional synapses, cycles between different locations in the presynaptic terminal (for review, see Shupliakov, 2009; Pechstein et al., 2010; Haucke et al., 2011).

Remarkably, we detected two immunologically distinct forms of clathrin heavy chain in the presynaptic photoreceptor terminal, CHC-V1 and CHC-V2. CHC-V1 was associated with the synaptic ribbon complex, whereas CHC-V2 was not localized at synaptic ribbons. CHC-V1 immunosignals at the synaptic ribbon complex largely overlapped with the dynamin immunoreactivity at that site. In support of these light microscopic data, we showed by immunogold electron microscopy that CHC-V1 is preferentially localized at the presynaptic plasma membrane in close vicinity to the active zone and synaptic ribbon. The antibodies against CHC-V2 did not work for postembedding immunogold electron microscopy. But the CHC-V2 immunosignals were clearly localized a large distance ( $\approx 580\ \text{nm}$ ) from the bassoon-labeled active zone in the proximal part of the presynaptic terminal and thus cannot contribute to periactive zone endocytosis. The identity and function of this CHC-V2-containing compartment needs to be elucidated in detail by future investigations. The molecular difference between CHC-V1 and CHC-V2 is unknown, but could involve differential splicing and/or differential post-translational modifications.

Our proposal of periactive zone endocytosis in photoreceptor synapses is in agreement with electron microscopic data that demonstrated coated buds and coated vesicles at the presynaptic

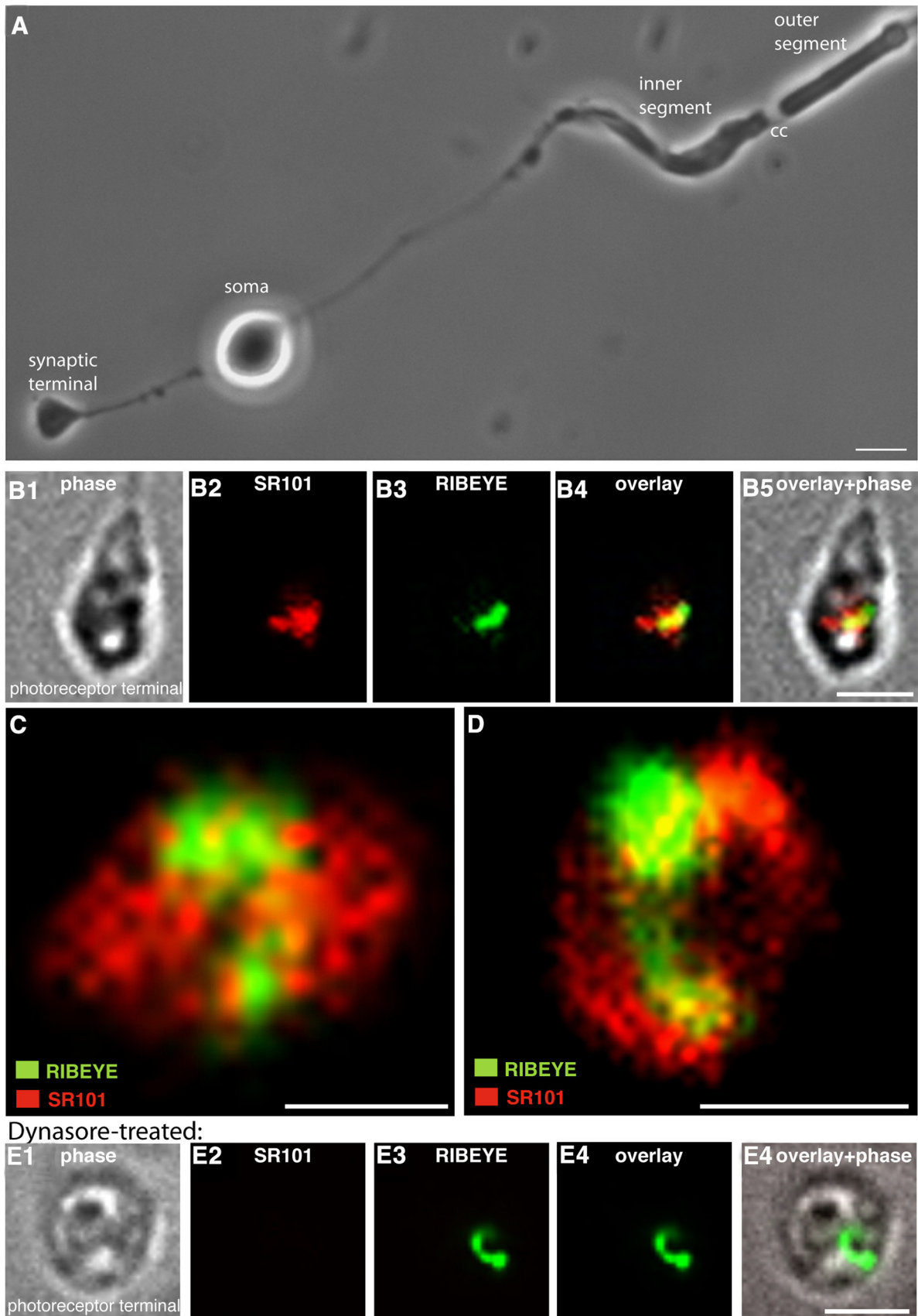


**Figure 16.** Imaging of synaptic ribbon-associated endocytosis in isolated mouse photoreceptors. Isolated mouse photoreceptors (shown in **A**) were incubated for 2 min with sulforhodamine (SR101), which is taken up by fluid-phase endocytosis. Afterward, SR101-loaded photoreceptors were fixed and immunolabeled with antibodies against RIBEYE(B)-domain/CtBP2. A hotspot of SR101 uptake is found in close association with the synaptic ribbon (**B–D**; and data not shown). **B** was obtained by conventional imaging; **C** and **D** are maximum projections of z-stacks from confocal imaging. Pretreatment with dynasore, a specific inhibitor of dynamin (100  $\mu$ M), completely inhibited the synaptic ribbon-associated uptake of SR101 (red channel) (**E** and data not shown). Scale bars, 1  $\mu$ m.

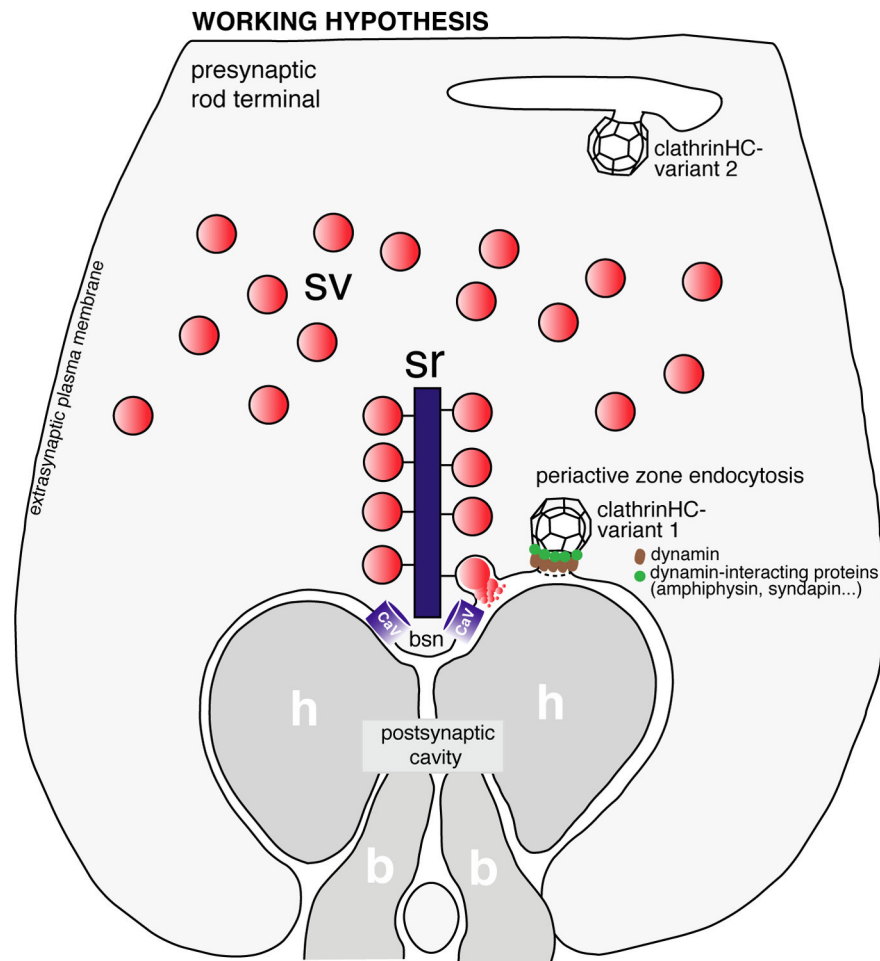


**Figure 17.** Simplified, schematic summary of the immunolocalization data presented in the manuscript. Key players of endocytic membrane traffic, including dynamin, dynamin-binding proteins, and CHC-V1, are enriched in a periactive zone of photoreceptor synapses. Besides CHC-V1, CHC-V2 is also present in the presynaptic photoreceptor terminal. In contrast to CHC-V1, CHC-V2 is located a large distance from the periactive zone, possibly on an endosomal compartment in the proximal region of the presynaptic terminal. Endosomal-like membrane compartments have been previously observed by transmission electron microscopy in this part of the photoreceptor terminal (Ripps et al., 1976; Schacher et al., 1976; Schaeffer and Raviola, 1978; Cooper and McLaughlin, 1983). The drawing of the photoreceptor terminal is modified based on a drawing of Gray and Pease (1971). sr, Synaptic ribbon; sv, synaptic vesicles; clathrinHC-V1, clathrin heavy chain variant 1, CHC-V1; clathrinHC-V2, CHC-V2; CaV, voltage-gated calcium channels of the photoreceptor active zone; h, postsynaptic dendritic tip of a horizontal cell; b, postsynaptic dendritic tip of an invaginating bipolar cell; bsn, bassoon.

plasma membrane lateral to the synaptic ribbon (Gray and Pease, 1971). These coated membranes were located in pouches of the presynaptic terminals located lateral to the synaptic ribbon and opposite to the dendritic tips of horizontal cells. These are exactly the sites where we found a strong enrichment of dynamin and a clathrin heavy chain variant (CHC-V1) using immunogold electron microscopy.

Previous analyses, mostly obtained from electrophysiological analyses of retinal bipolar cells and inner ear hair cells, revealed at least two distinct modes of endocytosis in ribbon synapses: a fast phase and a slow phase of endocytosis (Neves and Lagnado, 1999; Moser and Beutner, 2000; Beutner et al., 2001; Wu et al., 2007; for review, see LoGiudice and Matthews, 2007; Smith et al., 2008; Royle and Lagnado, 2010), with time constants of  $\approx 1$  and  $\approx 15$ – $30$  s. Future analyses need to show to which mode periactive endocytosis will contribute. In terms of its localization, it would be ideally suited to serve fast endocytosis in photoreceptors. In retinal bipolar cells, fast endocytosis was found to be clathrin independent however (Jockusch et al., 2005).

The local periactive zone endocytic machinery in photoreceptor synapses will be exposed to fluctuations of presynaptic  $[Ca^{2+}]_i$  that result from  $Ca^{2+}$  influx through voltage-gated  $Ca^{2+}$  channels at the active zone. The role of  $Ca^{2+}$  in endocytosis is not completely understood (for review, see Smith et al., 2008; Shupliakov, 2009; Yamashita, 2012). But many recent studies have demonstrated that increases of  $[Ca^{2+}]_i$  can promote and activate endocytosis (Neves and Lagnado, 1999; Beutner et al., 2001; Neves et al., 2001; Wu et al., 2005, 2007, 2009a; Hosoi et al., 2009; Babai et al., 2010; Schnee et al., 2011). Recent analyses suggested that vesicle recycling occurs close to presynaptic voltage-gated  $Ca^{2+}$  channels in photoreceptor ribbon synapses and could be stimulated by increases of presynaptic  $Ca^{2+}$  (Babai et al., 2010).

We found calcineurin, a  $Ca^{2+}$ -activated calmodulin-dependent phosphatase, localized in close vicinity to the synaptic ribbon. In conventional synapses, calcineurin is a  $Ca^{2+}$ -dependent regulator of endocytosis that adjusts activity-dependent endocytosis by dephosphorylating endocytic proteins (e.g., dynamin). By this way, it controls functionally important protein–protein interactions in endocytic networks (for review, see Cousin and Robinson, 2001; Clayton and Cousin, 2009; Yamashita, 2012). Thus, calcineurin is a potential  $Ca^{2+}$  sensor that could adjust local, ribbon-associated endocytosis to different levels of synaptic activity also in photoreceptor ribbon synapses. Calcineurin specifically binds to the dynamin-1Xb splice isoform of dynamin-1 (Bodmer et al., 2011; Xue et al., 2011), predicting that this dynamin splice variant is present at synaptic ribbons of photoreceptor synapses. Clearly,

further possibilities could also apply. In conventional synapses, various mechanisms are known to be installed that regulate endocytosis (for review, see Südhof, 2004, 2012; Shupliakov, 2009; Koch and Holt, 2012; Yamashita, 2012; Yao et al., 2012).

Recently, it was demonstrated that CtBP proteins perform an important role in mediating certain aspects of endocytosis (Bonazzi et al., 2005; Amstutz et al., 2008; Liberali et al., 2008; for review, see Hansen and Nichols, 2009). RIBEYE is also a member of the CtBP protein family and could possibly fulfill a similar role in the ribbon synapse. Recently, the RIBEYE(B) domain was demonstrated to be a lysophosphatidic acid-acyltransferase that generates phosphatidic acid (PA) at the synaptic ribbon (Schwarz et al., 2011). PA promotes negative membrane curvature that favors vesicle budding and fission (Jenkins and Frohman, 2005; Roth, 2008; Yang et al., 2008). PA stimulates binding of dynamin to membranes (Burger et al., 2000; Andresen et al., 2002; Roth, 2008) and thus might play a role in distinct aspects of endocytotic membrane traf-

ficking (Donaldson, 2009; Fine et al., 2011; Lariccia et al., 2011; Malhotra and Campelo, 2011; Campelo and Malhotra, 2012).

Currently, we can only speculate how the endocytic machinery is anchored at the synaptic ribbon complex of photoreceptor synapses. The protein Munc119 is recruited to synaptic ribbons via interaction with RIBEYE (Alpadi et al., 2008). Interestingly, Munc119 was found in a protein complex with dynamin in T lymphocytes and shown to regulate dynamin function (Karim et al., 2010). Therefore, Munc119 might perform a similar role in photoreceptor ribbon synapses by anchoring the endocytic machinery to synaptic ribbons and/or regulating its activity.  $\beta$ -subunits of voltage-gated  $\text{Ca}^{2+}$  channels also bind dynamin (Gonzalez-Gutierrez et al., 2007; Miranda-Laferte et al., 2011; Xue et al., 2011) and thus could be also involved in recruiting the endocytotic machinery. One needs to keep in mind that endocytic retrieval might differ in different types of ribbon synapses. For example, bulk membrane retrieval (Cousin, 2009) is an important mechanism of membrane retrieval in retinal bipolar cells (Holt et al., 2003; Paillart et al., 2003) but is absent in photoreceptor terminals (Rea et al., 2004). Furthermore, multiple modes of endocytosis could coexist in a single synapse (Holt et al., 2003; Paillart et al., 2003; LoGiudice et al., 2009).

## References

- Aartsen WM, Arsanto JP, Chauvin JP, Vos RM, Versteeg I, Cardozo BN, Bivic AL, Wijnholds J (2009) PSD95beta regulates plasma membrane  $\text{Ca}^{2+}$ -pump localization at the photoreceptor synapse. *Mol Cell Neurosci* 41:156–165. [CrossRef Medline](#)
- Alpadi K, Magupalli VG, Käppel S, Köblitz L, Schwarz K, Seigel GM, Sung CH, Schmitz F (2008) RIBEYE recruits Munc119, the mammalian ortholog of the *Caenorhabditis elegans* protein unc119, to synaptic ribbons of photoreceptor synapses. *J Biol Chem* 283:26461–26467. [CrossRef Medline](#)
- Amstutz B, Gastaldelli M, Kälin S, Imelli N, Boucke K, Wandeler E, Mercer J, Hemmi S, Greber UF (2008) Subversion of CtBP1-controlled macropinocytosis by human adenovirus serotype3. *EMBO J* 27:956–969. [CrossRef Medline](#)
- Andresen BT, Rizzo MA, Shome K, Romero G (2002) The role of phosphatidic acid in the regulation of the Ras/MEK/Erk signalling cascade. *FEBS Lett* 531:65–68. [CrossRef Medline](#)
- Babai N, Bartoletti TM, Thoreson WB (2010) Calcium regulates vesicle replenishment at the cone ribbon synapse. *J Neurosci* 30:15866–15877. [CrossRef Medline](#)
- Bai J, Hu Z, Dittman JS, Pym EC, Kaplan JM (2010) Endophilin functions as a membrane-binding molecule and is delivered to endocytic zones by exocytosis. *Cell* 143:430–441. [CrossRef Medline](#)
- Bennett V (1983) Proteins involved in membrane-cytoskeleton association in human erythrocytes: spectrin, ankyrin and band 3. *Methods Enzymol* 96:313–324. [CrossRef Medline](#)
- Beutner D, Voets T, Neher E, Moser T (2001) Calcium dependence of exocytosis and endocytosis at the cochlear inner hair cell afferent synapse. *Neuron* 29:681–690. [CrossRef Medline](#)
- Bodmer D, Ascaño M, Kuruvilla R (2011) Isoform specific dephosphorylation of dynamin1 by calcineurin couples neurotrophin receptor endocytosis to axonal growth. *Neuron* 70:1085–1099. [CrossRef Medline](#)
- Bonazzi M, Spanò S, Turacchio G, Cericola C, Valente C, Colanzi A, Kweon HS, Hsu VW, Polishchuck EV, Polishchuck RS, Sallèse M, Pulvirenti T, Corda D, Luini A (2005) CtBP3/BARS drives membrane fission in dynamin-independent transport pathways. *Nat Cell Biol* 7:570–580. [CrossRef Medline](#)
- Brodsky FM (1985) Clathrin structure characterized with monoclonal antibodies. I. Analysis of multiple antigenic sites. *J Cell Biol* 101:2047–2054. [CrossRef Medline](#)
- Brodsky FM (2012) Diversity of clathrin function: new tricks for an old protein. *Annu Rev Cell Dev Biol* 28:309–336. [CrossRef Medline](#)
- Buckley K, Kelly RB (1985) Identification of a transmembrane glycoprotein specific for secretory vesicles of neuronal and endocrine cells. *J Cell Biol* 100:1284–1294. [CrossRef Medline](#)
- Burger KN, Demel RA, Schmid SL, de Kruijff B (2000) Dynamin is membrane-active: lipid insertion is induced by phosphoinositides and phosphatidic acid. *Biochemistry* 39:12485–12493. [CrossRef Medline](#)
- Campelo F, Malhotra V (2012) Membrane fission: the biogenesis of transport vesicles. *Annu Rev Biochem* 81:407–427. [CrossRef Medline](#)
- Clayton EL, Cousin MA (2009) The molecular physiology of activity-dependent bulk endocytosis of synaptic vesicles. *J Neurochem* 111:901–914. [CrossRef Medline](#)
- Cooper NG, McLaughlin BJ (1983) Tracer uptake by photoreceptor synaptic terminals. *J Ultrastruct Res* 84:252–267. [CrossRef Medline](#)
- Cousin MA (2009) Activity-dependent bulk synaptic vesicle endocytosis—a fast, high capacity membrane retrieval mechanism. *Mol Neurobiol* 39:185–189. [CrossRef Medline](#)
- Cousin MA, Robinson PJ (2001) The dephosphins: dephosphorylation by calcineurin triggers synaptic vesicle endocytosis. *Trends Neurosci* 24:659–665. [CrossRef Medline](#)
- Di Paolo G, Sankaranarayanan S, Wenk MR, Daniell L, Perucco E, Caldaroni BJ, Flavell R, Picciotto MR, Ryan TA, Cremona O, De Camilli P (2002) Decreased synaptic vesicle recycling efficiency and cognitive defects in amphiphysin 1 knockout mice. *Neuron* 33:789–804. [CrossRef Medline](#)
- Dittman J, Ryan TA (2009) Molecular circuitry of endocytosis at nerve terminals. *Annu Rev Cell Dev Biol* 25:133–160. [CrossRef Medline](#)
- Doherty GJ, McMahon HT (2009) Mechanisms of endocytosis. *Annu Rev Biochem* 78:857–902. [CrossRef Medline](#)
- Donaldson JG (2009) Phospholipase D in endocytosis and endosomal recycling pathways. *Biochim Biophys Acta* 1791:845–849. [CrossRef Medline](#)
- Donaldson JG, Porat-Shliom N, Cohen LA (2009) Clathrin-independent endocytosis: a unique platform for cell signalling and PM remodelling. *Cell Signal* 21:1–6. [CrossRef Medline](#)
- Drenckhahn D, Franz H (1986) Identification of actin-,  $\alpha$ -actinin-, and viculin-containing plaques at the lateral membrane of epithelial cells. *J Cell Biol* 102:1843–1852. [CrossRef Medline](#)
- Euler T, Hausselt SE, Margolis DJ, Breuninger T, Castell X, Detwiler PB, Denk W (2009) Eyecup scope—optical recordings of light stimulus-evoked fluorescence signals in the retina. *Pflugers Arch* 457:1393–1414. [CrossRef Medline](#)
- Ferguson SM, De Camilli P (2012) Dynamin, a membrane remodelling GTPase. *Nat Rev Mol Cell Biol* 13:75–88. [CrossRef Medline](#)
- Ferguson SM, Brasnjo G, Hayashi M, Wölfel M, Collesi C, Giovedi S, Raimondi A, Gong LW, Ariel P, Paradise S, O’toole E, Flavell R, Cremona O, Miesenböck G, Ryan TA, De Camilli P (2007) A selective activity-dependent requirement for dynamin 1 in synaptic vesicle endocytosis. *Science* 316:570–574. [CrossRef Medline](#)
- Fine M, Llaguno MC, Lariccia V, Lin MJ, Yaradanakul A, Hilgemann DW (2011) Massive endocytosis driven by lipidic forces originating in the outer plasmalemmal monolayer: a new approach to membrane recycling and lipid domains. *J Gen Physiol* 137:137–154. [CrossRef Medline](#)
- Frank T, Rutherford MA, Strenke N, Neef A, Pangršič T, Khimich D, Fetjova A, Gundelfinger ED, Liberman MC, Harke B, Bryan KE, Lee A, Egnér A, Riedel D, Moser T (2010) Bassoon and the synaptic ribbon organize  $\text{Ca}^{2+}$ -channels and vesicles to add release sites and promote refilling. *Neuron* 68:724–738. [CrossRef Medline](#)
- Gonzalez-Gutierrez G, Miranda-Laferte E, Neely A, Hidalgo P (2007) The src homology 3 domain of the  $\beta$ -subunit of voltage-gated calcium channels promotes endocytosis via dynamin interactions. *J Biol Chem* 282:2156–2162. [CrossRef Medline](#)
- Gray EG, Pease HL (1971) On understanding the organization of the retinal receptor synapses. *Brain Res* 35:1–15. [CrossRef Medline](#)
- Griesinger CB, Richards CD, Ashmore JF (2005) Fast vesicle replenishment allows indefatigable signalling at the first auditory synapse. *Nature* 435:212–215. [CrossRef Medline](#)
- Gustafsson MG, Shao L, Carlton PM, Wang CJ, Golubovskaya IN, Cande WZ, Agard DA, Sedat JW (2008) Three-dimensional resolution doubling in wide-field fluorescence microscopy by structured illumination. *Biophys J* 94:4957–4970. [CrossRef Medline](#)
- Hansen CG, Nichols BJ (2009) Molecular mechanisms of clathrin-independent endocytosis. *J Cell Sci* 122:1713–1721. [CrossRef Medline](#)
- Hauacke V, Neher E, Sigris SJ (2011) Protein scaffolds in the coupling of synaptic exocytosis and endocytosis. *Nat Rev Neurosci* 12:127–138. [CrossRef Medline](#)
- Heidelberger R, Thoreson WB, Witkovsky P (2005) Synaptic transmission

- at retinal ribbon synapses. *Prog Retin Eye Res* 24:682–720. [CrossRef Medline](#)
- Heymann JA, Hinshaw JE (2009) Dynamics at a glance. *J Cell Sci* 122:3427–3431. [CrossRef Medline](#)
- Hinshaw JE, Schmid SL (1995) Dynamin self-assembles into rings suggesting a mechanism for coated vesicle budding. *Nature* 374:190–192. [CrossRef Medline](#)
- Holt M, Cooke A, Wu MM, Lagnado L (2003) Bulk membrane retrieval in the synaptic terminal of retinal bipolar cells. *J Neurosci* 23:1329–1339. [Medline](#)
- Hosoi N, Holt M, Sakaba T (2009) Calcium dependence of exo- and endocytic coupling at a glutamatergic synapse. *Neuron* 63:216–229. [CrossRef Medline](#)
- Hua Y, Sinha R, Thiel CS, Schmidt R, Hüve J, Martens H, Hell SW, Egner A, Klingauf J (2011) A readily retrievable pool of synaptic vesicles. *Nat Neurosci* 14:833–839. [CrossRef Medline](#)
- Irie M, Hata Y, Takeuchi M, Ichtchenko K, Toyoda A, Hirao K, Takai Y, Rosahl TW, Südhof TC (1997) Binding of neuroligins to PSD-95. *Science* 277:1511–1515. [CrossRef Medline](#)
- Jackman SL, Choi SY, Thoreson WB, Rabl K, Bartoletti TM, Kramer RH (2009) Role of the synaptic ribbon in transmitting the cone light response. *Nat Neurosci* 12:303–310. [CrossRef Medline](#)
- Jenkins GM, Frohman MA (2005) Phospholipase D: a lipid centric review. *Cell Mol Life Sci* 62:2305–2316. [CrossRef Medline](#)
- Jockusch WJ, Praefcke GJ, McMahon HT, Lagnado L (2005) Clathrin-dependent and clathrin-independent retrieval of synaptic vesicles in retinal bipolar cells. *Neuron* 46:869–878. [CrossRef Medline](#)
- Karim Z, Vepachedu R, Gorska M, Alam R (2010) UNC119 inhibits dynamin and dynamin-dependent endocytic processes. *Cell Signal* 22:128–137. [CrossRef Medline](#)
- Keifer J, Vyas D, Houk JC (1992) Sulforhodamine labelling of neural circuits engaged in motor pattern generation in the in vitro turtle brainstem-cerebellum. *J Neurosci* 12:3187–3199. [Medline](#)
- Kirchhausen T, Macia E, Pelish HE (2008) Use of dynasore, the small molecule inhibitor of dynamin, in the regulation of endocytosis. *Methods Enzymol* 488:77–93. [CrossRef Medline](#)
- Koch D, Spiwojs-Becker I, Sabanov V, Sinning A, Dugladze T, Stellmacher A, Ahuja R, Grimm J, Schüler S, Müller A, Angenstein F, Ahmed T, Diesler A, Moser M, Tom Dieck S, Spessert R, Boeckers TM, Fässler R, Hübner CA, Balschun D, Gloveli T, Kessels MM, Qualmann B (2011) Proper synaptic vesicle formation and neuronal network activity critically rely on synapin I. *EMBO J* 30:4955–4969. [CrossRef Medline](#)
- Koch M, Holt M (2012) Coupling exo- and endocytosis: an essential role for PIP2 at the synapse. *Biochim Biophys Acta* 1821:1114–1132. [CrossRef Medline](#)
- Koulen P, Fletcher EL, Craven SE, Bredt DS, Wässle H (1998) Immunocytochemical localization of the postsynaptic density protein PSD-95 in the mammalian retina. *J Neurosci* 18:10136–10149. [Medline](#)
- Lariccia V, Fine M, Magi S, Lin MJ, Yaradanakul A, Llaguno MC, Hilgemann DW (2011) Massive calcium-activated endocytosis without involvement of classical endocytic proteins. *J Gen Physiol* 137:111–132. [CrossRef Medline](#)
- Liberali P, Kakkonen E, Turacchio G, Valente C, Spaar A, Perinetti G, Böckmann RA, Corda D, Colanzi A, Marjomaki V, Luini A (2008) The closure of Pak1-dependent macropinosomes requires the phosphorylation of CtBP1/BARS. *EMBO J* 27:970–981. [CrossRef Medline](#)
- Lichtman JW, Wilkinson RS, Rich MM (1985) Multiple innervation of tonic endplates revealed by activity-dependent uptake of fluorescent probes. *Nature* 314:357–359. [CrossRef Medline](#)
- Llobet A, Gallop JL, Burden JJ, Camdere G, Chandra P, Vallis Y, Hopkins CR, Lagnado L, McMahon HT (2011) Endophilin drives the fast mode of vesicle retrieval in a ribbon synapse. *J Neurosci* 31:8512–8519. [CrossRef Medline](#)
- LoGiudice L, Matthews G (2007) Endocytosis at ribbon synapses. *Traffic* 8:1123–1128. [CrossRef Medline](#)
- LoGiudice L, Sterling P, Matthews G (2009) Vesicle recycling at ribbon synapses in the finely branched axon terminals of mouse retinal bipolar neurons. *Neuroscience* 164:1546–1556. [CrossRef Medline](#)
- Macia E, Ehrlich M, Massol R, Boucrot E, Brunner C, Kirchhausen T (2006) Dynasore, a cell-permeable inhibitor of dynamin. *Dev Cell* 10:839–850. [CrossRef Medline](#)
- Malhotra V, Campelo F (2011) PKD regulates membrane fission to generate TGN to cell surface transport carriers. *Cold Spring Harb Perspect Biol* 3:a005280. [CrossRef Medline](#)
- Mayor HD, Hampton JC, Rosario B (1961) A simple method for removing the resin from epoxy-embedded tissue. *J Biophys Biochem Cytol* 9:909–910. [CrossRef Medline](#)
- Mercer AJ, Thoreson WB (2011) The dynamic architecture of photoreceptor ribbon synapses: cytoskeletal, extracellular matrix, and intramembrane proteins. *Vis Neurosci* 28:453–471. [CrossRef Medline](#)
- Midorikawa M, Tsukamoto Y, Berglund K, Ishii M, Tachibana M (2007) Different roles of ribbon-associated and ribbon-free active zones in retinal bipolar cells. *Nat Neurosci* 10:1268–1276. [CrossRef Medline](#)
- Milosevic I, Giovedi S, Lou X, Raimondi A, Collesi C, Shen H, Paradise S, O'Toole E, Ferguson S, Cremona O, De Camilli P (2011) Recruitment of endophilin to clathrin-coated pit necks is required for efficient vesicle uncoating after fission. *Neuron* 72:587–601. [CrossRef Medline](#)
- Miranda-Laferte E, Gonzalez-Gutierrez G, Schmidt S, Zeug A, Ponimaskin EG, Neely A, Hidalgo P (2011) Homodimerization of the src homology 3 domain of the calcium channel  $\beta$ -subunit drives dynamin-dependent endocytosis. *J Biol Chem* 286:22203–22210. [CrossRef Medline](#)
- Mizuno N, Jao CC, Langen R, Steven AC (2010) Multiple modes of endophilin-mediated conversion of lipid vesicles into coated tubes: implications for synaptic vesicle endocytosis. *J Biol Chem* 285:23351–23358. [CrossRef Medline](#)
- Moser T, Beutner D (2000) Kinetics of exocytosis and endocytosis at the cochlear inner hair cell afferent synapse of the mouse. *Proc Natl Acad Sci U S A* 97:883–888. [CrossRef Medline](#)
- Moser T, Brandt A, Lysakowski A (2006) Hair cell ribbon synapses. *Cell Tissue Res* 326:347–359. [CrossRef Medline](#)
- Murthy VN, De Camilli P (2003) Cell biology of the presynaptic terminal. *Annu Rev Neurosci* 26:701–728. [CrossRef Medline](#)
- Neves G, Lagnado L (1999) The kinetics of exocytosis and endocytosis in the synaptic terminal of goldfish retinal bipolar cells. *J Physiol* 515:181–202. [CrossRef Medline](#)
- Neves G, Gomis A, Lagnado L (2001) Calcium influx selects the fast mode of endocytosis in the synaptic terminal of retinal bipolar cells. *Proc Natl Acad Sci U S A* 98:15282–15287. [CrossRef Medline](#)
- Nimmerjahn A, Kirchhoff F, Kerr JN, Helmchen F (2004) Sulforhodamine 101 as a specific marker of astroglia in the neocortex in vivo. *Nat Methods* 1:31–37. [CrossRef Medline](#)
- Paillart C, Li J, Matthews G, Sterling P (2003) Endocytosis and vesicle recycling at a ribbon synapse. *J Neurosci* 23:4092–4099. [Medline](#)
- Pechstein A, Shupliakov O, Haucke V (2010) Intersectin 1: a versatile actor in the synaptic vesicle cycle. *Biochem Soc Trans* 38:181–186. [CrossRef Medline](#)
- Praefcke GJ, McMahon HT (2004) The dynamin superfamily: universal membrane tubulation and fission molecules? *Nat Rev Mol Cell Biol* 5:133–147. [CrossRef Medline](#)
- Punge A, Rizzoli SO, Jahn R, Wildanger JD, Meyer L, Schönle A, Kastrop L, Hell SW (2008) 3D reconstruction of high-resolution STED microscope images. *Microsc Res Tech* 71:644–650. [CrossRef Medline](#)
- Raimondi A, Ferguson SM, Lou X, Armbruster M, Paradise S, Giovedi S, Messa M, Kono N, Takasaki J, Cappello V, O'Toole E, Ryan TA, De Camilli P (2011) Overlapping role of dynamin isoforms in synaptic vesicle endocytosis. *Neuron* 70:1100–1114. [CrossRef Medline](#)
- Rea R, Li J, Dharria A, Levitan ES, Sterling P, Kramer RH (2004) Streamlined synaptic vesicle cycle in cone photoreceptor terminals. *Neuron* 41:755–766. [CrossRef Medline](#)
- Rebrük TI, Korenbrot JI (2004) In intact mammalian photoreceptors, Ca<sup>2+</sup>-dependent modulation of cGMP-gated ion channels is detectable in cones but not in rods. *J Gen Physiol* 123:63–75. [CrossRef Medline](#)
- Ripps H, Shakib M, MacDonald ED (1976) Peroxidase uptake by photoreceptor terminals of the skate retina. *J Cell Biol* 70:86–96. [CrossRef Medline](#)
- Roth MG (2008) Molecular mechanisms of PLD function in membrane traffic. *Traffic* 9:1233–1239. [CrossRef Medline](#)
- Royle SJ, Lagnado L (2010) Clathrin-mediated endocytosis at the synaptic terminal: bridging the gap between physiology and molecules. *Traffic* 11:1489–1497. [CrossRef Medline](#)
- Saheki Y, De Camilli P (2012) Synaptic vesicle endocytosis. *Cold Spring Harb Perspect Biol* 4:a005645. [CrossRef Medline](#)
- Sandvig K, Pust S, Skotland T, van Deurs B (2011) Clathrin-independent

- endocytosis: mechanisms and function. *Curr Opin Cell Biol* 23:413–420. [CrossRef Medline](#)
- Schacher S, Holtzman E, Hood DC (1976) Synaptic activity of frog photoreceptors: a peroxidase uptake study. *J Cell Biol* 70:178–192. [CrossRef Medline](#)
- Schaeffer SF, Raviola E (1978) Membrane recycling in the cone cell endings of the turtle retina. *J Cell Biol* 79:802–825. [CrossRef Medline](#)
- Schermelleh L, Carlton PM, Haase S, Shao L, Winoto L, Kner P, Burke B, Cardoso MC, Agard DA, Gustafsson MG, Leonhardt H, Sedat JW (2008) Subdiffraction multicolor imaging of the nuclear periphery with 3D structured illumination microscopy. *Science* 320:1332–1336. [CrossRef Medline](#)
- Schermelleh L, Heintzmann R, Leonhardt H (2010) A guide to super-resolution fluorescence microscopy. *J Cell Biol* 190:165–175. [CrossRef Medline](#)
- Schmid SL, Frolov VA (2011) Dynamin: fundamental design of a membrane fission catalyst. *Annu Rev Cell Dev Biol* 27:79–105. [CrossRef Medline](#)
- Schmitz F (2009) The making of synaptic ribbons: how they are built and what they do. *Neuroscientist* 15:611–624. [CrossRef Medline](#)
- Schmitz F, Königstorfer A, Südhof TC (2000) RIBEYE, a protein's journey through evolution provides insights into synaptic ribbon function. *Neuron* 28:857–872. [CrossRef Medline](#)
- Schmitz F, Natarajan S, Venkatesan JK, Wahl S, Schwarz K, Grabner CP (2012) EF hand-mediated Ca<sup>2+</sup> and cGMP-signaling in photoreceptor synaptic terminals. *Front Mol Neurosci* 5:26. [CrossRef Medline](#)
- Schnee ME, Santos-Sacchi J, Castellano-Muñoz M, Kong JH, Ricci AJ (2011) Calcium-dependent synaptic vesicle trafficking underlies indefatigable release of the hair cell afferent fiber synapse. *Neuron* 70:326–338. [CrossRef Medline](#)
- Schoch S, Gundelfinger ED (2006) Molecular organization of the presynaptic active zone. *Cell Tissue Res* 326:379–391. [CrossRef Medline](#)
- Schoch S, Mittelstaedt T, Kaeser PS, Padgett D, Feldmann N, Chevaleyre V, Castillo PE, Hammer RE, Han W, Schmitz F, Lin W, Südhof TC (2006) Redundant functions of RIM1alpha and RIM2alpha in Ca<sup>2+</sup>-triggered neurotransmitter release. *EMBO J* 25:5852–5863. [CrossRef Medline](#)
- Schwarz K, Natarajan S, Kassas N, Vitale N, Schmitz F (2011) The synaptic ribbon is a site of phosphatidic acid generation in ribbon synapses. *J Neurosci* 31:15996–16011. [CrossRef Medline](#)
- Scita G, Di Fiore PP (2010) The endocytic matrix. *Nature* 463:464–473. [CrossRef Medline](#)
- Shupliakov O (2009) The synaptic vesicle cluster: a source of endocytic proteins during neurotransmitter release. *Neuroscience* 158:204–210. [CrossRef Medline](#)
- Smith SM, Renden R, von Gersdorff H (2008) Synaptic vesicle endocytosis: fast and slow modes of membrane retrieval. *Trends Neurosci* 31:559–568. [CrossRef Medline](#)
- Snellman J, Mehta B, Babai N, Bartoletti TM, Akmentin W, Francis A, Matthews G, Thoreson W, Zenisek D (2011) Acute destruction of the synaptic ribbon reveals a role for the ribbon in vesicle priming. *Nat Neurosci* 14:1135–1141. [CrossRef Medline](#)
- Spassova MA, Avissar M, Furman AC, Crumling MA, Saunders JC, Parsons TD (2004) Evidence that rapid replenishment of the synaptic ribbon mediates recovery from short-term adaptation at the hair cell afferent synapse. *J Assoc Res Otolaryngol* 5:376–390. [CrossRef Medline](#)
- Südhof TC (2004) The synaptic vesicle cycle. *Annu Rev Neurosci* 27:509–547. [CrossRef Medline](#)
- Südhof TC (2012) Calcium control of neurotransmitter release. *Cold Spring Harb Perspect Biol* 4:a011353. [CrossRef Medline](#)
- Takahashi N, Kishimoto T, Nemoto T, Kadowaki T, Kasai H (2002) Fusion pore dynamics and insulin granule exocytosis in the pancreatic islet. *Science* 297:1349–1352. [CrossRef Medline](#)
- Takei K, McPherson PS, Schmid SL, De Camilli P (1995) Tubular membrane invaginations coated by dynamin rings are induced by GTP-γ-S in nerve terminals. *Nature* 374:186–190. [CrossRef Medline](#)
- Teng H, Cole JC, Roberts RL, Wilkinson RS (1999) Endocytic active zones: hot spots for endocytosis in vertebrate neuromuscular terminals. *J Neurosci* 19:4855–4866. [Medline](#)
- Tian M, Xu CS, Montpetit R, Kramer RH (2012) Rab3A mediates vesicle delivery at photoreceptor ribbon synapses. *J Neurosci* 32:6931–6936. [CrossRef Medline](#)
- tom Dieck S, Brandstätter JH (2006) Ribbon synapses of the retina. *Cell Tissue Res* 326:339–346. [CrossRef Medline](#)
- tom Dieck S, Altmann WD, Kessels MM, Qualmann B, Regus H, Brauner D, Fejtová A, Bracko O, Gundelfinger ED, Brandstätter JH (2005) Molecular dissection of the photoreceptor ribbon synapse: physical interaction of Bassoon and RIBEYE is essential for the assembly of the ribbon complex. *J Cell Biol* 168:825–836. [CrossRef Medline](#)
- Townes-Anderson E, MacLeish PR, Raviola E (1985) Solitary rod photoreceptors from mature salamander retina: ultrastructure and uptake of horseradish peroxidase. *J Cell Biol* 100:175–188. [CrossRef Medline](#)
- Townes-Anderson E, Dacheux RF, Raviola E (1988) Rod photoreceptors dissociated from the adult rabbit retina. *J Neurosci* 8:320–331. [Medline](#)
- Van Hook MJ, Thoreson WB (2012) Rapid synaptic vesicle endocytosis in cone photoreceptors of salamander retina. *J Neurosci* 32:18112–18123. [CrossRef Medline](#)
- Wakeham DE, Abi-Rached L, Towler MC, Wilbur JD, Parham P, Brodsky FM (2005) Clathrin heavy and light chain isoforms originated by independent mechanisms of gene duplication during chordate evolution. *Proc Natl Acad Sci U S A* 102:7209–7214. [CrossRef Medline](#)
- Warnock DE, Terlecky LJ, Schmid SL (1995) Dynamin GTPase is stimulated by crosslinking through the c-terminal proline-rich domain. *EMBO J* 14:1322–1328. [Medline](#)
- Wilbur JD, Hwang PK, Brodsky FM (2005) New faces of the familiar clathrin lattice. *Traffic* 6:346–350. [CrossRef Medline](#)
- Wojcik SM, Rhee JS, Herzog E, Sigler A, Jahn R, Takamori S, Brose N, Rosenmund C (2004) An essential role for vesicular glutamate transporter 1 (VGLUT1) in postnatal development and control of quantal size. *Proc Natl Acad Sci U S A* 101:7158–7163. [CrossRef Medline](#)
- Wu LG, Ryan TA, Lagnado L (2007) Modes of vesicle retrieval at ribbon synapses, calyx-type synapses and small central synapses. *J Neurosci* 27:11793–11802. [CrossRef Medline](#)
- Wu W, Xu J, Wu XS, Wu LG (2005) Activity-dependent acceleration of endocytosis at a central synapse. *J Neurosci* 25:11676–11683. [CrossRef Medline](#)
- Wu XS, McNeil BD, Xu J, Fan J, Xue L, Melicoff E, Adachi R, Bai L, Wu LG (2009a) Ca<sup>2+</sup> and calmodulin initiate all forms of endocytosis during depolarization of a nerve terminal. *Nat Neurosci* 12:1003–1010. [CrossRef Medline](#)
- Wu Y, Matsui H, Tomizawa K (2009b) Amphiphysin I and regulation of synaptic vesicle endocytosis. *Acta Med Okayama* 63:305–323. [Medline](#)
- Xue J, Graham ME, Novelle AE, Sue N, Gray N, McNiven MA, Smillie KJ, Cousin MA, Robinson PJ (2011) Calcineurin selectively docks with the dynamin1xb splice variant to regulate activity-dependent bulk endocytosis. *J Biol Chem* 286:30295–30303. [CrossRef Medline](#)
- Yamashita T (2012) Ca<sup>2+</sup>-dependent regulation of synaptic vesicle endocytosis. *Neurosci Res* 73:1–7. [CrossRef Medline](#)
- Yang JS, Gad H, Lee SY, Mironov A, Zhang L, Beznoussenko GV, Valente C, Turacchio G, Bonsra AN, Du G, Baldanzi G, Graziani A, Bourgoin S, Frohman MA, Luini A, Hsu VW (2008) A role for phosphatidic acid in COPI vesicle fission yields insights into Golgi maintenance. *Nat Cell Biol* 10:1146–1153. [CrossRef Medline](#)
- Yao LH, Rao Y, Varga K, Wang C-Y, Xiao P, Lindau M, Gong LW (2012) Synaptotagmin-1 is necessary for the Ca<sup>2+</sup> dependence of clathrin-mediated endocytosis. *J Neurosci* 32:3778–3785. [CrossRef Medline](#)
- Yoshida Y, Kinuta M, Abe T, Liang S, Araki K, Cremona O, Di Paolo G, Moriyama Y, Yasuda T, De Camilli P, Takei K (2004) The stimulatory action of amphiphysin on dynamin function is dependent on lipid bilayer curvature. *EMBO J* 23:3483–3491. [CrossRef Medline](#)
- Zenisek D (2008) Vesicle association and exocytosis at ribbon and extraribbon sites in retinal bipolar cell presynaptic terminals. *Proc Natl Acad Sci U S A* 105:4922–4927. [CrossRef Medline](#)
- Zenisek D, Steyer JA, Almers W (2000) Transport, capture and exocytosis of single synaptic vesicles at active zones. *Nature* 406:849–854. [CrossRef Medline](#)

# ArfGAP3 Is a Component of the Photoreceptor Synaptic Ribbon Complex and Forms an NAD(H)-Regulated, Redox-Sensitive Complex with RIBEYE That Is Important for Endocytosis

Mayur Dembla, Silke Wahl,\* Rashmi Katiyar,\* and Frank Schmitz

Saarland University, Medical School, Department of Neuroanatomy, 66421 Homburg/Saar, Germany

Ribbon synapses are tonically active synapses in the retina and inner ear with intense vesicle traffic. How this traffic is organized and regulated is still unknown. Synaptic ribbons, large presynaptic structures associated with numerous synaptic vesicles, appear to be essential for this process. The base of the synaptic ribbon is anchored at the active zone and is a hotspot of exocytosis. The synaptic ribbon complex is also important for vesicle replenishment. RIBEYE is a unique and major component of synaptic ribbons. It consists of a unique A-domain and an NAD(H)-binding, C-terminal B-domain. In the present study, we show that the Arf-GTPase activating protein-3 (ArfGAP3), a well characterized regulator of vesicle formation at the Golgi apparatus, is also a component of the synaptic ribbon complex in photoreceptor synapses of the mouse retina and interacts with RIBEYE as shown by multiple, independent approaches. ArfGAP3 binds to RIBEYE(B)-domain in an NAD(H)-dependent manner. The interaction is redox sensitive because NADH is more efficient than the oxidized NAD<sup>+</sup> in promoting ArfGAP3-RIBEYE interaction. RIBEYE competes with the GTP-binding protein Arf1 for binding to ArfGAP3. Thus, binding of RIBEYE(B) to ArfGAP3 could prevent inactivation of Arf1 by ArfGAP3 and provides the synaptic ribbon with the possibility to control Arf1 function. The interaction is relevant for endocytic vesicle trafficking because overexpression of ArfGAP3 in photoreceptors strongly inhibited endocytotic uptake of FM1–43.

**Key words:** ArfGAP3; endocytosis; photoreceptor synapse; ribbon synapse; RIBEYE; synaptic ribbon

## Introduction

Ribbon synapses, e.g., retinal photoreceptor synapses, are continuously active synapses with a high vesicle turnover. How this vesicle traffic is organized and regulated is still largely unknown. Synaptic ribbons, large presynaptic structures associated with numerous synaptic vesicles, appear to play a central role in this process. The basal end of the synaptic ribbon is anchored at the active zone where L-type voltage-gated channels are clustered. This site is a hotspot of exocytosis (Zenisek et al., 2000; Frank et al., 2010; Chen et al., 2013). The synaptic ribbon complex is also

relevant for vesicle recycling (Spassova et al., 2004; Griesinger et al., 2005; Jackman et al., 2009; Babai et al., 2010; Frank et al., 2010; Schnee et al., 2011; Snellman et al., 2011; Tian et al., 2012; Wahl et al., 2013). In photoreceptor synapses, synaptic vesicle retrieval occurs in the periaxial zone, in close proximity to the synaptic ribbon (Wahl et al., 2013). RIBEYE is a major and unique component of synaptic ribbons (Schmitz et al., 2000; for review, see Schmitz, 2009). It consists of an N-terminal A-domain and a C-terminal B-domain. The B-domain is largely identical with the protein CtBP2 and binds NAD(H) (for review, see Schmitz, 2009; Schmitz et al., 2012).

Small GTP-binding proteins of the Arf family are important regulators of intracellular membrane traffic (for review, see Gillingham and Munro, 2007). Arf proteins switch between a GTP-bound, active form and a GDP-bound, inactive form. Which nucleotide is bound is regulated by the activity of two classes of proteins, the ArfGEFs (Arf GTP-exchange factors) and the ArfGAPs (Arf-GTPase-activating proteins; for review, see Inoue and Randazzo, 2007; Kahn et al., 2008; Spang et al., 2010). ArfGAPs enhance the low intrinsic GTPase activity of Arfs. A large number of ArfGAPs have been identified in higher organisms. Conserved hallmark of ArfGAPs is an ~136 aa long, catalytically active GAP-domain (AGD) with a central Zn-finger motif that stimulates GTPase activity of the attached Arf (Cukierman et al., 1995; Goldberg, 1999). The regions outside of the

Received Sept. 8, 2013; revised Feb. 27, 2014; accepted March 7, 2014.

Author contributions: F.S. designed research; M.D., S.W., R.K., and F.S. performed research; M.D., S.W., R.K., and F.S. analyzed data; F.S. wrote the paper.

This work was supported by the German research community Deutsche Forschungsgemeinschaft (SFB894 and GRK1326). We thank Dr. Ching-Hwa Sung (Weill Medical College, Cornell University, New York) for the bovine retina YTH cDNA library, Dr. Rachel Wong (University of Washington, Seattle) for the kind gift of a retina incubation chamber and for her support and advice on retinal explant cultures, Dr. Andreas Beck (Saarland University, Department of Pharmacology) for advice for quantification of binding experiments, Dr. Kannan Alpadi for cloning of the bassoon-pGAD-T7 construct, Dr. Elmar Krause (platform project P1, SFB894) for help with the SIM microscope, and Dr. Jutta Schmitz-Kraemer for critically reading this manuscript.

\*S.W. and R.K. contributed equally to this work.

The authors declare no competing financial interests.

Correspondence should be addressed to Dr. Frank Schmitz, Saarland University, Medical School, Institute of Anatomy and Cell Biology, Department of Neuroanatomy, 66421 Homburg/Saar, Germany. E-mail: frank.schmitz@uks.eu.

DOI:10.1523/JNEUROSCI.3837-13.2014

Copyright © 2014 the authors 0270-6474/14/345245-16\$15.00/0

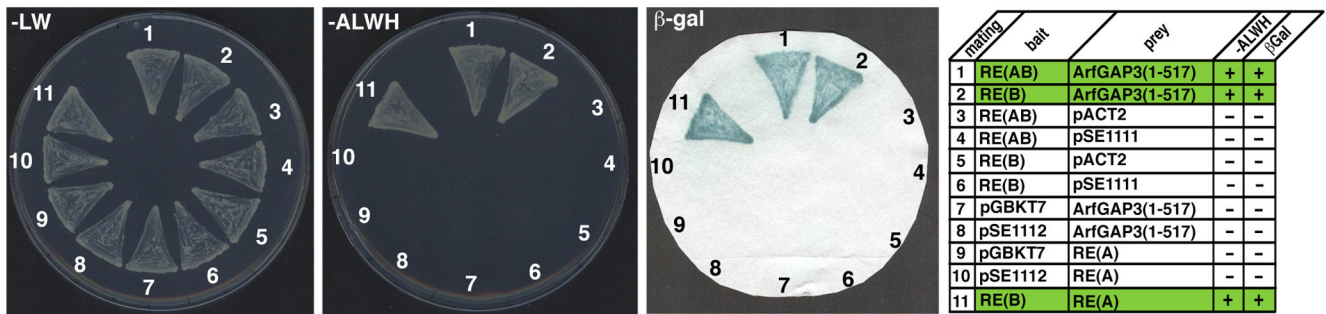


**Figure 1.** RIBEYE(B) and RIBEYE(AB) interact with ArfGAP3 in the YTH system. Summary plates of YTH analyses obtained with the indicated bait and prey plasmids. For convenience, experimental bait–prey pairs are underlayered in color (green in case of interacting bait–prey pairs; control matings are noncolored). RIBEYE(B) and also full-length RIBEYE [RIBEYE(AB)] interact with ArfGAP3 in the YTH system (matings 1 and 2). Mating 11 denotes an unrelated positive control (Magupalli et al., 2008). pSE1111 is an irrelevant prey vector and pSE1112 is an irrelevant bait vector (Tai et al., 1999; Magupalli et al., 2008). Negative control matings of the ArfGAP3 prey clone with empty bait clones (mating 7) or irrelevant bait clones (mating 8) demonstrate that the ArfGAP3 clone is not auto activating. The other matings represent negative control matings for the RIBEYE bait clones (matings 3–6) or RIBEYE prey clones (matings 9 and 10), demonstrating that these constructs are also not auto activating in the YTH system. RE(AB), full-length RIBEYE, containing both RIBEYE(A)- and RIBEYE(B)-domain; RE(A), RIBEYE(A)-domain; RE(B), RIBEYE(B)-domain; AGD, ArfGAP-domain of ArfGAP3.

AGD are divergent in different ArfGAPs. The prototypical yeast ArfGAPs gcs1p and glo3p possess mammalian orthologs in ArfGAP1 (for gcs1p) and ArfGAP2/ArfGAP3 (for glo3p). In these ArfGAPs, the conserved AGD is located at the N terminus. Both classes of ArfGAPs possess distinct motifs in their C terminus, which mediate membrane binding (Bigay et al., 2005; Kliouchnikov et al., 2009) as well as other functions (for review, see Spang et al., 2010).

In the present study, we identified ArfGAP3 as a new component of the synaptic ribbon complex in photoreceptor synapses of the mammalian retina. ArfGAP3 is a well known component of the Golgi apparatus where it regulates retrograde trafficking from the Golgi to the endoplasmic reticulum (for review, see Spang et al., 2010). We provide evidence that ArfGAP3 is important for controlling Arf1 activity at the synaptic ribbon complex and for regulating endocytic membrane traffic.

## Materials and Methods

### Plasmids

**Bacterial expression constructs.** These include *ArfGAP3(AGD)-pGEX-KG*, which encodes the ArfGAP-domain (AGD) (amino acids 1–136) of bovine ArfGAP3. The insert was excised from *GAP-dom(ArfGAP3)pACT2* with EcoRI and XhoI and cloned into the EcoRI/XhoI sites of pGEX-KG. *ArfGAP3(AGD)-pMal-C2*, encoding the ArfGAP-domain of bovine ArfGAP3. The insert was amplified from bovine ArfGAP3 cDNA (BC118087) using the following forward primer AAAAGAATTCA TGGGGGACCCAG and reverse primer AAAAGTGCACGCTAT-CAAGCCAGAG and cloned into the EcoRI/SalI sites of pMal-C2. Also included is *ArfGAP3(AGD-extended)-pMal-C2*, which encodes the extended ArfGAP-domain (AGD extended, amino acids 1–225 of bovine ArfGAP3). The insert was amplified from bovine ArfGAP3 cDNA (BC118087) using forward primer AAAAGAATTCATG GGGGAC-CCCAG reverse primer AAACGAGAAAGTCTCTTTTAGC and cloned into the EcoRI/SalI sites of pMal-C2. *ArfGAP3(AGD extended)-pSNAPtagT7* encodes the extended ArfGAP-domain. The insert was am-

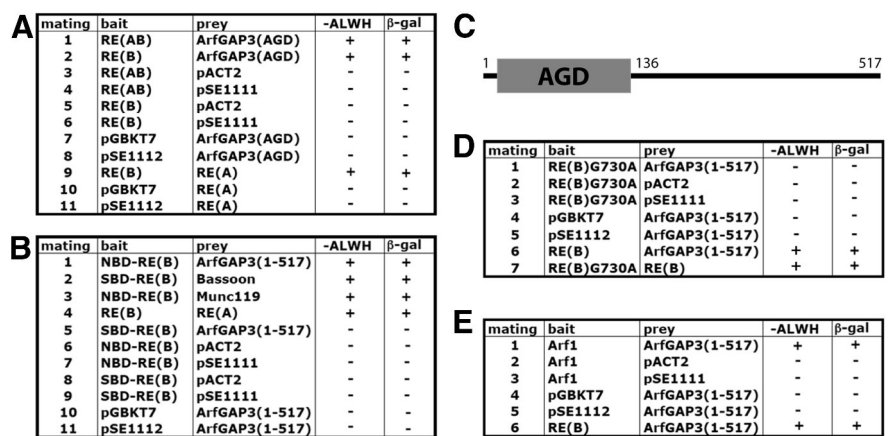


**Figure 2.** Summary tables of YTH matings. **A**, RIBEYE interacts with the ArfGAP-domain (AGD) of ArfGAP3. RIBEYE(B) and also full-length RIBEYE [RIBEYE(AB)] interact with the ArfGAP-domain (AGD) of ArfGAP3 in the YTH system (matings 1 and 2). Mating 9 denotes an unrelated positive control (Magupalli et al., 2008). The other matings are auto-activation controls. None of the yeast constructs is auto activating. **B**, The NAD(H)-binding subdomain of RIBEYE(B) interacts with ArfGAP3. The NAD(H)-binding subdomain of RIBEYE(B), the NBD, interacts with ArfGAP3 (mating 1), but not the substrate-binding subdomain of RIBEYE(B), the SBD (mating 5). Matings 2–4 are positive control matings—(Bassoon for SBD-RE(B); tom Dieck et al., 2005), Munc119 for NBD-RE(B) (Alpadi et al., 2008), RE(A) for RE(B) (Magupalli et al., 2008)—and matings 6–11 are negative controls (auto-activation controls). **C**, Schematic domain structures of ArfGAP3. **D**, An NAD(H)-binding-deficient mutant of RIBEYE(B), RE(B)G730A, does not interact with ArfGAP3 (mating 1), while wild-type RIBEYE does (mating 6). Mating 7 is a positive control mating for RE(B)G730A. **E**, Arf1 interacts with ArfGAP3 (mating 1). All constructs are non-auto activating as demonstrated by the negative control matings (2–5); mating 6 is a positive control mating. RE(A), RIBEYE(A)-domain; RE(B), RIBEYE(B)-domain; RE(B)G730A, RIBEYE(B)G730A; GAP-dom, GAP-domain (AGD) of ArfGAP3; NBD, NAD(H)-binding subdomain of RIBEYE(B); SBD, substrate-binding subdomain of RIBEYE(B).

plified from bovine ArfGAP3 cDNA (BC118087) using forward primer AAAAGGATCCATGGGGACCCCA and reverse primer AAACGAGAAAGTCC TCTTTTAGC and cloned into the BamHI/XhoI sites of pSNAPtagT7 (NEB). *ArfGAP3Cterm2-pGEX-KG* encodes amino acids 226–335 of bovine ArfGAP3. The insert was amplified from bovine ArfGAP3 cDNA using forward primer AAAGAATTCCGGCCAAAAAAG GAAGT and reverse primer AAACGAGCGTGA TTGGTGTTC and cloned into the EcoRI/XhoI sites of pGEX-KG. *ArfGAP3Cterm3-pGEX-KG* encodes amino acids 332–460 of bovine ArfGAP3. The insert was amplified from bovine ArfGAP3 cDNA using forward primer AAA-GAATTCAAACCAATCAGC GCG and reverse primer AAACGAG AGCTGAGCTGATGGA and cloned into the EcoRI/XhoI sites of pGEX-KG. *RIBEYE(B)-MBP* (Magupalli et al., 2008). The plasmid *pMal-C2* corresponds to the commercially available pMal-C2 vector (NEB) to which multiple STOP codons have been added in all reading frames at the end of the multiple cloning site using standard methods.

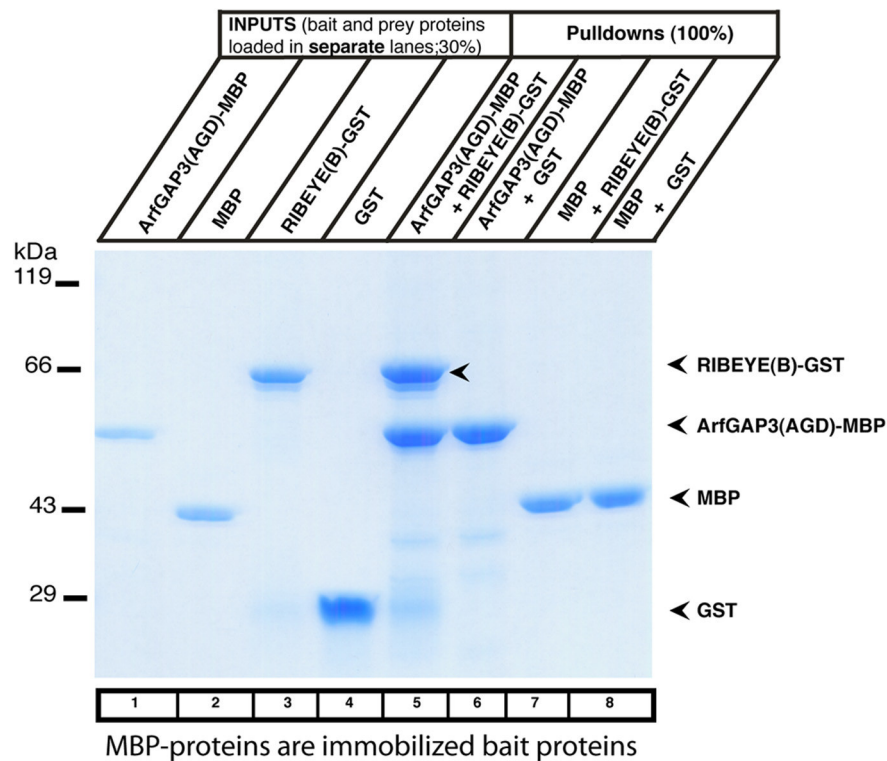


**Figure 3.** RIBEYE(B) specifically interacts with ArfGAP3 in fusion protein pull-down assays (SDS-PAGE analyses). Pull-down analyses of RIBEYE(B)/ArfGAP3 complexes were analyzed by Coomassie blue-stained polyacrylamide gel after SDS-PAGE. Lanes 1–4 show the indicated purified fusion proteins (input fractions). All input lanes represent 30% of the input fraction. Input proteins were loaded in separate lanes to demonstrate that the input fusion proteins display only a single, main protein band. In lanes 5–8, 100% of the pull-down reactions were loaded. MBP-tagged fusion proteins were used as immobilized bait proteins and GST-tagged proteins as soluble prey proteins. Only ArfGAP3-MBP pulled down RE(B)-GST (lane 5, arrowhead) but not MBP alone (lane 7). Neither MBP alone nor ArfGAP3-MBP pulled down GST alone (lanes 6 and 8). SDS-PAGE demonstrated that ArfGAP3-MBP specifically pulled down RIBEYE(B)-GST, demonstrating interaction of the two proteins in this assay system.

*RE(B)pGEX-KG* (Schmitz et al., 2000). *RE(B)G730ApGEX-KG* (Alpadi et al., 2008; Venkatesan et al., 2010). *Arf1-pGEX-KG*. The insert (~0.55 kb) was amplified from a bovine cDNA library using forward primer AAAACCATGGCGAATATCTTTGCAAAC and reverse primer AAAACTCGAGTCATTT CTGGTTC and cloned into the NcoI/XhoI sites of pGEX-KG. Plasmid constructs were verified by sequencing.

**Eukaryotic expression constructs.** *ArfGAP3-mCherry* encodes amino acids 1–517 of bovine ArfGAP3. Full-length ArfGAP3 was amplified by PCR using forward primer AAACCTCGAGGCCACCATGGGGGACCCAGCAAG, reverse primer AAAGAATTCCGGAACCGTAGCGATC, and ArfGAP3 cDNA as template. The ~1.5 kb PCR product was cloned into the XhoI/EcoRI sites of pCherry-N1 (Alpadi et al., 2008). *RE(B)-EGFP* (Schmitz et al., 2000).

#### Yeast vectors

*ArfGAP3-pACT2* encoding full-length bovine ArfGAP3 was obtained by yeast two-hybrid (YTH) screening with RIBEYE as bait construct. *ArfGAP3cDNA-pACT2*, encoding amino acids 1–517 of bovine ArfGAP3, was amplified from the full-length ArfGAP3 IMAGE clone #8081904 (BC118087) using forward primer AAAGAATTCTGATCATGGGGAC and reverse primer AAACCTCGAGTTAGGAAC CGTAGCG and cloned into the EcoRI/XhoI sites of pACT2. *ArfGAP3(AGD)pACT2* encodes the ArfGAP-domain of ArfGAP3. The insert was amplified by PCR using forward primer AAAGAATTCTGATCATGGGGAC, reverse primer AAACCTCGAGTTAGCTATC AAGCCA, and bovine ArfGAP3 cDNA (BC118087) as a template. The PCR product was cloned into the EcoRI/XhoI sites of pACT2. *CtermArfGAP3pACT2*, encoding amino acids 127–517 of bovine ArfGAP3, was amplified from bovine ArfGAP3 cDNA (BC118087) using forward primer AAA-

GAATTCAGCACGGGCACTGAC and reverse primer AAACCTCGAGTTAGGAACCGTAGC G and cloned into the EcoRI/XhoI sites of pACT2. The insert of *Arf1-pGBKT7* (~0.55 kb) was amplified from a bovine cDNA library (Alpadi et al., 2008) using forward primer AAAACCATGGCGAATATCTTTGCAAAC and reverse primer AAAACTCGAGTCATT TCTGGTTC and cloned into the NcoI/SalI sites of pGBKT7. *RE(AB)pGBK-T7* (Magupalli et al., 2008). *RE(B)pGBK-T7* (Magupalli et al., 2008). *RE(B)NBD-pGBK-T7* (Alpadi et al., 2008). *RE(B)SBD-pGBK-T7* (Alpadi et al., 2008). *RE(B)G730A-pGBK-T7* (Alpadi et al., 2008). *RE(A)pACT2* (Magupalli et al., 2008). *pGBK-T7* (empty bait plasmid) (Tai et al., 1999; Magupalli et al., 2008). *pSE1112* (control bait plasmid) (Tai et al., 1999; Magupalli et al., 2008). *pACT2* (empty prey plasmid) (Magupalli et al., 2008). *pSE1111* (control prey plasmid) (Tai et al., 1999; Magupalli et al., 2008). *Munc119pACT2* (Alpadi et al., 2008). Munc119 is known to interact with RIBEYE(B)-domain and was used as a positive control for yeast matings. *Bassoon pGAD-T7* (encoding amino acids 1638–2081 of rat bassoon, NP062019.2) was cloned by reverse-transcriptase-PCR using cDNA isolated from rat R28 cells (Alpadi et al., 2008), forward primer TTTTCATATGTGCGGATCTCCTCTGTCCCT, and reverse primer TTTTGAATTCC TGGGCCAGGCTGGCCTCTG and cloned into the NdeI/EcoRI sites of pGADT7. Bassoon pGAD-T7 was used as a positive control mating for RIBEYE(B) (tom Dieck et al., 2005). Plasmid constructs were verified by sequencing.

#### Antibodies

**Primary antibodies.** The following primary antibodies were used in the present study: mouse monoclonal anti-GST (Sigma; Alpadi et al., 2008) used at 1:10,000 dilution for Western blotting; mouse monoclonal anti-MBP (NEB; Alpadi et al., 2008) used at 1:10,000 dilution for Western blotting; rabbit polyclonal anti-RIBEYE(B)-domain (U2656; Schmitz et al., 2000) used at 1:10,000 for Western blotting for immunofluorescence microscopy at a 1:1000 dilution; mouse monoclonal antibodies against RIBEYE(B)-domain/CtBP2 (BD Transduction Laboratories; Alpadi et al., 2008; Schwarz et al., 2011; Wahl et al., 2013) used at a 1:1000 dilution; mouse monoclonal anti-Bassoon (Stressgen, VAM-PS003) used at a 1:100 dilution for immunofluorescence microscopy (Wahl et al., 2013); mouse monoclonal antibody against Arf1 (ARFS 1A9/5; Santa Cruz Biotechnology, sc-53168) used at a 1:500 dilution; and anti-dynamin (hudy-1; Millipore) used at a 1:50 dilution. The DyLight 650 directly labeled mouse monoclonal antibody against RIBEYE(B)/CtBP2 was diluted 1:2.

We generated two different polyclonal antisera against two different regions in the C terminus of ArfGAP3 (Cterm2 and Cterm3; see Fig. 7A). *ArfGAP3Cterm2-pGEX* and *ArfGAP3Cterm3-pGEX* were electroporated into Bl21(DE3) and fusion proteins were expressed and purified as previously described (Schmitz et al., 2000). For antibody production, the purified fusion proteins were injected into rabbits multiple times. Immune sera were screened for reactivity against the fusion protein and the endogenous protein. Pre-immune serum was used as control serum. Both ArfGAP3 antibodies (named ArfGAP3Cterm2- and ArfGAP3Cterm3-antisera) were used for Western blotting in a 1:3000 dilution for immunofluorescence microscopy in a dilution of 1:20. Affinity-purified ArfGAP3 antibodies were used at a concentration of 10 µg/ml for immunofluorescence microscopy. ArfGAP3Cterm2 and ArfGAP3Cterm3 antibodies worked well for Western blotting and

immunofluorescence microscopy. Unfortunately, they did not work at the electron microscopic level, both in pre-embedding and postembedding procedures with immunogold- and immunoperoxidase-based techniques with the procedures available in our laboratory. Also the following commercially available antibodies did not work in postembedding immunogold electron microscopy: rabbit and goat polyclonal anti-ArfGAP3 antibodies (AAS68618C and ASA34060; Antibody Verify), rabbit polyclonal anti-ArfGAP3 (NBP1-18921; Novus Biologicals), rabbit polyclonal anti-ArfGAP3 (HPA000638; Sigma), and rabbit polyclonal anti-ArfGAP3 (A302-032A; Biomol).

**Secondary antibodies (for immunofluorescence labeling).** The following secondary antibodies were used: chicken anti-mouse Alexa 488, donkey anti-rabbit Alexa 568, goat anti-mouse Alexa 488. All fluorophore-conjugated secondary antibodies were purchased from Invitrogen and used at a 1:1000 dilution for 1 h at room temperature (RT) for immunolabeling experiments.

#### Methods

**YTH analyses.** YTH assays were performed largely as previously described (Alpadi et al., 2008; Magupalli et al., 2008). The Gal4-based Matchmaker Yeast Two-Hybrid System (Clontech) was used according to manufacturer's instructions. For the YTH screening we used a bovine retinal YTH cDNA library from the retina (Tai et al., 1999; Alpadi et al., 2008; Venkatesan et al., 2010). The cDNA of the respective bait proteins were cloned in frame with the Gal4-DNA-binding domain of pGBKT7. The cDNA of the indicated prey proteins were cloned in frame with the Gal4-activation domain of pACT2 or pGADT7. The bait and prey plasmids confer tryptophan (W) and leucine (L) prototrophy to the respective auxotrophic yeast strains. Two yeast strains, Y187 and Y2HGold (Clontech), were used that contain distinct auxotrophic marker genes. (1) Y2HGold (Clontech): MAT $\alpha$ , trp1-901, leu2-3, 112, ura3-52, his3-200, gal4, gal80, LYS2::GAL1UAS–Gal1TATA–His3, GAL2UAS–Gal2TATA–Ade2, URA3::MEL1UAS–Mel1TATA, AU R1-C, MEL1. This strain contains distinct *ADE2*, *HIS3*, *MEL1*, and *AUR1-C* reporter constructs that are only expressed in the presence of GAL4-based protein interactions (Clontech). (2) Y187: MAT $\alpha$ , ura3-52, his3-200, ade2-101, trp1-901, leu2-3, 112, gal4, met, gal80, URA3::GAL1UASGAL1TATA–lacZ (Clontech) (Harper et al., 1993). Bait plasmids were electroporated into Y2HGold yeast and prey plasmids into Y187 yeast (Clontech). Preparation of electrocompetent yeasts and electroporation of yeasts were done as described previously (Magupalli et al., 2008). For identifying transformants, yeasts were plated on the respective selective plates to identify the resulting convertants to the respective prototrophy (dropout media; Clontech/ICN). For interaction analyses, Y2HGold yeasts containing the respective bait plasmid were mated with Y187 yeasts containing the respective prey plasmid. Mating was performed for 5 h at 30°C in 1 ml of YPD medium with heavy vortexing in a thermoshaker. For assessing mating efficiency, half of the mated sample was streaked on –LW plates, the other half was plated on –ALWH selective plates with 10 mM aminotriazole (3-amino 1,2,4-triazole) and 60 ng/ml aureobasidin. Growth of

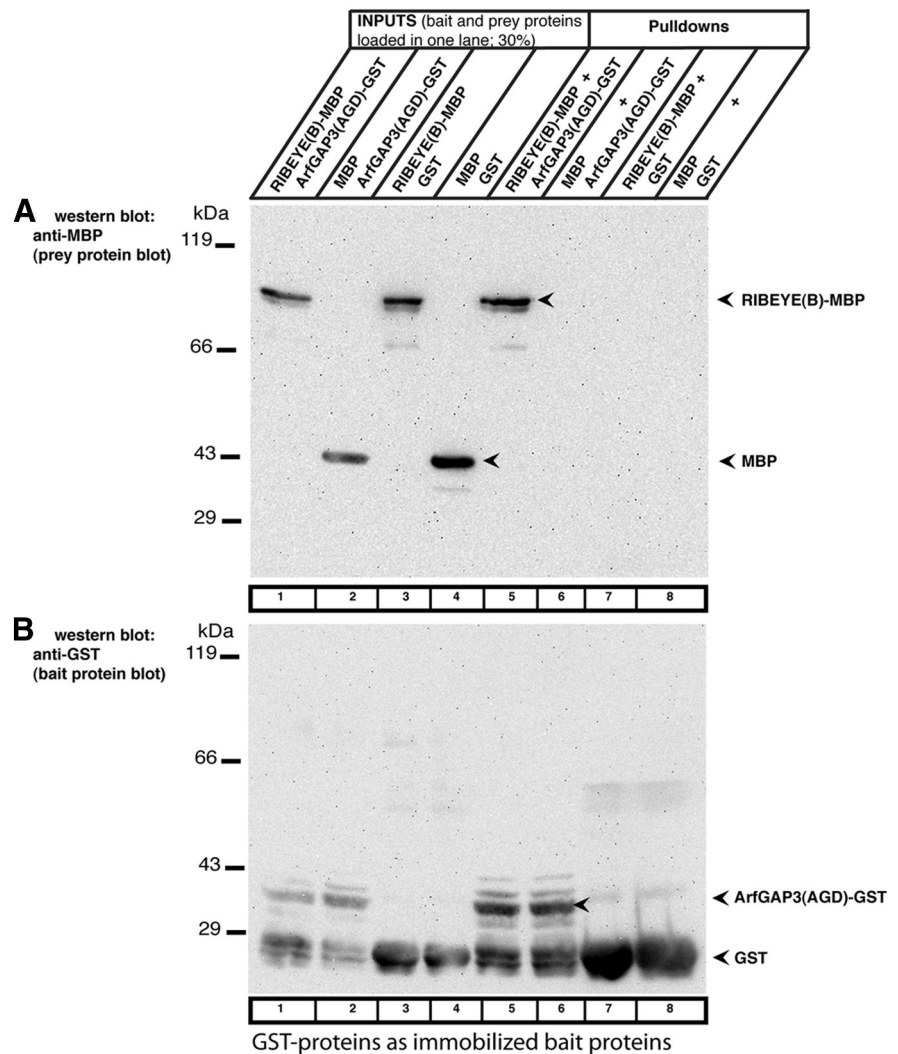


**Figure 4.** RIBEYE(B) specifically interacts with ArfGAP3 in fusion protein pull-down assays (Western blot analyses). To exclude that the tag has an importance for the pull-down results and to further exclude that any prey protein is unspecifically pulled down by bait-GST, we also analyzed the results of the pull-down assays by Western blotting with anti-MBP and anti-GST antibodies. The reaction buffer used for these experiments contained 1 mM  $\beta$ ME. GST-tagged fusion proteins were used as immobilized bait proteins and eluted MBP-tagged proteins as soluble prey proteins. Similar to the experiments described in Figure 3, only RIBEYE(B)-MBP (lane 5) and not MBP alone (lane 6) is pulled down by the ArfGAP3(AGD)-GST. GST alone (lane 7) and MBP alone (lane 8) do not pull down RIBEYE(B)-MBP, as shown by Western blotting with antibodies against MBP (Fig. 4A), demonstrating the specificity of the interaction. The Western blot data fully confirm the results shown in Figure 3 that were obtained by SDS-PAGE analyses. In Figure 4B, the same blot as analyzed in Figure 4A was reprobed (after stripping of the blot) with antibodies against GST to show equal loading of the bait proteins. RE(B)-MBP, RIBEYE(B)-MBP; ArfGAP3(AGD)-MBP, MBP-tagged ArfGAP-domain (AGD) of ArfGAP3.

mated yeasts on –LW selective medium demonstrates presence of both bait and prey plasmids; growth on –ALWH selective medium [and expression of  $\beta$ -galactosidase ( $\beta$ -gal) activity] indicates interaction of bait and prey proteins taking place. For the matings, pSE1111 and pSE1112 that encode irrelevant proteins (Magupalli et al., 2008) as well as the empty bait and prey vectors were used as negative controls (auto-activation controls). Expression of  $\beta$ -gal marker gene activity was qualitatively analyzed by filter assays as described previously (Magupalli et al., 2008).

**Fusion protein pull-down assay.** For fusion protein pull-down experiments, either GST-tagged or maltose-binding protein (MBP)-tagged fusion proteins were used as immobilized bait proteins. If GST-tagged proteins were used as immobilized bait protein, the MBP-tagged protein was used as solubilized prey protein and vice versa. Bait and prey proteins were used in equimolar amounts [0.3  $\mu$ M in incubation buffer containing 100 mM Tris, pH 8.0, 150 mM NaCl, 1 mM EDTA, 0.25% (w/v) Triton

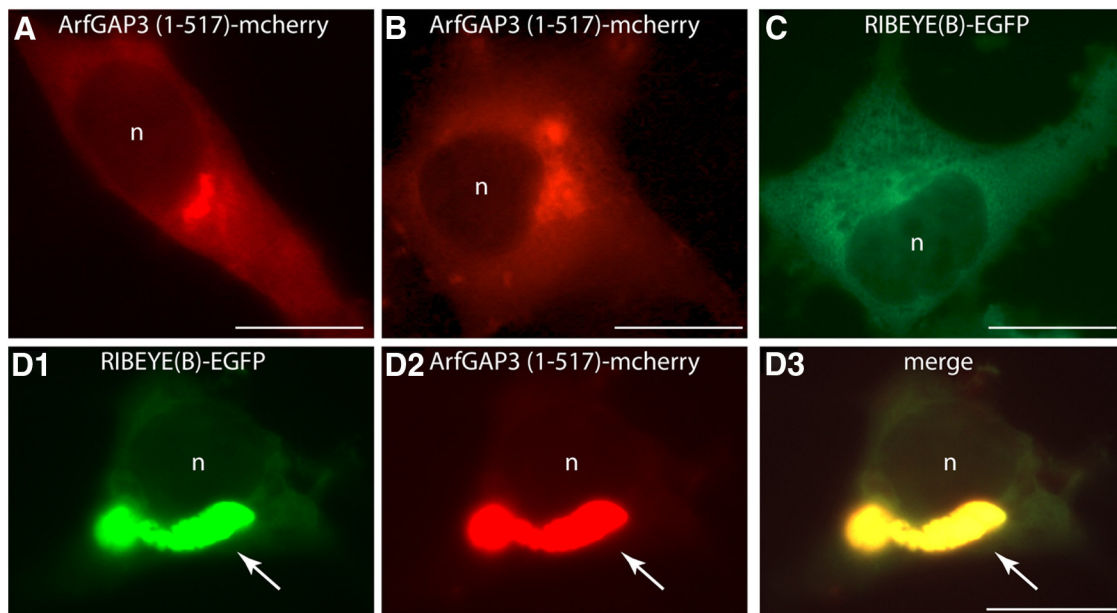


**Figure 5.** RIBEYE(B) is recruited by ArfGAP3 into a Golgi-like distribution in transfected COS cells. COS7 cells were transfected with the indicated mcherry-tagged ArfGAP3 or EGFP-tagged RIBEYE(B) constructs. Transfected cells were analyzed for the intracellular distribution of the respective proteins via direct epifluorescence microscopy. Cells transfected with ArfGAP3-mcherry alone show the typical enrichment at the Golgi apparatus in a perinuclear localization (**A, B**), as already previously shown (Dogic et al., 1999; Eugster et al., 2000; Lewis et al., 2004; Watson et al., 2004; Frigerio et al., 2007; Kartberg et al., 2010; Yu et al., 2012). In contrast, RIBEYE(B) is diffusely distributed in single-transfected cells (**C**; Schmitz et al., 2000). If RIBEYE(B)-EGFP is cotransfected with ArfGAP3-mcherry, RIBEYE(B) virtually completely redistributed from a diffuse distribution into the Golgi-like, perinuclear localization indicating interaction between RIBEYE(B) and ArfGAP3 (**D**). n, nucleus. The arrow in **D** points to the Golgi-like localization to which the RIBEYE(B)-EGFP signal is translocated in ArfGAP3-mcherry-transfected cells. Scale bars: **A–D**, 10  $\mu\text{m}$ .

X-100 (Tx-100), and 1 mM  $\beta$ -mercaptoethanol ( $\beta$ ME) if not denoted otherwise]. GST and MBP alone served as control proteins. Protein concentrations were determined using the Bradford method (Bradford, 1976). For pull-down experiments, fusion protein eluates were pre-cleared with 10  $\mu\text{l}$  of empty Sepharose beads (per 1 ml of eluate) for 1 h at 4°C. Incubations were typically done in a volume of 500  $\mu\text{l}$ . After overnight incubation at 4°C, immobilized beads were allowed to settle (20 min, at 4°C). Samples were washed by repeated centrifugation of the beads (3000 rpm, 2 min, 4°C) and subsequent resuspension with binding buffer. This procedure was repeated three times. Afterward, the final pellets were boiled with SDS-sample buffer (96°C, 10 min) and subjected to SDS-PAGE and/or Western blotting.

**Pre-absorption experiments.** Pre-absorption experiments were performed exactly as previously described (Wahl et al., 2013) using 50  $\mu\text{g}$  of the respective GST-fusion protein. Pre-absorbed ArfGAP3Cterm2 and ArfGAP3Cterm3 immunosera were used at a 1:20 dilution for immunofluorescence microscopy and at a 1:3000 dilution for Western blotting.

**Affinity purification of antibodies.** Antibodies were affinity purified by the method of Olmsted (1981). In brief,  $\sim$ 50  $\mu\text{g}$  of fusion protein was loaded on a 10% SDS-PAGE and transferred to nitrocellulose. The ArfGAP3Cterm-GST/ArfGAP3Cterm2 fusion protein bands at  $\sim$ 35 kDa were cut out with a scalpel blade. These fusion protein-loaded nitrocellulose strips were used for affinity purification of the antisera and treated with 5% skim milk powder in PBS (for  $\sim$ 30 min at RT). Next, nitrocellulose strips were incubated with the respective antisera (diluted 1:10 in 5% skim milk dissolved in PBS) and incubated overnight at 4°C. The nitrocellulose strips were washed several times with PBS. Bound antibodies were eluted from the nitrocellulose strips with a minimal volume (typically 200  $\mu\text{l}$ ) of 0.2 M glycine, pH 2.7, for 3–4 min (at 4°C). The antibody eluate was neutralized by the addition of 50  $\mu\text{l}$  of 1 M Tris, pH 8.5. Antibody was diluted to a concentration of 0.1 mg/ml and complemented with BSA (0.1 mg/ml) for stabilization.

**Direct labeling of primary antibodies (mouse anti-RIBEYE(B)-domain/CtBP2) with fluorophores (DyLight 650).** Direct labeling of mouse monoclonal antibodies against RIBEYE(B)/CtBP2 (BD) was performed exactly as previously described (Wahl et al., 2013) using the Thermo Scientific DyLight 650 Microscale Antibody Labeling Kit (Thermo Scientific #84536) according to the manufacturer's instructions.

**Heterologous protein expression in eukaryotic cell lines.** For heterologous expression, COS7 cells were used that were transfected with lipofection, as previously described (Magupalli et al., 2008; Schwarz et al., 2011). Transfected cells were typically analyzed 24 h after transfection.

**Coimmunoprecipitation from bovine retina.** For each immunoprecipitation, a single isolated bovine retina was incubated in 1 ml lysis buffer, containing 100 mM Tris-HCl, pH 8.0, 150 mM NaCl, 1 mM EDTA, and 1%Tx-100 for 45 min on vertical rotator at 4°C. The samples were mechanically cracked by forcefully ejecting the retinal lysates through a 20 gauge needle (20 $\times$ ). The samples were sonicated (Bandelin; Sonoplus) at 1% output for 20 half-second pulse ON/OFF cycles on ice. Afterward, the extracts were centrifuged at 13,000 rpm for 30 min at 4°C. The supernatants were transferred into new Eppendorf tubes. The centrifugation step was repeated one time to remove all cell debris. The resulting lysate was pre-cleared by the addition of 15  $\mu\text{l}$  of pre-immune serum and 20  $\mu\text{l}$  of washed protein A-Sepharose beads (2 h incubation at 4°C with an overhead rotator). Next, samples were centrifuged at 13,000 rpm for 30 min at 4°C (Biofuge Fresco; Heraeus; #3328 rotor). The supernatant was split in two equal volumes—for the control and experimental assays. For negative control immunoprecipitation, 15  $\mu\text{l}$  of ArfGAP3-Cterm3 pre-immune serum was added; for the experimental immunoprecipitation, 15  $\mu\text{l}$  of ArfGAP3-Cterm3 immune serum was added. Samples were incubated overnight at 4°C using an overhead rotator. Afterward, beads were allowed to settle (for 20 min, on ice). The supernatants were removed and saved; the bead pellets were resuspended in 1.0 ml of lysis buffer and washed thrice by repeated centrifugation (3000 rpm, 1 min, 4°C). The final pellet was boiled in 10  $\mu\text{l}$  of SDS sample buffer, subjected to SDS-PAGE, and analyzed by Western blotting with the indicated antibodies.

**Immunofluorescence microscopy of transfected COS cells.** Conventional fluorescence microscopy of transfected cells was done as previously described using a Zeiss Axiovert 200M equipped with the respective filter blocks (Schmitz et al., 2000; Magupalli et al., 2008; Wahl et al., 2013).

**Immunolabeling of 0.5- $\mu\text{m}$ -thick retinal resin sections.** Epon-embedded samples of mouse and bovine retinas were prepared as previously described (Wahl et al., 2013). From the tissue blocks, 0.5- $\mu\text{m}$ -thick sections were cut with a Reichert ultramicrotome. Epon was removed as described previously (Wahl et al., 2013). Afterward, sections were

incubated with the respective primary and secondary antibodies as described previously (Schmitz et al., 2000; Alpadi et al., 2008; Wahl et al., 2013). Immunolabeled sections were either analyzed by conventional epifluorescence microscopy or by super-resolution structured illumination microscopy (SR-SIM) as indicated. The immunofluorescence data shown in Figures 9–13 were obtained from incubations of mouse retinal sections. Qualitatively similar images were obtained from incubations of thin sections of the bovine retina (data not shown).

**SR-SIM.** To further improve the spatial resolution of our immunolabeling analyses, we applied multicolor SR-SIM analyses (Schermele et al., 2008, 2010; Wahl et al., 2013). SR-SIM was performed exactly as previously described using the Elyra PS1 setup (Wahl et al., 2013). Images were taken with a 63× Plan-Apochromat objective (NA 1.4) with excitation light wavelengths of 488, 561, and 650 nm, and then processed for SR-SIM to obtain higher resolutions (Gustafsson et al., 2008; for review, see Schermelleh et al., 2008, 2010), as previously described (Wahl et al., 2013). The Zeiss setup used for SR-SIM was checked for chromatic aberration in X-, Y-, and Z-direction using multicolor beads. For acquisition and processing, the Zen2010 software (Zeiss) was used.

**Triple immunolabeling of thin retinal sections.** Triple immunolabeling experiments were performed as previously described (Wahl et al., 2013). We used a directly labeled mouse monoclonal antibody against RIBEYE(B)-domain/CtBP2 (BD) conjugated with DyLight 650, and two other primary antibodies (one from mouse, the second from rabbit [as indicated in the respective experiments]), which were not directly fluorophore labeled. First, sections were incubated with the two unlabeled primary antibodies at the same time overnight (at the dilutions given above). On the next day, sections were washed three times with PBS and afterward incubated with the respective secondary antibodies (donkey anti-rabbit Alexa 568 and chicken anti-mouse Alexa 488). After 1 h incubation, sections were washed again three times with PBS and finally incubated with the directly DyLight 650-labeled CtBP2 primary antibody (in the dilutions summarized above) overnight at 4°C. After overnight incubation, sections were washed three times with PBS and embedded with anti-fade solution containing n-propyl gallate (NPG) as previously described (Schmitz et al., 2000).

**Control incubation.** Control incubations for immunolabeling experiments were done by omitting the primary antibody and only incubating with secondary antibody. No immunofluorescent signal was observed in photoreceptor synapses in these control incubations. In further control experiments, antibodies were pre-absorbed with the respective antigen as described below and processed for immunolabeling.

All experiments were done with mouse and bovine retinas of either sexes. Mice were killed in the early afternoon. Mouse eyes were collected at environmental daylight conditions (luminance of ~2 cd/m<sup>2</sup>). Bovine eyes were obtained from a local slaughterhouse. Similar data as shown for the mouse retina were also obtained with the bovine retina (of either sexes; data not shown).

**Preparation of retinas from the adult mouse for electroporation.** Retinas were isolated from adult mice within 5 min postmortem (in dim ambient light). The enucleated eyes were bisected at the equatorial plane and the posterior eye cup was transferred into ice-cold artificial CSF (ACSF) containing the following (in mM): 119 NaCl, 2.5 KCl, 2.5 CaCl<sub>2</sub>, 1.3

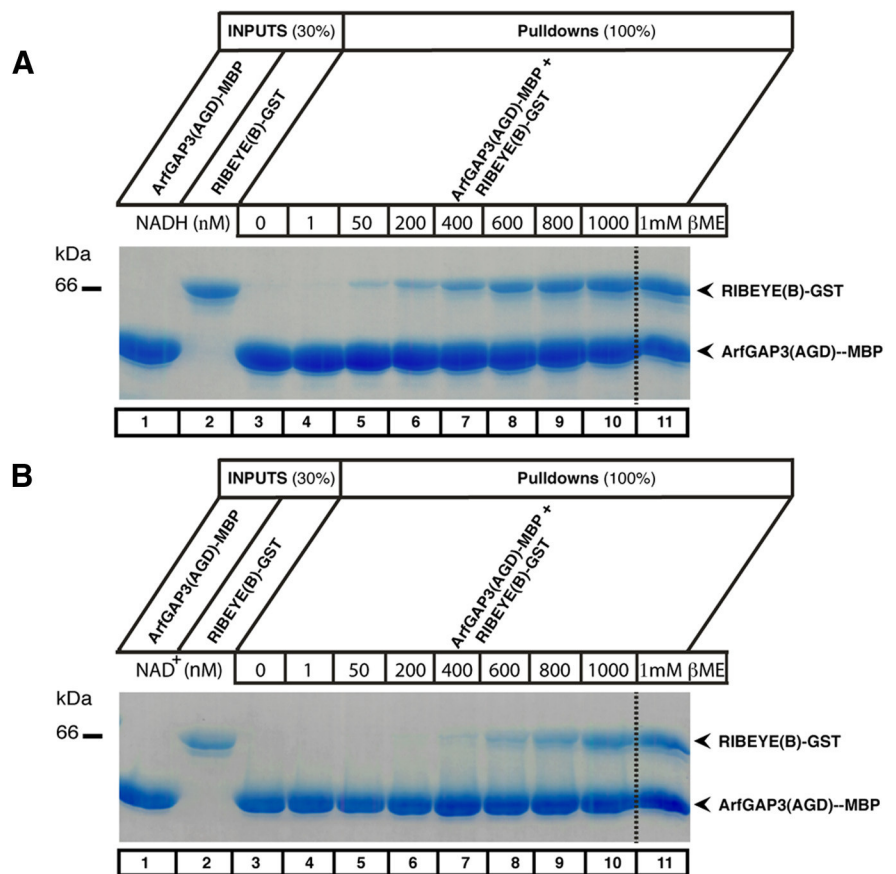


**Figure 6.** The binding between RIBEYE(B)-domain and the ArfGAP-domain (AGD) of ArfGAP3 is stimulated by NAD(H) in a redox-sensitive manner. **A, B.** Pull-down experiments were performed as in Figure 3 both in the absence (lanes 3–10; **A, B**) or presence (lane 11; **A, B**) of 1 mM  $\beta$ ME. RIBEYE binds to the ArfGAP-domain (AGD) of ArfGAP3 only in the presence of 1 mM  $\beta$ ME (lane 11; **A, B**) but not in the absence of 1 mM  $\beta$ ME (lane 3; **A, B**). Lanes 1 and 2 show the respective input fractions (30% input). We tested whether addition of NADH (**A**) or NAD<sup>+</sup> (**B**) could substitute for the presence of 1 mM  $\beta$ ME in promoting ArfGAP3/RIBEYE(B) interaction. As a matter of fact, increasing concentrations of both NADH (**A**) as well as NAD<sup>+</sup> (**B**) could promote binding of RIBEYE(B)-GST to the AGD of ArfGAP3 even in the absence of 1 mM  $\beta$ ME (lanes 4–10; **A, B**). The reduced form of the dinucleotide, NADH (**A**), was more effective than the oxidized form, NAD<sup>+</sup> (**B**), to promote RIBEYE(B)/ArfGAP3 interaction. Semiquantitative evaluation of the binding experiments ( $n = 4$ ) demonstrated that ~450 nM NADH and ~700 nM NAD<sup>+</sup> are promoting half-maximal binding of ArfGAP3 to RIBEYE(B) in the pull-down assays.

MgCl<sub>2</sub>, 1 NaH<sub>2</sub>PO<sub>4</sub>, 20 glucose, and 11 HEPES, pH 7.4, osmolarity ~300 mOsm/L. ACSF was saturated with 5% CO<sub>2</sub>/95% O<sub>2</sub> (carbogen) before use. From the posterior eyecup, the retina was gently peeled off from the pigment epithelium. Isolated retinas were transferred to black-gridded nitrocellulose filter membranes (Millipore, #HABG01300) with the ganglion cell side facing the nitrocellulose membrane. Thus, photoreceptors were facing the free surface and were in direct contact with the DNA plasmid solutions added to them in the electroporation experiments (see below). The filters with the attached retinas were transferred to sterile Petri dishes (3 cm diameter) containing ~1.0 ml of AMES' medium, pH 7.4 (A1420, Sigma-Aldrich) pre-incubated at 37°C.

**Electroporation of isolated mouse retinas and retinal explant culture.** Electroporation of adult mouse retinas was performed largely as previously described (Donovan and Dyer, 2006; Briggman and Euler, 2011; Vergara et al., 2013). Electroporation was performed with a square wave pulse electroporator (ECM 830; BTX) and a tweezer electrode electroporation device (BTX; #45-0118, #45-0204). Both electrodes of tweezer electrode were dipped in ACSF buffer to obtain a good electrical connection. Excess of ACSF was removed with filter paper to avoid dilution of the DNA. Before electroporation, DNA was column purified. For each electroporation, 50  $\mu$ g of purified DNA was used. Immediately after isolation, the retina was placed in between the tweezer electrode. The retina attached to the nitrocellulose was facing the positive electrode with the ganglion cell side

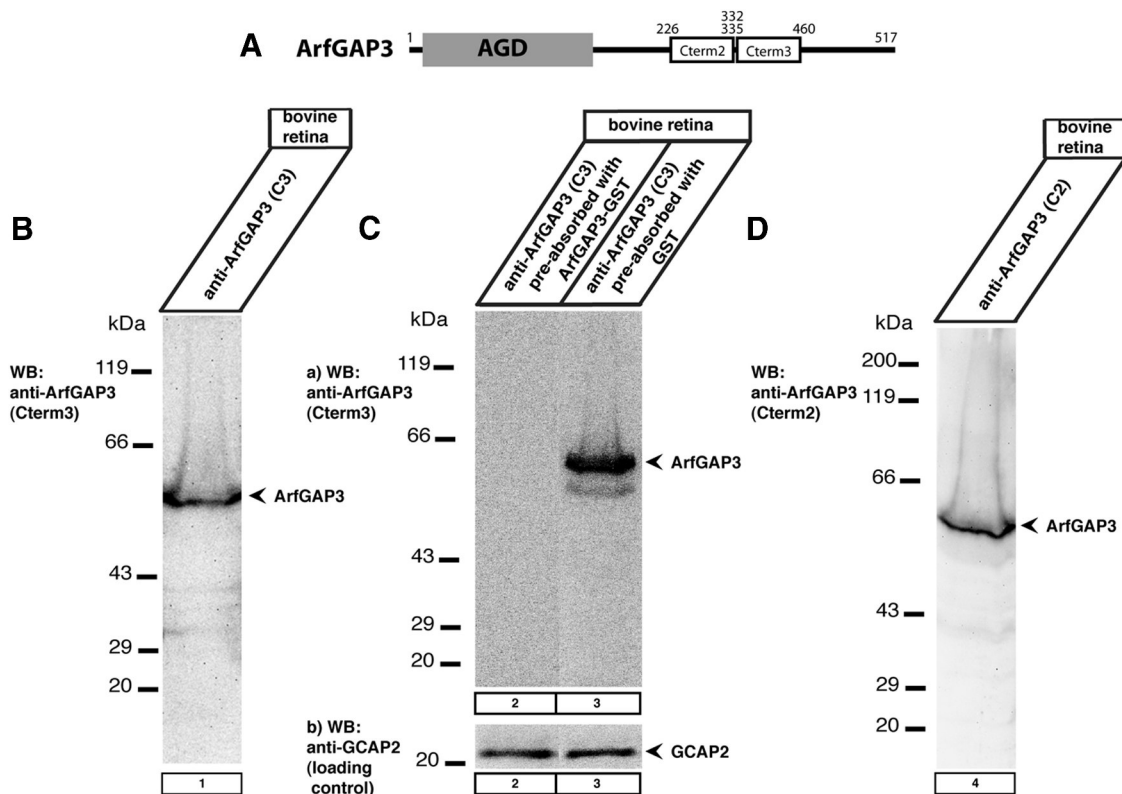


**Figure 7.** Western blot analyses of two antibodies that were generated against the C terminus of ArfGAP3. **A**, Schematic drawing denotes the areas against which the two polyclonal ArfGAP3 antibodies (Cterm2 and Cterm3) were generated. **B–D**, In Western blot analyses, both antibodies (Cterm2 and Cterm3) detected a single band at the expected running position of ArfGAP3 at ~55 kDa. This ArfGAP3 Western blot band could be blocked by pre-absorption of the antibody with the respective ArfGAP3-GST fusion protein (lane 2; *C*; data not shown) but not by pre-incubation with GST alone (*C*, lane 3; data not shown). **Cb**, Loading control (immunoblotting of the same blot as shown in **Ca**) after stripping of the blot and reprobing with an antibody against GCAP2 (Venkatesan et al., 2010), demonstrating equal protein loading.

while the plasmid DNA solution was added to the photoreceptor side at the negative electrode in hanging drop manner. The distance between the two electrodes was optimized to ~3–4 mm. Electroporation was done at 20 V, 950 ms OFF, 20 ms ON (10 pulses). Electroporated retinas were transferred back to Petri dishes containing 1.0 ml of AMES' medium, pH 7.4. Retinas were transferred to open Petri dishes that were placed in an incubation chamber, as previously described (Morgan et al., 2011; Williams et al., 2013). Temperature was continuously maintained at 32°C using a feedback temperature controller (TC324B; Warner Instruments) and a transparent ITO heater attached to the incubation chamber (HI-25Dp; MicroControls). The incubation chamber was filled with distilled H<sub>2</sub>O to the lower edge of stage where the Petri dish with the retina was placed and continuously gassed with carbogen (5% CO<sub>2</sub>/95% O<sub>2</sub>). Retinas were incubated inside the light-protected incubation chamber typically for 18–24 h.

**Loading of photoreceptors with FM1–43.** Isolated, electroporated retinas were incubated for 15 min in LCS containing 20 μM FM1–43 (fixable FM1–43: FM1–43FX; Invitrogen, #F35355) at 37°C in the dark, similar to the procedure described by Rea et al. (2004). We used this method, because it favors specific FM1–43 uptake in photoreceptor synaptic terminals (Rea et al., 2004). After labeling, the retinas were rinsed thrice with LCS and processed for the isolation of photoreceptor cells (see below).

**Dissociation of electroporated retinas and isolation of photoreceptors.** Twenty-four hours after electroporation, photoreceptors were isolated from the retina with a papain digestion procedure, largely as previously described (Wahl et al., 2013). The papain solution containing 6 U/ml papain (Sigma, #76220-25G) in low Ca<sup>2+</sup>-containing saline solution (LCS solution; containing 132 mM NaCl, 3 mM KCl, 1 mM MgCl<sub>2</sub> × 6H<sub>2</sub>O, 0.5 mM CaCl<sub>2</sub>, 10 mM sodium pyruvate, 10 mM glucose, and 10 mM HEPES, pH 7.4, ~300 mOsm/L) was activated with 2.7 mM L-cysteine at 37°C for 20 min before the experiments.

Isolated retinas were incubated in 1 ml of the cysteine-activated papain solution (containing 6 U papain/ml LCS) for 10 min at 25°C. LCS was saturated with 5% CO<sub>2</sub>/95% O<sub>2</sub> before use. After removal of the papain solution, the retina was gently washed three times with 1 ml of LCS solution containing 2% FCS and 0.01 mg/ml DNase (Sigma, #DN25-110MG). To dissociate photoreceptor cells, papain-treated retinas were very gently triturated (1–2 times) with a wide-bore plastic Pasteur pipette. The resulting cell suspension was plated on Concanavalin A (Sigma, #C7275-250 mg)-coated coverslips. For coating of a 25 mm round coverslip, ~200 μl of 1 mg/ml Concanavalin A (in LCS solution) was added for 1 h at RT. Unbound Concanavalin A was removed by three washes with LCS before the addition of the dissociated cells. Cells were allowed to settle on the coverslips for 30 min at 37°C for tight attachment. Unbound retinal cells were removed by gentle washes with LCS. Photoreceptors were identified based on their typical morphology. Photoreceptors were fixed with 4% PFA in PBS for 15 min at RT. After several washes with PBS, cells were mounted with NPG antifade as previously described (Wahl et al., 2013).

**Miscellaneous procedures.** SDS-PAGE and Western blotting were performed as previously described (Schmitz et al., 2000). Fusion proteins were expressed in BL21(DE3) bacteria for pGEX and pMal-C2 constructs as previously described (Schmitz et al., 2000). For expression of SNAP-tagged fusion proteins, *Escherichia coli* T7 Express bacteria (NEB; #C2566) were used. Expression and purification of SNAP-tagged fusion proteins were performed according to the manufacturer's instructions (NEB). SNAP-tagged fusion proteins were visualized SNAP-Vista Green (NEB; #S9147S) and covalently immobilized with SNAP-capture pull-down resin according to the manufacturer's instructions. Conventional immunofluorescence microscopy was performed as previously described (Schmitz et al., 2000) using a Zeiss Axiovert 200M equipped with the respective filter blocks.

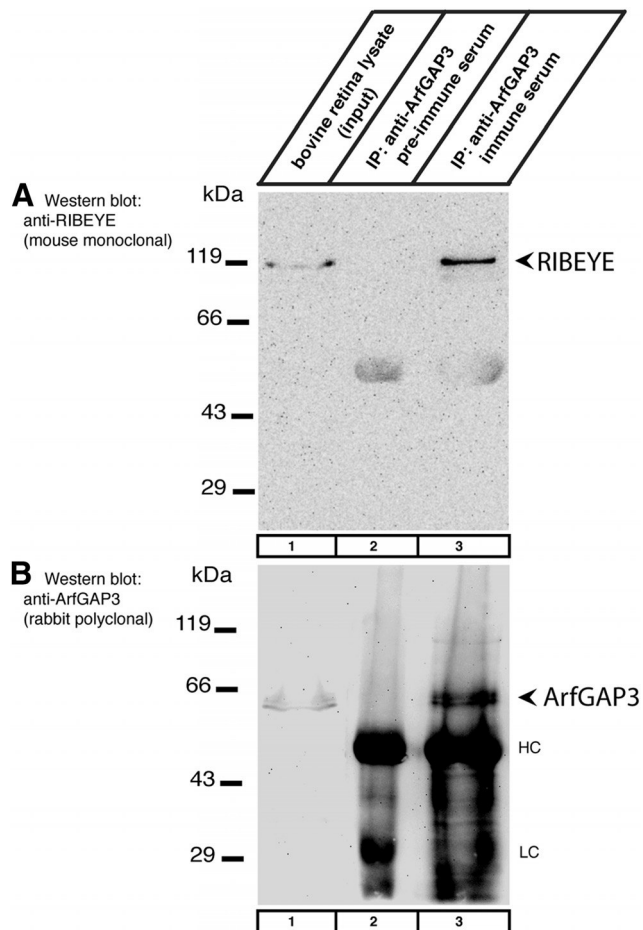


**Figure 8.** Coimmunoprecipitation of RIBEYE and ArfGAP3 from the bovine retina (Western blot analyses). **A**, ArfGAP3 immune serum (lane 3) and ArfGAP3 pre-immune serum (lane 2) were tested for their capability to coimmunoprecipitate RIBEYE from the bovine retina. Lane 1 shows the input fraction (1% of total input). RIBEYE is coimmunoprecipitated by ArfGAP3 immune serum (Cterm3 antiserum; lane 3) but not by ArfGAP3 pre-immune serum (lane 2). **B**, Shows the same blot as in **A** but reprobed with anti-ArfGAP3 antibodies (after stripping of the blot). This blot shows that ArfGAP3 was successfully immunoprecipitated by the immune serum (lane 3) but not by the control pre-immune serum (lane 2). HC and LC indicate the Ig heavy and light chains, respectively.

## Results

### ArfGAP3 binds to RIBEYE(B)-domain in the YTH system

Using RIBEYE(B) as bait, we obtained full-length ArfGAP3 as a RIBEYE-interacting YTH prey clone. The original ArfGAP3 prey clone contained a deletion of 8 aa in the Zn-finger motif of the ArfGAP-domain (data not shown). To exclude an artificial interaction of these proteins in the YTH system, we recloned full-length ArfGAP3 cDNA from an IMAGE clone (IMAGE #8081904, BC118087; encoding full-length bovine ArfGAP3 with no deletion in the Zn-finger) into the pACT2 prey vector. Then, we retested whether this entirely full-length ArfGAP3 prey interacts with RIBEYE(B) in the YTH system. Similar as observed for the original ArfGAP3 prey clone, we obtained a strong interaction between RIBEYE(B) and the recloned full-length ArfGAP3, as judged by growth on  $-ALWH$  selective medium and expression of  $\beta$ -gal activity (Fig. 1, matings 1 and 2) indicating that the interaction between ArfGAP3 and RIBEYE(B) is real in the YTH system. Negative control matings (Fig. 1, matings 3–10) demonstrated that ArfGAP3/RIBEYE interaction is not due to auto activation.

### Mapping of RIBEYE-ArfGAP3 interaction in the YTH system: the NAD(H)-binding subdomain RIBEYE(B) binds to the AGD-domain of ArfGAP3

Next, we tested with the YTH system which part of ArfGAP3 mediates the interaction with RIBEYE(B). We found that the AGD encoding amino acids 1–136 of ArfGAP3 is responsible for the interaction with RIBEYE(B) (Fig. 2A, matings 1 and 2). The C terminus of ArfGAP3 did not interact with RIBEYE(B) (data not shown). RIBEYE(B) consists of an NADH-binding subdomain (NBD) and a substrate-binding subdomain (SBD; Kumar et al., 2002; Nardini et al., 2003; for review, see Schmitz, 2009; Schmitz et al., 2012). Further YTH analyses demonstrated that the NBD of RIBEYE(B) interacts with ArfGAP3 (Fig. 2B, mating 1). The SBD did not promote ArfGAP3/RIBEYE(B) interaction in the YTH system (Fig. 2B, mating 5). Negative control matings (Fig. 2A, matings 3–8, 10, and 11; B, matings 6–11) demonstrated that bait and prey clones were not auto activating.

### RIBEYE(B) interacts with ArfGAP3 in fusion protein pull-down assays

We used various independent approaches to verify the interaction between RIBEYE(B)-domain and the ArfGAP-domain (AGD) of ArfGAP3. First, we performed pull-down experiments using bacterially expressed and purified fusion protein (Fig. 3). We used MBP-tagged fusion proteins (ArfGAP3(AGD)-MBP and MBP alone) as immobilized bait proteins and GST-tagged proteins (RIBEYE(B)-GST and GST alone) as soluble prey proteins. For the pull-down experiments demonstrated in Figures 3 and 4, the buffer contained 1 mM  $\beta$ ME (see Materials and Methods). ArfGAP3(AGD)-MBP (lane 5; but not MBP alone, lane 7) interacted with RIBEYE(B)-GST (but not with GST alone, lanes 6 and 8) as judged by protein pull-down analyses in SDS-PAGE (Fig. 3). Specificity of interaction was consistently shown both by SDS-PAGE (Fig. 3) and by Western blot analyses (Fig. 4; and data not shown). Identical results were obtained when tags were switched. In Figure 4, RIBEYE(B) was tagged with MBP and ArfGAP3(AGD) with GST. Also with these switched tags, a strong interaction was observed between RIBEYE(B) and ArfGAP3. Typically,  $> \sim 30\%$  of the input fraction of the RIBEYE(B) prey protein was bound to the immobilized ArfGAP3 bait fusion protein.

### ArfGAP3 interacts with RIBEYE(B) in transfected COS cells

Next, we tested whether RIBEYE(B) and ArfGAP3 would interact with each other in transfected COS cells (Fig. 5). ArfGAP3 and RIBEYE(B) were tagged with different fluorescent proteins, i.e., ArfGAP3 with mCherry and RIBEYE(B) with EGFP. When ArfGAP3 was transfected alone, ArfGAP3 was enriched at a perinuclear region that represents the Golgi apparatus (Fig. 5A, B) similarly as previously described (Dogic et al., 1999; Eugster et al., 2000; Lewis et al., 2004; Watson et al., 2004; Frigerio et al., 2007; Kliouchnikov et al., 2009). When RIBEYE(B)-EGFP was transfected alone (Fig. 5C), it was largely diffusely distributed throughout the entire cell (as previously described; Schmitz et al., 2000). In contrast, when RIBEYE(B) was cotransfected with ArfGAP3, RIBEYE(B) was nearly completely recruited to the ArfGAP3-typical Golgi-like perinuclear localization (Fig. 5D) indicating interaction of RIBEYE(B) and ArfGAP3 in cotransfected COS cells.

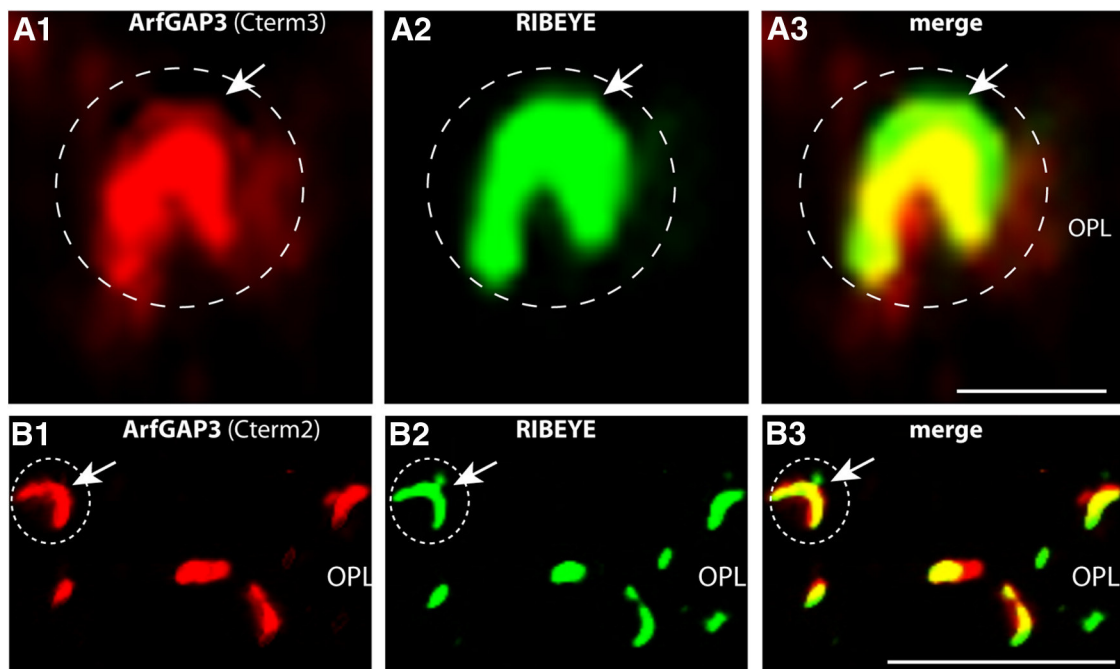


**Figure 9.** ArfGAP3 is strongly enriched at synaptic ribbons of photoreceptor synapses *in situ* (conventional imaging). ArfGAP3 colocalizes with synaptic ribbons. The 0.5- $\mu\text{m}$ -thick retinal sections are double immunolabeled with antibodies against ArfGAP3 and monoclonal antibodies against RIBEYE(B)/CtBP2 (**A, B**). ArfGAP3 Cterm3-antibody was used in **A**, and ArfGAP3 Cterm2 was used for immunolabeling of ArfGAP3 in **B**. Strong ArfGAP3 immunosignals were found in an identical manner with both ArfGAP3 antibodies at the RIBEYE-immunolabeled synaptic ribbons and in close vicinity to synaptic ribbons. The dashed circles denote single immunolabeled photoreceptor presynaptic terminals. Arrows in **B** and **C** point to single immunolabeled synaptic ribbons. No immunosignals were observed in the presynaptic terminals if pre-immune serum was used (data not shown). **A** and **B** were obtained by conventional imaging. OPL, Outer plexiform layer. Scale bars: **A**, 1  $\mu\text{m}$ ; **B**, 5  $\mu\text{m}$ .

### Interaction between ArfGAP3(AGD) and RIBEYE(B) is regulated by NAD(H) in a redox-sensitive manner

The fusion protein pull-down binding experiments shown above in Figures 3 and 4 were done with buffer that contained 1 mM  $\beta\text{ME}$ . If  $\beta\text{ME}$  was omitted, there was no binding between ArfGAP3 and RIBEYE(B) (Fig. 6A, B, compare lane 3 with lane 11). Previously, it has been shown that 1 mM  $\beta\text{ME}$  promotes a conformation of RIBEYE(B) that can be also induced by the addition of NAD(H) (Venkatesan et al., 2010). Furthermore, we demonstrated that the NAD(H)-binding subdomain of RIBEYE(B), the NBD, is responsible for the interaction with ArfGAP3 (see above). Therefore, we tested whether the addition of NAD(H) could replace  $\beta\text{ME}$  in promoting ArfGAP3/RIBEYE(B) interaction. Indeed, NAD(H) was very efficient in promoting RIBEYE(B)/ArfGAP3 interaction (Fig. 6A). The reduced form, NADH, was more efficient in promoting RIBEYE(B)/ArfGAP3 interaction in the absence of  $\beta\text{ME}$  than its oxidized form,  $\text{NAD}^+$  (Fig. 6A, B;  $K_d \sim 450$  nM for NADH;  $K_d \sim 700$  nM for  $\text{NAD}^+$ ). From these experiments we concluded that NAD(H), particularly the reduced NADH, promotes RIBEYE(B)/ArfGAP3 interaction. In line with this proposal is our finding that an NAD(H)-binding-deficient RIBEYE(B) point mutant, RIBEYE(B) G730A (Alpadi et al., 2008; Schwarz et al., 2011), did not interact with ArfGAP3(AGD) in the YTH system (Fig. 2D, mating 1).

### ArfGAP3 can be coimmunoprecipitated with RIBEYE from the bovine retina

We generated two different polyclonal antibodies against ArfGAP3 to analyze the relation between RIBEYE and ArfGAP3 *in situ*. The two different antibodies against ArfGAP3 were directed against two different portions in the divergent C terminus of ArfGAP3 (ArfGAP Cterm2 and ArfGAP Cterm3; see Fig. 7A). Both antibodies immunodetected a typical single, major band at

$\sim 55$  kDa in crude bovine retinal homogenates in Western blot analyses (Fig. 7; data not shown) that was absent in the pre-immune serum and that could be specifically blocked by the respective ArfGAP3-GST fusion protein but not by GST alone (Fig. 7C; data not shown).

Next, we tested whether antibodies against ArfGAP3 coimmunoprecipitated endogenous retinal RIBEYE. ArfGAP3 (Cterm3) immune serum (lane 3, but not ArfGAP3 pre-immune serum, lane 2) coimmunoprecipitated RIBEYE (Fig. 8A) together with ArfGAP3 (Fig. 8B), showing interaction of these proteins also in the retina *in situ* (Fig. 8). Both RIBEYE and ArfGAP3 were strongly enriched in the experimental (Fig. 8, lane 3) but not in the control (Fig. 8, lane 2) immunoprecipitates. Since RIBEYE is exclusively present at synaptic ribbons in the mature retina (Schmitz et al., 2000), the coimmunoprecipitation experiments suggested that ArfGAP3 is a component of the synaptic ribbon complex *in situ*.

### ArfGAP3 is present at the photoreceptor synaptic ribbon complex

To get further insights about the *in situ* localization of ArfGAP3 in the retina, we performed immunolabeling analyses with both ArfGAP3 antibodies (ArfGAP3 Cterm3 and ArfGAP3 Cterm2; Fig. 9). Both ArfGAP3 antibodies strongly labeled the outer plexiform layer (OPL) where photoreceptor ribbon synapses are localized (Fig. 9; data not shown). Identical results were obtained independent of whether crude antisera or affinity-purified antibodies were used (compare Figs. 9, 11, 12). To define the relation between ArfGAP3 and synaptic ribbons, we performed double immunolabelings with rabbit polyclonal antibodies against ArfGAP3 and mouse monoclonal antibodies against RIBEYE(B)-domain/CtBP2 (Fig. 9). The ArfGAP3 immunosignals largely

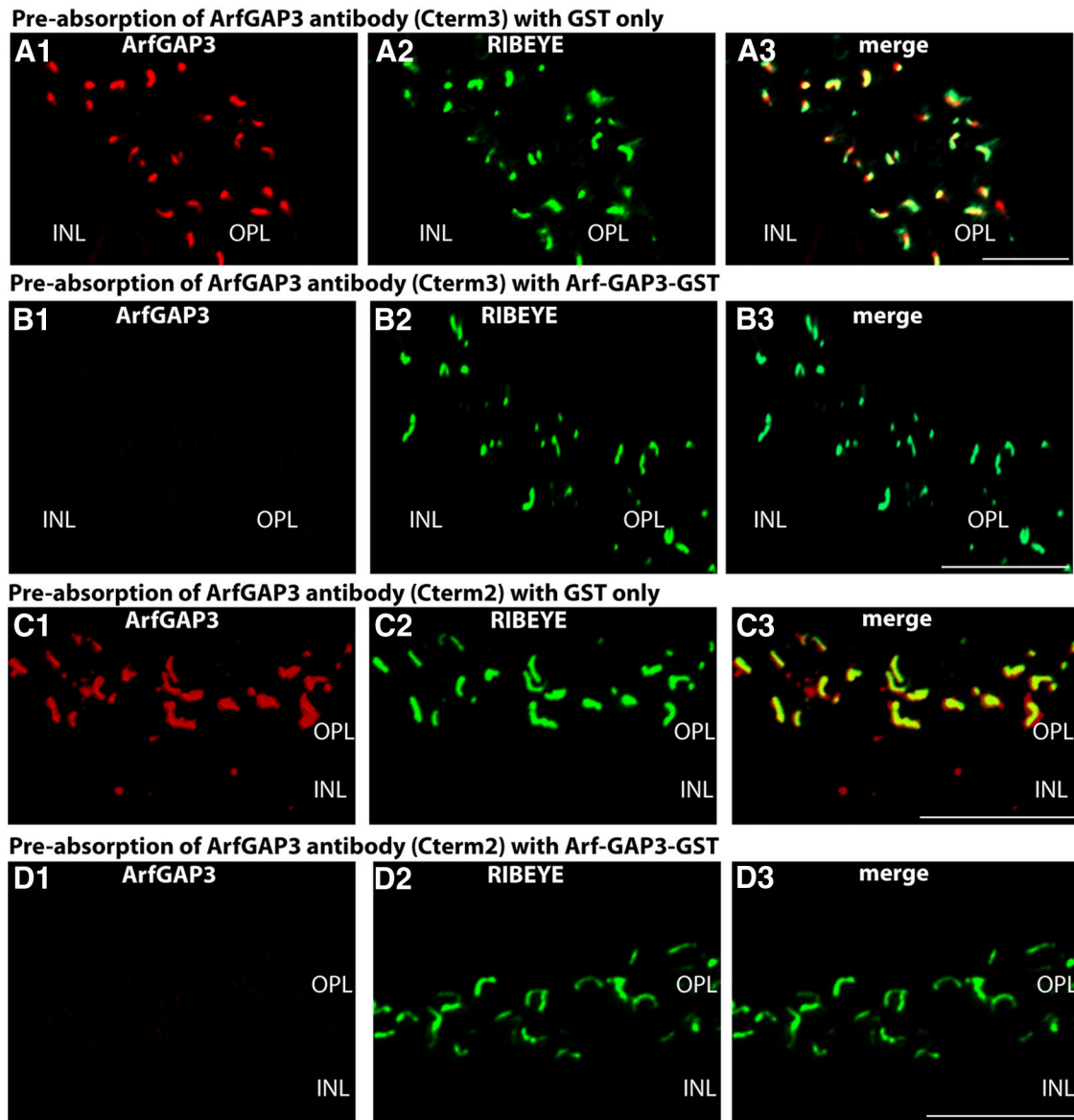


**Figure 10.** *A, B*, Pre-absorption control experiments for the immunolabeling analyses shown in Figure 9*A*. Double immunolabeling of 0.5- $\mu$ m-thick mouse retinal sections with ArfGAP3 (Cterm3) antibody pre-absorbed either with ArfGAP3-GST-fusion protein (*B*) or with GST alone (*A*). To visualize ribbon synapses, sections were coimmunolabeled with mouse monoclonal antibodies against RIBEYE(B)-domain/CtBP2. Pre-absorption with ArfGAP3Cterm3-GST fusion protein completely blocked the ArfGAP3 immunosignals at the synaptic ribbon (*B*), whereas GST alone had no influence on the ArfGAP3 immunosignals (*A*), demonstrating the specificity of the previous immunolabeling results. *C, D*, Pre-absorption control experiments for the immunolabeling analyses shown in Figure 9*B*. Double immunolabeling of 0.5- $\mu$ m-thick mouse retinal sections with ArfGAP3 (Cterm2) antibody pre-absorbed with either ArfGAP3Cterm2-GST-fusion protein (*D*) or with GST alone (*C*). Synaptic ribbons were coimmunolabeled with mouse monoclonal antibodies against RIBEYE(B)-domain/CtBP2. Pre-absorption with the specific fusion protein completely blocked the ArfGAP3 immunosignals at the synaptic ribbon (*D*), whereas GST alone had no influence on the ArfGAP3 immunosignals (*C*), demonstrating the specificity of the previous immunolabeling results. *A–D* were obtained by conventional imaging. OPL, Outer plexiform layer; INL, inner nuclear layer. Scale bars: *A–D*, 5  $\mu$ m.

overlapped at the photoreceptor ribbon synapse with the RIBEYE immunosignals indicating that ArfGAP3 is strongly enriched at the synaptic ribbon complex (Fig. 9*A, B*). Identical immunolabeling results were obtained with both ArfGAP3 antibodies (Fig. 9), further demonstrating that the immunoreactivity at the RIBEYE-immunolabeled synaptic ribbon is due to ArfGAP3 and not due to an unrelated protein. The described ArfGAP3 immunosignals obtained with both ArfGAP3 antibodies could be specifically blocked by pre-absorption with the respective ArfGAP3-GST fusion protein but not by GST alone, demonstrating the specificity of the immunolabeling results (Fig. 10). To further corroborate these findings, we performed SR-SIM of thin retinal sections double immunolabeled with affinity-purified

rabbit polyclonal antibodies against ArfGAP3 and mouse monoclonal antibodies against RIBEYE(B)/CtBP2 (Fig. 11). Also, SR-SIM analyses demonstrated a strong enrichment of the ArfGAP3 immunosignals at the synaptic ribbons (Fig. 11). In the SR-SIM analyses, the ArfGAP3 immunosignal was slightly shifted toward the inner nuclear layer (INL) compared with the RIBEYE immunosignal, which could indicate a localization of ArfGAP3 more toward the base of the synaptic ribbon (Fig. 11*A*; see also discussion). The ArfGAP3 immunosignals also showed a strong colocalization with the active zone protein bassoon (Fig. 11*B*). In the SR-SIM analyses, the ArfGAP3 immunosignal was slightly shifted toward the ONL compared with the bassoon immunosignal, also indicating an ArfGAP3 localization in the basal portions at the

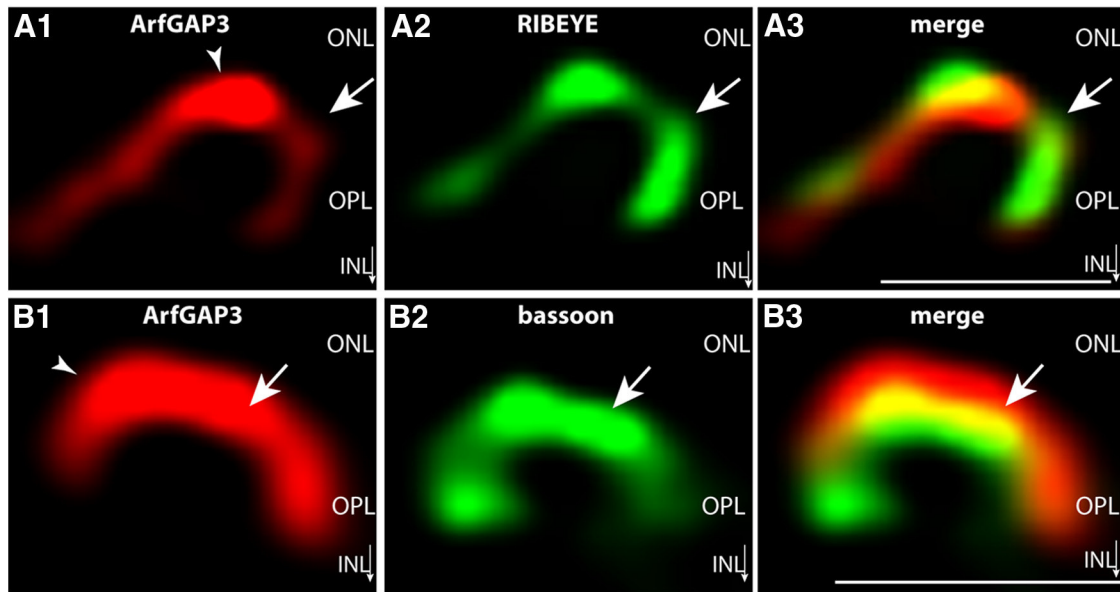


**Figure 11.** ArfGAP3 is strongly enriched at the synaptic ribbon of photoreceptor synapses *in situ* (SR-SIM imaging with ArfGAP3 Cterm3 antibody). **A**, 0.5- $\mu$ m-thick retinal sections double immunolabeled with affinity-purified rabbit antibodies against ArfGAP3 (ArfGAP3 Cterm3 antibody) and mouse monoclonal antibodies against RIBEYE(B)/CtBP2. **B**, Shows 0.5- $\mu$ m-thick retinal sections double immunolabeled with affinity-purified rabbit antibodies against ArfGAP3 (Cterm3 antibody) and mouse monoclonal antibodies against the active zone protein bassoon. Arrows in **A** and **B** point to single immunolabeled synaptic ribbons. Arrowheads denote ArfGAP3 immunoreactivity at the synaptic ribbon. **A** and **B** were obtained by SR-SIM imaging. ONL, Outer nuclear layer; OPL, outer plexiform layer; INL, inner nuclear layer. Scale bars: **A**, **B**, 1  $\mu$ m.

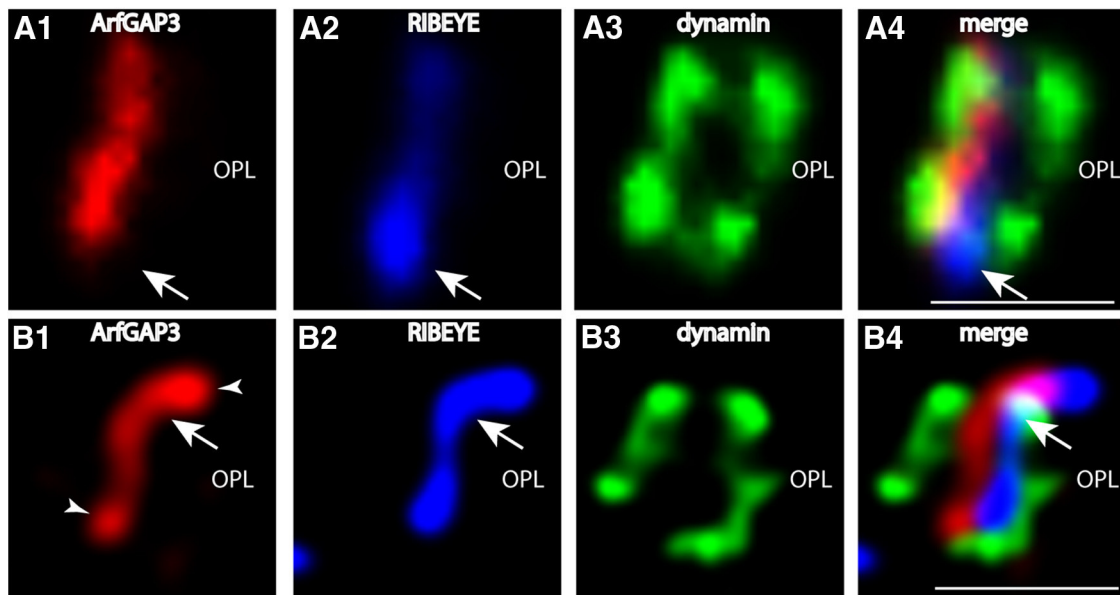


**Figure 12.** Localization of ArfGAP3 in the presynaptic photoreceptor terminal in relation to other presynaptic proteins. The 0.5- $\mu$ m-thick retinal sections were triple immunolabeled with affinity-purified rabbit polyclonal antibodies against ArfGAP3 (Cterm3), mouse monoclonal antibodies against dynamin (hudy-1), and DyLight 650 directly labeled primary antibodies against RIBEYE(B)/CtBP2. ArfGAP3 and RIBEYE are located very close to each other (**A**, **B**). The ArfGAP3 immunosignal is located within the ring-like dynamin immunosignal that demarcates the presynaptic plasma membrane of the periaxial zone that surrounds the synaptic ribbon (Wahl et al., 2013). **A** was obtained by conventional imaging; **B** is a micrograph obtained by SR-SIM imaging. Arrows in **A** and **B** point to immunolabeled single synaptic ribbons. Arrowheads indicate ArfGAP3 immunoreactivity at the synaptic ribbon. OPL, Outer plexiform layer. Scale bars: **A**, **B**, 1  $\mu$ m.

synaptic ribbon (Fig. 11B; see also discussion). Bassoon is localized to the arciform density and anchors the base of the synaptic ribbon (tom Dieck et al., 2005).

Previously, we have shown that dynamin is highly enriched at the presynaptic plasma membrane in close vicinity to the synaptic ribbon (Wahl et al., 2013). The dynamin immunosignal surrounds the synaptic ribbon in a ring-like manner in a very short distance (Wahl et al., 2013). Immunogold electron microscopy previously demonstrated that this ring of dynamin-1 immunore-

activity corresponded to the plasma membrane of the periaxial zone (Wahl et al., 2013). We used dynamin as a landmark protein to further define the localization of ArfGAP3 at the synaptic ribbon complex using high-resolution fluorescence microscopy. We performed triple immunolabeling analyses with rabbit polyclonal antibodies against ArfGAP3, mouse monoclonal antibodies against dynamin (hudy-1), and Alexa 650 directly labeled primary mouse monoclonal antibodies against RIBEYE(B)-domain/CtBP2 (Fig. 12). In these triple immunolabeling analyses,

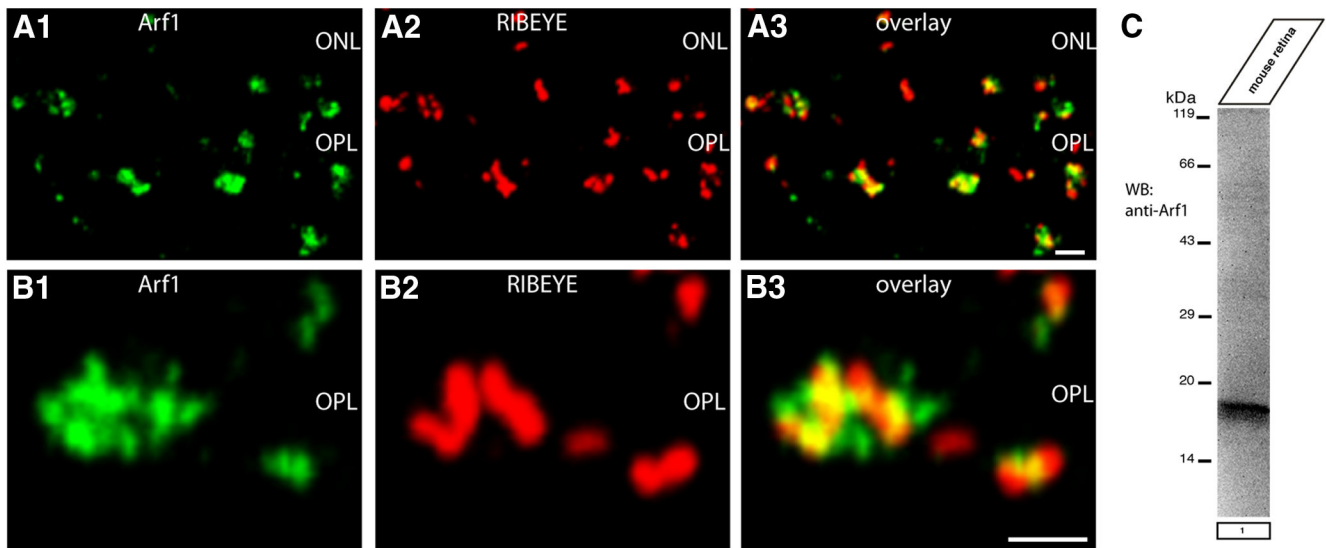


**Figure 13.** The ArfGAP3 effector Arf1 is enriched at the synaptic ribbon complex of photoreceptor synapses. **A, B,** Double immunolabeling experiments of 0.5- $\mu\text{m}$ -thick retinal sections with mouse monoclonal antibodies against Arf1 and rabbit polyclonal antibodies against RIBEYE (U2656) demonstrated a close enrichment of Arf1 around the synaptic ribbon complex. ONL, Outer nuclear layer; OPL, outer plexiform layer. Scale bars: **A, B,** 1  $\mu\text{m}$ . **(C)** Western blot analyses demonstrated that Arf1 is strongly expressed in the mouse retina.

the ArfGAP3 immunosignals were located very close to the RIBEYE-labeled synaptic ribbon and within the ring-like dynamin immunosignals that surrounded the synaptic ribbon (Fig. 12). Unfortunately, all the ArfGAP3 antibodies that we generated as well as various commercially available antibodies did not work at the ultrastructural level, so the ultrastructural localization remains to be elucidated by future examinations. ArfGAP3 is only weakly expressed in the inner plexiform layer (IPL) of the retina, which is probably due to the smaller size of the synaptic ribbons in bipolar cell terminals (data not shown).

#### RIBEYE(B) competes with Arf1 for binding to ArfGAP3

To get functional insights into the importance of the ArfGAP3/RIBEYE interaction we determined which Arf protein is interacting with ArfGAP3. In agreement with previous reports (Liu et al., 2001; Kartberg et al., 2010), we found that ArfGAP3 interacts with Arf1 (but not with Arf6; Fig. 2E, mating 1; data not shown). Western blot analyses demonstrated that Arf1 is strongly expressed in the retina and immunofluorescence microscopy documented enrichment of Arf1 in close vicinity to the synaptic ribbon complex (Fig. 13A–C).

Similar to RIBEYE(B), Arf1 also binds to the ArfGAP-domain of ArfGAP3 (data not shown). Therefore, we tested whether Arf1 and RIBEYE(B) can bind simultaneously to ArfGAP3 or whether they compete with each other in binding to ArfGAP3 (Fig. 14). To address this question, we used fusion protein pull-down experiments. We tested whether increasing concentrations of Arf1 (Fig. 14A) added to a fixed concentration of immobilized ArfGAP3 (0.15  $\mu\text{M}$ ) would inhibit binding of RIBEYE(B) to ArfGAP3. RIBEYE(B) was kept at a constant concentration in these experiments (0.15  $\mu\text{M}$ ). Similarly, we also tested whether increasing concentrations of RIBEYE(B) (Fig. 14B) added to a fixed concentration of immobilized ArfGAP3 (0.15  $\mu\text{M}$ ) would inhibit binding of Arf1 to ArfGAP3. Arf1 was kept at a constant concentration in these latter experiments (0.15  $\mu\text{M}$ ). In both sets of experiments, we observed a competitive behavior between Arf1 and RIBEYE(B) in binding to ArfGAP3: if Arf1 was increased, binding of RIBEYE(B) to ArfGAP3 was diminished and, vice versa, increasing concentrations of RIBEYE(B) inhibit binding of Arf1 to

ArfGAP3. These data demonstrate that RIBEYE(B) competes with Arf1 for binding to a common binding site on ArfGAP3, indicating that binding of RIBEYE(B) and Arf1 to ArfGAP3 is mutually exclusive.

#### ArfGAP3 is involved in endocytic vesicle retrieval at the photoreceptor synapse

Next, we wanted to find out for which synaptic process ArfGAP3 is relevant at the synaptic ribbon. The synaptic ribbon is a site of intense membrane retrieval (Jackman et al., 2009; Snellman et al., 2011; Chen et al., 2013; Wahl et al., 2013). Therefore, we tested whether ArfGAP3 is involved in this process (Fig. 15). We added FM1–43 to the extracellular medium to compare endocytic uptake in photoreceptors that were either electroporated with ArfGAP3-mcherry or mcherry alone. In mcherry-electroporated photoreceptors, there was an intense uptake of FM1–43 (Fig. 15A, B). The uptake of FM1–43 in mcherry-transfected photoreceptors was similar to the FM1–43 uptake in nontransfected photoreceptors (data not shown). In contrast to mcherry-transfected photoreceptors, ArfGAP3-overexpressing transfected photoreceptors showed a very strong inhibition of FM1–43 uptake (Fig. 15C, D) indicating that ArfGAP3 is essentially involved in endocytosis at the photoreceptor synapse (see discussion).

#### Discussion

In the present study, we demonstrated that the Arf-GTPase-activating protein-3, ArfGAP3, is a novel component of the photoreceptor synaptic ribbon complex using various independent assays. Conventional immunofluorescence microscopy as well as SR-SIM on thin retinal resin sections demonstrated that ArfGAP3 is highly enriched at the photoreceptor synaptic ribbon complex *in situ*. ArfGAP3 is more weakly expressed in the IPL than in photoreceptor synapses of the OPL (data not shown). This is most likely because synaptic ribbons in the IPL are smaller than in photoreceptor synapses of the OPL and because the IPL is dominated by conventional, nonribbon-containing synapses.

ArfGAP3 has been previously characterized as a component of the Golgi apparatus (for review, see Spang et al., 2010). At the Golgi apparatus, ArfGAP3 regulates vesicle trafficking in an Arf1-



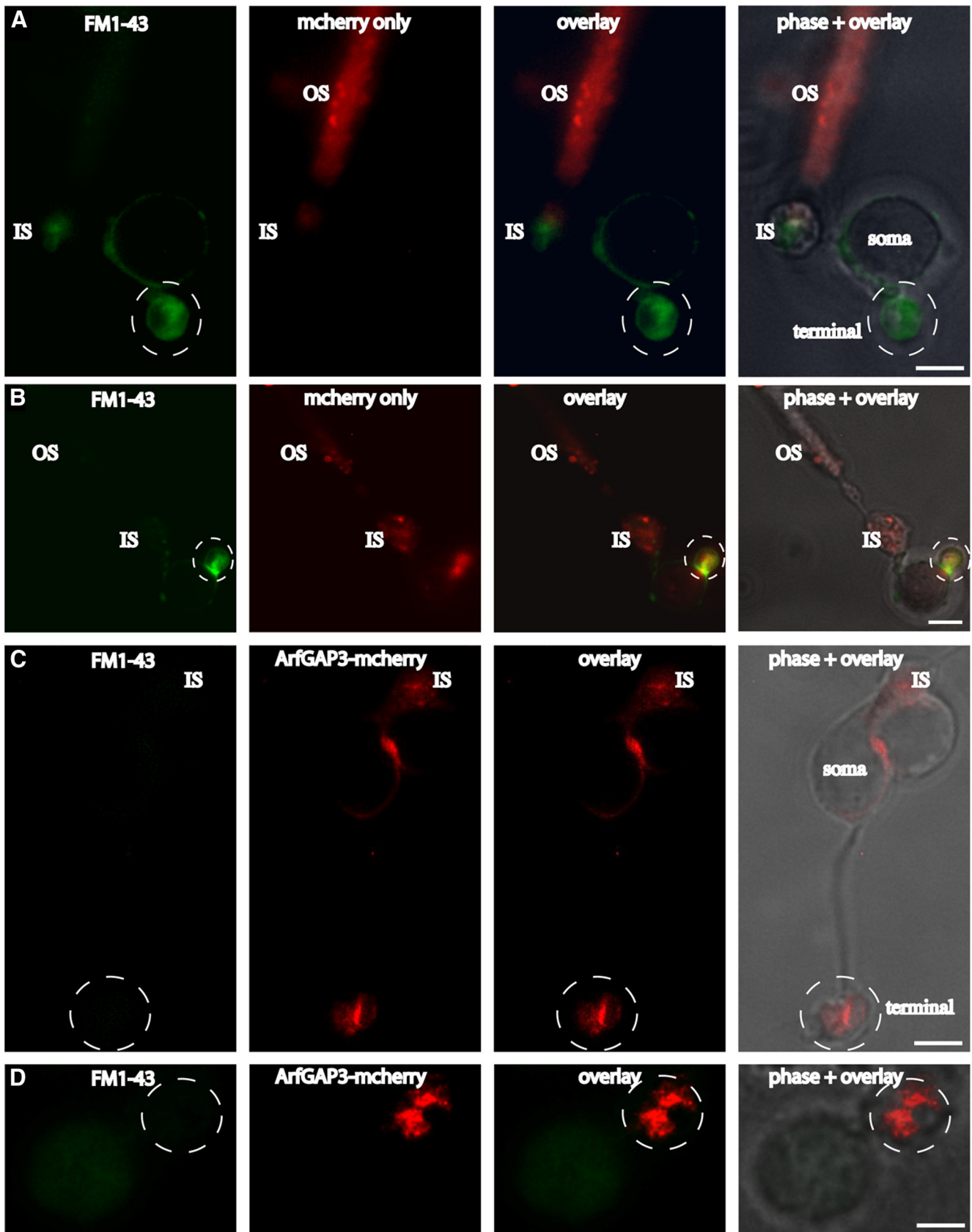


**Figure 15.** Overexpression of ArfGAP3 in mouse photoreceptors inhibits endocytic uptake of FM1-43. FM1-43 was used to compare endocytic uptake in photoreceptors that were either electroporated with mcherry alone (**A, B**) or ArfGAP3-mcherry (**C, D**). In mcherry-electroporated photoreceptors, there was an intense uptake of FM1-43 in the synaptic terminals (**A, B**). The uptake of FM1-43 in mcherry-transfected photoreceptors was similar to the FM1-43 uptake in nontransfected photoreceptors (data not shown). In contrast to mcherry-transfected photoreceptors, ArfGAP3-mcherry-overexpressing photoreceptors showed a strong inhibition of FM1-43 uptake in the synaptic terminals (**C, D**), indicating that ArfGAP3 is essential involved in endocytosis at the photoreceptor synapse. OS, Outer segment; IS, inner segment; Scale bars: **A–C**, 1  $\mu\text{m}$ ; **D**, 0.75  $\mu\text{m}$ .

2002, 2006; Fjeld et al., 2003). A main function of this redox-sensitive interaction in ribbon synapses appears to be controlling Arf1 function. The small GTP-binding protein Arf1, an ArfGAP3 effector, is enriched at the synaptic ribbon. Arf1 is an important regulator of vesicle traffic at various intracellular compartments, including the Golgi apparatus and endosomal compartments (Gillingham and Munro, 2007; Kahn et al., 2008; Donaldson and Jackson, 2011) and might perform a similar role at the photoreceptor synaptic ribbon complex. We demonstrated that Arf1 and RIBEYE cannot bind at the same time. When RIBEYE is bound, e.g., at high levels of NADH, Arf1 can no longer bind to ArfGAP3. As a consequence, its GTPase activity will remain low and Arf1 will stay in its active, GTP-bound form.

Unfortunately, the antibodies against ArfGAP3 were not suitable for ultrastructural analyses. Super-resolution immunofluorescent microscopy indicated a particularly high enrichment of ArfGAP3 at the base of synaptic ribbon complex. Similarly, ArfGAP3 was also found close to bassoon, which is located at the base of the ribbon, and within the ring-like dynamin signal that surrounds the synaptic ribbon in the periaxial zone. Dynamin was previously shown to be enriched at the presynaptic plasma membrane at the periaxial zone (Wahl et al., 2013). Therefore, ArfGAP3 probably exerts its function at the base of the ribbon and in close proximity to the plasma membrane of the periaxial zone. Clearly, future electron microscopic analyses need to demonstrate whether ArfGAP3 and Arf1 function directly at the presynaptic plasma membrane or on an endosomal compartment close to the plasma membrane.

Overexpression of ArfGAP3 in electroporated photoreceptors resulted in a strong inhibition of endocytic membrane retrieval as judged by an inhibition of uptake of FM1–43. Therefore, we propose that the RIBEYE/ArfGAP3 complex is involved in endocytic membrane retrieval at the synaptic ribbon. Recent studies demonstrated that the synaptic ribbon complex is important for endocytic membrane traffic in the tonically active ribbon synapse (Spasova et al., 2004; Griesinger et al., 2005; Khimich et al., 2005; Jackman et al., 2009; Babai et al., 2010; Frank et al., 2010; Schnee et al., 2011; Snellman et al., 2011; Tian et al., 2012; Chen et al., 2013; Wahl et al., 2013). Still, the molecular details and mechanisms used to accomplish this remain to be elucidated.

CtBP1/BARS, a close relative of RIBEYE(B)-domain/CtBP2 and component of the Golgi complex, is also localized to the synaptic ribbon complex (tom Dieck et al., 2005; for a review, see Corda et al., 2006). At the Golgi apparatus, CtBP1/BARS interacts with ArfGAP1 (Yang et al., 2005). This interaction has been proposed to be essential for vesicle formation and vesicle scission at the Golgi complex (Yang et al., 2002, 2005, 2006; Corda et al., 2006). The function of CtBP1/BARS at the synaptic ribbon is still unclear (Vaithianathan et al., 2013). There is a remarkable difference between the CtBP1/ArfGAP1 interaction compared with the RIBEYE/ArfGAP3 interaction. Interaction between CtBP1 and ArfGAP1 at the Golgi apparatus is mediated by the SBD of CtBP1, while the interaction between RIBEYE(B) domain and ArfGAP3 at the synaptic ribbons is mediated by the NBD of RIBEYE(B)-domain.

The recruitment of ArfGAP3 to the synaptic ribbon via an inducible, redox-dependent manner provides the synaptic ribbon with the possibility to regulate endocytic vesicle trafficking. The catalytically active ArfGAP-domain could control Arf1 activity in a redox-switchable manner by a competitive interaction with RIBEYE. The C terminus of ArfGAP3 could be involved in different tasks, e.g., the cargo sorting. The C terminus of ArfGAP3 has been shown to be involved in membrane-binding and

cargo-binding/coat protein-binding at the Golgi apparatus (Rein et al., 2002; for review, see Nie and Randazzo, 2006; Schindler and Spang, 2007; Kliouchnikov et al., 2009; Schindler et al., 2009; Spang et al., 2010). A similar function might also apply in the ribbon synapse and would provide the RIBEYE-ArfGAP3 complex a central position in the vesicle recycling machinery.

## References

- Alpadi K, Magupalli VG, Käppel S, Köblitz L, Schwarz K, Seigel GM, Sung CH, Schmitz F (2008) RIBEYE recruits a mammalian ortholog of the *C. elegans* protein unc119 to synaptic ribbons of photoreceptor synapses. *J Biol Chem* 283:26461–26467. [CrossRef Medline](#)
- Babai N, Bartoletti TM, Thoreson WB (2010) Calcium regulates vesicle replenishment at the cone ribbon synapse. *J Neurosci* 30:15866–15877. [CrossRef Medline](#)
- Bigay J, Casella JF, Drin G, Mesmin B, Antony B (2005) ArfGAP1 responds to membrane curvature through the folding of a lipid packing sensor motif. *EMBO J* 24:2244–2253. [CrossRef Medline](#)
- Bradford MM (1976) A rapid and sensitive method for the quantitation of microgram quantities of protein utilizing the principle of protein-dye binding. *Anal Biochem* 72:248–254. [CrossRef Medline](#)
- Briggman KL, Euler T (2011) Bulk electroporation and population calcium imaging in the adult mammalian retina. *J Neurophysiol* 105:2601–2609. [CrossRef Medline](#)
- Chen M, Van Hook MJ, Zenisek D, Thoreson WB (2013) Properties of ribbon and non-ribbon release from rod photoreceptors revealed by visualizing individual synaptic vesicles. *J Neurosci* 33:2071–2086. [CrossRef Medline](#)
- Corda D, Colanzi A, Luini A (2006) The multiple activities of CtBP/BARS proteins: the Golgi view. *Trends Cell Biol* 16:167–173. [CrossRef Medline](#)
- Cukierman E, Huber I, Rotman M, Cassel D (1995) The Arf1 GTPase-activating protein: zinc finger motif and Golgi complex localization. *Science* 270:1999–2002. [CrossRef Medline](#)
- Dogic D, de Chasse B, Pick E, Cassel D, Lefkiri Y, Hennecke S, Cosson P, Letourneur F (1999) The ADP-ribosylation factor GTPase-activating protein glo3p is involved in ER retrieval. *Eur J Cell Biol* 78:305–310. [CrossRef Medline](#)
- Donaldson JG, Jackson CL (2011) Arf family G proteins and their regulators: roles in membrane transport, development and disease. *Nat Rev Mol Cell Biol* 12:362–375. [CrossRef Medline](#)
- Donovan SL, Dyer MA (2006) Preparation and square wave electroporation of retinal explant cultures. *Nat Protoc* 1:2710–2718. [CrossRef Medline](#)
- Eugster A, Frigerio G, Dale M, Duden R (2000) COP I domains required for coatamer integrity and novel interactions with Arf and ArfGAP. *EMBO J* 19:3905–3917. [CrossRef Medline](#)
- Fjeld CC, Birdsong WT, Goodman RH (2003) Differential binding of NAD<sup>+</sup> and NADH allows the transcriptional corepressor C-terminal binding protein to serve as a metabolic sensor. *Proc Natl Acad Sci U S A* 100:9202–9207. [CrossRef Medline](#)
- Frank T, Rutherford MA, Strenze N, Neef A, Pangrsic T, Khimich D, Fejtova A, Gundelfinger ED, Liberman MC, Harke B, Bryan KE, Lee A, Egner A, Riedel D, Moser T (2010) Bassoon and the synaptic ribbon organize Ca<sup>2+</sup>-channels and vesicles to add release sites and promote refilling. *Neuron* 68:724–738. [CrossRef Medline](#)
- Frigerio G, Grimsey N, Dale M, Majoul I, Duden R (2007) Two human ArfGAPs associated with COP-I-coated vesicles. *Traffic* 8:1644–1655. [CrossRef Medline](#)
- Gillingham AK, Munro S (2007) The small G proteins of the Arf family and their regulators. *Annu Rev Cell Dev Biol* 23:579–611. [CrossRef Medline](#)
- Goldberg J (1999) Structural and functional analysis of the Arf1-Arfgap complex reveals a role for coatamer in GTP hydrolysis. *Cell* 96:893–902. [CrossRef Medline](#)
- Griesinger CB, Richards CD, Ashmore JF (2005) Fast vesicle replenishment allows indefatigable signalling at the first auditory synapse. *Nature* 435:212–215. [CrossRef Medline](#)
- Gustafsson MG, Shao L, Carlton PM, Wang CJ, Golubovskaya IN, Cande WZ, Agard DA, Sedat JW (2008) Three-dimensional resolution doubling in wide-field fluorescence microscopy by structured illumination. *Biophys J* 94:4957–4970. [CrossRef Medline](#)
- Harper JW, Adami GR, Wei N, Keyomarsi K, Elledge SJ (1993) The p21 Cdk-interacting protein Cip1 is a potent inhibitor of G1 cyclin-dependent kinases. *Cell* 75:805–816. [CrossRef Medline](#)

- Inoue H, Randazzo PA (2007) Arf GAPs and their interacting proteins. *Traffic* 8:1465–1475. [CrossRef Medline](#)
- Jackman SL, Choi SY, Thoreson WB, Rabl K, Bartoletti TM, Kramer RH (2009) Role of the synaptic ribbon in transmitting the cone light response. *Nat Neurosci* 12:303–310. [CrossRef Medline](#)
- Kahn RA, Bruford E, Inoue H, Logsdon JM Jr, Nie Z, Premont RT, Randazzo PA, Satake M, Theibert AB, Zapp ML, Cassel D (2008) Consensus nomenclature of the human ArfGAP domain-containing proteins. *J Cell Biol* 182:1039–1044. [CrossRef Medline](#)
- Kartberg F, Asp L, Dejgaard SY, Smedh M, Fernandez-Rodriguez J, Nilsson T, Presley JF (2010) ArfGAP2 and ArfGAP3 are essential for COP I coat assembly on the Golgi membrane of living cells. *J Biol Chem* 285:36709–36720. [CrossRef Medline](#)
- Katsumata O, Ohara N, Tamaki H, Niimura T, Naganuma H, Watanabe M, Sakagami H (2009) IQ-ArfGEF/BRAG1 is associated with synaptic ribbons in the mouse retina. *Eur J Neurosci* 30:1509–1516. [CrossRef Medline](#)
- Khimich D, Nouvian R, Pujol R, Tom Dieck S, Egner A, Gundelfinger ED, Moser T (2005) Hair cell synaptic ribbons are essential for synchronous auditory signalling. *Nature* 434:889–894. [CrossRef Medline](#)
- Kliouchnikov L, Bigay J, Mesmin B, Parnis A, Rawet M, Goldfeder N, Antonny B, Cassel D (2009) Discrete determinants in ArfGAP2/3 conferring Golgi localization and regulation by the COPI coat. *Mol Biol Cell* 20:859–869. [CrossRef Medline](#)
- Kumar V, Carlson JE, Ohgi KA, Edwards TA, Rose DW, Escalante CR, Rosenfeld MG, Aggarwal AK (2002) Transcription corepressor CtBP is an NAD(+) regulated dehydrogenase. *Mol Cell* 10:857–869. [CrossRef Medline](#)
- Lewis SM, Poon PP, Singer RA, Johnston GC, Spang A (2004) The ArfGAP Glo3 is required for the generation of COP I vesicles. *Mol Biol Cell* 15:4064–4072. [CrossRef Medline](#)
- Liu X, Zhang C, Xing G, Chen Q, He F (2001) Functional characterization of novel human ArfGAP3. *FEBS Lett* 490:79–83. [CrossRef Medline](#)
- Magupalli VG, Schwarz K, Alpadi K, Natarajan S, Seigel GM, Schmitz F (2008) Multiple RIBEYE-RIBEYE interactions create a dynamic scaffold for the formation of synaptic ribbons. *J Neurosci* 28:7954–7967. [CrossRef Medline](#)
- Morgan JL, Soto F, Wong RO, Kerschensteiner D (2011) Development of cell type-specific connectivity patterns of converging excitatory axons in the retina. *Neuron* 71:1014–1021. [CrossRef Medline](#)
- Nardini M, Spanò S, Cericola C, Pesce A, Massaro A, Millo E, Luini A, Corda D, Bolognesi M (2003) CtBP/BARS: a dual-function protein involved in transcriptional corepression and Golgi membrane fission. *EMBO J* 22:3122–3130. [CrossRef Medline](#)
- Nie Z, Randazzo PA (2006) Arf GAPs and membrane traffic. *J Cell Sci* 119:1203–1211. [CrossRef Medline](#)
- Olmsted JB (1981) Affinity purification of antibodies from diazotized paper blots of heterogeneous protein samples. *J Biol Chem* 256:11955–11957. [Medline](#)
- Rea R, Li J, Dharia A, Levitan ES, Sterling P, Kramer RH (2004) Streamlined synaptic vesicle cycle in cone photoreceptor terminals. *Neuron* 41:755–766. [CrossRef Medline](#)
- Rein U, Andag U, Duden R, Schmitt HD, Spang A (2002) ArfGAP-mediated interaction between ER-Golgi v-SNAREs and the COP I coat. *J Cell Biol* 157:395–404. [CrossRef Medline](#)
- Saitoh A, Shin HW, Yamada A, Waguri S, Nakayama K (2009) Three homologous ArfGAPs participate in coat protein I-mediated transport. *J Biol Chem* 284:13948–13957. [CrossRef Medline](#)
- Schermelleh L, Carlton PM, Haase S, Shao L, Winoto L, Kner P, Burke B, Cardoso MC, Agard DA, Gustafsson MG, Leonhardt H, Sedat JW (2008) Subdiffraction multicolor imaging of the nuclear periphery with 3D structured illumination microscopy. *Science* 320:1332–1336. [CrossRef Medline](#)
- Schermelleh L, Heintzmann R, Leonhardt H (2010) A guide to superresolution fluorescence microscopy. *J Cell Biol* 190:165–175. [CrossRef Medline](#)
- Schindler C, Spang A (2007) Interaction of SNAREs with ArfGAPs precedes recruitment of sec18p/NSF. *Mol Biol Cell* 18:2852–2863. [CrossRef Medline](#)
- Schindler C, Rodriguez F, Poon PP, Singer RA, Johnston GC, Spang A (2009) The GAP domain and the SNARE, coatomer and cargo interaction region of the ArfGAP2/3 glo3 are sufficient for glo3 function. *Traffic* 10:1362–1375. [CrossRef Medline](#)
- Schmitz F (2009) The making of synaptic ribbons: how they are built and what they do. *Neuroscientist* 15:611–624. [CrossRef Medline](#)
- Schmitz F, Königstorfer A, Südhof TC (2000) RIBEYE, a component of ribbon synapses: a protein's journey through evolution provides insight into synaptic ribbon function. *Neuron* 28:857–872. [CrossRef Medline](#)
- Schmitz F, Natarajan S, Venkatesan JK, Wahl S, Schwarz K, Grabner CP (2012) EF hand-mediated Ca and cGMP signaling in photoreceptor synaptic terminals. *Front Mol Neurosci* 5:26. [CrossRef Medline](#)
- Schnee ME, Santos-Sacchi J, Castellano-Muñoz M, Kong JH, Ricci AJ (2011) Calcium-terminal synaptic vesicle trafficking underlies indefatigable release of the hair cell afferent fiber synapse. *Neuron* 70:326–338. [CrossRef Medline](#)
- Schwarz K, Natarajan S, Kassas N, Vitale N, Schmitz F (2011) The synaptic ribbon is a site of phosphatidic acid generation in ribbon synapses. *J Neurosci* 31:15996–16011. [CrossRef Medline](#)
- Snellman J, Mehta B, Babai N, Bartoletti TM, Akmentin W, Francis A, Matthews G, Thoreson W, Zenisek D (2011) Acute destruction of the synaptic ribbon reveals a role for the ribbon in vesicle priming. *Nat Neurosci* 14:1135–1141. [CrossRef Medline](#)
- Spang A, Shiba Y, Randazzo PA (2010) ArfGAPs: gatekeepers of vesicle generation. *FEBS Lett* 584:2646–2651. [CrossRef Medline](#)
- Spassova MA, Avissar M, Furman AC, Crumling MA, Saunders JC, Parsons TD (2004) Evidence that rapid replenishment of the synaptic ribbon mediates recovery from short-term adaptation at the hair cell afferent synapse. *J Assoc Res Otolaryngol* 5:376–390. [CrossRef Medline](#)
- Tai AW, Chuang JZ, Bode C, Wolfrum U, Sung CH (1999) Rhodopsin's carboxyterminal cytoplasmic tail acts as a membrane receptor for cytoplasmic dynein by binding to the dynein light chain Tctex-1. *Cell* 97:877–887. [CrossRef Medline](#)
- Tian M, Xu CS, Montpetit R, Kramer RH (2012) Rab3a mediates vesicle delivery at photoreceptor ribbon synapses. *J Neurosci* 32:6931–6936. [CrossRef Medline](#)
- tom Dieck S, Altmann WD, Kessels MM, Qualmann B, Regus H, Brauner D, Fejtová A, Bracko O, Gundelfinger ED, Brandstätter JH (2005) Molecular dissection of the photoreceptor ribbon synapse: physical interaction of Bassoon and RIBEYE is essential for the assembly of the ribbon complex. *J Cell Biol* 168:825–836. [CrossRef Medline](#)
- Vaithianathan T, Akmentin W, Henry D, Matthews G (2013) The ribbon-associated protein C-terminal-binding protein 1 is not essential for the structure and function of retinal ribbon synapses. *Mol Vis* 19:917–926. [Medline](#)
- Venkatesan JK, Natarajan S, Schwarz K, Mayer SI, Alpadi K, Magupalli VG, Sung CH, Schmitz F (2010) Nicotinamide adenine dinucleotide-dependent binding of the neuronal Ca<sup>2+</sup> sensor protein GCAP2 to photoreceptor synaptic ribbons. *J Neurosci* 30:6559–6576. [CrossRef Medline](#)
- Vergara MN, Gutierrez C, O'Brien DR, Canto-Soler MV (2013) Ex vivo electroporation of retinal cells: a novel, high efficiency method for functional studies in primary retinal cultures. *Exp Eye Res* 109:40–50. [CrossRef Medline](#)
- Wahl S, Katiyar R, Schmitz F (2013) A local, periaxonal zone endocytic machinery at photoreceptor synapses in close vicinity to photoreceptor synaptic ribbons. *J Neurosci* 33:10278–10300. [CrossRef Medline](#)
- Watson PJ, Frigerio G, Collins BM, Duden R, Owen DJ (2004) gamma-COP appendage domain-structure and function. *Traffic* 5:79–88. [CrossRef Medline](#)
- Williams PR, Morgan JL, Kerschensteiner D, Wong RO (2013) In vitro imaging of retinal whole mounts. *Cold Spring Harb Protoc* 2013. pii:pdb-prot072645. [CrossRef Medline](#)
- Yang JS, Lee SY, Gao M, Bourgoin S, Randazzo PA, Premont RT, Hsu VW (2002) ArfGAP1 promotes the formation of COPI vesicles, suggesting function as a component of the coat. *J Cell Biol* 159:69–78. [CrossRef Medline](#)
- Yang JS, Lee SY, Spanò S, Gad H, Zhang L, Nie Z, Bonazzi M, Corda D, Luini A, Hsu VW (2005) A role for BARS at the fission step of COP I vesicle formation from the Golgi membrane. *EMBO J* 24:4133–4143. [CrossRef Medline](#)
- Yang JS, Zhang L, Lee SY, Gad H, Luini A, Hsu VW (2006) Key components of the fission machinery are interchangeable. *Nat Cell Biol* 8:1376–1382. [CrossRef Medline](#)
- Yu X, Breitman M, Goldberg J (2012) A structure-based mechanism for Arf1-dependent recruitment of coatomer to membranes. *Cell* 148:530–542. [CrossRef Medline](#)
- Zenisek D, Steyer JA, Almers W (2000) Transport, capture and exocytosis of single synaptic vesicles at active zones. *Nature* 406:849–854. [CrossRef Medline](#)
- Zhang Q, Piston DW, Goodman RH (2002) Regulation of corepressor function by nuclear NADH. *Science* 295:1895–1897. [Medline](#)
- Zhang Q, Wang SY, Nottke AC, Rocheleau JV, Piston DW, Goodman RH (2006) Redox sensor CtBP mediates hypoxia-induced tumor cell migration. *Proc Natl Acad Sci U S A* 103:9029–9033. [CrossRef Medline](#)



# EF hand-mediated $\text{Ca}^{2+}$ - and cGMP-signaling in photoreceptor synaptic terminals

Frank Schmitz\*, Sivaraman Natarajan, Jagadeesh K. Venkatesan†, Silke Wahl, Karin Schwarz and Chad P. Grabner\*

Department of Neuroanatomy, Medical School Homburg/Saar, Institute for Anatomy and Cell Biology, Saarland University, Saarland, Germany

## Edited by:

Karl-Wilhelm Koch, Carl von Ossietzky University Oldenburg, Germany

## Reviewed by:

Karl-Wilhelm Koch, Carl von Ossietzky University Oldenburg, Germany  
Florentina Soto, Washington University in St. Louis, USA

## \*Correspondence:

Frank Schmitz and Chad P. Grabner, Department of Neuroanatomy, Medical School Homburg/Saar, Institute for Anatomy and Cell Biology, Saarland University, Kirrbergerstrasse, University Campus, 66421 Homburg/Saar, Germany.  
e-mail: frank.schmitz@uks.eu; chadgrabner@gmail.com

## † Present Address:

Department of Experimental Orthopedics, Saarland University, University Hospital of Orthopedics, Homburg/Saar, Germany.

Photoreceptors, the light-sensitive receptor neurons of the retina, receive and transmit a plethora of visual informations from the surrounding world. Photoreceptors capture light and convert this energy into electrical signals that are conveyed to the inner retina. For synaptic communication with the inner retina, photoreceptors make large active zones that are marked by synaptic ribbons. These unique synapses support continuous vesicle exocytosis that is modulated by light-induced, graded changes of membrane potential. Synaptic transmission can be adjusted in an activity-dependent manner, and at the synaptic ribbons,  $\text{Ca}^{2+}$ - and cGMP-dependent processes appear to play a central role. EF-hand-containing proteins mediate many of these  $\text{Ca}^{2+}$ - and cGMP-dependent functions. Since continuous signaling of photoreceptors appears to be prone to malfunction, disturbances of  $\text{Ca}^{2+}$ - and cGMP-mediated signaling in photoreceptors can lead to visual defects, retinal degeneration (rd), and even blindness. This review summarizes aspects of signal transmission at the photoreceptor presynaptic terminals that involve EF-hand-containing  $\text{Ca}^{2+}$ -binding proteins.

**Keywords:** photoreceptor, ribbon synapse, synaptic ribbon, GCAP, RIBEYE, CaBP4,  $\text{Ca}_v1.4$  calcium channel, EF-hands

## INTRODUCTION

Vision belongs to the most important senses of the human body. The light-sensitive retina within our eyes screens the optical world around us and transmits this information to the brain. At the beginning of the complex task of visual perception, photoreceptors physically detect light energy and transmit the information to the inner retina where further processing takes place. The retina employs two different classes of photoreceptors, rod and cones, to begin sorting out different components of light. Rod photoreceptors are specialized to operate at the lowest level of light, single

photon detection, and are thus saturated in daylight (Pahlberg and Sampath, 2011). Cone photoreceptors mediate color vision and operate at higher light intensities. In primates, e.g., humans, three different types of cones with long (L)-, medium (M)-, and short (S)- wavelength sensitivities provide color vision; simpler, non-primate mammals, e.g., mice, are dichromatic and possess only two types of cones (L-S-cones, for review, see Abramov and Gordon, 1994).

Mammalian photoreceptors in general are slender, highly polarized neurons with a bipolar morphology (Figure 1). The outer segment (OS) is the distal process that contacts the pigment epithelium and this is where phototransduction takes place. At the molecular level, phototransduction principally occurs via a light-induced transduction cascade that finally leads to closure of cGMP-gated cation channels (CNG-channels; cyclic nucleotide-gated (CNG) channels) which causes the cell to hyperpolarize from about  $-35$  mV to  $-40$  mV in the dark to about  $-70$  mV in very bright light (for review, see Burns and Baylor, 2001; Chen, 2005). At the “opposite” (vitread) end of the photoreceptor, the presynaptic terminal transmits the light information to dendrites of secondary neurons, bipolar, and horizontal cells (Figures 1A,B). The vast array of light information detected by the photoreceptor OS must be transmitted at the first synapse

**Abbreviations:** NCS, neuronal  $\text{Ca}^{2+}$ -sensor proteins; ROS-GC rod outer segment guanylate cyclase; GC, guanylate cyclase; OS, outer segments; IS, inner segments; OPL, outer plexiform layer (containing photoreceptor ribbon synapses); PDE6, cGMP phosphodiesterase 6; CNG, cyclic nucleotide-gated; CNG channel, cyclic nucleotide-gated channel; HCN channel, hyperpolarization-activated, cyclic nucleotide-gated channel; LTCC, L-type calcium channels; VGCC, voltage-gated calcium channels; CSNB, congenital stationary night blindness; GCAP, guanylate cyclase-activating protein;  $[\text{Ca}^{2+}]_i$ , cytoplasmic concentration of free  $\text{Ca}^{2+}$ ; ER, endoplasmic reticulum; CDI, calcium-dependent inactivation; VDI, voltage-dependent inactivation; KHD, kinase homology domain; CTR, carboxy-terminal region; LCA, Leber congenital amaurosis; CORD, cone-rod dystrophy; ON-bipolar cells, bipolar cells that depolarize in response to illumination; OFF-bipolar cells, bipolar cells that hyperpolarize in response to illumination; ERG, electroretinogram; KO, knockout; SIM, structured illumination microscopy.

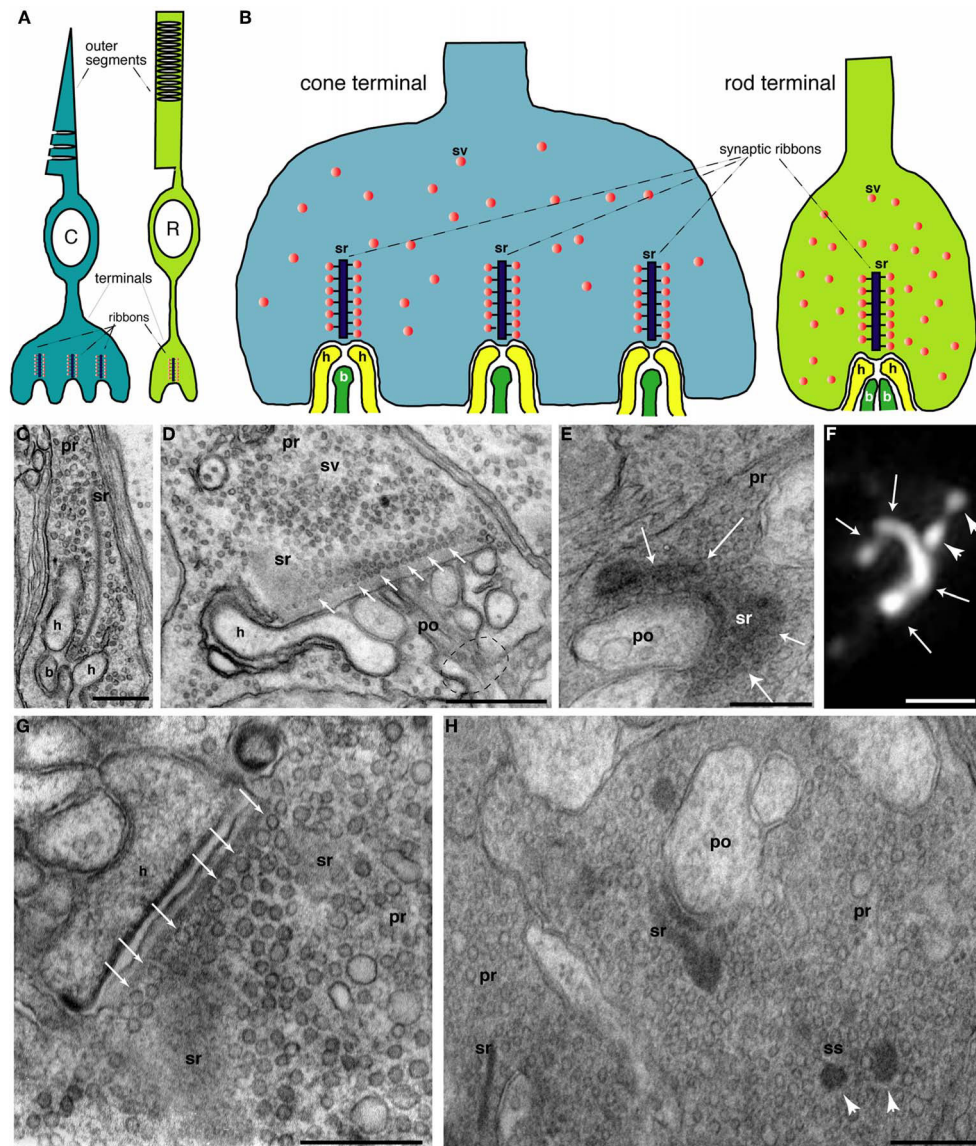


**FIGURE 1 | (A)** Schematic, simplified drawing of rod (R) and cone (C) photoreceptors. Outer segments (OS) in which phototransduction occurs are depicted as well as the presynaptic terminal where light information is passed from photoreceptors to the secondary neurons, bipolar, and horizontal cells (depicted in yellow and dark green colors in **Figure 1B**). Subcellular details of photoreceptors including the inner segments were omitted for sake of clarity. **(B)** Schematic, simplified drawing of rod and cone photoreceptor presynaptic terminals. Rod synapses possess only a single, large active zone with a single synaptic ribbon (sr) whereas cones possess multiple active zones (20–50). Only invaginating ribbon synapses are depicted. Non-invaginating, non-ribbon type synapses (Regus-Leidig and Brandstätter, 2011) are not shown. **(C–E, G–H)** Electron micrographs of photoreceptor terminals. **(C)** Shows a cross-sectioned ribbon (sr) with its typical bar-shaped appearance in a rod terminal. The synaptic ribbon is associated with large numbers of synaptic vesicles (sv) **(D)**. The rod photoreceptor in **(D)** is largely sectioned parallel to the plate-like synaptic ribbon. In the left part, the section passes through the synaptic ribbon (sr); more to the right, the plane of section is parallel, but close to the plate-like synaptic ribbon. Many docked synaptic vesicles can be observed at the base of the synaptic ribbon (small white arrows). The dashed circle indicates the site where the postsynaptic dendrites enter the postsynaptic cavity formed

by the invagination of the presynaptic photoreceptor terminal. **(E)** Also shows a tangential view of the synaptic ribbon. The plate-like character of the ribbon is visible. White arrows denote the ribbon plate which is bended along the presynaptic plasma membrane in a horseshoe-like manner. The horseshoe-shaped appearance of the synaptic ribbon can be also visualized by immunolabeling with anti-RIBEYE antibodies and super-resolution, structured illumination microscopy (SIM) (white arrows in **F**). White arrowheads in **(F)** show spherical synaptic spheres (ss), intermediate structures in the assembly and disassembly of plate-shaped synaptic ribbons [see also below; in **(H)**]; for review, see Schmitz (2009)]. **Figure (G)** demonstrates many docked synaptic vesicles at the base of the synaptic ribbon (white arrows) which are probably readily releasable. **(H)** Electron micrograph of an immature, developing terminal from the early, postnatal mouse retina (postnatal day 6). The ribbon complex is not yet fully assembled. Besides bar-shaped ribbons (sr), spherical precursors of synaptic ribbons, the synaptic spheres (ss), are also present in the presynaptic terminal. Abbreviations: C, cone photoreceptor; R, rod photoreceptor; sr, synaptic ribbon; ss, synaptic spheres; sv, synaptic vesicle; pr, presynaptic terminal; po, postsynaptic dendrite; h, horizontal cell postsynaptic dendrite; b, bipolar cell postsynaptic dendrite. Scale bars: 400 nm **(C)**; 800 nm **(D)**; 320 nm **(E)**; 1  $\mu$ m **(F)**; 400 nm **(G)**, 500 nm **(H)**.

of the visual system, the photoreceptor synapse (for review, see Wässle, 2004; Heidelberger et al., 2005; Schmitz, 2009; Matthews and Fuchs, 2010; Regus-Leidig and Brandstätter, 2011).

### STRUCTURAL AND FUNCTIONAL SPECIALIZATIONS OF PHOTORECEPTOR RIBBON SYNAPSES: A SYNAPSE TUNED FOR PHASIC AND CONTINUOUS RELEASE

Both types of photoreceptors, rods, and cones, form ribbon synapses to communicate with their secondary neurons, i.e., bipolar and horizontal cells in the outer plexiform layer of the retina. In mammals, ribbon synapses are also made by retinal bipolar cells, photoreceptor-like neurons in the pineal gland as well as auditory and vestibular hair cells (Schmitz, 2009; Matthews and Fuchs, 2010; Regus-Leidig and Brandstätter, 2011). Ribbon synapses are characterized by large, electron-dense structures, the synaptic ribbons (**Figure 1**; for review, see Schmitz, 2009). Synaptic ribbons in photoreceptor synapses are plate-like structures which appear bar-shaped in electron micrographs if cross-sectioned (**Figure 1**; Schmitz, 2009). In rod synapses, typically one synaptic ribbon is contained at a single active zone; in cone synapses 20–50 active zones are present with each usually containing one synaptic ribbon (Wässle, 2004; Regus-Leidig and Brandstätter, 2011). In hair cell ribbon synapses, most synaptic ribbons are spherical in shape (for review, see Matthews and Fuchs, 2010). The synaptic ribbon is associated along its entire surface area with a large number of synaptic vesicles that are filled with the neurotransmitter glutamate. It is anchored at the active zone of the presynaptic plasma membrane; in photoreceptors via the electron-dense arciform density (for review, see Schmitz, 2009; Matthews and Fuchs, 2010; Regus-Leidig and Brandstätter, 2011). RIBEYE is the major component of synaptic ribbons (Schmitz et al., 2000; Magupalli et al., 2008; Schmitz, 2009; Uthaiyah and Hudspeth, 2010). It consists of a large and unique aminoterminal A-domain, and a carboxyterminal B-domain which is largely identical with the nuclear co-repressor C-terminal-binding protein 2 (CtBP2). The B-domain/CtBP2 and a related protein, CtBP1, have developed from a family of dehydrogenases and both specifically bind NAD(H) (for review, see Schmitz, 2009).

Typically, ribbon synapses do not respond to bursts of action potentials but are specialized to transmit a large bandwidth of stimulus intensities via fine, graded changes in membrane potential. To report even small changes of receptor potential in response to differing light stimuli, ribbon synapses modulate the rate of tonic vesicle exocytosis (for review, see Heidelberger et al., 2005; Matthews and Fuchs, 2010; Wan and Heidelberger, 2011). Photoreceptor terminals may contain up to several hundred thousands of highly motile synaptic vesicles depending upon the species and type of synapse (for review, see Schmitz, 2009; Matthews and Fuchs, 2010), which support the high basal synaptic vesicle turnover driven by the synaptic ribbon (**Figure 1**). Various studies, mostly done with fish retinal bipolar cells, indicated that ribbon-associated vesicles are primed and readily-releasable (for review, see Heidelberger et al., 2005; Matthews and Fuchs, 2010; Wan and Heidelberger, 2011). Synaptic ribbons were proposed to capture and prime synaptic vesicles for immediate release. By this way of thinking, the synaptic ribbons

would provide a battery of ready-to-go vesicles that could support continuous release for extended periods of time (Jackman et al., 2009). Synaptic ribbons are hot spots of exocytosis as visualized with TIRF-microscopy (Zenisek et al., 2000), and more recently by the analyses of terminals with photodamaged synaptic ribbons that showed strongly depressed release (Snellman et al., 2011). At the base of the synaptic ribbons, voltage-gated L-type calcium channels are highly enriched (tom Dieck et al., 2005). These channels allow voltage-dependent  $\text{Ca}^{2+}$ -influx at the ribbon synapse which triggers synaptic vesicle release (for review, see Heidelberger et al., 2005; Schmitz, 2009; Striessnig et al., 2010). L-type calcium channels are considered ideally suited to serve the continuously active ribbon synapses (see below). Submicromolar (average) concentrations of  $\text{Ca}^{2+}$  are capable of supporting tonic exocytosis in photoreceptors (for review, see Heidelberger et al., 2005). Specific signaling properties of ribbon synapses could require higher  $\text{Ca}^{2+}$ -concentrations that might be achieved at the base of the synaptic ribbons (Beutner et al., 2001; Choi et al., 2008; Jackman et al., 2009; Jarsky et al., 2010; Graydon et al., 2011). A recent study predicted concentrations up to 100  $\mu\text{M}$  around the presynaptic  $\text{Ca}^{2+}$ -channels (Graydon et al., 2011), which could support coordinated multivesicular release (Singer et al., 2004; Khimich et al., 2005; Jarsky et al., 2010; Graydon et al., 2011). RIBEYE is involved in the clustering of  $\text{Ca}^{2+}$ -channels in inner ear hair cells (Sheets et al., 2011), and in agreement with this, several studies found a correlation between the ribbon size and the dimension of  $\text{Ca}^{2+}$ -microdomains (Johnson et al., 2008; Frank et al., 2009, 2010).

The size and number of synaptic ribbons can vary considerably (Hull et al., 2006; Johnson et al., 2008; Frank et al., 2009, 2010; Regus-Leidig et al., 2010; Liberman et al., 2011; for review, see Vollrath and Spiwoкс-Becker, 1996; Schmitz, 2009; Regus-Leidig and Brandstätter, 2011). The plate-shaped synaptic ribbons in photoreceptors appear to assemble and disassemble via spherical intermediates, the synaptic spheres (for review, see Schmitz, 2009; Mercer and Thoreson, 2011b). In the mouse retina, structural changes of synaptic ribbons are activity- (illumination-) dependent; structural changes of fish synaptic ribbons are also strongly influenced by circadian signals (Emran et al., 2010; for review, see Vollrath and Spiwoкс-Becker, 1996; Regus-Leidig and Brandstätter, 2011). The activity-dependent plasticity of the synaptic ribbon complex is related to the performance of the visual system also at the systems level (Balkema et al., 2001). At photoreceptor ribbon synapses, postsynaptic dendrites of bipolar and horizontal cells contact the presynaptic release sites in an invagination of the presynaptic terminal (**Figure 1**). At this site, the released glutamate is detected by the metabotropic glutamate receptor 6 (mGluR6) on the tips of ON-bipolar cells; horizontal cells as well as OFF-bipolar cells employ ionotropic glutamate receptors (Wässle, 2004; DeVries et al., 2006; Morgans et al., 2010).

Recent data revealed that EF-hand-containing proteins play an important role in the activity-dependent adaptational processes at the photoreceptor synapse. These findings suggest that the photoreceptor synaptic apparatus is adjusted during changes in illumination, thus allowing synaptic communication to continue in a

senseful manner if background illumination changes over a broad range. The processes in the presynaptic photoreceptor terminals that involve EF-hand-containing proteins, including distinct neuronal  $\text{Ca}^{2+}$ -sensor (NCS) - proteins and  $\text{Ca}^{2+}$ -binding proteins (CaBPs), will be summarized in the present review. Postsynaptic activity-dependent signaling is covered by other recent reviews (Burgoyne, 2007; Koike et al., 2010; Morgans et al., 2010).

## **$\text{Ca}^{2+}$ -IONS AND EF-HAND-CONTAINING $\text{Ca}^{2+}$ -BINDING PROTEINS: OUTLINE**

$\text{Ca}^{2+}$ -ions are crucial intracellular messengers that have central roles in synaptic transmission ranging from triggering of synaptic vesicle exocytosis, vesicle recruitment, and recovery as well as different aspects of synaptic plasticity (for review, Neher and Sakaba, 2008).  $\text{Ca}^{2+}$ -binding EF-hand-containing proteins are perfect candidates for participating in photoreceptor signaling. These proteins are characterized by high-affinity  $\text{Ca}^{2+}$ -binding motifs and consist of a helix-loop-helix motif (Burgoyne, 2007). The loop region, typically 12 residues long, is rich in acidic amino acids that chelate the  $\text{Ca}^{2+}$  (as well as  $\text{Mg}^{2+}$ ). The founder molecule is calmodulin, and related to calmodulin are two classes of EF-hand-containing proteins (**Figures 2 and 3**): (1) the family of neuronal calcium sensor (NCS) proteins that include the guanylate cyclase activating proteins (GCAPs) and (2) the family of calcium-binding proteins (CaBPs) that include calcium-binding protein 4 (CaBP4) (for review, see Haeseleer et al., 2002; Burgoyne, 2007). Furthermore, individual proteins contain EF-hand motifs as important functional parts of their primary structure, e.g., the  $\alpha 1$ -subunit of L-type voltage-gated  $\text{Ca}^{2+}$ -channels (VGCCs).

## **$[\text{Ca}^{2+}]_i$ IN PRESYNAPTIC PHOTORECEPTOR TERMINALS**

EF-hand-containing proteins typically bind  $\text{Ca}^{2+}$  in the submicromolar range and are regulated by  $[\text{Ca}^{2+}]_i$ . In photoreceptor terminals, presynaptic  $[\text{Ca}^{2+}]_i$  is controlled by various mechanisms. These include  $[\text{Ca}^{2+}]_i$ -influx through calcium-permeable channels in the presynaptic plasma membrane (VGCCs, probably also CNG- and hyperpolarization-activated, cyclic nucleotide-gated (HCN)-channels),  $\text{Ca}^{2+}$ -buffering systems in the presynaptic terminals,  $\text{Ca}^{2+}$ -release from the ER (e.g.,  $\text{Ca}^{2+}$ -induced  $\text{Ca}^{2+}$ -release) as well as extrusion from the cytosol into the ER and the extracellular space (e.g., via plasma membrane  $\text{Ca}^{2+}$ -ATPase;  $\text{Na}^+/\text{Ca}^{2+}$ ,  $\text{K}^+$ -exchanger) (Rieke and Schwartz, 1994; Savchenko et al., 1997; Krizaj and Copenhagen, 2002; Suryanarayanan and Slaughter, 2006; Johnson et al., 2007; Knop et al., 2008; Szikra et al., 2008, 2009; Babai et al., 2010; Seeliger et al., 2011). Importantly,  $\text{Ca}^{2+}$ -concentrations in the presynaptic terminals of photoreceptors have been imaged *in-situ* using two-photon-microscopy (Choi et al., 2008; Jackman et al., 2009). In the anole lizard (*Anolis sagrei*), 360–600 nm global (average)  $\text{Ca}^{2+}$  were measured in cone terminals of dark-adapted retinas; 190–250 nm of global average  $\text{Ca}^{2+}$  after bright illumination at physiological extracellular  $\text{Ca}^{2+}$ -concentrations. At the base of the synaptic ribbon,  $[\text{Ca}^{2+}]_i$  could be much higher than these average values ( $>4 \mu\text{M}$ ) (Choi et al., 2008; Jackman et al., 2009).

These  $[\text{Ca}^{2+}]_i$  values in the presynaptic terminal differ from  $[\text{Ca}^{2+}]_i$  values in the OS. In the OS of mouse retinas, dark values

of 250 nm were measured; down to 23 nm  $[\text{Ca}^{2+}]_i$  were measured in the OS of mice at saturating illumination (Olshevskaya et al., 2002; Woodruff et al., 2002; Koch, 2006; Baehr and Palczewski, 2009). Species-dependent differences in OS  $[\text{Ca}^{2+}]_i$  values have been observed: dark values of  $\approx 700$  nm  $[\text{Ca}^{2+}]_i$  were measured in salamander rod OS; many species have dark  $[\text{Ca}^{2+}]_i$  values of  $\approx 500$  nm (Olshevskaya et al., 2002; Woodruff et al., 2002; Koch, 2006; Karan et al., 2010). Differences of  $[\text{Ca}^{2+}]_i$  between presynaptic terminals and outer/inner segments could result from the elongated, slender shape of photoreceptors and various  $\text{Ca}^{2+}$ -extrusion mechanisms between OSs and presynaptic terminals (Krizaj and Copenhagen, 2002). Additionally, signals in the presynaptic terminals are shaped by feedback responses from secondary neurons (Jackman et al., 2010; Regus-Leidig and Brandstätter, 2011).

## **L-TYPE VOLTAGE-GATED CALCIUM CHANNELS IN PHOTORECEPTOR PRESYNAPTIC TERMINALS**

The rate of synaptic vesicle exocytosis at ribbon synapses is highly dependent on changes in membrane potential, and the role of voltage-gated calcium channels in this process has been intensively investigated. Synaptic vesicle exocytosis in rod and cone photoreceptor synapses is triggered via  $\text{Ca}^{2+}$ -influx through L-type voltage-gated calcium channels (LTCCs) at the active zones (for review, see Morgans et al., 2005; Striessnig et al., 2010; Catterall, 2011). The  $\alpha 1$ -subunit is the largest subunit of LTCCs.  $\text{Ca}_v1.4$  (often also denoted as  $\alpha 1\text{F}$ -subunit (Cacna1f); Catterall et al., 2005) is believed to represent the main pore forming  $\alpha 1$ -subunit of LTCCs involved in neurotransmitter release at photoreceptor synapses. This assumption is based on several findings: (1) immunocytochemical analyses (Nachman-Clewner et al., 1999; Morgans, 2001; for review, see Morgans et al., 2005); (2) analyses of spontaneous and engineered  $\text{Ca}_v1.4$  mouse knockouts (for review, see Doering et al., 2007; Striessnig et al., 2010). (3) human patients suffering from congenital stationary night blindness (CSNB) show mutations in the  $\text{Ca}_v1.4$  gene (for review, see Doering et al., 2007; Striessnig et al., 2010). Some studies also observed expression of  $\text{Ca}_v1.3$  (also denoted as  $\alpha 1\text{D}$ -subunit (Cacna1d); Catterall et al., 2005) in photoreceptor synapses (Xiao et al., 2007; Kersten et al., 2010). Inner ear hair cell ribbon synapses employ  $\text{Ca}_v1.3$  as pore-forming  $\text{Ca}^{2+}$ -channel  $\alpha 1$ -subunit (for review, see Striessnig et al., 2010). But while hearing is severely impaired, vision appears to be normal in  $\text{Ca}_v1.3$  knockout mice (for review, see Striessnig et al., 2010).

$\text{Ca}_v1.4$  ( $\alpha 1\text{F}$ ) is  $\approx 2000$  amino acids long and organized into four homologous domains (domain I–IV) (Catterall et al., 2005; Catterall, 2011). Both N- and C-terminus reside in the cytoplasm (**Figure 2**). The C-terminus (CTR) of  $\text{Ca}_v1.4$  possesses important regulatory functions and consists of a  $\text{Ca}^{2+}$ -binding EF-hand domain, a pre-IQ and IQ-domain as well as an important regulatory region at the very carboxyterminus, the so-called CTM (C-terminal modulator) or ICDI (inhibitor of CDI) (Singh et al., 2006; Wahl-Schott et al., 2006; Striessnig et al., 2010). The CTM performs functionally important intramolecular interactions with the carboxyterminus of  $\text{Ca}_v1.4$  (see below). The  $\alpha 1$ -subunit associates with cytoplasmic  $\beta$ -subunits, predominantly at the loop region between domain I and II of  $\text{Ca}_v1.4$  (Dolphin,

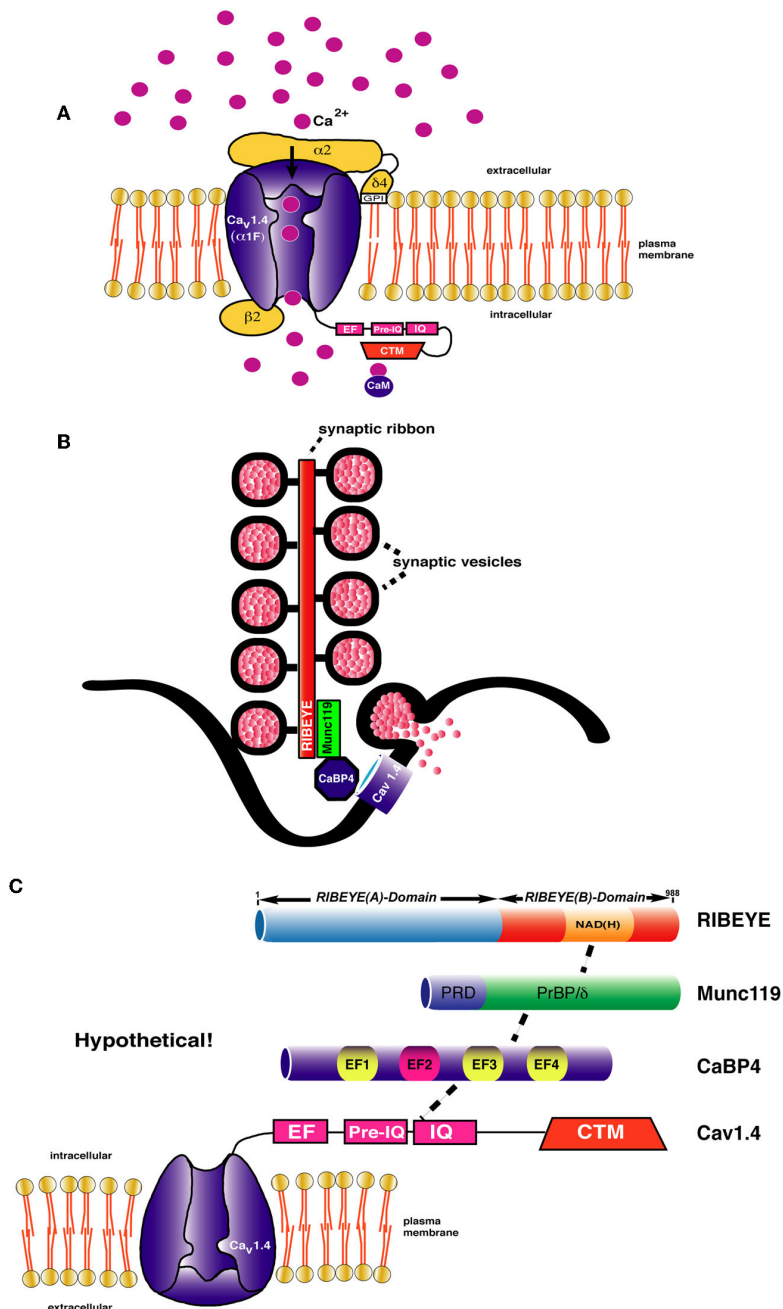


**FIGURE 2 | (A)** Schematic representation of L-type  $\text{Ca}^{2+}$ -channel composition of rod photoreceptor synapses [drawn modified based on Lacinova (2005)]. The channels are immobilized at the active zone close to the base of the synaptic ribbon. The  $\alpha 1$ F-subunit is considered the pore-forming subunit that supports voltage-dependent entry of  $\text{Ca}^{2+}$ .  $\text{Ca}^{2+}$  ions are depicted as pink spheres. The cytoplasmic C-terminus of  $\text{Ca}_v1.4$   $\alpha 1$ -subunit contains an EF-hand, Pre-IQ-, and IQ-domain. In other  $\text{Ca}_v1$  channels, e.g.,  $\text{Ca}_v1.2$ , these carboxyterminal domains mediate  $\text{Ca}^{2+}$ -dependent inactivation [for review, see Striessnig et al. (2010)]. In  $\text{Ca}_v1.4$ , CDI is prevented by the additional CTM region that forms an intramolecular interaction with the above mentioned domains [Singh et al. (2006); Wahl-Schott et al. (2006)]. The  $\beta 2$ -subunit interacts with the  $\alpha 1$ -subunit at the cytoplasmic loop connecting domain I with domain II [Catterall (2011)]. The  $\alpha 2$ -delta4 ( $\alpha 2\delta 4$ )-subunit, linked to each other with disulfide-bridges (not shown), complements the channel composition [Wycisk et al. (2006); Mercer

et al. (2011a)]. The  $\delta$ -subunit possesses a single transmembrane segment which is post-translationally cleaved off and replaced by a GPI anchor [Davies et al. (2010)] **(B,C)** Schematic depiction of the synaptic ribbon. Protein-protein interaction cascades are shown that could link RIBEYE to presynaptic calcium channels. Although all individual interactions (e.g., RIBEYE-Munc119; Munc119-CaBP4; CaBP4-Cav1.4) have been demonstrated [Alpadi et al. (2008); Haeseleer et al. (2004, 2008)], it is not clear whether all shown interactions can occur at the same time. Other interactions that might link the ribbons to presynaptic calcium channels, e.g., via association with RIM-proteins are not shown. Domain structures of the interacting proteins are only schematically depicted. CaBP4 contains 4 EF-hands from which EF2 (depicted in red) is non-functional. EF1, EF3, and EF4 are functional EF-hands (depicted in yellow). Abbreviations: CaM, calmodulin; PrBP/ $\delta$ , prenyl-binding protein delta homology domain; PRD, proline-rich domain; IQ, IQ-domain; NAD(H), nicotine amide dinucleotide; CTM, C-terminal modulator.

2003; Buraei and Yang, 2010). The  $\beta 2$ -protein appears to be the main  $\beta$ -channel subunit in photoreceptor LTCCs (Ball et al., 2002, 2011).  $\beta$ -subunits are important for the trafficking of the  $\alpha 1$ -subunit and for the kinetics of channel opening (Dolphin, 2003; Buraei and Yang, 2010). The  $\text{Ca}_V1.4$  channel is complemented by an  $\alpha 2\delta$ -subunit, which is the  $\alpha 2\delta 4$  protein in photoreceptor synapses (Wycisk et al., 2006; Mercer et al., 2011a).

The properties of  $\text{Ca}_V1.4$  and  $\text{Ca}_V1.3$  can be modulated over a wide range (for review, see Striessnig et al., 2010). In some contexts,  $\text{Ca}_V1.4$  and  $\text{Ca}_V1.3$  open at relatively negative membrane potentials (below  $-40$  mV) which is an important requirement for photoreceptors that vary their membrane potential between  $-35$  and  $-40$  mV (in the dark) to less than  $-55$  mV in the light (see above). Furthermore, for the tonically active photoreceptor synapses it is important that a sufficient  $\text{Ca}^{2+}$ -concentration is maintained that allows sustained, continuous exocytosis. This could be well accomplished by a calcium channel that does not inactivate or inactivates only very slowly.  $\text{Ca}_V1.4$  shows no  $\text{Ca}^{2+}$ -dependent inactivation (CDI) and very slow voltage-dependent inactivation (VDI) (Singh et al., 2006; Wahl-Schott et al., 2006; Striessnig et al., 2010). This low degree or lack of inactivation could very well support continuous  $\text{Ca}^{2+}$ -influx and subsequently tonic exocytosis. Further supplies of  $\text{Ca}^{2+}$  that may help maintain sustained release could come from  $\text{Ca}^{2+}$ -induced  $\text{Ca}^{2+}$  release or store-operated  $\text{Ca}^{2+}$ -entry (Suryanarayanan and Slaughter, 2006; Szikra et al., 2008, 2009; Babai et al., 2010).

The biological purpose of CDI (and VDI), in general, is to provide neurons with a negative feedback mechanism that can protect from  $\text{Ca}^{2+}$ -overflow and subsequent cell death. CDI is mediated by the EF-hand, the pre-IQ-domain, and the IQ-domain in the CTR of  $\text{Ca}_V1.4$  to which  $\text{Ca}^{2+}$ /calmodulin can bind (for review, see Doering et al., 2007; Striessnig et al., 2010). In  $\text{Ca}_V1.4$ , CDI is absent because of a modulatory domain in the CTR of  $\text{Ca}_V1.4$  that prevents binding of  $\text{Ca}^{2+}$ -calmodulin to the pre-IQ/IQ-domain. CDI would probably not be compatible with the need of continuous, tonic exocytosis at photoreceptor synapses that also requires tonic  $\text{Ca}^{2+}$ -influx to drive exocytosis. Mutations in the  $\text{Ca}_V1.4$  gene are associated with incomplete stationary night blindness (CSNB2) (for review, see Striessnig et al., 2010). Inhibition of CDI in inner ear hair cells is mediated by the binding of CaBP4 to the CTR of  $\text{Ca}_V1.3$  (Yang et al., 2006). CaBP4 is an EF-hand-containing protein of the CaBP-family (Haeseleer et al., 2004; Haeseleer, 2008).

In photoreceptor synapses, CaBP4 could have an additional function. Binding of CaBP4 to the IQ-domain of  $\text{Ca}_V1.4$  shifts the activation curve of the channel to more negative values (Haeseleer et al., 2004), thereby extending the operational range of the channel. At  $-40$  mV, the membrane potential in the dark, the depolarized condition, the channel is at the very beginning of its activation curve (for review, see Striessnig et al., 2010). At  $-50$  mV, a membrane potential which is easily achieved during illumination, the  $\text{Ca}_V1.4$  channel would be closed. A CaBP4-induced hyperpolarizing shift of the  $\text{Ca}_V1.4$  activation curve (shift of approximate  $10$ – $15$  mV) would allow the channel to operate at more negative membrane potentials. It should be kept in mind that many of the biophysical characterizations were obtained from powerful, but simplified, model systems, e.g., transfected

HEK cells. Channel regulation in the synapse could be more complex.

Mutations in the CaBP4 gene lead to autosomal recessive CSNB and Leber's congenital amaurosis (LCA)-like phenotype in humans (Zeit et al., 2006; Aldahmesh et al., 2010); CaBP4 knockout mice have severe disturbances in synaptic transmission emphasizing the physiological importance of this protein. Interestingly, RIBEYE, the main component of synaptic ribbons binds to Munc119 (Alpadi et al., 2008), a protein which has been linked with a cone-rod dystrophy (CORD) (Kobayashi et al., 2000). Munc119, on the other hand, interacts with CaBP4 (Haeseleer, 2008; Alpadi and Schmitz, unpublished data). This multicomponent molecular connection could influence the gating of  $\text{Ca}^{2+}$ -channels at the active zone of photoreceptors (Figure 2).

The  $\beta$ -subunit of LTCC—together with other channel subunits (i.e.,  $\alpha 2\delta 4$ ; Figure 2) and further channel-associated proteins—plays an important role in the regulation of the kinetics of  $\text{Ca}^{2+}$ -channel opening, intracellular channel trafficking, and density at the plasma membrane (Dolphin, 2003; Davies et al., 2007; Buraei and Yang, 2010; Striessnig et al., 2010). Deletion of  $\beta 2$ -subunit cause similar phenotypes as in CSNB2 patients with  $\text{Ca}_V1.4$  mutations (Ball et al., 2002).  $\beta$ -subunit might be involved in the positional priming of calcium channels and the exocytotic machinery.  $\beta$ -subunits of LTCC bind to the RIM family of active zone proteins (Kiyonaka et al., 2007; Miki et al., 2007; Gebhart et al., 2010) via a carboxyterminal region that includes the C2B-domain of RIMs. RIM proteins are important for vesicle exocytosis, various steps of presynaptic plasticity and for the immobilization of  $\text{Ca}^{2+}$ -channels as shown mostly for conventional synapses (Han et al., 2011; Kaeser et al., 2011). RIMs are also components of the active zone complex of photoreceptors including the synaptic ribbons (Wang et al., 1997). Via the proline-rich region, RIM proteins bind to the RIM-binding proteins (RBPs) which associate with the  $\beta$ -subunit of L-type  $\text{Ca}^{2+}$ -channels (Hibino et al., 2002). Most interestingly, RIM knockouts lead to loss of  $\text{Ca}^{2+}$ -channel immobilization in conventional synapses (Han et al., 2011; Kaeser et al., 2011, for review, see Kaeser, 2011). RIM proteins are also important in modulating voltage-gated  $\text{Ca}^{2+}$ -channels as judged by a mutation in the C2A-domain of RIM1 that causes cone-rod dystrophy (CORD7) (Miki et al., 2007).

In conclusion, modulation of L-type  $\text{Ca}^{2+}$ -channel properties appears to have a powerful influence on synaptic transmission at the photoreceptor synapse (Striessnig et al., 2010). The plasticity is mediated by the EF-hand/Pre-IQ/IQ-domain-containing carboxyterminal region of the  $\alpha$ -channel subunits. Tuning of the  $\text{Ca}^{2+}$ -channels could be involved in the adjustment of synaptic transmission during different levels of illumination and/or for slower, adaptation of the exocytotic machinery for overall changes of light- and dark-adaptation during day- and night time. Interestingly, L-type calcium channel expression in photoreceptors is likely under circadian control (Ko et al., 2007).

#### EF-HAND PROTEINS AND $\text{Ca}^{2+}$ -cGMP-DEPENDENT PLASTICITY AT THE SYNAPTIC RIBBON

As described above, EF-hand motif-containing proteins are important  $\text{Ca}^{2+}$ -dependent modulators of presynaptic

voltage-gated  $\text{Ca}^{2+}$ -channel functions. Also the synaptic ribbons are subject to  $\text{Ca}^{2+}$ -dependent dynamic changes which in turn could feedback on presynaptic  $\text{Ca}^{2+}$ -levels. Presynaptic  $\text{Ca}^{2+}$ -channels are anchored at the active zone of photoreceptor synapses by the synaptic ribbons. RIBEYE appears to have a central role in the clustering of  $\text{Ca}^{2+}$ -channels in inner ear hair cells (Sheets et al., 2011). Ribbon-associated proteins, e.g., the above mentioned RIM proteins or the protein bassoon, could potentially also play an important role (Wang et al., 1997; tom Dieck et al., 2005; Frank et al., 2010; Han et al., 2011; Kaeser et al., 2011). The ribbon-associated protein bassoon anchors synaptic ribbons to the active zone probably via its interaction with RIBEYE (tom Dieck et al., 2005). Bassoon is important for ribbon synapse development and maintaining the stability of the synaptic ribbon complex (Dick et al., 2003; tom Dieck et al., 2005; Regus-Leidig et al., 2010).

Recent studies suggested that activity-dependent structural changes of photoreceptor synaptic ribbons, i.e., assembly and disassembly of synaptic ribbons, are mediated by GCAP2, the guanylate cyclase-activating protein 2 (Venkatesan et al., 2010). GCAP2 belongs to a family of small  $\text{Ca}^{2+}$ -regulated, EF-hand-containing proteins of the NCS protein family (Koch, 2006; Burgoyne, 2007; Koch et al., 2010; Sharma, 2010). GCAPs are well known to regulate guanylate cyclase (GC) activity in photoreceptor OSs in a  $\text{Ca}^{2+}$ -dependent manner. How GCAPs could work in the presynaptic photoreceptor terminals to regulate synaptic plasticity is unclear. Current knowledge and ideas about GCAP/GC/cGMP-mediated signaling events in the presynaptic terminals will be summarized in the present review. To elucidate possible similarities between regulatory mechanisms in the OS and synaptic terminals, some key events of OS phototransduction will be also included.

### GUANYLATE CYCLASE-ACTIVATING PROTEINS (GCAPs) IN PHOTORECEPTORS

Guanylate cyclase-activating proteins (GCAPs) are small, EF-hand-containing  $\text{Ca}^{2+}$ -binding proteins of  $\approx 24$  kDa (Figure 3). GCAPs belong to the subfamily of NCS proteins (Koch, 2006; Burgoyne, 2007). They contain four EF-hands, and the first EF-hand in GCAPs is non-functional due to exchanges of critical amino acids in the  $\text{Ca}^{2+}$ -binding loop (Figure 3). Instead, EF1 provides a binding interface for the membrane-bound photoreceptor guanylate cyclases (ROS-GCs; Ermilov et al., 2001; see below). EF2–4 are functionally active and bind  $\text{Ca}^{2+}$  (as well as  $\text{Mg}^{2+}$ ). In the OSs, the free intracellular  $\text{Mg}^{2+}$ -concentration is largely constant (at  $\approx 1$  mM) and not affected by changes in illumination (Chen, 2005; Peshenko et al., 2011a). In contrast, free intracellular  $\text{Ca}^{2+}$  levels change strongly upon illumination as described above. If  $\text{Ca}^{2+}$  (and cGMP) is high (in the dark),  $\text{Ca}^{2+}$  will replace the bound  $\text{Mg}^{2+}$  at the EF-hands of GCAPs (Stephen et al., 2008; Dizhoor et al., 2010; Peshenko et al., 2011a). The replacement of  $\text{Mg}^{2+}$  by  $\text{Ca}^{2+}$  at the EF-hands of GCAPs is functionally important because this changes the character of interaction with important effector proteins, the guanylate cyclases (GC, see below). GCAP proteins are myristoylated at their N-terminus (for review, see Palczewski et al., 2004; Koch, 2006; Baehr and Palczewski, 2007, 2009). In contrast to

the recoverin-like NCS proteins, GCAPs do not perform a  $\text{Ca}^{2+}$ -dependent myristoyl-switch (Stephen et al., 2007; Ames and Lim, 2011). Irrespective whether  $\text{Ca}^{2+}$  is bound or not, the myristoyl chain remains buried inside the molecule and is not involved in  $\text{Ca}^{2+}$ -dependent membrane anchoring (Figure 3). Instead, the myristoyl residue has been suggested to stabilize the conformation of the protein (Stephen et al., 2007).

Three GCAP isoforms (GCAP1, GCAP2, and GCAP3) are expressed in mammalian retinas with species-dependent differences (Palczewski et al., 2004; Koch, 2006; Baehr and Palczewski, 2007, 2009; Dizhoor et al., 2010). In rod photoreceptors of mouse retinas, both GCAP1 and GCAP2 are expressed. GCAP1 appears to be the predominant isoform in cones (Palczewski et al., 2004; Koch, 2006; Baehr and Palczewski, 2007, 2009). Consistently, mutations of the GCAP1 gene lead to cone-dominated dystrophies in the human retina as well as in the respective mouse models (Jiang et al., 2005; Buch et al., 2011). GCAP3 expression is restricted to cone photoreceptors in the human retina; in the mouse retina GCAP3 is not expressed arguing that GCAP3 is probably dispensable for vision in mice (for review, see Baehr and Palczewski, 2007, 2009). Despite strong sequence similarities, biophysical and biochemical properties of GCAP proteins differ (e.g.,  $\text{Ca}^{2+}$ -affinities, dimerization properties, and activation of GCs; Ermilov et al., 2001; Olshevskaya et al., 2002; Koch et al., 2010). In photoreceptor outer segments (OS), GCAPs constitutively associate with membranes via interaction with ROS-GCs (Olshevskaya et al., 2002; Stephen et al., 2007; Ames and Lim, 2011). Mice with a deletion of GCAP1 and GCAP2 genes showed increased amplitudes of single photon responses and a delayed recovery phase (for review, see Palczewski et al., 2004; Baehr and Palczewski, 2007, 2009).

### GCAP EFFECTOR PROTEINS IN PHOTORECEPTOR OUTER SEGMENTS

In photoreceptor OSs, GCAP effector proteins have been extensively characterized (Karan et al., 2010; Hunt et al., 2010; Koch et al., 2010). Main effectors of GCAP proteins are the  $\approx 115$  kDa membrane-bound rod outer segment-guanylate cyclases (ROS-GCs). Two ROS-GCs are found in mammalian photoreceptors: ROS-GC1 (retGC1, GC-E) and ROS-GC2 (retGC2, GCF) (for review, see Olshevskaya et al., 2002; Potter, 2011). ROS-GCs are large, type 1 transmembrane proteins ( $\approx 1100$  aa; Figure 4) with an extracellular domain, a transmembrane domain, and a cytoplasmic domain that consists of a short juxtamembrane domain (JMD), a kinase homology domain (KHD), a dimerization domain (DD), a catalytic domain (CCD) that converts GTP into cGMP and C-terminal extension (CTE). Both ROS-GC1 and ROS-GC2 are expressed in rods; ROS-GC2 appears to be absent from mouse cone photoreceptors (Haire et al., 2006; Karan et al., 2010). ROS-GCs play a crucial role in photoreceptor OS phototransduction. A light-induced conformational change of rhodopsin leads to a transducin-mediated activation of phosphodiesterase 6 (PDE6) and subsequently reduced levels of cGMP (Burns and Baylor, 2001). Thus, light generates a drop in cGMP levels in the OSs and subsequent closure of cGMP-gated CNG-channels (Biel and Michalakakis, 2009). As a result of light-induced closure of CNG channels intracellular  $\text{Ca}^{2+}$  levels drop in the OS from about 250 nM (dark) to less than  $<50$  nM

**A**

mGCAP1	MG-----NIMEGKSVEELSSTECHQWYKKFMT <b>ECPS</b> QLTLYEF <b>RQFFG</b>	44
mGCAP2	MGQQLSWEEAEAAA---GEMDVAELQEWYKKFV <b>VECP</b> S <b>T</b> LFMHE <b>FKRFFK</b>	47
bGCAP2	MGQQFSWEEAEENGAVGAADAA <b>QLQEWYKKFLE</b> ECPS <b>T</b> LFMHE <b>FKRFFK</b>	50
	<b>EF1</b>	
mGCAP1	LKNLSPSASQYVEQMFET <b>PDFN</b> KDGYIDFMEYVAALS <b>LV</b> LK <b>GV</b> E <b>Q</b> KL <b>RW</b>	44
mGCAP2	VTG-NEEASQYVESM <b>FR</b> FDK <b>NG</b> DNTIDF <b>LE</b> YVAAL <b>N</b> LV <b>R</b> GS <b>LE</b> HK <b>L</b> K <b>W</b>	96
bGCAP2	-VPDNEEA <b>TOY</b> VEAM <b>FR</b> FD <b>T</b> NGDNTIDF <b>LE</b> YVAAL <b>N</b> LV <b>R</b> GT <b>LE</b> HK <b>L</b> K <b>W</b>	99
	<b>EF2</b>	
mGCAP1	YFKLYD <b>V</b> D <b>G</b> NGC <b>I</b> DR <b>DE</b> LL <b>T</b> I <b>R</b> A <b>I</b> -----RTINPWS <b>D</b> SS <b>S</b> MA <b>E</b> EF	135
mGCAP2	TFKIYDKDRNGC <b>I</b> DR <b>LE</b> LL <b>D</b> I <b>VE</b> AIYK <b>L</b> KACRAEL <b>D</b> LE <b>H</b> Q <b>G</b> QL <b>T</b> PE <b>E</b> V	146
bGCAP2	TFKIYDKDRNGC <b>I</b> DR <b>Q</b> EL <b>L</b> D <b>I</b> VE <b>S</b> IYK <b>L</b> KAC <b>S</b> VEVEAE <b>Q</b> Q <b>G</b> K <b>L</b> L <b>T</b> PE <b>E</b> V	149
	<b>EF3</b>	
mGCAP1	TDTVFAKID <b>I</b> NGD <b>G</b> EL <b>S</b> LE <b>F</b> ME <b>G</b> VQ <b>K</b> D <b>Q</b> ML <b>L</b> DT <b>I</b> TRSLD <b>L</b> TG <b>I</b> VR <b>R</b> L <b>Q</b> N	185
mGCAP2	VDRI <b>F</b> LL <b>V</b> D <b>E</b> NGD <b>G</b> Q <b>L</b> SL <b>T</b> EF <b>I</b> EGARR <b>D</b> K <b>W</b> VM <b>K</b> ML <b>Q</b> MD <b>I</b> NP <b>G</b> C <b>W</b> IT <b>Q</b> Q <b>R</b> R	196
bGCAP2	VDRI <b>F</b> LL <b>V</b> D <b>E</b> NGD <b>G</b> Q <b>L</b> SL <b>N</b> EF <b>V</b> EGARR <b>D</b> K <b>W</b> VM <b>K</b> ML <b>Q</b> MD <b>L</b> NP <b>S</b> SW <b>I</b> S <b>Q</b> Q <b>R</b> R	149
	<b>EF4</b>	
mGCAP1	GEHEEAGTGD <b>L</b> AA <b>E</b> AA <b>G</b>	202
mGCAP2	RSAMF	201
bGCAP2	KSAMF	204

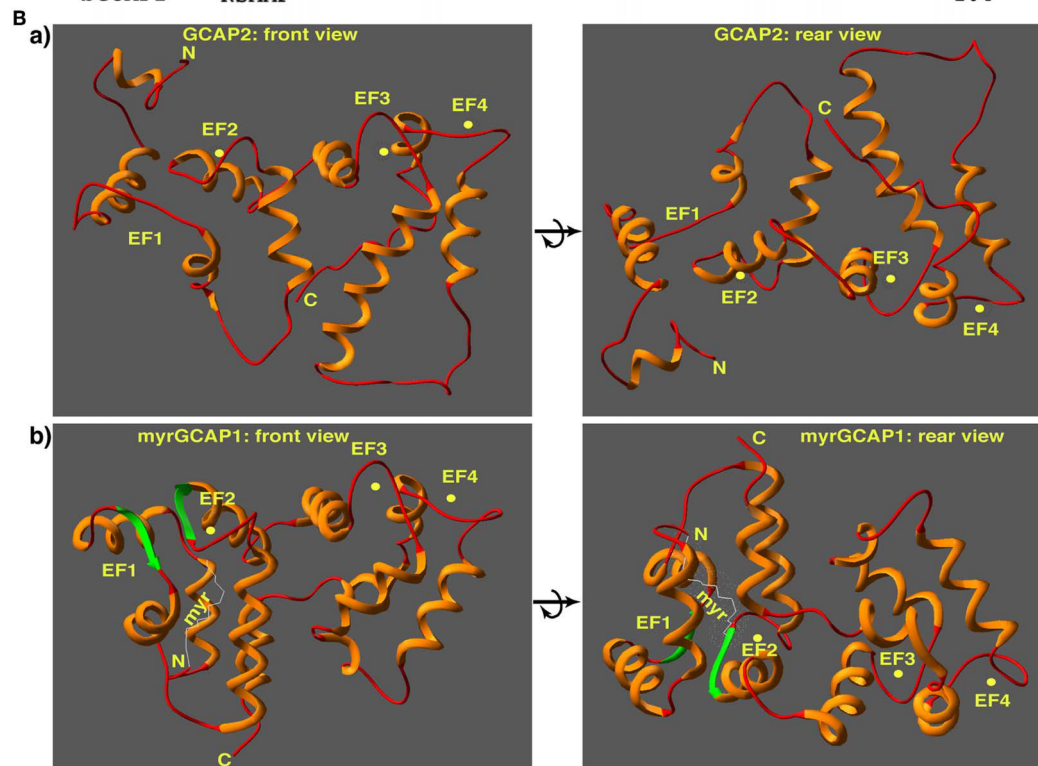


**FIGURE 3 | (A)** Sequence alignment of GCAP1 and GCAP2 from the indicated species (mGCAP1: NP032215, GI: 40254633; mGCAP2: NP\_666191, GI: 22122571; bGCAP2: NP\_777211, GI: 27807519). Amino acid residues identical in all three indicated GCAP proteins are highlighted in green. Underlined below the aligned amino acid sequences is the  $\text{Ca}^{2+}$ -/ $\text{Mg}^{2+}$ -chelating loop region located between the E- and F-helices of the respective EF-hands. It is flanked on both sides by an  $\alpha$ -helix (underlined in amber). The amino acid sequences of the EF-hands of GCAP1 and GCAP2 are highly homologous. Amino acids identical in mGCAP1, mGCAP2, and bGCAP2 are highlighted in green. EF-hands are highly conserved; the C-terminus of GCAP1 of GCAP2 is divergent. The CTR of GCAP2, but not of GCAP1, binds to the NADH-binding sub-domain of RIBEYE(B)

[Venkatesan et al. (2010)]. Amino acids in GCAP2 highlighted in red appear to be involved in the interaction with ROS-GCs [Ames et al. (1999)]. Residues in the loop region of EF1 that are incompatible with  $\text{Ca}^{2+}$ -chelation and also involved in ROS-GC target interaction are shown in orange [Ames et al. (1999); Hwang et al. (2004)]. Abbreviations: mGCAP1, mouse GCAP1; mGCAP2, mouse GCAP2; bGCAP2, bovine GCAP2. **(B)** Structure of unmyristoylated GCAP2 (a) [Ames et al. (1999); pdb-file: 1jba] and myristoylated GCAP1 (b) [Stephen et al. (2007); pdb-file: 2R2I]. The structure is shown from the front (left) with the  $\text{Ca}^{2+}$ -chelating loops on top as well as from the back (right) to document the location of the CTR region that binds to RIBEYE(B) in the case of GCAP2 [Venkatesan et al. (2010)].  $\text{Ca}^{2+}$  ions are schematically depicted as yellow spheres.

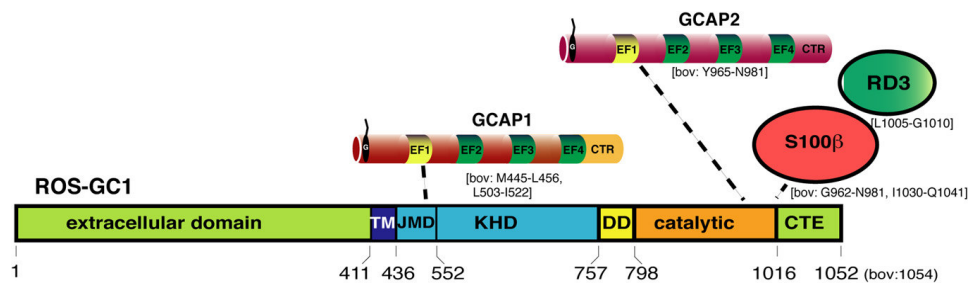


**FIGURE 4 | Schematic representation of ROS-GC1 and**

**ROS-GC1-interaction partners in photoreceptors.** ROS-GC1 contains an aminoterminal extracellular domain, transmembrane domain (TM), kinase homology domain (KHD), dimerization domain (DD), and the catalytic domain that converts GTP into cGMP. The aminoterminal portion of the KHD is also referred to as juxtamembrane domain (JMD) [Lange et al. (1999)]. The borders of the respective domains are schematically depicted in the amino acid sequence of human ROS-GC1 (NP\_000171, GI: 4504217). Numbers indicated correspond to the mature ROS-GC1 protein (without leader sequence). The borders of the individual domains were determined by the analyses of various ROS-GC1 constructs; the precise structure of photoreceptor ROS-GC1 (e.g., X-ray-structure) is not yet available. At the intracellular domains of ROS-GC1, different NCS proteins bind at different locations. GCAP1 binds to the JMD, the aminoterminal portion of the kinase homology domain of ROS-GC1 probably via its aminoterminal EF1 hand. In contrast, S100β and GCAP2 bind close to each other to the catalytic domain. The binding of GCAPs appears to compete with the binding of the retinal degeneration protein 3 (RD3). While GCAPs inhibit

mostly ROS-GC1 activity at high  $Ca^{2+}$ -concentrations, S100β stimulates ROS-GC1 activity at high  $Ca^{2+}$ . The  $Ca^{2+}$ -concentrations needed by S100β to stimulate ROS-GC1 activity is high but could be achieved at the active zone of photoreceptors close to presynaptic  $Ca^{2+}$ -channels. The numbers below the schematic depiction of ROS-GC1 domains depict the respective borders in human ROS-GC1 sequence. Most of the mapping of the ROS-GC1 interacting proteins has been done with bovine ROS-GC1 reviewed in Sharma (2010). For some interactions (e.g., GCAP1), multiple interaction sites were reported. GCAP1 was also reported to bind to the catalytic domain though with lower affinity than at the KHD [for review, Sharma (2002, 2010)]. The respective amino acid regions of bovine ROS-GC1 involved in the interaction with the indicated proteins are indicated in square brackets. Non-photoreceptor-interacting proteins of ROS-GC1 [Sharma, (2010)] are not depicted. Abbreviations: TM, transmembrane domain; JMD, juxtamembrane domain; DD, dimerization domain; CTE, carboxyterminal extension; RD3, retinal degeneration 3. Proteins and protein domains are only schematically depicted and not drawn in scale.

(light) in the mouse retina. Light-induced decreased levels of cGMP need to be replenished in order to be able to detect the next flash of light. Recovery of cGMP levels is accomplished by a  $Ca^{2+}$ -dependent feedback mechanism mediated by GCAP proteins. After illumination (at low  $Ca^{2+}$ ), GCAPs are in the  $Mg^{2+}$ -bound state and stimulate GC activity. In contrast, in the  $Ca^{2+}$ -bound state (at high  $Ca^{2+}$  in the dark) GCAPs inhibit GC activity (Koch, 2006; Sharma, 2010; Sakurai et al., 2011). Thus, GCAPs work as bimodal regulators of GCs: as an inhibitor of GC activity function (if  $Ca^{2+}$  is bound) and as an activator of GC function (and cGMP synthesis) if  $Mg^{2+}$  is bound. At low  $Ca^{2+}$  levels (light), GCAPs activate GCs and thus raise cGMP levels to restore pre-flash cGMP levels. These fundamental properties of GCAP proteins are crucial for the  $Ca^{2+}$ -dependent feedback of the phototransduction cascade. This is necessary to make the OS responsive to new flashes of light and to reset the sensitivity of the phototransduction cascade to different levels of illumination. Particularly EF-hand 3 (EF3) emerged as key region that determines whether GCAPs act as an activator or inhibitor of GCs (Olshevskaya et al., 2002; Baehr and Palczewski, 2007, 2009).

GCAP1 binds to the juxtamembrane KHD of ROS-GCs (for review, see Koch et al., 2010). GCAP2 binds directly to the catalytic domain of ROS-GCs. Despite high sequence similarities, GCAPs are not functionally equivalent; many regulatory properties differ (for review, see Koch, 2006; Dizhoor et al., 2010; Koch et al., 2010). GCAP2 has a higher affinity for  $Ca^{2+}$  than GCAP1 (for review, see Koch, 2006; Dizhoor et al., 2010). Different  $Ca^{2+}$ -affinities of GCAPs could enhance the operational range of  $Ca^{2+}$ -regulation of GCs and give rise to the  $Ca^{2+}$ -relay model of

GC activation/inhibition in the OS (for review, see Koch, 2006; Burgoyne, 2007). At intermediate levels,  $Ca^{2+}$  is still bound to GCAP2 whereas GCAP1 is already  $Ca^{2+}$ -free ( $Mg^{2+}$ -bound version). As a consequence, GCAP1 would stimulate GC activity at these intermediate concentrations, whereas GCAP2 would still be inhibitory. Recently, it was found that the RD3 protein, which is associated with LCA, also binds to the carboxyterminal of ROS-GC and inhibits GC activity by an allosteric mechanism (Azadi et al., 2010; Peshenko et al., 2011b). RD3 binding to ROS-GCs promotes dissociation of GCAPs from the ROS-GC complex.

### GCAPS IN PHOTORECEPTOR PRESYNAPTIC TERMINALS AND THEIR INVOLVEMENT IN ACTIVITY-DEPENDENT CHANGES OF SYNAPTIC RIBBONS

Various studies demonstrated the presence of GCAP proteins in photoreceptor presynaptic terminals (Otto-Bruc et al., 1997; Kachi et al., 1999; Cuenca et al., 1998; Pennesi et al., 2003; Makino et al., 2008; Venkatesan et al., 2010). But the significance of GCAP proteins in the presynaptic terminals is not well understood. One function of GCAP-mediated signaling appears to mediate the  $Ca^{2+}$ -dependent regulation of synaptic ribbon plasticity (Venkatesan et al., 2010). Synaptic ribbons are dynamic structures (for review, see Vollrath and Spiwox-Becker, 1996; Schmitz, 2009). The synaptic ribbon undergoes activity- (illumination-) dependent changes. Illumination leads to smaller and less numerable synaptic ribbons in the mouse retina (Spiwox-Becker et al., 2004). The dynamics of these structures is known to be dependent upon  $Ca^{2+}$  and cGMP (Vollrath and Spiwox-Becker, 1996). Chelating intracellular  $Ca^{2+}$  leads to a disassembly of synaptic



Venkataraman et al., 2003; Sharma, 2010). S100 $\beta$  binds to the catalytic domain of ROS-GC and subsequently enhances ROS-GC1 activity at high Ca<sup>2+</sup>-concentrations. These Ca<sup>2+</sup>-concentrations could be achieved close to the synaptic ribbon (Choi et al., 2008; Jackman et al., 2009; Graydon et al., 2011). Thus, S100 $\beta$  binds to ROS-GC1 at the catalytic domain, similar to GCAP2 (Duda et al., 2002, 2005; Sharma, 2002, 2010). It is possible that S100 $\beta$  competes with GCAP2 for binding to ROS-GC1.

The regulation of cGMP levels could be the key in the regulation of activity-dependent synaptic ribbon plasticity. cGMP was reported to stabilize synaptic ribbons in the pineal gland (Seidel et al., 1990; Spessert et al., 1992). cGMP-dependent protein kinases could be effectors that might mediate the stabilizing effect of cGMP on synaptic ribbons. cGMP-dependent kinases have been localized to photoreceptor synapses (Feil et al., 2005). But the involvement of these kinases in ribbon dynamics has not yet been elucidated. Interestingly, the RD3 protein, which blocks binding of GCAP2 to ROS-GC1, is present in the presynaptic terminals (Azadi et al., 2010; Peshenko et al., 2011b). Thus, a complex interplay of several proteins that compete for binding to ROS-GCs modulates cGMP-dependent signaling in the photoreceptor synapse in a complex manner. The recruitment of GCAP2 to synaptic ribbons and the subsequent disassembly of synaptic ribbons could be due to changes in cGMP levels that induce further downstream effects or due to increased GCAP2-mediated Ca<sup>2+</sup>-buffering. Future investigations have to discriminate between these possibilities. The importance of cGMP and cGMP-dependent protein kinases for synaptic ribbon dynamics is supported by a recent study that showed a synaptic ribbon-protective effect of cGMP in an inner ear trauma model (Jaumann et al., 2012). In this study, the authors demonstrated that inhibition of cGMP-hydrolyzing PDE5 leads to stabilization of synaptic ribbons in a cGMP-regulated protein kinase 1-dependent manner in inner hair cells. Analyses of GCAP1/2 double knockout mice also pointed to a synaptic function of GCAPs proteins at the photoreceptor synapse (Okawa et al., 2010). GCAP1/2 knockout mice show disturbed signal processing at the synapse: although the single-photon-responses in OS of GCAP knockout mice were much larger than in wildtype mice, the synaptic processing of this information, as measured by recordings from postsynaptic bipolar cells, was more inefficient. A main synaptic function of GCAPs appears to improve the signal-to-noise ratio of synaptic transmission (Okawa et al., 2010). The underlying molecular mechanisms are still unknown but could involve structural changes of the synapse.

### **cGMP IS AN IMPORTANT MODULATOR OF SYNAPTIC PLASTICITY IN PHOTORECEPTOR TERMINALS**

Various other aspects of plasticity in photoreceptor presynaptic terminals are mediated by cGMP (Rieke and Schwartz, 1994; Vollrath and Spiwox-Becker, 1996; Savchenko et al., 1997; Zhang and Townes-Anderson, 2002; Zhang et al., 2005). The group of Townes-Anderson showed that outgrowth of neurites in rods and cones photoreceptor depends upon influx of Ca<sup>2+</sup> (for review, see Townes-Anderson and Zhang, 2006). In cones, Ca<sup>2+</sup> enters the presynaptic terminal through cGMP-gated Ca<sup>2+</sup>-channels to mediate this type of synaptic

plasticity. Hyperpolarization-activated, cyclic nucleotide-gated (HCN) channels could be further effectors of presynaptic cGMP. HCN1 channels have been demonstrated in presynaptic photoreceptor terminals (Müller et al., 2003; Knop et al., 2008; Seeliger et al., 2011; Tanimoto et al., 2012). cGMP-regulated channels could extend the range of synaptic transmission e.g., at very negative membrane potentials at which L-type calcium channels might already be closed (Rieke and Schwartz, 1994; Savchenko et al., 1997). Soluble GCs could also contribute to the generation of cGMP. Several studies suggest that this source of cGMP production could play a role in neurotransmitter release and structural plasticity in photoreceptor terminals (Savchenko et al., 1997; Kourennyi et al., 2004; Zhang et al., 2005; Blom et al., 2009; Sato et al., 2011).

### **IMBALANCE OF cGMP AND Ca<sup>2+</sup>-HOMEOSTASIS IN PHOTORECEPTORS LEADS TO DISEASE**

As described above, cGMP and Ca<sup>2+</sup> homeostasis are intimately related and possess a central role for phototransduction and light-adaptation. Tight control of cGMP and Ca<sup>2+</sup>-levels are of central importance for the survival of photoreceptors (Hunt et al., 2010). Various severe neurodegenerative diseases of the retina are associated with disturbances of the cGMP/Ca<sup>2+</sup>-homeostasis (Fain, 2006; Barabas et al., 2010; Paquet-Durand et al., 2011). These include Retinitis pigmentosa (RP), LCA, and distinct forms of cone and rod dystrophies (Baehr and Palczewski, 2009; Jiang and Baehr, 2010; Paquet-Durand et al., 2011). Mutations in the ROS-GC1 gene can lead to LCA, a devastating degeneration leading to childhood blindness, or a cone-rod-dystrophy (CORD 6) (for review, see Hunt et al., 2010). Diseases associated with ROS-GC2 are not known. The gene for GCAP1 has been associated with a form of cone-rod dystrophy, CORD3 (for review, see Jiang and Baehr, 2010). Missense mutations in GCAP1 cause loss of photoreceptors, particularly cones. Many of the disease-causing mutations are located in EF3 and EF4 or indirectly affect the structure of these EF-hands. The disease mutants lead to a decrease in Ca<sup>2+</sup>-sensitivity thus making these mutants to constitutive, Ca<sup>2+</sup>-insensitive activators of GCs. As a result, cGMP and Ca<sup>2+</sup> levels are pathologically increased leading to photoreceptor cell death (Baehr and Palczewski, 2009; Jiang and Baehr, 2010; Paquet-Durand et al., 2011). The retinal degeneration 1 (rd1) mouse is characterized by a loss-of-function mutation in the gene encoding for the  $\beta$ -subunit of the photoreceptor-specific PDE6 (for a recent review, see Barabas et al., 2010). Consequently, rd1 mice have low PDE6 activity and high levels of cGMP which lead to photoreceptor cell death, predominantly in rods. Also the proteins discussed above, i.e., Cav1.4, Munc119, RIM, and CaBP4, have high clinical relevance; mutations in the respective genes cause various severe degenerative diseases of the retina, as described above.

### **OPEN QUESTIONS/PERSPECTIVES**

Activity-dependent, adaptive signaling in photoreceptor presynaptic terminals is just at the beginning of being understood. Currently, knowledge about these processes in the synapse lags behind to what is known about dynamic processes in the OS. Ca<sup>2+</sup>, cGMP, and EF-hand-containing proteins likely play

numerous roles in signaling at the photoreceptor synapse and activity-dependent synaptic changes. Dynamics of synaptic ribbons at a molecular level may involve control of RIBEYE-RIBEYE interactions. How these interactions are controlled at a molecular level is currently not known. The involved effector molecules and molecular pathways need to be elucidated. Differences between rod and cone dynamic signaling need to be worked out since the purpose of synaptic transmission at these two different types of photoreceptor synapses is different (although related). Are there differences in adaptative signaling in cone and rod synapses and eventually also between the different active zones present in cone synapses? Recent  $\text{Ca}^{2+}$ -imaging analyses strongly argue that this is the case (Johnson et al., 2007; Sheng et al., 2007). Most of our current knowledge about the physiology of retinal ribbon

synapses was obtained from goldfish bipolar cells and salamander photoreceptors. The mouse retina with its powerful genetic possibilities just entered the stage. Mouse knockout models as well as the possibility of manipulating the mouse retina with recombinant viruses can be expected to provide further important insights into signal processing at the photoreceptor synapse.

## ACKNOWLEDGMENTS

Work by the authors is supported by the German Research Community (DFG) SFB894 TPA7, GRK1326 and the Human Frontiers Science Organization HFSP. Thanks to Dr. Jutta Schmitz-Kraemer for critically reading the manuscript. The authors apologize that not all relevant original papers could be mentioned due to limitations in space.

## REFERENCES

- Abramov, I., and Gordon, J. (1994). Color appearance: on seeing red- or yellow, or green, or blue. *Ann. Rev. Psychol.* 45, 451–485.
- Aldahmesh, M. A., Al-Owain, M., Alqahtani, F., Hazzaa, S., and Alkurya, F. S. (2010). A null mutation in CaBP4 causes Leber's congenital amaurosis-like phenotype. *Mol. Vis.* 16, 207–212.
- Alpadi, K., Magupalli, V. G., Käppel, S., Köblitz, L., Schwarz, K., Seigel, G. M., Sung, C. H., and Schmitz, F. (2008). RIBEYE recruits Munc119, the mammalian ortholog of the *Caenorhabditis elegans* protein unc119 to synaptic ribbons of photoreceptor synapses. *J. Biol. Chem.* 283, 26461–26467.
- Ames, J. B., Dizhoor, A. M., Ikura, M., Palczewski, K., and Stryer, L. (1999). Three-dimensional structure of guanylyl cyclase activating protein-2, a calcium-sensitive modulator of photoreceptor guanylyl cyclases. *J. Biol. Chem.* 274, 19329–19337.
- Ames, J. B., and Lim, S. (2011). Molecular structure and target recognition of neuronal calcium sensor proteins. *Biochim. Biophys. Acta* [Epub ahead of print].
- Azadi, S., Molday, L. L., and Molday, R. S. (2010). RD3, the protein associated with Leber congenital amaurosis type 12, is required for guanylate cyclase trafficking in photoreceptor cells. *Proc. Natl. Acad. Sci. U.S.A.* 107, 21158–21163.
- Babai, N., Morgans, C. W., and Thoreson, W. B. (2010). Calcium-induced calcium release contributes to synaptic release from mouse rod photoreceptors. *Neuroscience* 165, 1447–1456.
- Baehr, W., and Palczewski, K. (2007). Guanylate-cyclase-activating proteins and retina disease. *Subcell. Biochem.* 45, 71–91.
- Baehr, W., and Palczewski, K. (2009). Focus on molecules: guanylate cyclase-activating proteins (GCAPs). *Exp. Eye Res.* 89, 2–3.
- Balkema, G. W., Cusick, K., and Nguyen, T. H. (2001). Diurnal variation in synaptic ribbon length and visual threshold. *Vis. Neurosci.* 18, 789–792.
- Ball, S. L., McEnery, M. W., Yunker, A. M., Shin, H. S., and Gregg, R. G. (2011). Distribution of voltage gated calcium channel  $\beta$  subunits in the mouse retina. *Brain Res.* 1412, 1–8.
- Ball, S. L., Powers, P. A., Shin, H. S., Morgans, C. W., Peachey, N. S., and Gregg, R. G. (2002). Role of the  $\beta 2$  subunit of voltage-dependent  $\text{Ca}^{2+}$  channels in the retinal outer plexiform layer. *Invest. Ophthalmol. Vis. Sci.* 43, 1595–1603.
- Barabas, P., Peck, C. C., and Krizaj, D. (2010). Do calcium channel blockers rescue dying photoreceptors in the *Pde6brd1* mouse? *Adv. Exp. Med. Biol.* 664, 491–499.
- Beutner, D., Voets, T., Neher, E., and Moser, T. (2001). Calcium dependence of exocytosis and endocytosis at the cochlear inner hair cell afferent synapse. *Neuron* 29, 681–690.
- Biel, M., and Michalakakis, S. (2009). Cyclic nucleotide-gated channels. *Handb. Exp. Pharmacol.* 191, 111–136.
- Blom, J. J., Blute, T. A., and Eldred, W. D. (2009). Functional localization of the nitric oxide/cGMP pathway in the salamander retina. *Vis. Neurosci.* 26, 275–286.
- Buch, P. K., Mihelec, M., Cottrill, P., Wilkie, S. E., Pearson, R. A., Duran, Y., West, E. L., Michaelides, M., and Hunt, D. M. (2011). Dominant cone-rod dystrophy: a mouse model generated by gene targeting of the GCAP1/Guca1a gene. *Plos One* 3, 18089. doi: 10.1371/journal.pone.0018089
- Buraci, Z., and Yang, Y. (2010). The  $\beta$ -subunit of  $\text{Ca}^{2+}$  channels. *Physiol. Rev.* 90, 1461–1506.
- Burgoyne, R. D. (2007). Neuronal calcium sensor proteins: generating diversity in neuronal  $\text{Ca}^{2+}$ -signalling. *Nat. Rev. Neurosci.* 8, 182–193.
- Burns, M. E., and Baylor, D. A. (2001). Activation, deactivation, and adaptation in vertebrate photoreceptor cells. *Ann. Rev. Neurosci.* 24, 779–805.
- Catterall, W. A., Perez-Reyes, E., Snutch, T. P., and Striessnig, J. (2005). International union of pharmacology. XLVIII. Nomenclature and structure-function relationships of voltage-gated calcium channels. *Pharmacol. Rev.* 57, 411–425.
- Catterall, W. A. (2011). Voltage-gated calcium channels. *Cold Spring Harb. Persp. Biol.* 3, a003947.
- Chen, K. (2005). The vertebrate phototransduction cascade: amplification and termination mechanisms. *Rev. Physiol. Biochem. Pharmacol.* 154, 101–121.
- Choi, S. Y., Jackman, S., Thoreson, W. B., and Kramer, R. H. (2008). Light regulation of  $\text{Ca}^{2+}$  in the cone photoreceptor synaptic terminal. *Vis. Neurosci.* 25, 693–700.
- Cooper, N., Liu, N., Yoshida, A., Pozdnyakov, N., Margulies, A., and Sitarumayya, A. (1995). The bovine rod outer segment guanylate cyclase, ROS-GC, is present in both outer segment and synaptic layers of the retina. *J. Mol. Neurosci.* 6, 211–222.
- Cuenca, N., Lopez, S., Howes, K., and Kolb, H. (1998). The localization of guanylyl cyclase-activating proteins in the mammalian retina. *Invest. Ophthalmol. Vis. Sci.* 39, 1249–1250.
- Davies, A., Hendrich, J., Van Minh, A. T., Wratten, J., Douglas, L., and Dolphin, A. C. (2007). Functional biology of the  $\alpha(2)\delta$  subunits of voltage-gated calcium channels. *Trends Pharmacol. Sci.* 28, 220–228.
- Davies, A., Kadurin, I., Alvarez-Laviada, A., Douglas, L., Nieto-Rostro, M., Bauer, C. S., Pratt, W. S., and Dolphin, A. C. (2010). The  $\alpha 2\delta$  subunits of voltage-gated calcium channels form GPI-anchored proteins, a posttranslational modification essential for function. *Proc. Natl. Acad. Sci. U.S.A.* 107, 1654–1659.
- DeVries, S. H., Li, W., and Saszik, S. (2006). Parallel processing in two transmitter microenvironments at the cone photoreceptor synapse. *Neuron* 50, 735–748.
- Dick, O., tom Dieck, S., Altmock, W. D., Ammermüller, J., Weiler, R., Garner, C. C., Gundelfinger, E. D., and Brandstätter, J. H. (2003). The presynaptic active zone protein bassoon is essential for photoreceptor ribbon synapse formation in the retina. *Neuron* 37, 775–786.
- Dizhoor, A. M., Olshevskaya, E. V., and Peshenko, I. V. (2010).  $\text{Mg}^{2+}/\text{Ca}^{2+}$  cation binding cycle of guanylyl cyclase activating proteins (GCAPs): role in the regulation of photoreceptor guanylyl cyclase. *Mol. Cell. Biochem.* 334, 117–124.
- Doering, C. J., Peloquin, J. B., and McRory, J. E. (2007). The  $\text{CaV}1.4$  channel. *Channels* 1, 3–10.
- Dolphin, A. C. (2003).  $\beta$  subunits of voltage-gated calcium channels. *J. Bioenerg. Biomembr.* 35, 599–620.
- Duda, T., Fik-Rymarkiewicz, E., Venkataraman, V., Krishnan, R., Koch, K. W., and Sharma, R. K. (2005). The calcium-sensor guanylate cyclase activating protein type 2 specific site in rod outer segment membrane guanylate cyclase type 1. *Biochemistry* 44, 7336–7345.
- Duda, T., Koch, K. W., Venkataraman, V., Lange, C., Beyermann, M.,

- and Sharma, R. K. (2002). Ca<sup>2+</sup>-sensor S100 $\beta$ -modulated sites of membrane guanylate cyclase in the photoreceptor-bopolar synapse. *EMBO J.* 21, 2547–2556.
- Emran, F., Rihel, J., Adolph, A. R., and Dowling, J. E. (2010). Zebrafish larvae lose vision at night. *Proc. Natl. Acad. Sci. U.S.A.* 107, 6034–6039.
- Ermilov, A. N., Olshevskaya, E. V., and Dizhoor, A. M. (2001). Instead of binding calcium, one of the EF-hand structures in guanylyl cyclase activating protein 2 is required for targeting photoreceptor guanylyl cyclase. *J. Biol. Chem.* 276, 48143–48148.
- Fain, G. L. (2006). Why photoreceptors die and why they don't. *Bioessays* 28, 344–354.
- Feil, S., Zimmermann, A., Knorn, A., Brummer, S., Schlossmann, J., Hofmann, F., and Feil, R. (2005). Distribution of cGMP-dependent protein kinase type I and its isoform in the mouse brain and retina. *Neuroscience* 135, 863–868.
- Frank, T., Khimich, D., Neef, A., and Moser, T. (2009). Mechanisms contributing to synaptic Ca<sup>2+</sup> signals and their heterogeneity in hair cells. *Proc. Natl. Acad. Sci. U.S.A.* 106, 4483–4488.
- Frank, T., Rutherford, M. A., Strenzke, N., Neef, A., Pangrsic, T., Khimich, D., Fejtova, D., Gundelfinger, E. D., Liberman, M. C., Harke, B., Bryan, K. E., Lee, A., Egner, A., Riedel, D., and Moser, T. (2010). Bassoon and the synaptic ribbon organize Ca<sup>2+</sup>-channels and vesicles to add release sites and promote refilling. *Neuron* 68, 724–738.
- Gebhart, M., Juhasz-Vedres, G., Zuccotti, A., Brandt, N., Engel, J., Trockenbacher, A., Kaur, G., Obermair, G. J., Knipper, M., Koschak, A., and Striessnig, J. (2010). Modulation of CaV1.3 channel gating by Rab3 interacting molecule. *Mol. Cell. Neurosci.* 44, 246–259.
- Graydon, C. W., Cho, S., Li, G. L., Kachar, B., and von Gersdorff, H. (2011). Sharp Ca<sup>2+</sup> nanodomains beneath the ribbon promote highly synchronous multivesicular release at hair cell synapses. *J. Neurosci.* 31, 16637–16650.
- Haeseleer, F., Imanishi, Y., Maeda, T., Possin, D. E., Maeda, A., Lee, A., Rieke, F., and Palczewski, K. (2004). Essential role of Ca<sup>2+</sup>-binding protein 4, a CaV1.4 channel regulator, in photoreceptor synaptic function. *Nat. Neurosci.* 7, 1079–1087.
- Haeseleer, F., Imanishi, Y., Sokal, I., Filipek, S., and Palczewski, K. (2002). Calcium-binding proteins: intracellular sensors from the calmodulin superfamily. *Biochem. Biophys. Res. Commun.* 290, 615–623.
- Haeseleer, F. (2008). Interaction and colocalization of CaBP4 and unc119 (MRG4) in photoreceptors. *Invest. Ophthalmol. Vis. Sci.* 49, 2366–2375.
- Haire, S. E., Pang, J., Boye, S. L., Sokal, I., Craft, C. M., Palczewski, K., Hauswirth, M. M., and Semple-Rowland, S. L. (2006). Light-driven cone arrestin translocation in cones of postnatal guanylate cyclase-1 knockout mouse retina treated with AAV-GC1. *Invest. Ophthalmol. Vis. Sci.* 47, 3745–3753.
- Han, Y., Kaeser, P. S., Südhof, T. C., and Schneggenburger, R. (2011). RIM determines Ca<sup>2+</sup> channel density and vesicle docking at the presynaptic active zone. *Neuron* 69, 304–316.
- Heidelberger, R., Thoreson, W. B., and Witkovsky, P. (2005). Synaptic transmission at retinal ribbon synapses. *Prog. Retin. Eye Res.* 24, 682–720.
- Hibino, H., Pironkova, R., Onwumere, O., Vologodskaya, M., Hudspeth, A. J., and Lesage, F. (2002). RIM binding proteins (RBPs) couple Rab3-interacting molecules (RIMs) to voltage-gated Ca<sup>2+</sup>-channels. *Neuron* 34, 411–423.
- Hull, C., Studholme, K., Yazulla, S., and von Gersdorff, H. (2006). Diurnal changes in exocytosis and the number of synaptic ribbons at active zones of an ON-type bipolar cell terminal. *J. Neurophysiol.* 96, 2025–2033.
- Hunt, D. M., Buch, P., and Michaelidis, M. (2010). Guanylate cyclases and associated activator proteins in retinal disease. *Mol. Cell. Biochem.* 334, 157–168.
- Hwang, J.-Y., Schlesinger, R., and Koch, K. W. (2004). Irregular dimerization of guanylate cyclase-activating protein 1 mutants causes loss of target activation. *Eur. J. Biochem.* 271, 3785–3793.
- Jackman, S. L., Babai, N., Chambers, J. J., Thoreson, W. B., and Kramer, R. H. (2010). A positive feedback synapse from horizontal cells to cone photoreceptors. *Plos Biol.* 9, e1001057. doi: 10.1371/journal.pbio.1001057
- Jackman, S. L., Choi, S. Y., Thoreson, W. B., Rabl, K., Bartoletti, T. M., and Kramer, R. H. (2009). Role of the synaptic ribbon in transmitting the cone light response. *Nat. Neurosci.* 12, 303–310.
- Jarsky, T., Tian, M., and Singer, J. H. (2010). Nanodomain control of exocytosis is responsible for the signalling capability of a retinal ribbon synapse. *J. Neurosci.* 30, 11885–11895.
- Jaumann, M., Dettling, J., Gubelt, M., Zimmermann, U., Gerling, A., Paquet-Durand, F., Feil, S., Wolpert, S., Franz, C., Varakina, K., Xiong, H., Brandt, N., Kuhn, S., Geisler, H. S., Rohbock, K., Ruth, P., Schlossmann, J., Hütter, J., Sandner, P., Feil, R., Engel, J., Knipper, M., and Rüttiger, L. (2012). cGMP-Prkg1 signaling and Pde5 inhibition shelter cochlear hair cells and hearing function. *Nat. Med.* 18, 252–259.
- Jiang, L., and Baehr, W. (2010). GCAP1 mutations associated with autosomal dominant cone dystrophy. *Adv. Exp. Med. Biol.* 664, 273–282.
- Jiang, L., Katz, B. J., Yang, Z., Zhao, Y., Faulkner, N., Hu, J., Baird, J., Baehr, W., Creel, D. J., and Zhang, K. (2005). Autosomal dominant cone dystrophy caused by a novel mutation in the GCAP1 gene (GucalA). *Mol. Vis.* 11, 143–151.
- Johnson, J. E. Jr., Perkins, G. A., Anand Giddabasappa, C. S., Chaney, S., Xiao, W., White, A. D., Brown, J. M., Waggoner, J., Ellisman, M. H., and Fox, D. A. (2007). Spatiotemporal regulation of ATP and Ca<sup>2+</sup> dynamics in vertebrate rod and cone ribbon synapses. *Mol. Vis.* 13, 887–919.
- Johnson, S. L., Forge, A., Knipper, M., Münkner, S., and Marcotti, W. (2008). Tonotopic variation in the calcium dependence of neurotransmitter release and vesicle pool replenishment at mammalian auditory ribbon synapses. *J. Neurosci.* 28, 7670–7678.
- Joselevitch, C., and Zenisek, D. (2010). The cytomatrix protein bassoon contributes to fast transmission at conventional and ribbon synapses. *Neuron* 68, 604–606.
- Kachi, S., Nishizawa, Y., Olshevskaya, E., Yamazaki, A., Miyake, Y., Wakabashi, T., Dizhoor, A. M., and Usukura, J. (1999). Detailed localization of photoreceptor guanylate cyclase activating protein-1 and -2 in mammalian retinas using light and electron microscopy. *Exp. Eye Res.* 68, 465–473.
- Kaeser, P. (2011). Pushing vesicles over the RIM. *Cell. Logist.* 1, 106–110.
- Kaeser, P. S., Deng, L., Wang, Y., Dulubova, I., Liu, X., Rizo, J., and Südhof, T. C. (2011). RIM tethers Ca<sup>2+</sup> channels to presynaptic active zones via a direct PDZ-domain interaction. *Cell* 144, 282–295.
- Karan, S., Frederick, J. M., and Baehr, W. (2010). Novel functions of photoreceptor guanylate cyclases revealed by targeted deletion. *Mol. Cell. Biochem.* 334, 141–155.
- Kersten, F. J. K., van Wijk, E., van Reenwijk, J., van der Zwaag, B., Märker, T., Peters, T. A., Katsanis, N., Wolfrum, U., Keunen, J. E. E., Roepman, R., and Kremer, H. (2010). Association of whirlin with CaV1.3( $\alpha$ 1D) channels in photoreceptors, defining a novel member of the Usher protein network. *Invest. Ophthalmol. Vis. Sci.* 51, 2338–2346.
- Khimich, D., Nouvian, R., Pujol, R., tom Dieck, S., Egner, A., Gundelfinger, E. D., and Moser, T. (2005). Hair cell synaptic ribbons are essential for synchronous auditory signalling. *Nature* 434, 889–894.
- Kiyonaka, S., Wakamori, M., Miki, T., Uriu, Y., Nonaka, M., Bito, H., Beedle, A. M., Mori, E., Hara, Y., De Waard, M., Kanagawa, M., Itakura, M., Takahashi, M., Campbell, K. P., and Mori, Y. (2007). RIM1 confers sustained activity and neurotransmitter vesicle anchoring to presynaptic Ca<sup>2+</sup>-channels. *Nat. Neurosci.* 10, 691–701.
- Knop, G. C., Seeliger, M. W., Thiel, F., Mataruga, A., Kaupp, U. B., Friedburg, C., Tanimoto, N., and Kaupp, U. B. (2008). Light responses in the mouse retina are prolonged upon targeted deletion of the HCN1 channel gene. *Eur. J. Neurosci.* 28, 2221–2230.
- Ko, M. L., Liu, Y., Dryer, S. E., and Ko, G. Y. (2007). The expression of L-type voltage-gated calcium channels in retinal photoreceptors is under circadian control. *J. Neurochem.* 103, 784–792.
- Kobayashi, A., Higashide, T., Hamasaki, D., Kubota, S., Sakuma, A., An, W., Fujimaki, T., McLaren, M. J., Weleber, R. G., and Inana, G. (2000). HRG4 (UNC119) mutation found in cone-rod dystrophy causes retinal degeneration in a transgenic model. *Invest. Ophthalmol. Vis. Sci.* 41, 3268–3277.
- Koch, K. W. (2006). GCAPs, the classical neuronal calcium sensors in the retina. In: Calcium binding proteins. *Landes Biosci.* 1, 3–6.
- Koch, K. W., Duda, T., and Sharma, R. K. (2010). Ca<sup>2+</sup>-modulated vision-linked ROS-GC guanylate cyclase transduction machinery. *Mol. Cell. Biochem.* 334, 105–115.
- Koike, C., Numata, T., Ueda, H., Mori, Y., and Furukawa, T. (2010). TRPM1: a vertebrate TRP channel responsible for retinal ON bipolar function. *Cell Calcium* 48, 95–101.
- Kourennyi, D. E., Liu, X. D., Hart, J., Mahmud, F., Baldrige, W. H., and Barnes, S. (2004). Reciprocal modulation of calcium dynamics at rod and cone photoreceptor synapses

- by nitric oxide. *J. Neurophysiol.* 92, 477–483.
- Krizaj, D., and Copenhagen, D. R. (2002). Calcium regulation in photoreceptors. *Front. Biosci.* 7, 2023–2044.
- Lacinova, L. (2005). Voltage-dependent calcium channels. *Gen. Physiol. Biophys.* 24(S1), 1–78.
- Lange, C., Duda, T., Beyermann, M., Sharma, R. K., and Koch, K.-W. (1999). Regions in vertebrate photoreceptor guanylyl cyclase ROS-GC1 involved in Ca<sup>2+</sup>-dependent regulation by guanylyl cyclase-activating protein GCAP-1. *FEBS Lett.* 460, 27–31.
- Lieberman, L. D., Wang, H., and Liberman, M. C. (2011). Opposing gradients of ribbon size and AMPA receptor expression underlie sensitivity differences among cochlear-nerve/hair-cell synapses. *J. Neurosci.* 31, 801–808.
- Liu, X., Seno, K., Nishizawa, Y., Hayashi, E., Yamazaki, A., Matsumoto, H., Wakabayashi, T., and Usukura, J. (1994). Ultrastructural localization of retinal guanylate cyclase in human and monkey retina. *Exp. Eye Res.* 59, 761–768.
- Magupalli, V. G., Schwarz, K., Alpadi, K., Natarajan, S., Seigel, G. M., and Schmitz, F. (2008). Multiple RIBEYE – RIBEYE interactions create a dynamic scaffold for the formation of synaptic ribbons. *J. Neurosci.* 28, 7954–7967.
- Makino, C. L., Peshenko, I. V., Wen, X. H., Olshevskaia, E. V., Barrett, R., and Dizhoor, A. M. (2008). A role for GCAP2 in regulating the photoreceptor response: guanylyl cyclase activation and rod physiology in GUC1A1B knockout mice. *J. Biol. Chem.* 283, 29135–29143.
- Matthews, G., and Fuchs, P. (2010). The diverse roles of ribbon synapses in sensory neurotransmission. *Nat. Rev. Neurosci.* 11, 812–822.
- Mercer, A. J., Chen, M., and Thoreson, W. B. (2011a). Lateral mobility of presynaptic L-type calcium channels at photoreceptor ribbon synapses. *J. Neurosci.* 31, 4397–4406.
- Mercer, A. J., and Thoreson, W. B. (2011b). The dynamic architecture of photoreceptor ribbon synapses: cytoskeletal, extracellular matrix, and intramembrane proteins. *Vis. Neurosci.* 28, 453–471.
- Miki, T., Kiyonaka, S., Uriu, Y., deWaard, M., Wakamori, M., Beedle, A. M., Campbell, K., and Mori, Y. (2007). Mutation associated with an autosomal dominant cone-rod dystrophyCORD7 modifies RIM1-mediated modulation of voltage-gated Ca<sup>2+</sup>-channels. *Channels* 1, 144–147.
- Morgans, C. W. (2001). Localization of the  $\alpha 1F$  calcium channel subunit in the rat retina. *Invest. Ophthalmol. Vis. Sci.* 42, 2414–2418.
- Morgans, C. W., Bayley, P. R., Oesch, N., Ren, G., Akileswaran, L., and Taylor, W. R. (2005). Photoreceptor calcium channels: insight from night blindness. *Vis. Neurosci.* 22, 561–568.
- Morgans, C. W., Brown, R. L., and Duvoisin, R. M. (2010). TRPM1: an endpoint of the mGluR6 signal transduction cascade in retinal ON-bipolar cells. *Bioessays* 32, 609–614.
- Müller, F., Scholten, A., Ivanova, E., Haverkamp, S., Kremmer, E., and Kaupp, U. B. (2003). HCN channels are expressed differentially in retinal bipolar cells and concentrated at synaptic terminals. *Eur. J. Cell Biol.* 17, 2084–2096.
- Nachman-Clewner, M., St Jules, R., and Townes-Anderson, E. (1999). L-type calcium channels in the photoreceptor synapse: localization and role in synaptic plasticity. *J. Comp. Neurol.* 415, 1–16.
- Neher, E., and Sakaba, T. (2008). Multiple roles of calcium ions in the regulation of neurotransmitter release. *Neuron* 59, 861–872.
- Okawa, H., Miyagishima, J., Arman, A. C., Hurley, J. B., Field, G. F., and Sampath, A. P. (2010). Optimal processing of photoreceptor signals is required to maximize behavioural sensitivity. *J. Physiol.* 588, 1947–1960.
- Olshevskaia, E. V., Ermilov, A. N., and Dizhoor, A. M. (2002). Factors that affect regulation of cGMP synthesis in vertebrate photoreceptors and their genetic link to human retinal degeneration. *Mol. Cell. Biochem.* 230, 139–147.
- Otto-Bruc, A., Fariss, R. N., Haeseleer, F., Huang, J., Buczylo, J., Surgocheva, I., Baehr, W., Milam, A. H., and Palczewski, K. (1997). Localization of guanylate cyclase-activating protein 2 in mammalian retina. *Proc. Natl. Acad. Sci. U.S.A.* 94, 4727–4732.
- Pahlberg, J., and Sampath, A. P. (2011). Visual thresholds is set by linear and nonlinear mechanisms: how neural circuits in the retina improve the signal-to-noise ratio of the single photon response. *Bioessays* 33, 438–447.
- Paquet-Durand, F., Beck, S., Michalakakis, S., Goldmann, T., Huber, S., Mühlfriedel, R., Trifunovic, D., Fischer, M. D., Fahl, E., Duetsch, G., Becirovic, E., Wolfrum, U., van Veen, T., Biel, M., Tanimoto, N., and Seeliger, M. W. (2011). A key role for cyclic nucleotide gated (CNG) channels in cGMP related retinitis pigmentosa. *Hum. Mol. Genet.* 20, 941–947.
- Palczewski, K., Sokal, I., and Baehr, W. (2004). Guanylate cyclase-activating proteins: structure, function and diversity. *Biochem. Biophys. Res. Comm.* 322, 1123–1130.
- Pennesi, M. E., Howes, K. A., Baehr, W., and Wu, S. M. (2003). Guanylate cyclase activating protein (GCAP1) 1 rescues cone recovery kinetics in GCAP1/GCAP2 knockout mice. *Proc. Natl. Acad. Sci. U.S.A.* 100, 6783–6788.
- Peshenko, I. V., Olshevskaia, E. V., Savchenko, A. B., Karan, S., Palczewski, K., Baehr, W., and Dizhoor, A. M. (2011a). Enzymatic properties and regulation of the native isozymes of retinal membrane guanylyl cyclase (RetGC) from mouse photoreceptors. *Biochemistry* 50, 5590–5600.
- Peshenko, I. V., Olshevskaia, E. V., Azadi, S., Molday, L. L., Molday, R. S., and Dizhoor, A. M. (2011b). Retinal degeneration 3 (RD3) protein inhibits catalytic activity of retinal membrane guanylyl cyclase (RetGC) and its stimulation by activating proteins. *Biochemistry* 50, 9511–9519.
- Potter, L. R. (2011). Guanylyl cyclase structure, function and regulation. *Cell Signal* 23, 1921–1926.
- Rambotti, M. G., Spreca, A., Giambanco, I., Sorci, G., and Donato, R. (2002). Ultracytochemistry as a tool for the study of the cellular and subcellular localization of membrane-bound guanylate cyclases (GC) activity. Applicability to both receptor-activated and receptor-independent GC activity. *Mol. Cell. Biochem.* 230, 85–96.
- Regus-Leidig, H., and Brandstätter, J. H. (2011). Structure and function of a complex sensory synapse. *Acta Physiol. (Oxf)* [Epub ahead of print].
- Regus-Leidig, H., Specht, D., tom Dieck, S., and Brandstätter, J. H. (2010). Stability of active zone components at the photoreceptor ribbon complex. *Mol. Vis.* 16, 2690–2770.
- Rieke, F., and Schwartz, E. A. (1994). A cGMP-gated current can control exocytosis at cone synapses. *Neuron* 13, 863–873.
- Sakurai, K., Chen, J., and Kefalov, V. J. (2011). Role of guanylyl cyclase modulation in mouse cone phototransduction. *J. Neurosci.* 22, 7991–8000.
- Sato, M., Ohtsuka, T., and Stell, W. K. (2011). Endogenous nitric oxide enhances the light-response of cones during light-adaptation in the rat retina. *Vis. Res.* 51, 131–137.
- Savchenko, A., Barnes, S., and Kramer, R. H. (1997). Cyclic-nucleotide-gated channels mediate synaptic feedback by nitric oxide. *Nature* 390, 694–698.
- Schmitz, F. (2009). The making of synaptic ribbons: how they are built and what they do. *Neuroscientist* 15, 611–624.
- Schmitz, F., Königstorfer, A., and Südhof, T. C. (2000). RIBEYE, a component of synaptic ribbons: a protein's journey through evolution provides insights into synaptic ribbon function. *Neuron* 28, 857–872.
- Seeliger, M. W., Brombas, A., Weiler, R., Humphries, P., Knop, G., Tanimoto, N., and Müller, F. (2011). Modulation of rod photoreceptor output by HCN1 channels is essential for regular mesopic cone vision. *Nat. Commun.* 2, 532.
- Seidel, A., Kantarjian, A., and Vollrath, L. (1990). A possible role for cyclic guanosine monophosphate in the rat pineal gland. *Neurosci. Lett.* 110, 227–231.
- Sharma, R. K. (2002). Evolution of the membrane guanylate cyclase transduction system. *Mol. Cell. Biochem.* 230, 3–30.
- Sharma, R. K. (2010). Membrane guanylate cyclase is a beautiful signal transduction machinery. *Mol. Cell. Biochem.* 334, 3–36.
- Sheets, L., Trapani, J. G., Mo, W., Obholzer, N., and Nicolson, T. (2011). RIBEYE is required for presynaptic Ca(V)1.3 channel localization and afferent innervation of sensory hair cells. *Development* 138, 1309–1319.
- Sheng, Z., Choi, S. Y., Dharia, A., Li, J., Sterling, P., and Kramer, R. H. (2007). Synaptic Ca<sup>2+</sup> in darkness is lower in rods than in cones, causing slower tonic release of vesicles. *J. Neurosci.* 27, 5033–5042.
- Singer, J. H., Lassová, L., Vardi, N., and Singer, J. S. (2004). Coordinated multivesicular release at a mammalian ribbon synapse. *Nat. Neurosci.* 7, 826–833.
- Singh, A., Hamedinger, D., Hoda, J. C., Gebhart, M., Koschak, A., Romanin, C., and Striessnig, J. (2006). C-terminal modulator controls Ca<sup>2+</sup>-dependent gating of Ca(v)1.4 L-type Ca<sup>2+</sup> channels. *Nat. Neurosci.* 9, 1108–1116.

- Snellman, J., Mehta, B., Babai, N., Bartoletti, T. M., Akmentin, W., Francis, A., Matthews, G., Thoreson, W. B., and Zenisek, D. (2011). Acute destruction of the synaptic ribbon reveals a role for the ribbon in vesicle priming. *Nat. Neurosci.* 14, 1135–1141.
- Spessert, R., Gupta, B. B. P., Seidel, A., Maitra, S. K., and Vollrath, L. (1992). Involvement of cyclic guanosine monophosphate (cGMP) and cytosolic guanylate cyclase in the regulation of synaptic ribbon numbers in the rat pineal gland. *Brain Res.* 570, 231–236.
- Spiwojs-Becker, I., Glas, M., Lasarzik, I., and Vollrath, L. (2004). Synaptic ribbons lose and regain material in response to illumination changes. *Eur. J. Neurosci.* 19, 1559–1571.
- Stephen, R., Bereta, G., Golczak, M., Palczewski, K., and Souza, M. C. (2007). Stabilizing function for myristoyl group revealed by the crystal structure of a neuronal calcium sensor, guanylate cyclase-activating protein 1. *Structure* 15, 1392–1402.
- Stephen, R., Filipek, S., Palczewski, K., and Souza, M. C. (2008). Ca<sup>2+</sup>-dependent regulation of phototransduction. *Photochem. Photobiol.* 84, 903–910.
- Striessnig, J., Bolz, H. J., and Koschak, A. (2010). Channelopathies in CaV1.1, CaV1.3, and CaV1.4 voltage-gated L-type Ca<sup>2+</sup>-channels. *Pflugers Arch.* 460, 361–374.
- Suryanarayanan, A., and Slaughter, M. M. (2006). Synaptic transmission mediated by internal calcium stores in rod photoreceptors. *J. Neurosci.* 26, 1759–1766.
- Szikra, T., Barabas, P., Bartoletti, T. M., Huang, W., Akopian, A., Thoreson, W. B., and Krizaj, D. (2009). Calcium homeostasis and cone signalling are regulated by interactions between calcium stores and plasma membrane ion channels. *Plos One* 4, e6723. doi: 10.1371/journal.pone.0006723
- Szikra, T., Cusato, K., Thoreson, W. B., Barabas, P., Bartoletti, T. M., and Krizaj, D. (2008). Depletion of calcium stores regulates calcium influx and signal transmission in rod photoreceptors. *J. Physiol.* 586, 4859–4875.
- Tanimoto, N., Brombas, A., Müller, F., and Seeliger, M. W. (2012). HCN1 channels significantly shape retinal photoresponses. *Adv. Exp. Med. Biol.* 723, 807–812.
- tom Dieck, S., Altmann, W. D., Kessels, M. M., Qualmann, B., Regus, H., Brauner, D., Fejtova, A., Bracko, O., Gundelfinger, E. D., and Brandstätter, J. H. (2005). Molecular dissection of the photoreceptor ribbon synapse: physical interaction of bassoon and Ribeye is essential for the assembly of the ribbon complex. *J. Cell Biol.* 168, 825–836.
- Townes-Anderson, E., and Zhang, N. (2006). “Synaptic plasticity and structural remodelling of rod and cone cells,” in *Plasticity of the Visual System: From Genes to Circuits*, eds R. Pinaud, L. A. Tremere, and P. DeWeerds, (Berlin, Heidelberg, NY: Springer Science), 13–31.
- Uthaiyah, R. C., and Hudspeth, A. J. (2010). Molecular anatomy of the hair cell’s ribbon synapse. *J. Neurosci.* 30, 12387–12399.
- Venkataraman, V., Duda, T., Vardi, N., Koch, K. W., and Sharma, R. K. (2003). Calcium-modulated guanylate cyclase transduction machinery in the photoreceptor-bipolar synaptic region. *Biochemistry* 42, 5640–5648.
- Venkatesan, J. K., Natarajan, S., Schwarz, K., Mayer, S. I., Alpadi, K., Magupalli, V. G., Sung, C. H., and Schmitz, F. (2010). Nicotinamide adenine dinucleotide-dependent binding of the neuronal Ca<sup>2+</sup> sensor protein GCAP2 to photoreceptor synaptic ribbons. *J. Neurosci.* 30, 6559–6567.
- Vollrath, L., and Spiwojs-Becker, I. (1996). Plasticity of retinal ribbon synapses. *Microsc. Res. Tech.* 35, 472–487.
- Wahl-Schott, C., Baumann, L., Cuny, H., Eckert, C., Griessmaier, K., and Biel, M. (2006). Switching off calcium-dependent inactivation in L-type calcium channels by an autoinhibitory domain. *Proc. Natl. Acad. Sci. U.S.A.* 103, 15657–15662.
- Wan, Q. F., and Heidelberger, R. (2011). Synaptic release at mammalian bipolar cell terminals. *Vis. Neurosci.* 28, 109–119.
- Wang, Y., Okamoto, M., Schmitz, F., Hofmann, K., and Südhof, T. C. (1997). RIM is a putative effector in regulating synaptic-vesicle fusion. *Nature* 388, 593–598.
- Wässle, H. (2004). Parallel processing in the mammalian retina. *Nat. Rev. Neurosci.* 5, 1–12.
- Woodruff, M. L., Sampath, A. P., Matthews, H. R., Krasnoperova, N. V., Lem, J., and Fain, G. L. (2002). Measurement of cytoplasmic calcium concentration in the rods of wild-type and transducin knock-out mice. *J. Physiol.* 542, 843–854.
- Wycisk, K. A., Budde, B., Feil, S., Skosyrski, S., Buzzi, F., Neidhardt, J., Glaus, E., Nürnberg, P., Rüter, K., and Berger, W. (2006). Structural and functional abnormalities of retinal ribbon synapses due to Cacna2d4 mutation. *Invest. Ophthalmol. Vis. Sci.* 47, 3523–3530.
- Xiao, H., Chen, X., and Steele, Jr. E. C. (2007). Abundant L-type calcium channel CaV1.3 (alpha1D) subunit mRNA is detected in rod photoreceptors of the mouse retina via in-situ hybridization. *Mol. Vis.* 13, 764–771.
- Yang, P. S., Alseikhan, B. A., Hiel, H., Grant, L., Mori, M. X., Yang, W., Fuchs, P. A., and Yue, D. T. (2006). Switching of the Ca<sup>2+</sup>-dependent inactivation of CaV1.3-channels by calcium binding proteins of auditory hair cells. *J. Neurosci.* 26, 10677–10689.
- Zeitze, C., Kloeckener-Gruissem, B., Forster, U., Kohl, S., Magyar, I., Wissinger, B., Mátyás, G., Borruat, F. X., Schorderet, D. F., Zrenner, E., Munier, F. L., and Berger, W. (2006). Mutations in CABP4, the gene encoding the Ca<sup>2+</sup>-binding protein 4, cause autosomal recessive night blindness. *Am. J. Hum. Genet.* 79, 657–667.
- Zenisek, D., Steyer, J. A., and Almers, W. (2000). Transport, capture and exocytosis of synaptic vesicles at active zones. *Nature* 406, 849–854.
- Zhang, N., and Townes-Anderson, E. (2002). Regulation of structural plasticity by different channel types in rod and cone photoreceptors. *J. Neurosci.* 22, 7065–7079.
- Zhang, N., Beuve, A., and Townes-Anderson, E. (2005). The nitric-cGMP signalling pathway differentially regulates presynaptic structural plasticity in cone and rod cells. *J. Neurosci.* 25, 2761–2770.

**Conflict of Interest Statement:** The authors declare that the research was conducted in the absence of any commercial or financial relationships that could be construed as a potential conflict of interest.

Received: 09 January 2012; paper pending published: 25 January 2012; accepted: 15 February 2012; published online: 29 February 2012.

Citation: Schmitz F, Natarajan S, Venkatesan JK, Wahl S, Schwarz K and Grabner CP (2012) EF hand-mediated Ca<sup>2+</sup>- and cGMP-signaling in photoreceptor synaptic terminals. *Front. Mol. Neurosci.* 5:26. doi: 10.3389/fnmol.2012.00026

Copyright © 2012 Schmitz, Natarajan, Venkatesan, Wahl, Schwarz and Grabner. This is an open-access article distributed under the terms of the Creative Commons Attribution Non Commercial License, which permits non-commercial use, distribution, and reproduction in other forums, provided the original authors and source are credited.